

# **Electro Discharge Machining for Micro Manufacturing**

A thesis submitted to the Cardiff University

for the degree of

Doctor of Philosophy

by

Atanas Ivanov

Cardiff University

United Kingdom

2008

UMI Number: U585147

All rights reserved

INFORMATION TO ALL USERS

The quality of this reproduction is dependent upon the quality of the copy submitted.

In the unlikely event that the author did not send a complete manuscript and there are missing pages, these will be noted. Also, if material had to be removed, a note will indicate the deletion.



UMI U585147

Published by ProQuest LLC 2013. Copyright in the Dissertation held by the Author.  
Microform Edition © ProQuest LLC.

All rights reserved. This work is protected against  
unauthorized copying under Title 17, United States Code.



ProQuest LLC  
789 East Eisenhower Parkway  
P.O. Box 1346  
Ann Arbor, MI 48106-1346

Others can stop you temporarily, but only you can do it permanently

**To my family**

# Synopsis

Due to the high precision and good surface quality that it can give, Electrical Discharge Machining (EDM) is potentially an important process for the fabrication of micro tools, micro components and parts with micro features. However, a number of issues remain to be solved before micro EDM can become a reliable process with repeatable results and its full capabilities as a micro manufacturing technology can be realised.

This work presents some developments in advancing the state-of-the-art in the micro EDM process. EDM drilling and EDM milling are regarded as separate processes as they require different approaches in investigating and implementing the results of the study. At the beginning, special attention is paid to factors and procedures influencing the accuracy achievable, including positioning approaches during EDM and electrode grinding. In particular, the main parameters affecting the size and position of a machined feature are discussed and new techniques for minimising errors are proposed. The technological capabilities of different methods of setting up and dressing the electrode on the machine are analysed.

Factors contributing to electrode wear, the main systematic cause for inaccuracy of the dimensions achieved, during the micro EDM process are studied. A method for calculating the volumetric wear ratio based only on geometrical information obtained from the process is proposed. This study investigates the suitability of micro EDM electrode wear compensation methods. Electrode shape deformation and random variations in the volumetric wear are also investigated as the



two main factors affecting the applicability of the wear compensation methods as well as indicating the accuracy achievable with micro EDM.

When producing features and parts on the micro scale, the phenomena that take place between the electrodes in EDM is not fully understood. A barrier to a complete exploitation of the potential natural tolerance of this process and to the further development of the process towards the production of components on the nano-scale is therefore in place. An analytical micro EDM model of electrode wear based on electrode shape deformation and wear ratio is suggested, verification of which requires experimental work with pure metals. Electrode-tool wear is studied during the micro EDM process of pure metals and the effect of electrode wear on the process accuracy and process variability. Objectives in this case are to advance the experimental knowledge of the electrical discharges during micro EDM operations which often conflicts with existent theoretical models of the EDM process. In particular, the remit of this investigation is to identify the effects that electrode materials have on selected electrical characteristics of the discharge process. An exploratory data analysis (EDA) approach is adopted in order to draw conclusions from the performed experimental activity.

The material removal mechanism in the micro EDM process was confirmed to be mainly attributed to the melting and vaporisation phenomenon. Metal removal takes place as a result of the extremely high temperature generated by the discharge sparks. It was also found in this study that the volumetric wear ratio depends not only on the sparking conditions but also on the electrode materials. In addition, the research also proved that the electrode material severely influences the energy distribution between the electrodes during the sparks.

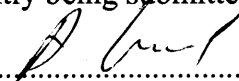
# **Acknowledgement**

I gratefully acknowledge Prof. Pham for his guidance and encouragement in this work, and for the use of the departmental facilities for the project.

# Declaration

## Statement 1

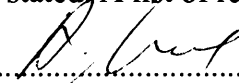
This work has not been accepted in substance for any degree and is not concurrently being submitted in candidature for any other degree.

Signed:  (Atanas Ivanov - candidate)

Date: 28/05/08

## Statement 2

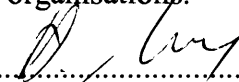
This thesis is the result of the candidate's own investigations, except where otherwise stated. A list of references is appended.

Signed:  (Atanas Ivanov - candidate)

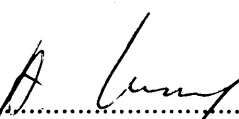
Date: 28/05/08

## Statement 3

I hereby give consent for my thesis, if accepted, to be available for photocopying and for inter-library loan and for the title and summary to be available to outside organisations.

Signed:  (Atanas Ivanov - candidate)

Date: 28/05/08

Signed:  (Professor D.T. Pham - supervisor)

Date: 28/05/08

# Table of Contents

Synopsis .....	iii
Acknowledgement .....	v
Declaration .....	vi
Table of Contents .....	vii
List of Figures .....	xi
List of Tables .....	xvii
Notations .....	xx
Chapter 1 .....	1
<b>1. Introduction .....</b>	<b>2</b>
1.1. Motivation .....	3
1.2. Aims and Objectives .....	6
1.3. Outline of the Thesis .....	7
Chapter 2 .....	10
<b>2. Literature Review .....</b>	<b>11</b>
2.1. Micro Manufacturing Technologies and Micro EDM .....	11
2.2. An overview of the EDM process .....	18
2.3. Theories of Material Removal .....	24
2.4. Growth of the EDM Industry .....	25
2.5. EDM as a Micro Technology - problematic issues .....	28
2.5.1. Micro EDM Issues .....	32
2.5.1.1. Handling of Electrodes and Parts .....	32
2.5.1.2. Electrode and workpiece preparation .....	35

2.5.1.3. The Micro EDM process.....	36
2.5.1.4. Measurements .....	39
2.6. Surface Integrity and Process Characterisation Research in micro EDM .....	40
2.7. Micro EDM Process Improvement and Open Research Issues .....	42
2.8. Summary .....	44
Chapter 3 .....	46
<b>3. Accuracy Requirements for Micro EDM Process.....</b>	<b>47</b>
3.1. Process Specific .....	47
3.2. Accumulation of Errors.....	48
3.2.1. Process Definition .....	48
3.2.2. Factors affecting hole diameter .....	51
3.2.3. Factors affecting the position of the hole.....	52
3.3. Description of the factors affecting the accuracy .....	54
3.3.1. Accuracy and Repeatability of Positioning.....	54
3.3.1.1. Dressing Position .....	57
3.3.1.2. Hole Position .....	58
3.3.2. Spark gaps and effective electrode diameter .....	58
3.3.2.1. Gap between electrode and workpiece .....	58
3.3.2.2. Gap between electrode and dressing unit.....	58
3.3.2.3. Effective Diameter .....	59
3.3.2.4. Estimation of $g_e$ and $\Delta g_e$ .....	64
3.3.3. Temperature instability error .....	65
3.3.4. Measurement errors .....	65
3.3.4.1. Workpiece surface detection error ( $\Delta X_{meas}$ , $\Delta Y_{meas}$ ).....	65
3.3.4.2. Surface position detection error ( $\Delta g_{meas}$ ) .....	66

3.4. Experimental set up.....	71
3.5. Summary .....	73
Chapter 4.....	74
<b>4. Micro EDM electrode wear investigation .....</b>	<b>75</b>
4.1. Wear estimation .....	76
4.1.1. Electrode shape deformation.....	76
4.1.2. Volumetric wear.....	83
4.2. Wear ratio calculation .....	84
4.3. Experiments .....	90
4.3.1. Wear measurements for the three different materials .....	91
4.3.2. Electrode wear variation .....	98
4.3.3. Spark gap variation .....	102
4.4. Summary .....	106
Chapter 5.....	107
<b>5. Natural tolerances of the Micro EDM process.....</b>	<b>108</b>
5.1. Factors affecting electrode shape change .....	109
5.2. Factors affecting electrode wear ratio in micro EDM .....	116
5.2.1. Experimental set up.....	121
5.2.2. Results.....	124
5.2.3. Analysis of the results .....	131
5.3. Estimation of the effects of the electrode material on the electrical discharge in micro EDM .....	136
5.3.1. Investigation set-up.....	138
5.3.2. Results from the investigation .....	143
5.4. Summary .....	154

Chapter 6 .....	155
<b>6. Contributions, conclusions and future work .....</b>	<b>156</b>
6.1. Contributions.....	156
6.2. Discussion and conclusions .....	157
6.3. Future work .....	161
Appendix A.....	163
Appendix B.....	186
Appendix C .....	204
Appendix D.....	209
Appendix E .....	215
Appendix F.....	218
References.....	218

# List of Figures

## Chapter 2

		page
<b>2.1</b>	Classification of micro manufacturing technologies	17
<b>2.2</b>	The Lazarenkos basic EDM circuit which provided the foundation of the modern EDM industry	17
<b>2.3</b>	Schematic and explanations of the discharge process stages	20
<b>2.4</b>	Leading institutions and centres for EDM research	27
<b>2.5</b>	Problematic areas in micro EDM	31
<b>2.6</b>	Dressing unit and ceramic guiding system	34
<b>2.7</b>	Three types of electrode grinding devices	34



## Chapter 3

		page
3.1	Example of micro EDM equipment and its elements	49
3.2	Example of micro EDM machining elements	49
3.3	Example of achieved dimensions when machining a single hole	50
3.4	Achieved diameter $\varnothing H$ of EDM drilled hole	50
3.5	Schematic of micro EDM dressing process	50
3.6	Dimensions affecting the hole position	53
3.7	Schematic of the setting up process	53
3.8	X axis positioning results	55
3.9	Y axis positioning results	55
3.10	Z axis positioning results	56
3.11	Single spot positioning accuracy	60
3.12	Effect of the clearance gap between the ceramic guide and the electrode	60
3.13	Possible error in long dressed electrode	63
3.14	Accuracy of a hole produced with rotating and stationary electrodes	63
3.15	Machine body deformation due to temperature variations	67
3.16	Accuracy of surface detection using touch probe on a WC block	67
3.17	Schematic of surface detection with $\Delta D$ influence	69
3.18	Surface detection using electrode on a WC block	69
3.19	Hole diameter variation for 4 dressing positions	72

## Chapter 4

		page
<b>4.1</b>	The shapes of a $\varnothing 150 \mu\text{m}$ rod electrode (a) before and (b) and (c) after two erosion depths  a) Before erosion  b) After $25 \mu\text{m}$ erosion depth  c) After $100 \mu\text{m}$ erosion depth	78
<b>4.2</b>	Evolution of the cavity/electrode shape during EDM drilling of tool steel with $\varnothing 170 \mu\text{m}$ WC electrode  a) hole/electrode shape evolution during drilling  b) constant hole/electrode shape after $180 \mu\text{m}$ erosion depth	79
<b>4.3</b>	Electric field intensity dependency on the electrode shape changes  a) The highest intensity is on the edge of the cylindrical electrode  b) The position of the highest intensity field shifts towards the centre with the rounding of the edge of the cylindrical electrode  c) The uniform field intensity with constant electrode shape	80
<b>4.4</b>	Groove shapes obtained for two different milling depths  a) Top view of EDM milling passes  b) End view of the milling passes	82
<b>4.5</b>	Schematics of erosion to a fixed depth $Z$ with rod and tubular electrode  a) Rod electrode  b) Tubular electrode	87

<b>4.6</b>	Repeatability of electrode measurements a) Datum plane erosion after 100 measurements b) Error of surface detection	88
<b>4.7</b>	Electrode wear graphs a) Brass workpiece and tubular electrode b) Brass workpiece and rod electrode c) Aluminium workpiece and tubular electrode d) Aluminium workpiece and rod electrode e) Steel workpiece and tubular electrode f) Steel workpiece and rod electrode	92
<b>4.8</b>	Variation of electrode wear a) wear variation using WC rod and tubular electrode with steel, aluminium and brass workpieces b) wear variation using WC rod electrode with aluminium and brass workpieces	100
<b>4.9</b>	Variation of the spark gap a) WC rod electrode in steel workpiece b) WC tube electrode in steel workpiece c) WC rod electrode in brass workpiece d) WC tube electrode in brass workpiece e) WC rod electrode in aluminium workpiece f) WC tube electrode in aluminium workpiece	104

## Chapter 5

		page
5.1	Examples of different final shapes achieved by different sparking conditions	113
5.2	Electric field strength $ E $ (V/m) in the sparking gap area <ul style="list-style-type: none"> <li>a) Electro static field intensity <math> E </math> of electrode at start</li> <li>b) Electro static field intensity <math> E </math> of electrode after 10<math>\mu</math>m depth</li> <li>c) Electro static field intensity <math> E </math> of electrode after 40<math>\mu</math>m depth</li> <li>d) Electro static field intensity <math> E </math> of electrode after 60<math>\mu</math>m depth</li> <li>e) Electrostatic field intensity <math> E </math> of electrode after 60<math>\mu</math>m depth and progressing down</li> </ul>	113
5.3	Voltage current spark pulses assumption for the wear ratio modelling. Nominal pulse shape: typical set-up parameters of a power generator (in boxes) and measured quantities	117
5.4	'S' control chart for the mass measuring process	126
5.5	Wear ratio in mass (anode over cathode removal)	126
5.6	Wear ratio in mass in excess of the median	129
5.7	Images of the eroded surfaces on the anode	130
5.8	The obtained empirical distribution	135
5.9	Schema of the test rig	139
5.10	Interpretation of $T_{ON}$ and $T_{OFF}$ : on channel 2, just 2 current pulses are	142

	visible, whereas the train of voltage still continues the $T_{ON} - T_{OFF}$ pattern	
<b>5.11</b>	Oscilloscope waveforms for each material investigated: $i(t)$ current average discharge pulses, $v(t)$ voltage average discharge pulses and $p(t)$ instant power average discharge pulses  a) Silver (Ag) $t_e=1080$ ns b) Copper (Cu) $t_e=976$ ns c) Nickel (Ni) $t_e=872$ ns d) Titanium (Ti) $t_e=1136$ ns e) Tungsten (W) $t_e=748$ ns	146
<b>5.12</b>	Effect of the five experimental units (I, II, III, IV, V) on the nine response variables	151
<b>5.13</b>	Effect of the five electrode materials considered (Ag,, Cu, Ni, Ti, W) on the nine response variables	152

# List of Tables

## *Chapter 3*

		page
3.1	Data for experimentally determined $\Delta H$	72

## ***Chapter 4***

		page
<b>4.1</b>	Data for electrode wear variation	103
<b>4.2</b>	Data for spark gap variation	103

## ***Chapter 5***

		page
<b>5.1</b>	Set up parameters of the EDM generator	123
<b>5.2</b>	Main physical properties of the hydrocarbon dielectric	123
<b>5.3</b>	Oscilloscope and current probe main characteristics	139



# Notations

## Chapter 3

Notations :	
<b>d</b>	effective dressed diameter of electrode
<b>D</b>	initial effective diameter of the electrode
<b>D<sub>guide</sub></b>	diameter of the ceramic guide
<b>D<sub>init</sub></b>	initial diameter of the electrode
<b>D<sub>init_min</sub></b>	minimum initial diameter of the electrode
<b>g<sub>d</sub></b>	spark gap during dressing of the electrode
<b>g<sub>e</sub></b>	spark gap during erosion of the workpiece
<b>g<sub>meas</sub></b>	spark gap during measuring cycle
<b>H</b>	achieved hole diameter
<b>L<sub>guide</sub></b>	length of the guide
<b>t<sub>meas</sub></b>	time interval between each contact signal check
<b>V<sub>meas</sub></b>	speed of measuring cycle movement
<b>X<sub>H</sub></b>	X coordinate of the hole relative to the workpiece reference
<b>X<sub>meas</sub></b>	X coordinate of the measured point of contact between electrode and workpiece surface
<b>X<sub>pos</sub></b>	X coordinate of the hole relative to the machine zero point

$y_d$	target dressing position in Y axis
$y_{d\_init}$	an initial target dressing position
$Y_H$	Y coordinate of the hole relative to the workpiece reference
$Y_{meas}$	Y coordinate of the measured point of contact between electrode and workpiece surface
$Y_{pos}$	Y coordinate of the hole relative to the machine zero point
$y_{unit}$	Y coordinate of the dressing point relative to the machine zero point
$z_{guide}$	length of electrode protruding from the ceramic guide
$\Delta d$	d variation
$\Delta D$	D variation
$\Delta g_d$	$g_d$ variation
$\Delta g_e$	$g_e$ variation
$\Delta g_{meas}$	$g_{meas}$ variation
$\Delta H$	H variation
$\Delta X_{meas}$	$X_{meas}$ variation
$\Delta X_{pos}$	$X_{pos}$ variation
$\Delta y_d$	$y_d$ variation
$\Delta Y_{meas}$	$Y_{meas}$ variation
$\Delta Y_{pos}$	$Y_{pos}$ variation
$\Delta y_{unit}$	$y_{unit}$ variation
$\epsilon$	Side error due to the tilting of the electrode in the ceramic guide

## Chapter 4

Notations :	
$D_e$	External diameter of the electrode (rod or tubular)
$d_e$	Internal diameter of the tube electrode
$D_p$	Diameter of the eroded hole
$g$	Spark gap
$M_{dif}^z$	Maximum difference between the smallest and the largest measured electrode wear
$Rw$	Volumetric wear ratio proportionality factor
$\overline{Rw}$	Mean value of the volumetric wear ratio proportionality factor
$Rw_i$	Value of the volumetric wear ratio proportionality factor for the $i^{th}$ data set
$V_e$	Volume removed from the electrode (electrode wear)
$V_p$	Volume removed from the workpiece (material removed)
$W_e$	Eroded length from the electrode
$W_e^{trend}$	Predicted electrode wear based on the linear regression equation
$W_p$	Eroded length from the workpiece
$Z$	Coordinate of the target depth of erosion
$\delta R w_i$	Relative deviation of the volumetric wear ratio proportionality factor for the $i^{th}$ data set

$\delta v_i$	Relative deviation of the electrode wear ratio for the $i^{\text{th}}$ data set
$\Delta v_i$	The absolute value of the difference between the value of the volumetric wear ratio for the $i^{\text{th}}$ data set and the mean value of the volumetric wear ratio
$v$	Volumetric wear ratio
$v_i$	Value of the volumetric wear ratio for the $i^{\text{th}}$ data set
$\bar{v}$	Mean value of the volumetric wear ratio

## Chapter 5

Notations :	
<b>c</b>	Speed of light
<b>c<sub>4</sub></b>	A constant which can be found tabulated or computed directly
$c_4(n_i)$	(Montgomery, 1996, page 212 and Appendix 6)
<b>c<sub>p</sub></b>	Specific heat capacity (J/kg °C)
<b>E</b>	Electric field intensity
<b>e e</b>	Discharge energy of the average discharge pulse
$E_{dis}^{anode}$	Discharge energy going to the anode
$E_{dis}^{cathode}$	Discharge energy going to the cathode
$E_{dis}^{dial}$	Discharge energy going to the dielectric
<b>E<sub>dis</sub></b>	Energy of the discharge
<b>E<sub>m</sub></b>	Energy required to melt certain amount of material (mass) (J)
<b>E<sub>v</sub></b>	Energy required to vaporize certain amount of material (mass) (J)
<b>F</b>	Electric force given by Coulomb's law
<b>H<sub>m</sub></b>	Enthalpy of melting (J/kg)
<b>H<sub>v</sub></b>	Enthalpy of vaporization (J/kg)
$\bar{i}$	Average current intensity during the measured time interval $t_e$

$I_{dis}$	Current of the discharge
$i_{max}$	Maximum value of current intensity during a discharge
$LCL_i$	Lower Control Limit
$L_m$	Latent heat for melting (J/kg)
$L_v$	Latent heat vaporization (J/kg)
$m$	Mass (kg)
$n_i$	Number of test measurements performed for obtaining the $i$ -th measurement result
$\bar{P}$	Average discharge electrical power
$P_{max}$	Maximum of the discharge instant power
$Q$	Charge of the particle creating the electric field
$q$	Electric charge
$r$	Distance from the particle with charge $Q$ to the E-field evaluation point
$\hat{r}$	Unit vector pointing from the particle with charge $Q$ to the E-field evaluation point
$\bar{S}$	Sample standard deviation
$T_0$	Starting (initial ambient) temperature (°C)
$t_0$	Time interval between successive pulses of voltage (time-off)
$t_e$	Time duration of the discharge
$t_i$	Time duration of the pulses (time-on)

$t_{ign}$	Time (share of the time duration of the pulse $t_i$ ) which is from the start of the pulse to registering the current start going through the spark gap
$T_m$	Temperature of melting ( $^{\circ}C$ )
$t_{max}$	Time interval between the initial flow of current, instant A, and the instant where the current is at its maximum, $i_{max}$
$T_v$	Temperature of vaporization ( $^{\circ}C$ )
$UCL_i$	Upper Control Limit
$V_{dis}^{anode}$	Volume removed material from the anode
$V_{dis}^{cathode}$	Volume removed material from the cathode
$V_{total}$	Total vaporized volume ( $m^3$ )
$W_t$	Power of the discharge
$\alpha$	Probability of a false alarm
$\epsilon_0$	Permittivity in vacuum
$\epsilon_r$	Dielectric constant
$\mu_0$	Permeability of vacuum
$\mu_{anode}$	The expected values (mean) of the measured mass from the anode
$\mu_{cathode}$	The expected values (mean) of the measured mass from the cathode
$v$	Volumetric wear ratio
$V_e$	Discharge voltage

$\bar{v}_e$	Average discharge voltage
$\bar{v}_0$	Average open circuit voltage measured 200 ns before the occurrence of the trigger
$\rho$	Density of the material of the anode and the cathode respectively (kg/m <sup>3</sup> )
$\rho_{\text{unit}}$	Charge density, or the amount of charge per unit volume
$\sigma_{\text{balance}}^2$	Variance of the weight measuring process (mg <sup>2</sup> )
$\hat{\sigma}_{\text{balance}}$	Standard deviation of the weight measuring process (mg)
$\sigma_{\text{EDM}}^2$	Variance caused by the EDM
$\hat{\sigma}_{\text{total}}^2$	Total variance
$\chi_e$	Electric susceptibility of the material



If you don't start, it's certain you won't arrive

# Chapter 1

## 1. Introduction

Micro-manufacture is in one of the specific areas for future research need, identified in the Final Report of the Manufacturing 2020 part of the UK Government's Foresight Programme. The total world market for Micro Electrical Mechanical Systems MEMS has grown from 14.4 Billion Euro in 1996 to 38 Billion Euro by the year 2003 which represents a growth rate of 18% per year in this sector. To achieve and sustain such impressive growth rates in subsequent years, significant advances are required in micro-fabrication technologies for micro-structuring not only in silicon but also in other materials like polymers, metals and ceramics. On the other hand, properties of the materials on a small scale can start changing due to larger surface areas per unit of mass and then the quantum effects can begin to dominate the behaviour of matter (Dowling et al., 2004). This enables the possibility of developing completely new applications.

A significant contribution to the development of micro-fabrication technologies, comes from existing manufacturing processes like milling, turning, grinding and Electro Discharge Machining (EDM), which now have extended capabilities and have to cover the new area of micro manufacturing (Masuzawa, 2000).

Increased demands for manufactured goods have raised the overall environmental impact and the energy requirements in order to support manufacturing growth especially in strategic areas like micro manufacturing. The latest micro EDM process developments have reached the stage where the process efficiency has increased, with a 70% reduction of the energy usage from the process being reported recently (Bleys & Kruth, 2001). This, together with

little or no waste products from the process, make EDM a very environmentally friendly process. Furthermore the EDM process has been on the manufacturing market for more than 50 years. There are well trained personnel and well formed communities of EDM users all over the world. With the new developments in the micro manufacturing, it would be relatively easy to promote the use of micro EDM to those communities. Broadening the application of this process will help to better secure jobs in manufacturing and specifically in the EDM sector by opening a new market in micro manufacturing, which could have a large social impact.

The main aim of this research is to develop and validate new techniques for the use of the micro-EDM process. This research work adds a new dimension and at the same time comes as a natural continuation of previous work by the investigator on the traditional EDM process, its capabilities and fields of application.

## **1.1 Motivation**

Once considered a “non-traditional” machining process, EDM has been replacing drilling, milling, grinding and other traditional machining operations in many industries throughout the world especially in difficult to machine materials. Following its early days, over 50 years ago, EDM has developed into one of the most advanced machining technologies. Today’s EDM equipment uses advanced Computer Numerical Control (CNC) with up to six-axis simultaneous operation and state-of-the-art power supply technology (Bleys & Kruth, 2001), which can produce a mirror surface finish and high accuracy products (Rzmasawmy & Blunt, 2002).

Although EDM represents only a small portion of the total machine tool industry worldwide, the number of laboratories throughout the world performing EDM research and development studies has been growing steadily over the years due to the exceptional process capabilities especially in the new rapidly developing micro and nano sector.

The more in-depth and well organized EDM research programmes at various technical centres are funded by the major EDM machine builders or through government research grants because the process has proven to be cost effective and it is simple and reliable and has justified its place in the micro and nano manufacturing market. Because of that, micro EDM has recently attracted a significant amount of research attention with the availability of new types of power generators capable of releasing very small amounts of energy (<http://www.smaltec.com/>). The new focus is not only on producing small holes and slots but also on developing trajectory micro EDM capable of continuous path producing features of micro water cooling channels and cavities for micro moulds and dies ([http://www.sarix.com/sx200\\_e.htm](http://www.sarix.com/sx200_e.htm)), which adds new dimensions to the process and makes it more desirable for the micro manufacturing industry.

The achieved high aspect ratio with good surface integrity (Lim et al, 2003; Yu et al, 2002) is unique among all of the micro manufacturing processes. However, to reveal the full potential of the process, more research is required. This includes the development of analytical and computer models of the micro EDM process, study of micro-electrode wear behaviour, development of CAM support for trajectory EDM, integration of on-line process monitoring systems

and incorporation of electrode on-the-machine measuring systems together with on-the-machine electrode grinding systems.

The negligible forces in the EDM process, in general, and its independence of the mechanical properties of the workpiece (Son et al, 2007) open a variety of alternatives for different applications. At the same time, the physical and chemical properties of the machined material may have strange effects on the process outcomes in an unpredictable way.

The new micro application field of the EDM process presents new challenges for the machine tool-builders. In spite of EDM being slow, which does not require quick movement of the machine parts, specific characteristics for accuracy would be required for the new machine-tool which is to accommodate the micro EDM process. For example, from a dimensional point of view, when reducing the size of a product it is expected that the size of the dimensional error (the tolerance) is also proportionally reduced. Masuzawa (Masuzawa, 2000) pointed out this concept by describing the equipment precision as a 'necessary condition for micromachining'. Measuring and inspection methods with an even higher level of precision should also be available to characterise both products and manufacturing processes in the micrometric and nanometric ranges.

Furthermore the material removal mechanism was never before considered as changeable when changing process parameters which brought large discrepancies between the modelled process outcome and the empirical findings from the process (Egashira et al, 2006; Singh & Ghosh, 1999).

Finally, each process has its natural limits imposed by the nature of the process. Changing the phenomenon of the material removal by severely altering

the processing conditions will modify the natural limits of the process. However, some limits of the process capabilities still exist and they have to be known which will help engineers to design parts with certain tolerances and to know what the ultimate possible process accuracy is. It is envisaged that not only manufacturing process designers but also product designers could benefit from this research. For example, designers of micro-fluidic devices, such as micro-pumps, micro-valves, micro-flow-meters and micro-mixers as well as production engineers who, based on the process limits, would be able to assign process tolerances for the different machining operations.

## **1.2 Aims and Objectives**

The scope of this investigation was:

- To investigate and extend the technological capabilities of the micro EDM process;
- To investigate the needed micro EDM process requirements and parameters for machine tool capabilities;
- To investigate the main systematic factors affecting the process performance and to establish links between process parameters and their influence on the systematic factors;
- To establish the quantitative characteristics of micro EDM (minimum and max energy of the discharge, speed of the discharge, spark phenomenon change) based on the thermal, electrical and physical properties of the used materials;
- To determine the micro EDM phenomenon change of the process and empirically to verify it;
- To determine the process constraints imposed by the nature of the processes and determine the limits of the process application in terms of accuracy, surface integrity, roughness, repeatability, etc;

- To investigate the influence of the material properties on the discharge characteristics of the process in order to facilitate the use of an appropriate compensation method for electrode wear.

### **1.3 Outline of the thesis**

This thesis has six chapters. Chapters 3 to 5 cover the main investigations. Chapter 2 reviews the relevant literature and Chapter 6 concludes the thesis with a summary of the contributions and future work.

Chapter 2 is devoted to a literature review and provides background knowledge for Chapters 3 to 6. This chapter consists of four interconnected sections relating to the main ideas given in Chapters 3-6. In the first section, the importance of the micro manufacturing sector is highlighted and the place of micro EDM is determined. In the second section, evidence of the already researched area of EDM and ongoing research topics are discussed. Furthermore, the fundamental principles adopted for EDM process modelling are shown and the best process models are discussed. Critical analysis of the research devoted to the investigation of electrode wear behaviour in micro electrical discharge machining is provided and the opening of a new niche for micro electrode wear investigation is highlighted.

In Chapter 3, a dimensional analysis of the micro EDM process is conducted, showing all possible errors which can be brought by the machine tool inaccuracy. This is achieved through investigating the errors due to machine positioning accuracy and repeatability and temperature instability. The

contribution to the final outcome of procedures such as setting up, measuring and on-the-machine electrode grinding are also discussed and the errors due to these procedures are investigated. All the errors are theoretically explained and empirically confirmed by conducting appropriate experiments.

By building upon the findings of Chapter 3, in Chapter 4, the main systematic factor, tool electrode wear is investigated. Special attention is paid to the deformation of the electrode shape and also to the dimensional wear of the electrode which affects directly the dimensions achieved during the process. A hypothesis for electrode shape deformation is suggested and empirically verified using Finite Element Analysis of the electrostatic field created in the continuum between the electrodes. A practical solution to the problem with the dimensional effect of the electrode wear is suggested based only on the geometrical information available from the process. Finally the wear charts and wear variations for three different materials (aluminium, brass and tool steel) and for two different electrode types (WC rod and tube  $\varnothing$  170 micrometers) are investigated.

In Chapter 5, following the findings in Chapter 4 and especially the suggested hypothesis of electrode wear due to the non-uniform electrostatic field intensity, a deeper investigation is conducted and a method for predicting shape change is suggested. The wear ratio is an inseparable part of this method and in order to explain the change in material removal regions in micro EDM, an analytical explanation of the electrode wear ratio is suggested. The theoretical investigation has led to an investigation of wear phenomena in pure metals in order to determine the ultimate limits of the process capabilities and to



assist in justification of a method to be used for electrode wear compensation. Using exploratory data analysis, it was discovered that the discharge characteristics strongly depend on the material despite the process parameters being the same.

Finally, Chapter 6 comprises conclusions summarising the author's thoughts on the proposed research, its findings and limitations. The chapter contains suggestions for further work to address some of the limitations identified.

Wisdom comes with experience, while intelligence is innate

# *Chapter 2*

## **2. Literature review**

This chapter introduces electro discharge machining (EDM) in general and as a micro manufacturing technology for two- and three-dimensional features. Some specific micro EDM machining strategies and equipment are discussed as well as the state-of-the-art in the process modelling, process characterisation research and some open research issues. The centrality of the concept of volumetric wear ratio in micro electrical discharge machining (micro EDM) operations is highlighted and the importance of electrode wear compensation methods is also emphasised. In addition, the chapter also discusses process characterisation research and the development of hybrid methods of machining in order to improve process parameters (accuracy, material removal rate, roughness etc).

### **2.1. Micro manufacturing technologies and Micro EDM**

It has been recognised that, to be competitive, manufacturing will need to focus on advanced high-value added rather than commodity products. Micro-manufacture is one such high-value added technology that is also time, energy and resource efficient making it highly compatible with economic sustainability requirements.

The use of micro components and products with micro features has spread rapidly over the last few years (Bleys & Kruth, 2001). A growth rate of 18% per year was reported in the world market for Mechanical Electrical Micro Systems (MEMS). Significant efforts are required to sustain such impressive growth rates, in both design and manufacturing of micro devices. There is an urgent need for

industrial technologies to cost effectively mass produce micro parts and components with micro details. This can be satisfied on the one hand by the use of replication techniques employing mould tools and on the other by developing appropriate mass production technologies. If the first approach is adopted, the performance of the replication techniques is strongly dependent on the corresponding micro mould, the quality of which defines and limits the behaviour of the final micro parts (Piotter et al, 2000) and it is seen as the immediate answer to the market demand, while the second approach is riskier and is accepted as a long term strategy for mass production of micro parts.

At present the industrial need is mainly for parts and components of small size (but not exactly micro) with some *features* in the micrometer range. However, the demand for micro parts is growing rapidly, and this is expected to have a high industrial impact in the medium term. There are many techniques for micro manufacturing with new ones continually under development. Most of these techniques are expensive, not well proven and consequently difficult to scale up and industrialise.

Until now, the main material for micro systems manufacture has been silicon (Si) (Senturia, 2001) even in spite of its drawbacks: expensive processing equipment, suitability only for 2.5D structures and problems in packaging. There is, however, a growing interest in new materials such as ceramics, polymers, active materials and biomaterials allowing increased functionality, and particularly the fabrication of 3D micro structures (Alting et al, 2003), which overcome some or all of the limitations associated with silicon. The current production of micro products remain predominantly as a result of a technology push from the semiconductor industry and are in the domain of the techniques resulting from the accumulated know-how in the

micro-electronics industry.

Currently Micro-Electro-Mechanical-Systems (MEMS) are also dominated by silicon based products due to the commercial opportunities presented by adopting the existing suite of Integrated Circuit (IC-processing) technologies. Currently available products are therefore also a result of the technology “push” from the semiconductor industry. To broaden the range of the micro systems based products, whilst multiplying their capabilities to enable market driven products, requires the introduction of new materials and manufacturing processes and their subsequent integration with IC-based, batch fabrication processes.

The present range of micro technologies can be clustered in two main groups (Fig. 2.1), micro systems (MST) and Micro Engineering Technologies (MET). MST are suitable for the manufacture of MEMS and Micro-Opto-Electro-Mechanical-Systems (MOEMS) and rely on processes such as photolithography & electroforming. MET enable the production of highly precise mechanical components, replication tools and micro-structured surfaces. An intermediate group of technologies includes Electro-Physico-Chemical processes such as Ion Beam Machining (IBM), Electron Beam Machining (EBM), Laser Beam Machining (LBM), Electro-Chemical Machining (ECM) and EDM that could be classified as both MST or MET. Finally, there is a fourth group of processes covering replication techniques, e.g. injection moulding, hot embossing, forging and casting which are very important for the serial manufacture of non-silicon micro components. It should be noted that there is a strong trend for technology convergence between the three groups.

The two greatest barriers facing industrial companies who wish to adopt such techniques are the cost of entry into micro manufacturing technologies and their rapid

rate of change. For large scale adoption, it must therefore be ensured that the probability of payback is maximised and that any investment required will not become obsolete before yielding full returns. Furthermore, micro manufacturers should have a good degree of knowledge of these processes. Most of them are adaptation of already existing processes in the Precision Engineering area and there are machine tools already available or easily modifiable to suit the purpose of micro manufacturing. For example:

- **Micro milling** originates from the watch making industry for manufacturing small parts. With new achievements in CNC control systems, powder metallurgy for sintering small super hard cutters and new spindles capable of over 100 000 rev/min (Weule et al , 2001), micro milling has become an important technology for producing micro moulds and dies (Schaller et al, 1999). Micro milling has recently been used for the direct manufacture of micro parts and micro features, however, minimum cutter size, aspect ratio, machine tool dynamic characteristics and spindle speed impose certain limitations on the process (Egashira & Mizutani, 2002). Lack of CAM support, condition-monitoring systems for small tools and machining strategies also restrict the use of the process and make results unpredictable (Bao & Tansel, 2000; Dimla & Dimla; 2000, Dimov et al, 2004).

- **Laser machining** has been applied to various industrial applications (Meijer et al, 2002) and with its small affected area during machining and the absence of an electrode or cutting tool it is an ideal candidate for the micro machining process. Commercially available laser systems compete successfully with conventional manufacturing methods in a number of applications where the latter methods have reached the limits of their capabilities and lasers can also be easily integrated into CNC machines turning them into flexible and efficient material processing machines.

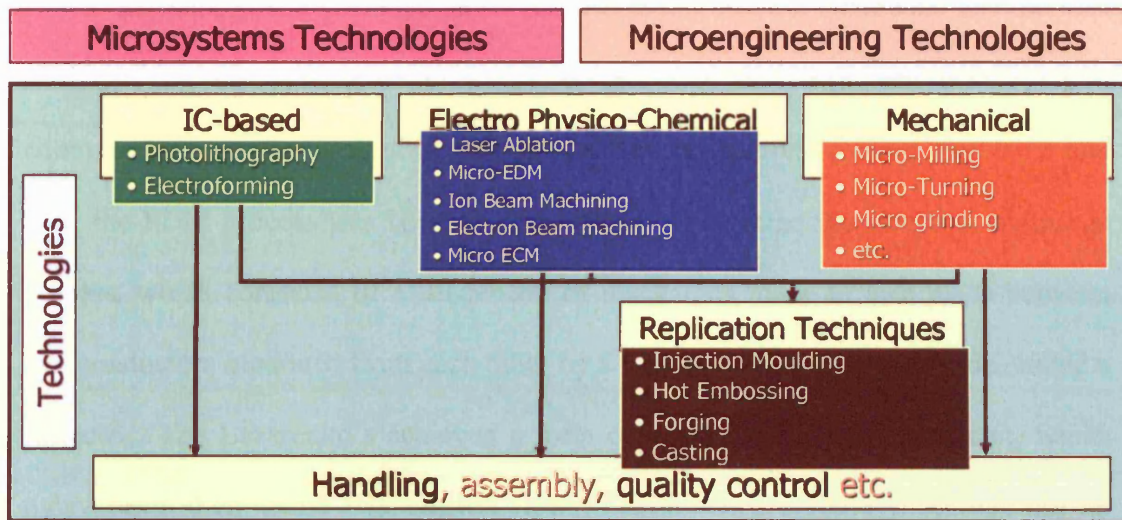
Laser milling processes (Pham et al, 2002) allow complex parts and tooling inserts to be fabricated *directly* from CAD data in a wide range of advanced engineering materials such as ceramics, hardened steel, titanium and nickel alloys (Pham et al, 2001). The type of laser needs to be chosen to suit the material to be machined and there are already different laser sources on the market, with different wavelengths and pulse durations, suitable for incorporation into machine tools for many 2.5D laser machining applications. The mathematical modelling of the process, however, still only covers a few specific cases and the laser ablation phenomena and the dependency of material removal rates, surface finish and surface integrity on wavelength and pulse duration has still have to be studied.

• **Ion Beam Machining (IBM)** is currently considered a *non-conventional* method of machining. In IBM, a stream of charged atoms (ions) of an inert gas, such as argon, is accelerated in a vacuum by high energies and directed toward a solid workpiece. The beam removes atoms from the workpiece by transferring energy and momentum to atoms on the surface of the object, when an atom strikes a cluster of atoms on the workpiece, it dislodges between 0.1 and 10 atoms from the workpiece. Focussed ion beam (FIB) systems are designed to structure nano and micro features in silicon or non-silicon materials by either 3D etching or deposition. Ions extracted from a plasma source, normally liquid gallium, are accelerated and bombard the surface of the processed material sputtering its surface atoms. If special (organic) gases are also applied in the vicinity of the surface the resulting collisions can give rise to the deposition of neutral species (Pt, W, C, Au, etc) on the surface. FIB systems can also be operated in two modes- direct writing and projection modes with the latter considered to be much faster than the former but requiring a mask to be fabricated for *each* new pattern.

• **Photo chemical machining (PCM)** is a general term for a variety of chemical and electrochemical processes which are still widely used in the semiconductor industry. Patterning using photoresist masks has progressed considerably through the development of photo exposure systems for IC. It is possible, via electro chemical reactions, to remove material from the workpiece and/or to deposit material in a predetermined pattern through photoresist etching. Chemical and electrochemical forming has been successfully used for machining large mechanical parts as well as for effective fabrication of small mechanical and electrical parts.

• **Micro EDM** has recently attracted a significant amount of research attention with the availability of new types of power generators capable of releasing very small amounts of energy. The new focus is not only on producing small holes and shafts (Masuzawa et al, 2002, 355-362) but also on developing trajectory micro EDM capable of machining 3 dimensional micro features for micro parts and micro moulds and dies (Yu et al, 1998). The prospect of achieving high aspect ratios (Lim et al, 2003) with good surface integrity is very tempting. However, to reveal the full potential of the micro EDM process more investigations need to be performed. This includes the development of analytical and computer models of the process ( Ho & Newman, 2003), study of electrode wear behaviour (Ozgedik & Cogun, 2006), development of CAM support for trajectory EDM (Dimov et al, 2003, 1633-1637), integration of adaptive control monitoring systems and incorporation of on the machine electrode measuring systems.





Adapted from Altung L., et al., Micro Engineering, Annals of CIRP, Vol. 52, 2003

Figure 2.1 Classification of micro manufacturing technologies

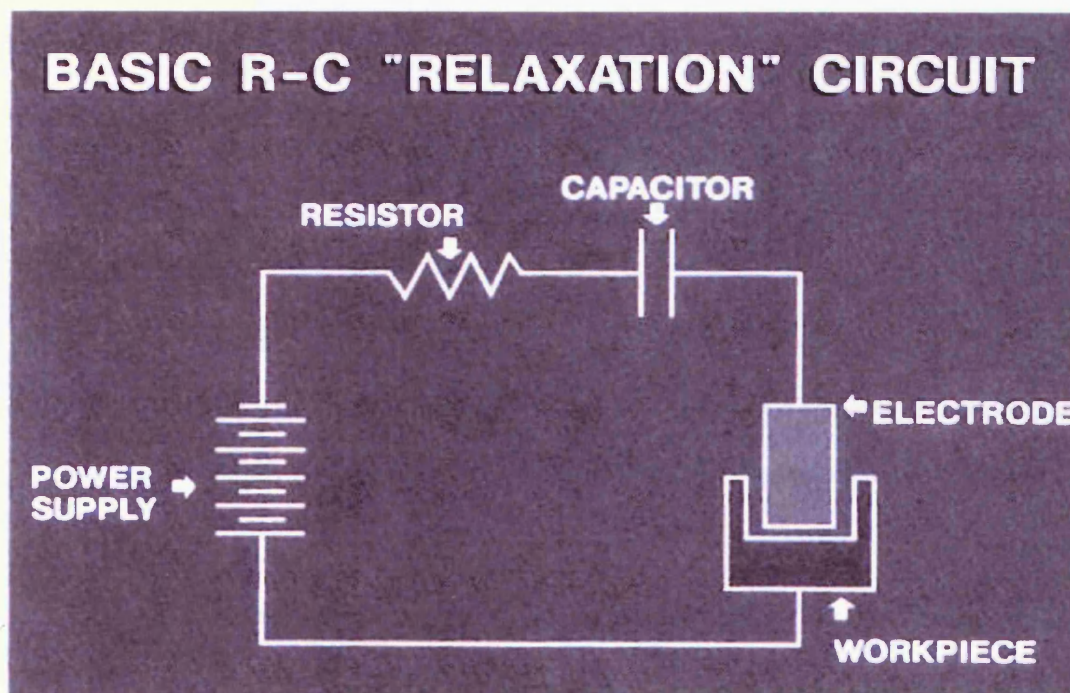


Figure 2.2 The Lazarenkos basic EDM circuit which provided the foundation of the modern EDM industry (Chetverikov et al 1964)

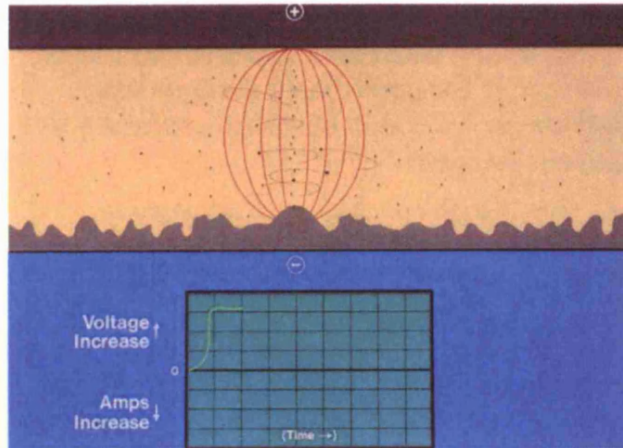
## 2.2. An Overview of the EDM process

In 1943, Soviet scientists Boris Lazarenko and Natalia Lazarenko had the idea of exploiting the destructive effect of an electrical discharge and developing a controlled process for machining materials that are conductors of electricity. With that idea, the EDM process was born. The Lazarenko's perfected the electrical discharge process, which consisted of a succession of discharges made to take place between two conductors separated from each other by a film of non-conducting liquid, called a dielectric. The Lazarenko's achieved a form of immortality with this circuit, which today bears their name (Панайотов, 1989). Today, many EDM machines use an advanced version of the Lazarenko's circuit (Fig.2.2). They also invented a simple servo controller that helped maintain the gap width between the tool and the workpiece. This reduced arcing and made EDM machining more reliable. This was the turning point in the history of the EDM process (Панайотов, 1989).

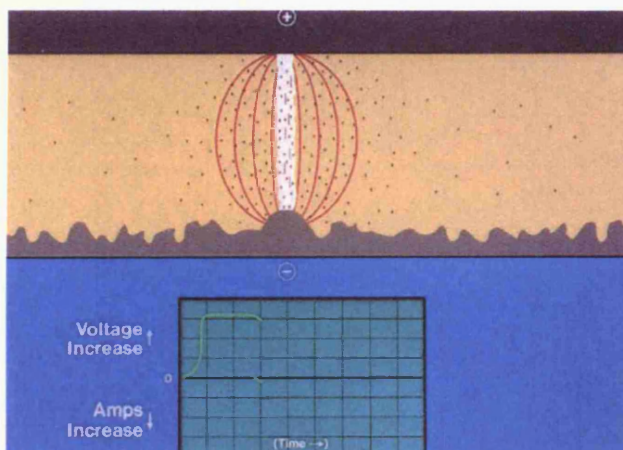
During the EDM process, a series of non-stationary, timed electrical pulses remove material from a workpiece. The electrode and the workpiece are held by the machine tool, which also contains the dielectric (Попилов, 1982). A power supply controls the timing and intensity of the electrical charges and the movement of the electrode in relation to the workpiece. At the spot where the electric field is strongest, a discharge is initiated. Under the effect of this field, electrons and positive free ions are accelerated to high velocities and rapidly form an ionized channel that conducts electricity. At this stage current can flow and the spark forms between the electrode and workpiece, causing a great number of collisions between the particles. During this process a bubble of gas develops and its pressure rises very steadily until a plasma zone is formed. The plasma zone quickly reaches very high temperatures, in the region of 8,000° to 12,000°C, due to the effect of the ever-increasing number of

collisions). This causes instantaneous local melting and vaporization of a certain amount of the material at the surface of the two conductors (Toren et al, 1975). When the current is cut off, the sudden reduction in temperature causes the bubble to implode, which projects the melted material away from the workpiece, leaving a tiny crater. The eroded material then resolidifies in the dielectric in the form of small spheres and is removed by the dielectric. All this without the electrode ever touching the workpiece (Schumacher, 2004). Figure 2.3 gives a detailed illustration and description of the different stages of the process (Панайотов, 1989).

The fact that EDM is a non-contact machining process allows achieving tighter tolerances and better finishes in a wide range of materials that are otherwise difficult or impossible to machine with traditional processes.



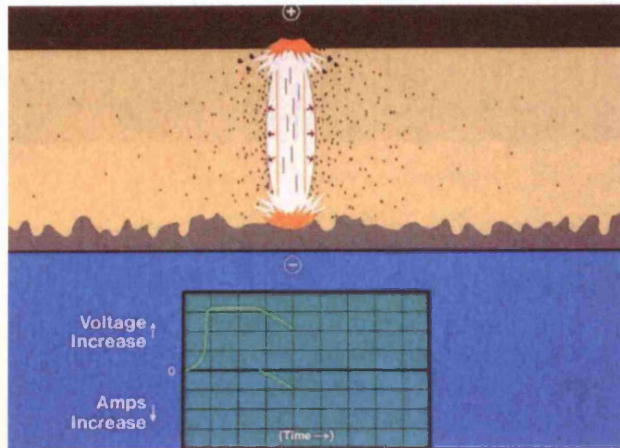
1. As the number of ionic (charged) particles increases, the insulating properties of the dielectric fluid begin to decrease along a narrow channel centered in the strongest part of the field. Voltage has reached its peak, but current is still zero.



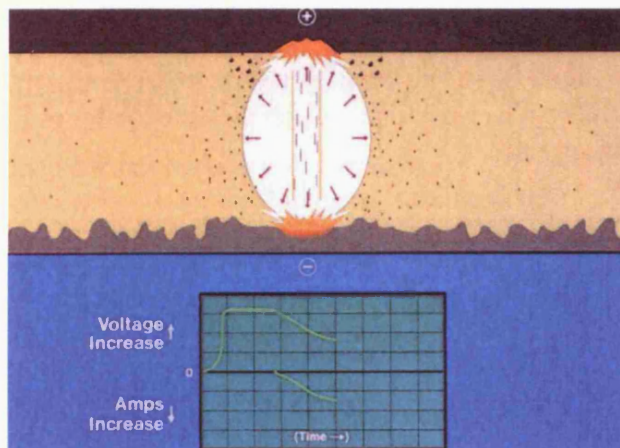
2. A current is established as the fluid becomes less insulating. Voltage begins to decrease.

Figure 2.3 Schematic and explanations of the discharge process stages

(to be continued)



3. Heat builds up rapidly as current increases, and the voltage continues to drop. The heat vaporizes some of the fluid, workpiece, and electrode, and a discharge channel begins to form between the electrode and workpiece.

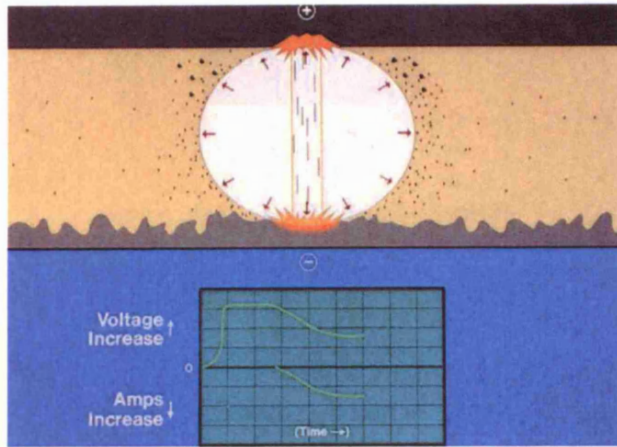


4. A vapour bubble tries to expand outward, but its expansion is limited by a rush of ions towards the discharge channel. These ions are attracted by the extremely intense electro-magnetic field that has built up. Current continues to rise and voltage drops further.

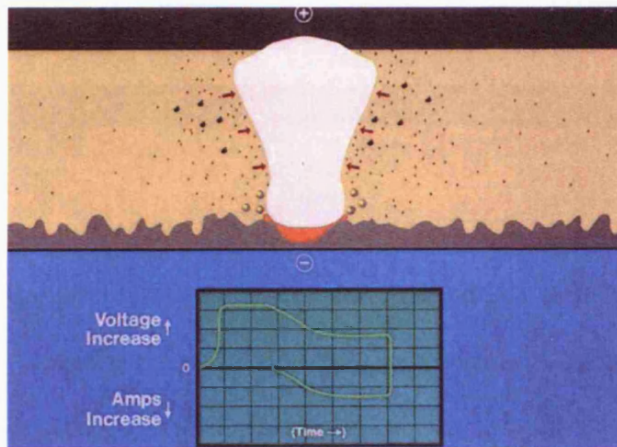
Figure 2.3 Schematic and explanations of the discharge process stages

(to be continued)





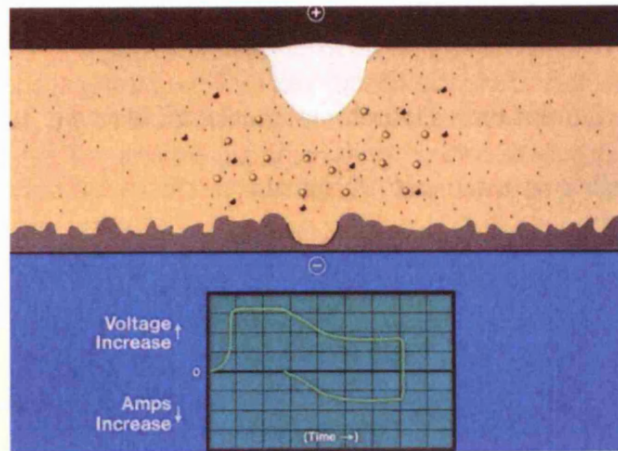
5. Near the end of the on-time, current and voltage have stabilized, heat and pressure within the vapour bubble have reached their maximum, and some metal is being removed. The layer of metal directly under the discharge column is in a molten state, but is held in place by the pressure of the vapour bubble. The discharge channel now consists of a superheated plasma made up of vaporized metal, dielectric oil, and carbon with an intense current passing through it.



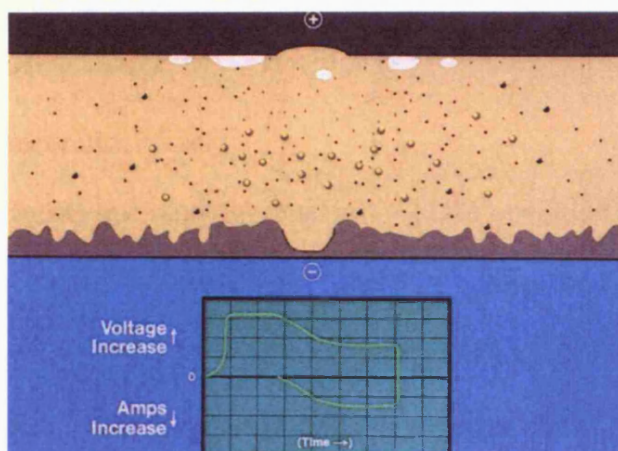
6. At the beginning of the off-time, current and voltage drop to zero. The temperature decreases rapidly, collapsing the vapor bubble and causing the molten metal to be expelled from the workpiece.

Figure 2.3 Schematic and explanations of the discharge process stages

(to be continued)



7. Fresh dielectric fluid rushes in, flushing the debris away and quenching the surface of the workpiece. Unexpelled molten metal solidifies to form what is known as the recast layer.



8. The expelled metal solidifies into small spheres dispersed in the dielectric oil along with bits of carbon from the electrode. The remaining vapor rises to the surface. Without a sufficient off-time, debris would collect causing the spark to be unstable. This situation could create a DC arc which can damage the electrode and the workpiece.

Figure 2.3 Schematic and explanations of the discharge process stages

(continued)

### **2.3. Theories of Material Removal**

The removal of material in electrical discharge machining is based upon the erosion effect of electric sparks occurring between the two electrodes (Fig. 2.3). Several theories have been forwarded in attempts to explain the complex phenomenon of "erosive spark" (Подураев, 1995; Toren et al, 1975).

- **Electro-mechanical theory**

This theory suggests that abrasion of material particles takes place as a result of the concentrated electric field. The theory proposes that the electric field separates the material particles of the workpiece as it exceeds the forces of cohesion in the lattice of the material. This theory neglects any thermal effects. Experimental evidence lacks supports for this theory.

- **Thermo-mechanical theory**

This theory suggests that material removal in EDM operations is attributed to the melting of material caused by "flame jets". These so - called flame jets are formed as a result of various electrical effects of the discharge. However, this theory does not agree with experimental data and fails to give a reasonable explanation of the effect of spark erosion.

- **Thermo-electric theory**

This theory, best-supported by experimental evidence, suggests that metal removal in EDM operations takes place as a result of the generation of extremely high temperature generated by the high intensity of the discharge current. Although well supported, this theory cannot be considered as definite and complete because of difficulties in interpretation.



## 2.4. Growth of the EDM industry

EDM has rapidly earned its place as a proactive, mainstream technology. EDM is best known for its ability to machine complex shapes in very hard and difficult to machine metals. The first and still the most common use of EDM is machining dies, tools and molds made of hardened steel, tungsten carbide, high-speed steel and other workpiece materials (Valentincic et al, 2006; Heeren et al, 1997). The process has also solved a number of problems related to the machining of "exotic" materials such as Hastelloy, Nitralloy, Waspaloy and Nimonic, which are used on a large scale in the aeronautical and aerospace industries. EDM has become an indispensable process in modern manufacturing industry because of its ability to produce complex shapes with high degrees of accuracy practically in any electrically conductive material. With developments in Computer Numerical Control, the versatility of EDM has increase greatly. Techniques like orbital EDM and EDM milling, which are a result of developments in CNC, play a very crucial role in the application field of EDM, particularly in the die and mould making industry (Curodeau et al, 2004). Today's EDM equipment uses advanced Computer Numerical Control, state-of-the-art power supply technology and machine tools with positional accuracies in the range of nanometers (Puertas et al, 2004; (<http://www.smaltec.com/gm703.cfm>)).

Due to the exceptional micro EDM process capabilities especially in the new rapidly developing micro sector the number of institutions engaging in micro EDM research and development has been growing for several years (Fig.2.4). Various Universities and other research institutions are funded mainly by the major EDM machine-builders to develop the process further and to explore the feasibility to machine different materials (including less or even none electrically conductive)

(Heeren et al, 1997) and to determine the limits of the process when micro and nano features are concerned.

Due to the rapidly growing micro and nano market, micro EDM has recently attracted a significant amount of research attention (Fuzhu, et al, 2004). The major focus is on producing trajectory micro EDM capable of machining 3D features and parts with predictable accuracy and timescale in different materials and this way solving many problems of micro moulds and dies. So far compared to the other processes given in figure 2.1, micro EDM is the process which achieves the highest aspect ratio on the features, very good surface integrity (compare to the material removal rate) and accuracy suitable for the micro and nano sector (Lim et al, 2003).

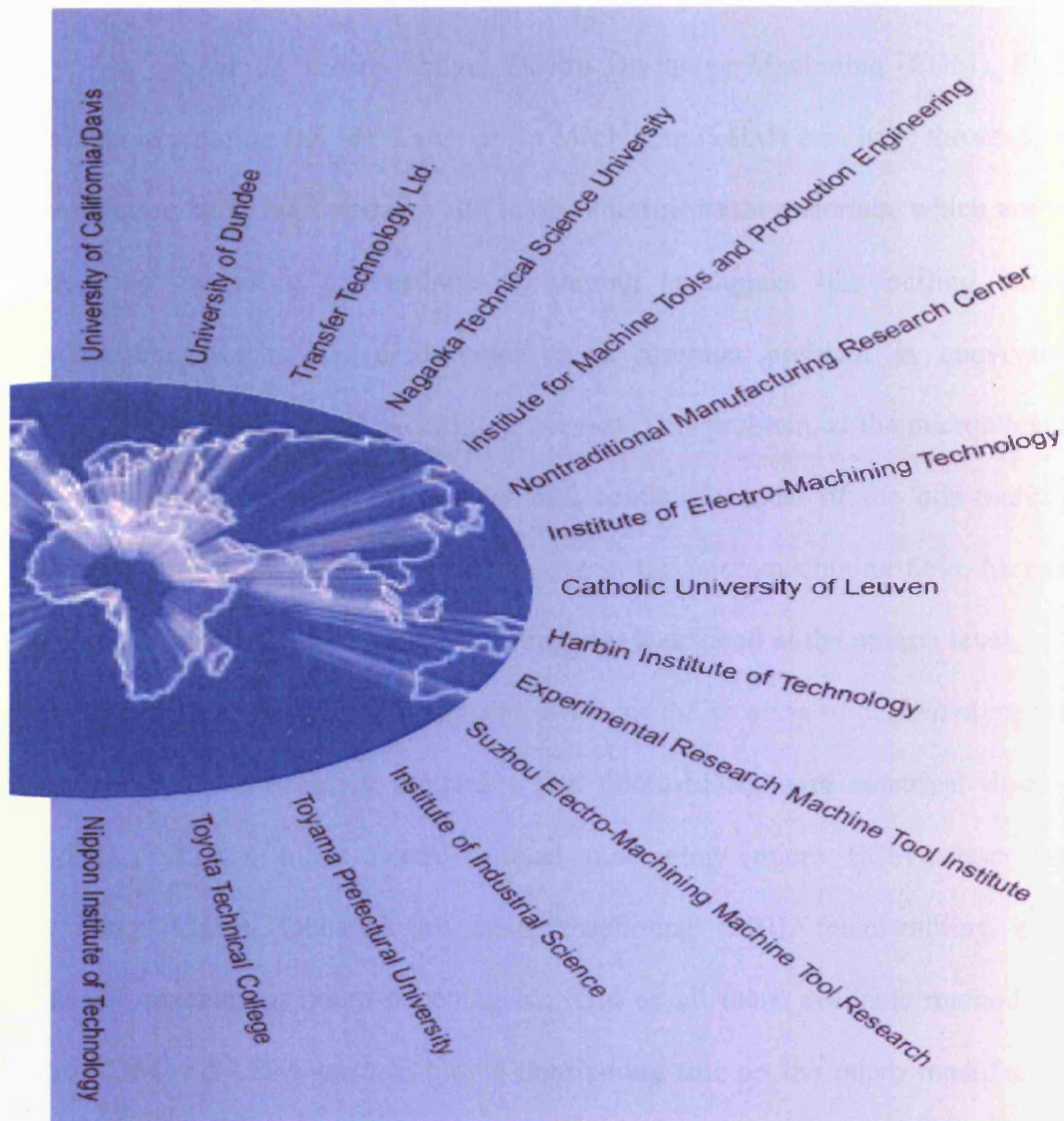


Figure 2.4 Leading institutions and centres for EDM research (Brink, 2006)

## **2.5. EDM as a micro technology - problematic issues**

As mentioned already above, Electro Discharge Machining (EDM), Electro Chemical Machining (ECM), Laser Beam Machining (LBM) etc., have the advantage of machining hard, high strength and temperature resistant materials, which are very difficult to cut using conventional machining techniques like milling, turning, grinding etc. Mechanical deformation is a common problem in conventional mechanical machining such as cutting processes. This problem, at the micron level, is serious. Since there is no mechanical tool contact in most of the non-traditional machining processes, they have a better edge in the micromachining field. Moreover the production of cutting tools like a milling tool is difficult at the micron level.

There is an ongoing development work for the creation of dedicated machine-tools using micromachining methods like micro-EDM, wire electrical discharge grinding (WEDG), micro-electrochemical machining (micro ECM), laser beam machining (LBM), focussed ion beam machining (FIB), micro-milling, micro-ultrasonic machining, micro-punching etc. Out of all these available methods only micro-EDM and LBM seem to play a dominating role on the micro manufacturing processes market which is due to the relation of these processes to the macro world on one side and the already available machine tools on which the new micro process can be tested with small changes in the machine parameters on the other.

It was explained earlier in 2.2, that the EDM process is based on the thermoelectric energy created between a workpiece and an electrode submerged in a dielectric fluid. When the workpiece and the electrode are separated by a specific small gap, the so-called 'spark gap', a pulsed discharge occurs which removes material from the workpiece through melting and evaporation (Toren et al, 1975). The same principle of EDM is applied at the micro level for micromachining. The process

is called micro-EDM. Generally in EDM, the amount of material removed is a function of the energy which crosses the discharge gap (Конрад & Крамлиц, 1990). Higher energy, results in a higher removal rate but a rougher surface because of the crater left behind in the workpiece. In micro-EDM, the key is to limit the energy in the discharge (Egashira et al, 2006). Since small energy is the key point to make micro products with high accuracy and good surface finish, the energy per single discharge should be minimized and discharge frequency should be increased. It is required for micromachining to maintain the energy of a single discharge in the order of  $10^{-6}$ J to  $10^{-7}$ J (Perez et al, 2004).

The numerous developments in micro EDM which have focused on the production of micro features have become possible due to the availability of new CNC systems and advanced spark generators that have helped to improve machined surface quality and process control. Also, the very small process forces very often negligible and fairly good repeatability of the process results have made micro EDM the best means for achieving high-aspect-ratio micro features with the tightest tolerances (Frank, et al, 2005).

Current micro EDM technology used for manufacturing micro features can be categorised into four different types (Pham et al, 2004):

- Micro wire EDM, where a wire of diameter down to 0.02mm is used to cut through a conductive workpiece.
- Die sinking micro EDM, where an electrode with micro features is employed to produce its mirror image in the workpiece.
- Micro EDM drilling, where micro electrodes (of diameters down to 5-10 microns) are used to “drill” micro holes in the workpiece.

- Micro EDM milling, where micro electrodes (of diameters down to 5-10 microns) are employed to produce 3D cavities by adopting a movement strategy similar to that in conventional milling.

Despite the number of publications extolling the improved capabilities of these processes, they are still not very widely used. This is mainly due to the fact that available machine tools and process characteristics are still not sufficiently reliable.

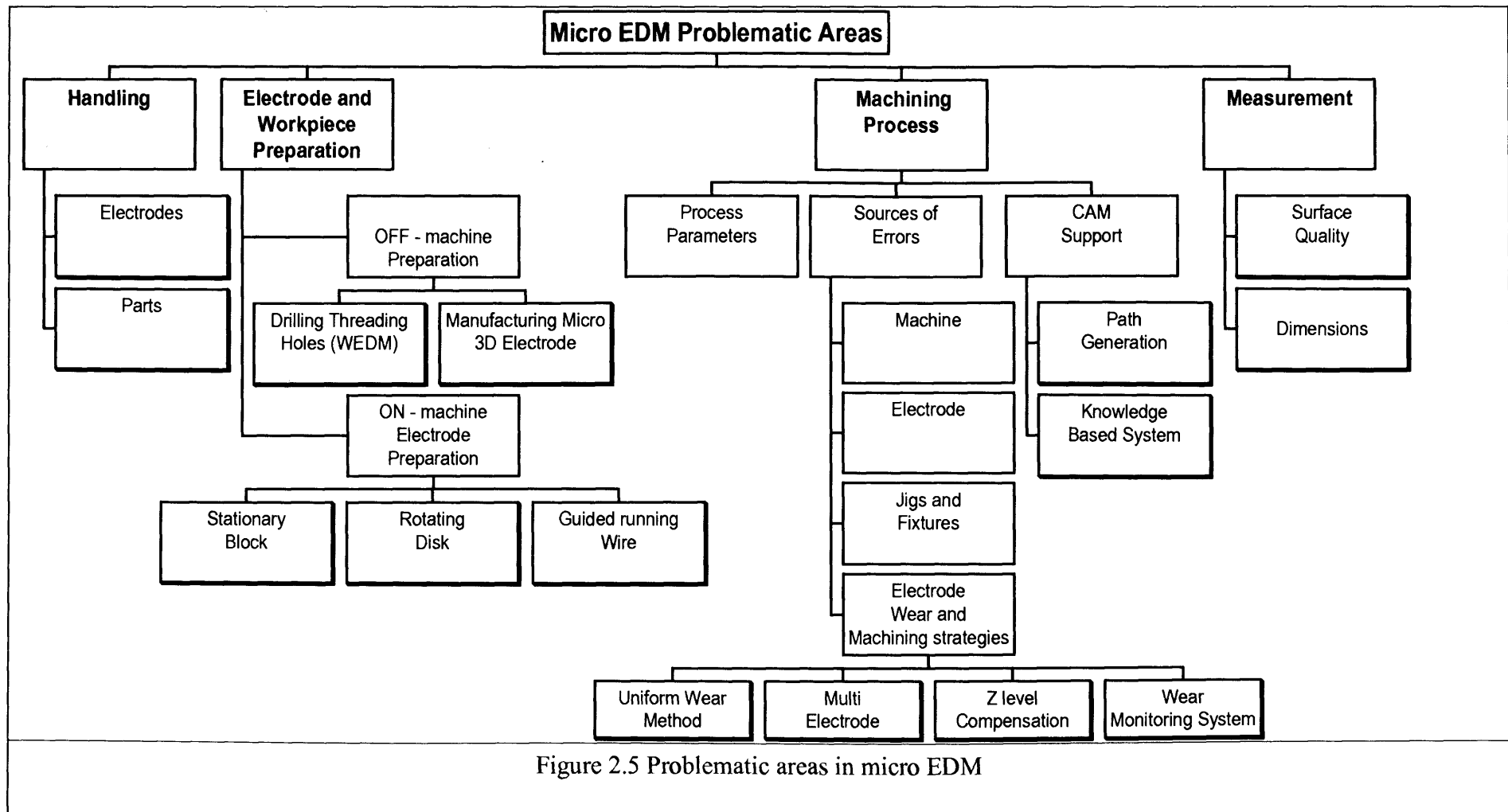


Figure 2.5 Problematic areas in micro EDM

### **2.5.1. MICRO EDM ISSUES**

Miniaturisation of the product requires a new approach to product and process design. This section discusses the above mentioned four types of micro EDM applications and identifies problematic areas with those applications. So far micro EDM has tended to be performed using conventional EDM machines modified to accommodate the micro manufacturing requirements, a number of problems have arisen. Figure 2.5 gives an overall view of the problems related to the use of the EDM process for micro machining.

#### **2.5.1.1. Handling of electrodes and parts**

In wire EDM machines, the trend to reduce the diameter of the wire used has caused many problems with handling electrodes and parts. At first the existing wire machines were adapted to take smaller diameter wires (down to 0.03mm), but this demanded significant time for machine preparation. Initially the distance from the spool position to the threading nozzle was long, and this caused a great deal of inconvenience for the installation of the wire. The existing dynamic forces on the brakes could not be taken easily by the new very thin wire. This resulted in frequent wire breaks, which required manual intervention and a slow process overall. Even on the newly developed micro wire machines, manipulating and handling of wires with diameters as small as 0.02 or 0.03mm can be difficult. When micro parts are manufactured on a wire machine, handling of the parts can also be challenging. Special measures should be considered after the separation cut to avoid losing parts into the tank of the machine.

In micro EDM die sinking, drilling or milling, different techniques and devices can be employed to help handling and manipulating small electrodes and parts. For



instance, the electrodes mainly used for EDM drilling and milling are W (tungsten) or WC (tungsten carbide) rods or tubes, of diameters within the range 0.1-0.4mm, and their handling is difficult as they can be easily damaged. Therefore, sub-systems are incorporated into micro EDM machines for on-the-machine manufacture and holding of the required micro electrodes. The most common subsystems are ceramic guides and dressing units such as Wire Electro Discharge Grinders (WEDG) (2.6) (Rees et al, 2007).

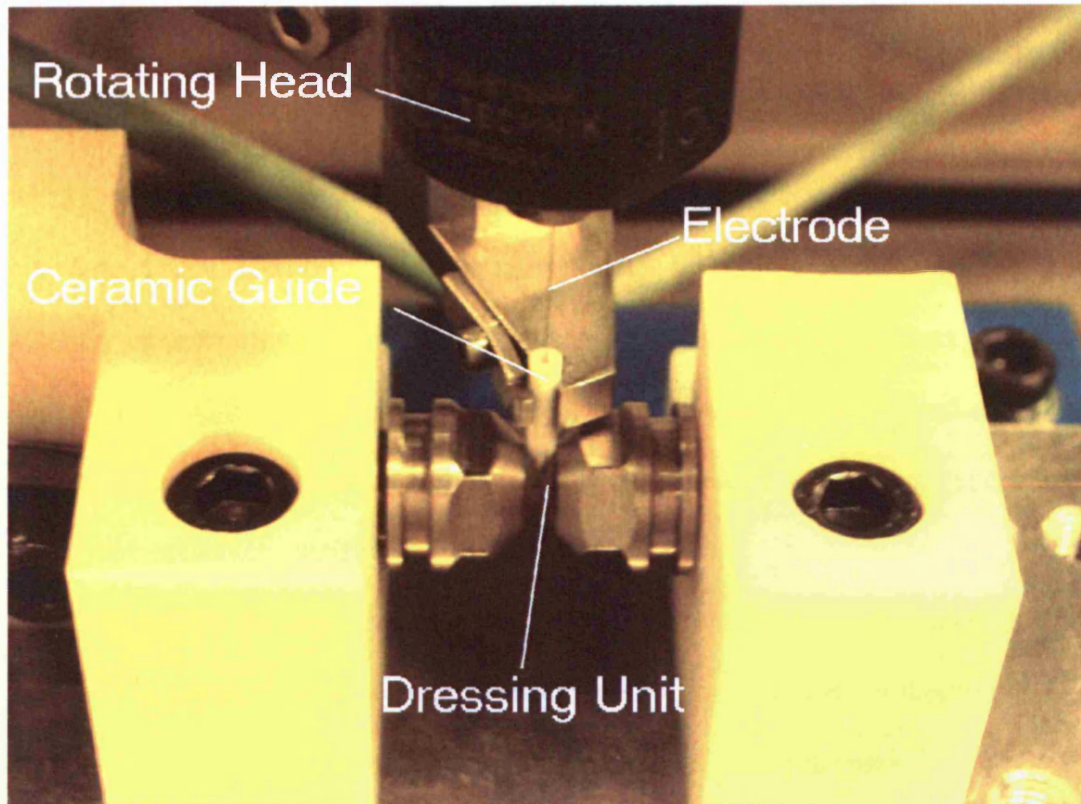


Figure 2.6 Dressing unit and ceramic guiding system

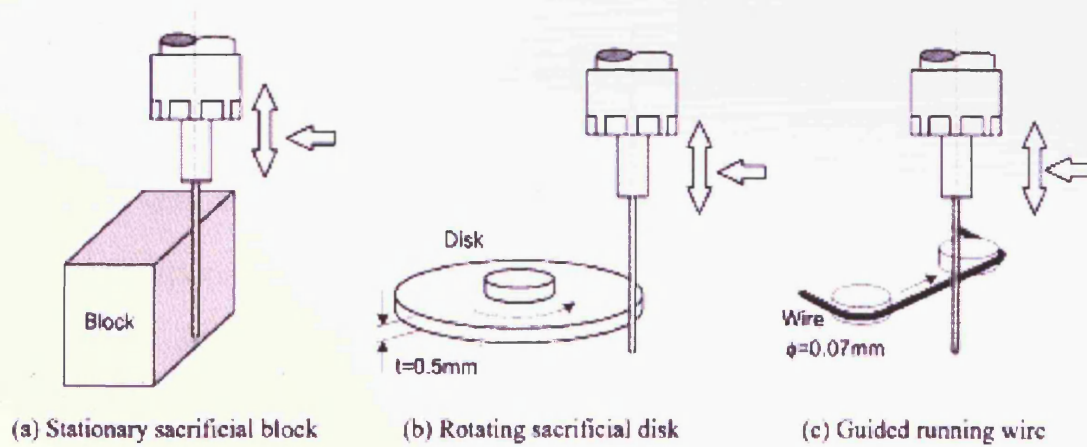


Figure 1.7 Three types of electrode grinding devices

### **2.5.1.2. Electrode and workpiece preparation**

With micro wire EDM, the main issues in workpiece preparation relate to the production of small holes used for threading the wire into the workpiece. Depending on the profile to be machined, these holes could have micro diameters with a very high aspect ratio. Usually they are produced either by drilling or EDM drilling. The accuracy of positioning of the hole(s) with respect to the measuring point should be high. This is to ease the automatic threading procedure and to avoid short-circuiting after threading, although automatic threading through such holes, even on specialised micro wire machines, is difficult.

When die sinking of micro features is required, one or more electrodes are produced in advance usually either by micro milling or by EDM. In this case micro features machined onto the electrode should be offset with the spark gap. Thus the feature size is further diminished which may cause distortion of the form, even making the geometry impossible. Production of such 3D profile electrodes is costly and time consuming.

Trajectory EDM (EDM milling) uses a simple shaped electrode, rod or tube of diameter between 0.1– 0.4mm. The electrode can be EDM ground if a smaller diameter is required. As mentioned previously, to avoid handling difficulties and error stack-up when the electrode is manufactured externally to the EDM machine, additional devices are used to prepare the electrode on the machine. The working electrode is eroded against a sacrificial electrode in an operation known as EDM grinding. Three different types of sacrificial electrodes are used (Figure 1.7). A problem is that the shape, dimension and roughness of the ground electrode is not easy to control (Lim et al, 2003).

### **2.5.1.3. The micro EDM process**

Process planning for micro EDM should be considered very carefully, as feature sizes are very small and so are the tolerances of the machined surfaces. During the preparation stage and the machining process itself, a number of errors occur which may lead to disappointing results. These errors are due to equipment imperfection on the one hand and the stochastic nature of the sparking process on the other.

Many papers target ways of optimising EDM performance measures like the material removal rate (MRR) (Wong et al, 2003), tool wear rate (TWR) (Ozgedik & Cogun, 2006) and surface quality (SQ) ( Ho & Newman, 2003). Process parameters for micro EDM are still at the development stage and their effects on performance measures have yet to be clarified. Because of the stochastic thermal nature of the micro EDM process, it is difficult to explain all of those effects fully. The optimisation of parameters is based on process analysis to reveal the influence of each process variable on the desired machining characteristic ( Ho & Newman, 2003). The lack of information in this field is the main reason for the inability to develop knowledge-based systems to help the planning of micro EDM operations.

Despite the use of advanced CNC controllers and the high degree of automation of EDM machines, there is still a lack of CAM tools to support micro EDM. One of the main reasons for the limited application of micro EDM milling to the machining of complex 3D cavities is the difficulty of generating tool paths using existing CAM systems. In particular, those systems do not permit electrode wear compensation, nor support variation of the slice thickness or allow the direction of cut to vary with each slice. Attempts to address these issues have been reported (Dimov et al, 2003).

Electrode wear is not a major problem for micro wire EDM, apart from the fact that a high rate of wear might cause more frequent wire breaks. This is due to the fact

that wear reduces the cross section of the micro wire and therefore the maximum tension the wire can take drops significantly.

Electrode wear becomes an important issue when employing electrodes with micro-features in die sinking as the combination of micro features and macro features on one electrode will introduce different wear ratios. The sparking area will change as the electrode moves down, which will bring different sparking conditions during the process and will reduce the quality of the machined part.

In micro EDM drilling, there are problems with the electrode wear when producing blind holes because wear constantly reduces the length of the electrode. As a result, when eroding down to a fixed depth, the real depth of the hole will be significantly smaller.

A method to achieve a specific depth in this case is to compensate for wear of the electrode by constant electrode feeding in the Z axis (Bleys et al 2002). This method requires an accurate model for estimating the volumetric wear ratio (the ratio of electrode wear and workpiece wear). Certain factors affecting the wear ratio are difficult to assess and control, like flushing conditions in a deep hole for instance. This could easily result in wrong estimation of the wear ratio and therefore in errors in the produced depth. One solution is to repeat the process a number of times with new or reground microelectrodes until the required depth is obtained. This is called the multiple electrode strategy. The main drawback is that it can be time consuming and difficult to predict the number of needed electrodes.

The problems created by electrode wear become more complicated when machining complex 3D micro cavities. Either wear is too severe to allow the use of complex-shape electrodes in a classical die-sinking process or electrode geometry is impossible. Thus, for the production of micro 3D cavities, the use of micro EDM

milling with simple shape-electrodes might be the preferred strategy. In this case a basic method is to use a layer-by-layer machining strategy that compensates for wear during the machining of each layer by constant electrode feeding in the Z-axis, based on estimation of the wear ratio. Some authors assumed that eroding of sufficiently thin layers would ensure that wear only occurs on the face of the electrode but not on the sides (Yu et al, 1998). Very accurate estimation of the amount of wear is required, because an error in the estimation would have a cumulative effect through the layers. However, even when using a very small layer thickness, side wear is not negligible and introduces errors in the machined profile.

In the Uniform Wear Method (UWM) (Yu et al, 1998; Yu et al, 1998, 7-12), the tool (electrode) path is specially designed to ensure that after the machining of each layer the original shape of the electrode is restored. This is done using a combination of carefully designed overlapping tool paths and very small layer thickness (0.5 to 10  $\mu\text{m}$ ). The use of thin layers results in good flushing conditions, a more stable erosion process and therefore more predictable wear.

According to Yu (Yu et al, 2003), UWM involves a time consuming empirical approach for selecting tool paths. The design of these tool paths derives from the values of the cross section area of the electrode, the area of the layer surface, the depth of cut and the volumetric wear ratio which are assumed to be constant. Any variation in one of these values could introduce discrepancies in the machined layer, and would affect the values of the parameters for the next layers.

As the sparking conditions and therefore the volumetric wear might not be constant during the erosion process, another type of compensation method has been proposed, which is based on the monitoring of the sparking conditions during the process in order to estimate wear on-line using a mathematical model of the sparking

efficiency. Such a method has been considered for conventional EDM (Dauw, 2002; Bleys et al 2002). However, because of the accuracy required, its development in micro EDM is still at a very early stage. A sufficiently accurate mathematical model representing the sparking phenomenon is yet to be found (Schumacher, 2004).

The main problem with previously presented wear compensation methods is that they rely highly on the accuracy of the wear estimation models they employ. Thus, with these methods under-estimation of the amount of wear could easily result in overcutting of the cavity. Many researchers have focused on the difficult problem of wear estimation (Yu et al, 2003; Mohri et al, 1995) but the accuracy of the proposed models still needs to be verified for use in micro EDM milling.

With improvements in wear estimation models, further developments in compensation methods may be expected. They are likely to focus on hybrid compensation approaches, where for instance UWM could be first used, ensuring no overcutting, and then a multiple electrode strategy would accurately finish the profile. The accuracy and reliability of these processes should be carefully assessed if they are to be applied industrially.

#### **2.5.1.4. Measurements**

Measuring the dimensions or the surface quality of micro features is not an easy task. There are not even standardised methods of determining the surface roughness, which is one of the most important characteristics especially for micro tooling. Estimation of the recast layer and heat-affected zone, which affect the properties of the machined surface, requires specialised equipment (Ayers & Moore, 1984).

On-the-machine measurement of electrode and feature dimensions is necessary to achieve good accuracy in micro EDM suitable for the achieved tolerances. This is because after a part that has been taken out of the machine for measurement and later

it is reinstated for more machining, the resetting error will drastically affect the final accuracy of the machined features. Work on on-line feature and electrode measurement has already been reported (Lim et al, 2003).

## **2.6. Surface integrity and process characterisation research in micro EDM**

The surface integrity is becoming more and more important to satisfy the increasing demands of sophisticated component performance, longevity, and reliability. Surface integrity is defined as the inherent or enhanced condition of a surface produced in a machining or other surface generating operation. The nature of the surface layer has been found in many cases to have a strong influence on the mechanical properties of the part. This association is more pronounced in some materials and under certain machining operations (CNMR, 2005).

As it is mentioned above in EDM process, in general, there is no direct physical contact between the electrodes and therefore no direct mechanical forces are exchanged between the workpiece and the tool (except the force caused by the explosion of a small vapour bubble). Therefore, the process has the capability of machining any electrically conductive material regardless of its mechanical properties (Abdullah, 1989). Several researchers reported studies on surface integrity of difficult to machine materials by the EDM process (Abdullah, 1989; Lee & Li, 2001). Zolotykh and Korobova (Zolotykh & Korobova, 1964) studied the magnitude of the defective layer due to the pulse duration and pulse energy of the spark. As an outcome, they pointed out optimum operating conditions in regards to the size of the defective layer produced by the process. Chetverikov and Foteev (Chetverikov & Foteev, 1964) showed that the Material Removal Rate (MRR) and average size of the side-sparking gap between the workpiece and the tool electrode increases with an



increasing Cobalt content when machining WC-Co composite. Gadalla and Tsai (Gadalla & Tsai, 1989) reported that again the cutting rate of WC-Co composites, using a wire EDM process, increases with the increase of cobalt content and WC grain size. Lenz (Lenz, et al, 1975) concluded that when machining WC-Co by using EDM, the number and size of cracks decreases with the increase of cobalt content and WC grains size. Verkhovurov (Verkhovurov, et al, 1983) pointed out that ED Machining of composites promotes a selective removal of the lower melting point material leading to inter-granular fracture along the phase boundaries. Lee and Li (Lee & Li, 2001), investigated the influence of EDM machining parameters on the material removal rate (MRR) and surface integrity of the workpiece. They reported that, the MRR increases with the increase of discharge current and pulse duration. There is a clear defective layer on the machined surface and the number and size of micro cracks increases with the increase of the current and pulse duration. In addition, it was also reported that there is no significant difference between the hardness of the machined surface and base material.

Whenever the EDM or micro EDM process is employed in machining of advanced materials, much attention should be paid to the machined surface characteristics as it may alter completely the mechanical properties and fatigue life of the basic material. The types of surface alterations are associated with: generation of hard recast superficial layer, recrystallization, phase transformations, intergranular attack, preferential removal of low melting point materials and micro-constituents, joining of high melting point contents, residual stress creation, hardening and brittling of the surface layer and as a result micro and macro cracking of the surface (CNMR, 2005; Abdullah, 1989). Due to these deficiencies and poor surface integrity, macro EDM has been avoided by aerospace industry for a long time.

Removing or diminishing the effect of the above layers or zones can be achieved either by careful balancing of the discharge energy and selection of electrode and workpiece material in the micro EDM process. Any additional processes aiming to improve the surface integrity are supplementary and will increase manufacturing cost and time and very often are not applicable when micro features are involved. Since these operations are very expensive or impossible to apply for micro manufacturing, it is advisable to overcome the difficulties by employing new hybrid machining methods, among which ultrasonic assisted EDM claims its share.

Much work is reported in ultrasonic assisted EDM and micro EDM of steel and some ceramics and composites (Kremer, et al, 1989; Lin et al, 2000). Kremer (Kremer, et al, 1989) reported that ultrasonic vibrations significantly improve the discharge efficiency, in machining of alloy steel with a graphite electrode. Murthy (Murthy & Philip, 1987) showed that ultrasonic assisted machining of steel significantly reduces inactive pulses in the process. Zhixin (Zhixin, 1997) reported increase of MRR when machining advanced ceramics, by ultrasonic assisted EDM. Lin and Yan (Lin et al, 2000) showed higher MRR and elimination of the recast layer using the same method.

## **2.7. Micro EDM- process improvement and open research issues**

In electrical discharge machining the reduction of the discharge energy during each breakdown of the dielectric liquid is a necessary condition for such a process to be considered a micromachining technology according Masuzawa and Tsai (Masuzawa, 2000; Tsai & Wang, 2001). In such working conditions providing low discharge energy, the ratio of the volume removed from the tool electrode to the volume removed from the work piece electrode, also known as volumetric wear ratio

( $V$ ), increases significantly. This is shown by Dibitonto, Patel and Eubank (DiBitonto et al, 1989; Patel et al, 1989; Eubank et al, 1993) via experimental data for a copper-made anode tool and steel-made cathode work piece. The range of data for low discharge energies, although still large for micro EDM operations, has been conveniently rearranged and wear ratio values have been also derived.

Moreover, in manufacturing micro through-holes with cylindrical electrodes and with constant low discharge energy settings, there is experimental evidence that the smaller the electrode diameter is, the larger the volumetric wear ratio becomes (Tsai & Masuzawa, 2003). In that sense the main consequence of a high volumetric wear ratio according Yu (Yu et al, 1998) is a quick change in the shape of the tool electrode. Several authors have proposed different techniques aiming to overcome the accuracy problems caused by the rapidly changing shape of the tool electrode during the micro electric die-sinking discharge machining of complex 3D cavities (Yu et al, 1998; Yu et al, 2003; Pham et al, 2004). However, these techniques, apart from the method presented by Pham (Pham et al, 2004), have relied on an a priori perfect knowledge of the volumetric wear ratio, which has been considered a deterministic constant quantity. Therefore, in order for those approaches to represent viable methods, a measurement procedure of the micro volumes removed from the tool and from the workpiece is needed. Pham (Pham et al, 2004) pointed out the need of more accurate measurement procedures for the volumetric wear ratio. In particular, these procedures should address the issue of estimating not only the reduction in length of the tool electrode, but also the changes in the shape of the tool electrode that has occurred during machining.

Tsai and Masuzawa (Tsai & Masuzawa, 2003) introduced a method for assessing the micro volumes removed from rotating cylindrical tool electrodes and

from workpiece electrodes in machining micro through-holes, which is needed to calculate the volumetric wear ratio. On the tool electrode, the removed micro volume was divided in two parts, corresponding to the reduction in the tool length and to the corner rounding. This approach was based on three different instruments. Firstly, an optical microscope with a resolution of  $0.1 \mu\text{m}$  was used for measuring the original diameter of the tool electrode. Secondly, the electrical contact system of the EDM machine used for measuring the difference in the end of tool position before and after machining. Thus, it was utilised to estimate the reduction in length of the tool electrode. Additionally scanning electron microscope (SEM) pictures were used to estimate the micro volume removed from the corner of the tool electrode. In particular, this volume was evaluated on the basis of an interpolating polynomial function passing through two points of the rounded corner in the SEM picture of the tool longitudinal profile. The micro volume removed from the work piece electrode was estimated by considering the micro through-hole as a conical frustum with height equal to the thickness of the workpiece. Nevertheless, no further details are provided on how the radii of the frustum were measured.

## **2.8 Summary**

In the first section of this chapter, a review of the main micro technologies was given and the place of the micro EDM described. An overview of the EDM and micro EDM process was given and advantages and disadvantages are explained together with the most popular hypothesis of material removal.

Further the growth of the EDM and micro EDM industry was described which was based on the key advantages of the process. The focus was then moved towards the problematic issues of the micro EDM process. These include the handling of small

parts or electrodes, workpiece preparation and setting, uncertainties in the process itself, and the measurement of small parts, electrodes and process parameters.

The practical need for a more accurate method of measuring micro volumes and the volumetric wear ratio in micro EDM was highlighted. Methods and equipment for measuring the electrode (tool) and features on the workpiece dimensions on the machine are urgently required.

The present world-wide process characterisation research in the area of micro EDM was described. This research mainly concerns surface integrity of the machined surface and machinability of different conductive materials including the use of hybrid methods of machining.

In addition, some particularly critical aspects of the micro EDM process and open research issues were highlighted. It was shown that the definition of micro EDM remains vague, whether the term is used to describe reduced size of electrode or features machined, or is related to specific process characteristics of the discharge. This results in uncertainty about the micro EDM process boundaries and application and even more the lack of information regarding the change of process mechanisms when the sparking conditions change severely.

The best way to escape your problem is to solve it

# *Chapter 3*

### **3. Accuracy requirements for micro EDM process**

As stated in chapter 2 micro EDM has proved to be an efficient technology for the machining of micro features ( Ho & Newman, 2003; Ehrfeld et al, 1996). Different techniques and different devices can be employed to help in handling and manipulating small electrodes and parts. On the machine dressing of the electrode is already considered as a standard feature for micro EDM but different approaches of electrode grinding can affect the final achievable accuracy (Rees et al, 2007).

This chapter investigates the influence of various factors on the final accuracy in micro EDM process. Although not all errors affecting the accuracy are described, the main factors affecting the size and the position of the machined features are discussed and appropriate techniques for minimising the effect of the errors are proposed.

This chapter also analyses the technological capabilities of different setting and dressing techniques used for on-the-machine fabrication of microelectrodes. The major sources of machining errors are identified and solutions are proposed to improve the accuracy and repeatability of the micro EDM process. The physical limitations of the process are also targeted. Experiments are conducted to confirm the theoretical findings.

#### **3.1. Process specifics**

The electrodes usually employed for micro EDM are made of tungsten (W) or tungsten –carbide (WC) rods or tubes, with a diameter of 0.1mm to 0.9mm, and 150 mm to 300mm long. Most often one end of the electrode is clamped in a high-speed spindle and the other end goes through a fixed ceramic guide positioned a few millimetres above the job (Figure 3.1). Rotating the electrode has proven to be more

successful for achieving bigger aspect ratios and a better surface finish due to the fact that a rotating electrode helps easier to remove the debris from the working zone and makes final roughness more independent on the initial roughness of the electrode. During the EDM process, the electrode wears and this can be compensated for with additional movement in the Z direction, while the ceramic guide remains at the same fixed position. When an electrode diameter, smaller than the smallest rod available (usually 0.1 mm) is needed, the electrode protruding out of the ceramic guide can be EDM 'ground' on the machine using either a WC block (Ravi & Chuan, 2002), or using a spinning WC wheel or a special wire grinding device (Masuzawa, et al, 1985; Lim et al, 2003).

## **3.2. Accumulation of errors**

### **3.2.1. Process Definition**

The aim of this chapter is to investigate the possible accuracy and accuracy requirements of the micro EDM process. As an example, micro EDM drilling of a small hole in a block of material, using single pass machining and a single dressed electrode is used (Figure 3.2).

The main dimensions achieved are (Figure 3.3):

**H** – diameter of the hole

**X<sub>H</sub>** and **Y<sub>H</sub>** – position of the hole in respect to the co-ordinate system.



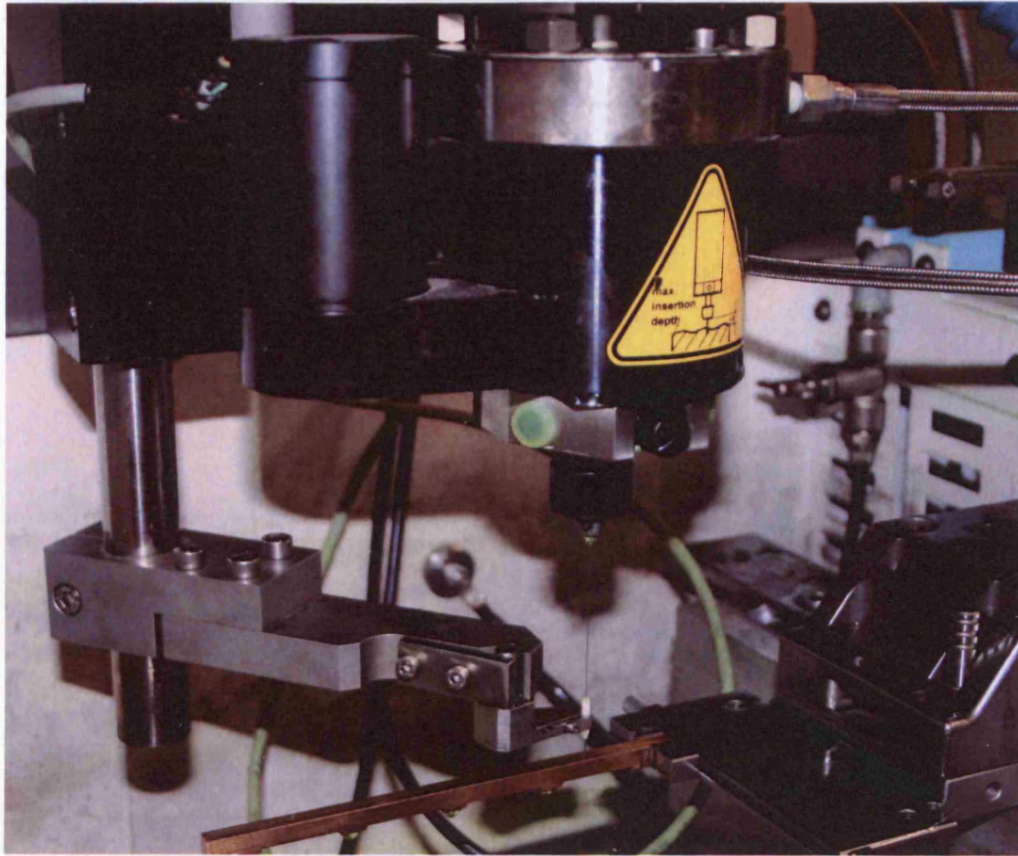


Figure 3.1 Example of micro EDM equipment and its elements

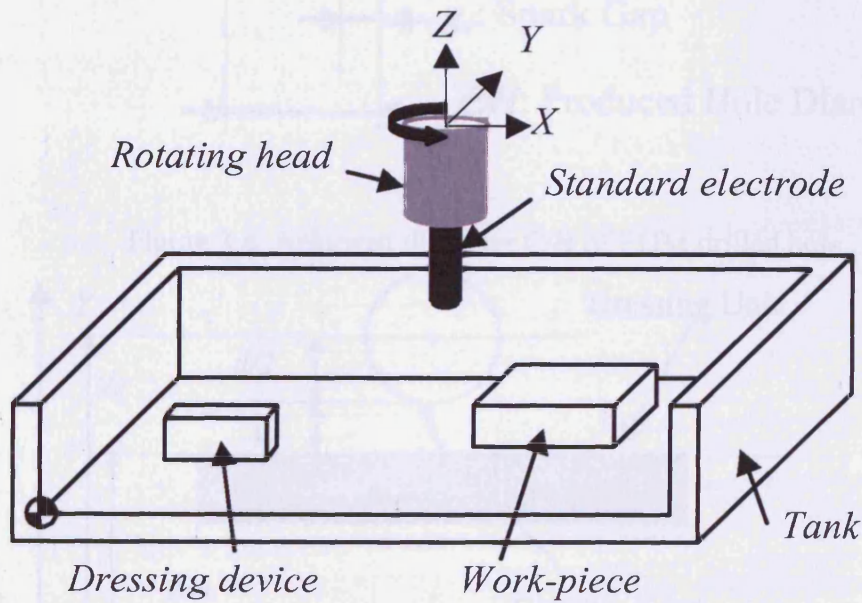


Figure 3.2 Example of micro EDM machining elements

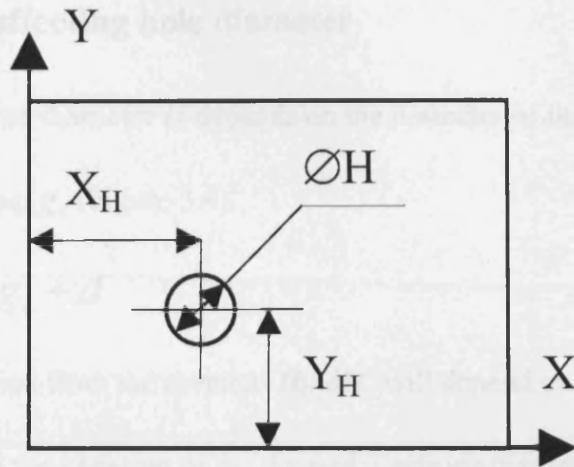


Figure 3.3 Example of achieved dimensions when machining a single hole

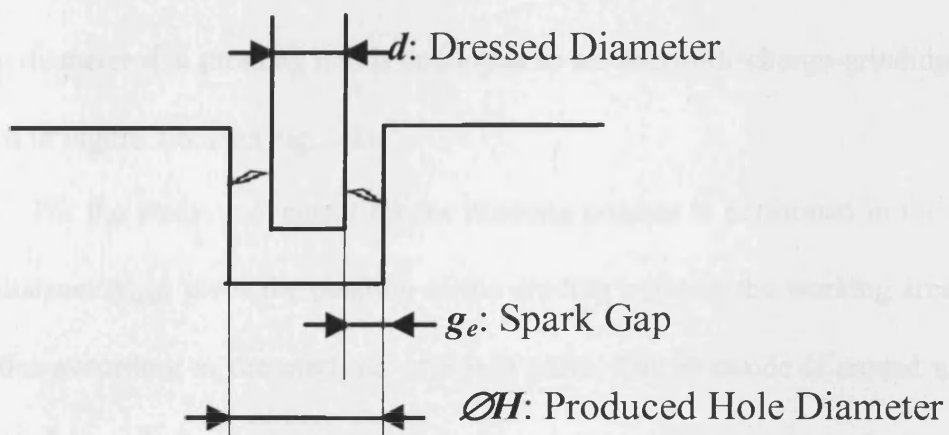


Figure 3.4 Achieved diameter  $\text{Ø}H$  of EDM drilled hole

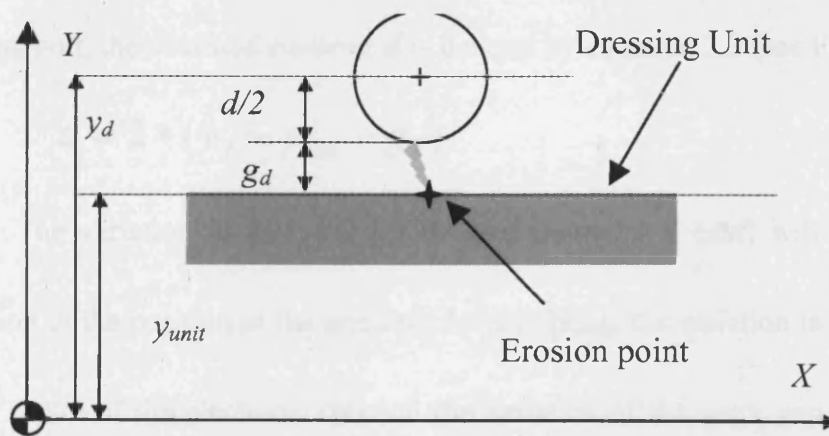


Figure 3.5 Schematic of micro EDM dressing process

### 3.2.2. Factors affecting hole diameter

The achieved diameter  $H$  depends on the diameter of the dressed electrode  $d$  and on the spark gap  $g_e$  (Figure 3.4).

$$H = 2 \cdot g_e + d \quad (3.1)$$

The deviation from the nominal  $H$  ( $\Delta H$ ) will depend on the variation of the spark gap  $\Delta g_e$  and the variation of the dressed electrode diameter  $\Delta d$ .

$$\Delta H = 2 * \Delta g_e + \Delta d \quad (3.2)$$

In order to reduce the initial diameter of the tungsten carbide rod  $D$  down to a micro diameter  $d$ , a dressing unit is employed as an electro-discharge-grinding unit as shown in Figure 2.6. (see Fig. 3.5).

For the study, movement for the dressing process is performed in the Y axis. The distance  $y_{unit}$  gives the position of the eroding point in the working area of the machine according to the machine reference point. The electrode is eroded until the centre of the spindle reaches a target position  $y_d$  resulting in a dressed electrode of diameter  $d$ . Taking into account the spark gap  $g_d$  between the electrode and the dressing unit, the obtained diameter  $d$  is defined by equation 3.3 (see Fig. 3.5).

$$d = 2 * (y_d - y_{unit} - g_d) \quad (3.3)$$

The variation in the effective dressed diameter  $d$  ( $\Delta d$ ) will depend on the deviation in the position of the grinding device  $\Delta y_{unit}$ , the variation in the positioning of the centre of the electrode  $\Delta y_d$  and the variation of the spark gap when grinding  $\Delta g_d$ .

$$\Delta d = 2 * (\Delta y_d + \Delta y_{unit} + \Delta g_d) \quad (3.4)$$

Finally the variation in the hole diameter drilled by a single dressed electrode will be determined by equation 3.6:

$$H = 2 \cdot (g_e + y_d - y_{unit} - g_d) \quad (3.5)$$

$$\Delta H = 2 \cdot (\Delta g_e + \Delta y_d + \Delta y_{unit} + \Delta g_d) \quad (3.6)$$

### 3.2.3. Factors affecting the position of the hole

The position of the hole is described by the following equations directly derived from Figure 3.6.

$$X_H = X_{pos} - X_{set} \quad (3.7)$$

$$Y_H = Y_{pos} - Y_{set} \quad (3.8)$$

In order to set up the workpiece position in the work area, an electrode of nominal effective diameter ( $D$ ) is employed. It should be noted that the use of probes or other setting devices has been ruled out as more errors would be introduced into the system because this would require reattachment of the high speed spindle and readjusting of the ceramic guide. The setting process is represented in Figure 3.7.

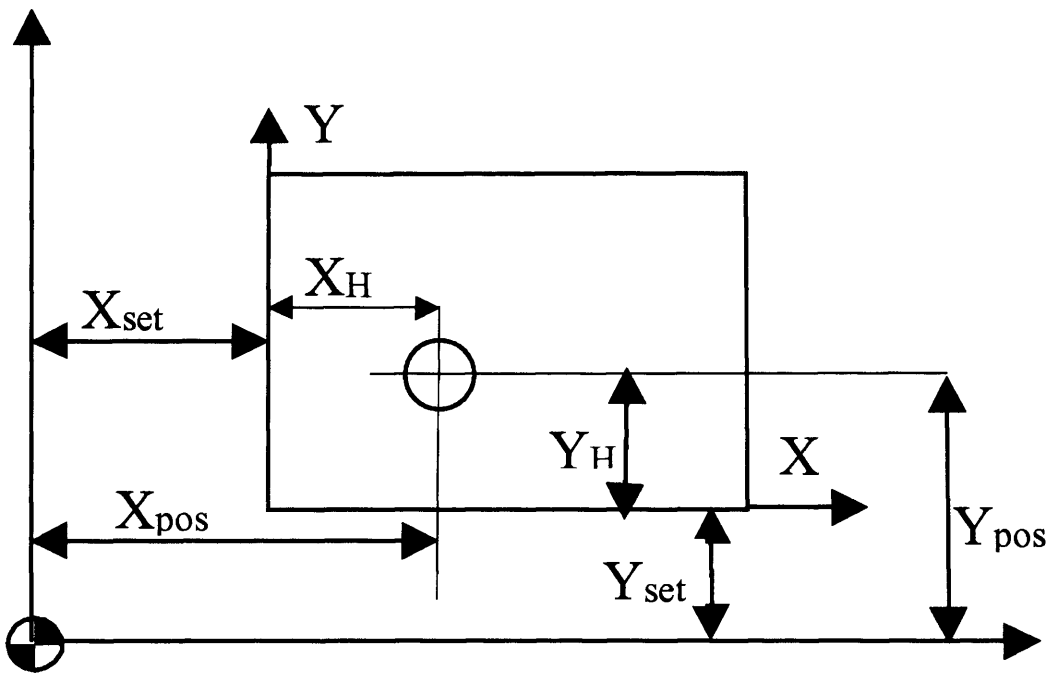


Figure 3.6 Dimensions affecting the hole position

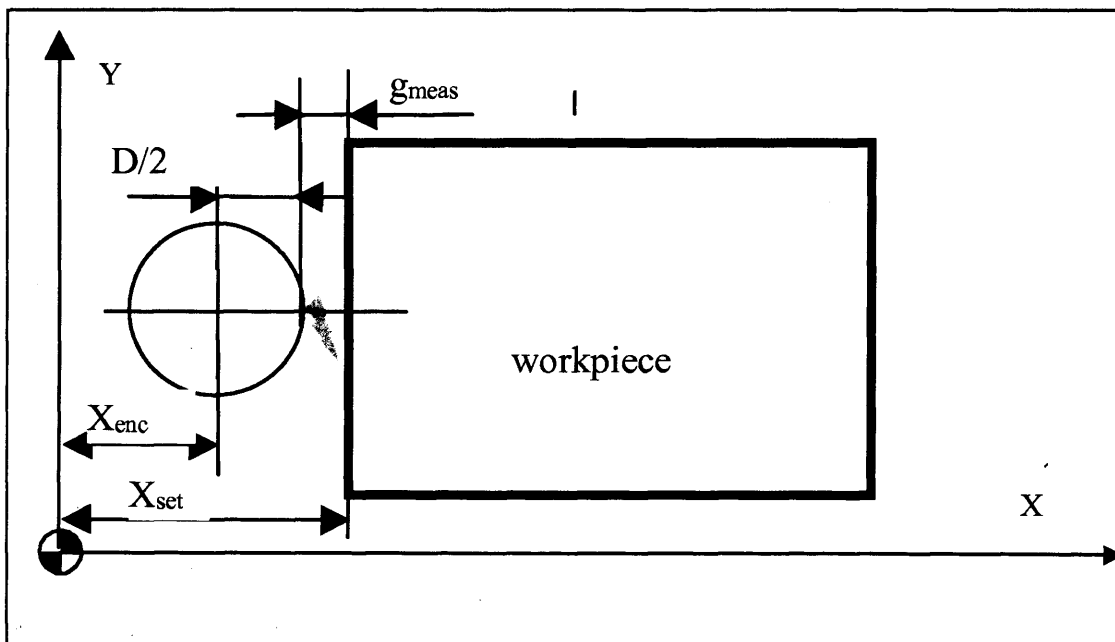


Figure 3.7 Schematic of the setting up process

$$X_H = X_{pos} - (X_{meas} + D/2 + g_{meas}) \quad (3.9)$$

$$Y_H = Y_{pos} - (Y_{meas} + D/2 + g_{meas}) \quad (3.10)$$

The deviations will be respectively:

$$\Delta X_H = \Delta X_{pos} + \Delta X_{meas} + \Delta D/2 + \Delta g_{meas} \quad (3.11)$$

$$\Delta Y_H = \Delta Y_{pos} + \Delta Y_{meas} + \Delta D/2 + \Delta g_{meas} \quad (3.12)$$

The accuracy of the position of the hole will depend on the accuracy of positioning of the machine ( $\Delta X_{pos}$ ,  $\Delta Y_{pos}$ ), the accuracy of detecting contact signal with the surface ( $\Delta X_{meas}$ ,  $\Delta Y_{meas}$ ,  $\Delta g_{meas}$ ) and the variation in the initial effective diameter of the electrode ( $\Delta D$ ).

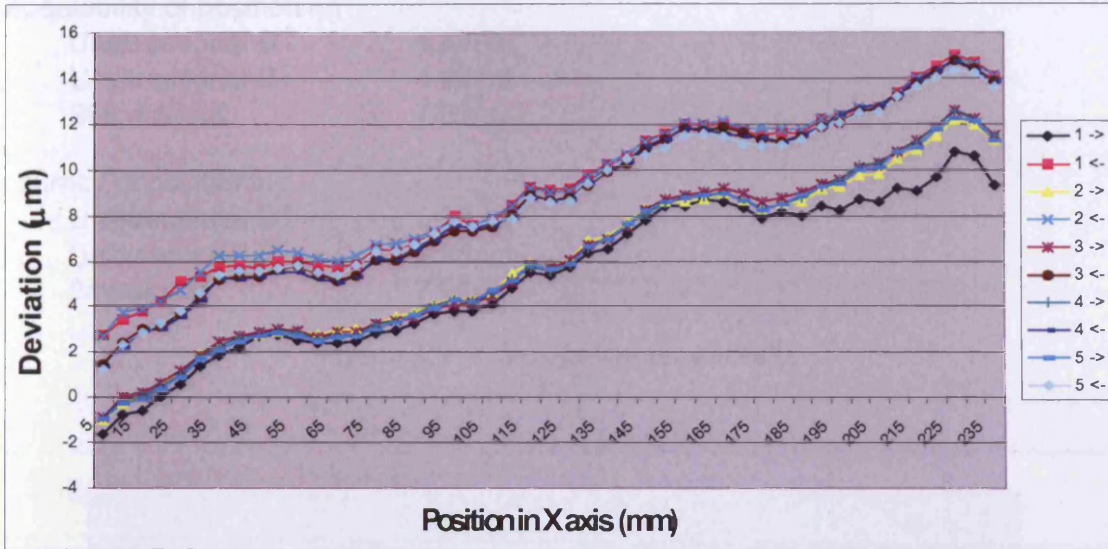
### 3.3. Description of the factors affecting the accuracy

#### 3.3.1. Accuracy and repeatability of positioning ( $\Delta y_d$ and $\Delta X_{pos}$ , $\Delta Y_{pos}$ )

The accuracy and repeatability of positioning ( $\Delta y_d$  and  $\Delta X_{pos}$ ,  $\Delta Y_{pos}$ ) of the machine were measured and assessed according to BS ISO 230-2:1997 and the results are given in Figure 3.8, Figure 3.9 and Figure 3.10 for the three axes of the machine. The data from the measurements is given in Appendix A.

Measurements were done using a Renishaw ML 10 laser interferometer for measuring bi-directional accuracy of machine movement.





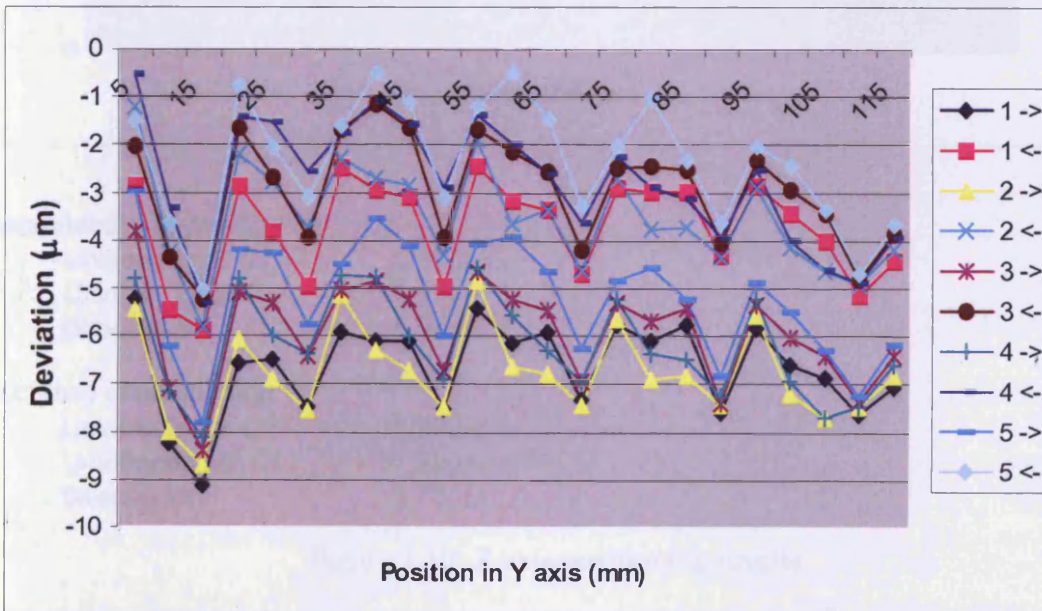
Repeatability of positioning

Unidirectional A $\uparrow$	3.76 $\mu\text{m}$
Unidirectional A $\downarrow$	2.95 $\mu\text{m}$
Bidirectional	5.33 $\mu\text{m}$

Accuracy of positioning

Unidirectional A $\uparrow$	14.03 $\mu\text{m}$
Unidirectional A $\downarrow$	11.85 $\mu\text{m}$
Bidirectional	15.7 $\mu\text{m}$

Figure 3.8 X axis positioning results



(to be continued)

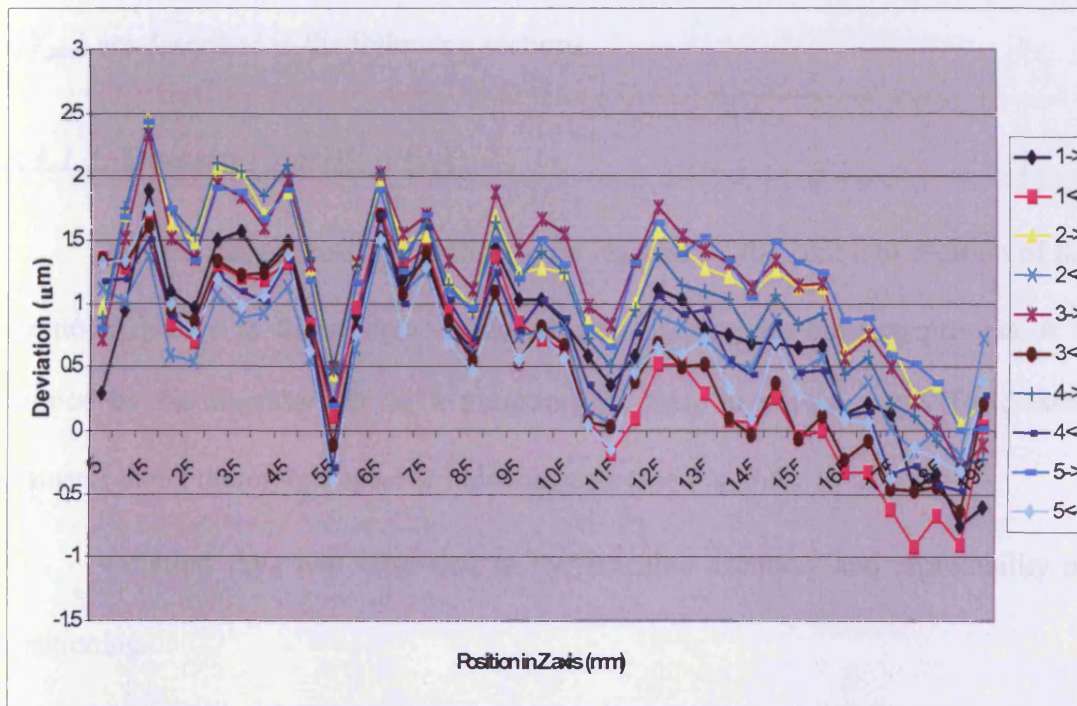
Repeatability of positioning

Unidirectional B $\uparrow$	4.49 $\mu\text{m}$
Unidirectional B $\downarrow$	4.92 $\mu\text{m}$
Bidirectional	7.83 $\mu\text{m}$

Accuracy of positioning

Unidirectional B $\uparrow$	5.03 $\mu\text{m}$
Unidirectional B $\downarrow$	5.18 $\mu\text{m}$
Birectional	7.91 $\mu\text{m}$

Figure 3.9 Y axis positioning results



Repeatability of positioning

Unidirectional C $\uparrow$	1.48 $\mu\text{m}$
Unidirectional C $\downarrow$	1.27 $\mu\text{m}$
Birectional	1.9 $\mu\text{m}$

Accuracy of positioning

Unidirectional C $\uparrow$	2.39 $\mu\text{m}$
Unidirectional C $\downarrow$	1.82 $\mu\text{m}$
Birectional	2.73 $\mu\text{m}$

Figure 3.10 Z axis positioning results



Machine tool manufactures should supply these data with the purchase of the machine, but it is advisable after installation and commissioning of the machine to have the machine checked again and recalibrated if necessary. Depending on the use of the machine, it should be tested periodically and accuracy of positioning and repeatability checked again on a regular basis.

The factors affected by the accuracy of machine movement ( $\Delta y_d$  and  $\Delta X_{pos}$ ,  $\Delta Y_{pos}$ ) are described in the following sections.

### 3.3.1.1. Dressing Position ( $y_d$ )

$y_d$  is the target dressing position to be reached by the centre of rotation of the electrode relative to the machine reference point during the dressing process. It is defined by the operator (or by a program) in order to obtain a specific dressed diameter  $d$  and therefore a specific hole diameter (see Fig. 3.5).

Variation  $\Delta y_d$  will arise due to the machine accuracy and repeatability of positioning.

An obvious way of reducing  $\Delta y_d$  during the dressing process is to always approach the position from the same direction (unidirectional approach). Another way of limiting the error is to identify an area on the machine and to fix the dressing unit where the repeatability of positioning is at its best.

For instance, when focusing on one single spot in the machine where the dressing unit is placed (Figure 3.11), the calculated repeatability of positioning according BS ISO 230-2:1997 in this case is  $2.2\mu\text{m}$ , which is much better compared to the values given in Figure 3.8-3.10. The measured value for  $\Delta y_d$  is  $1.98\mu\text{m}$  (Figure 3.11).

### **3.3.1.2. Hole position ( $X_{pos}$ and $Y_{pos}$ )**

$X_{pos}$  and  $Y_{pos}$  are the coordinates of the centre of the hole in the machine coordinate system. The position of the hole depends on the work-piece and its position in the working area. Thus the only way to improve  $\Delta X_{pos}$  and  $\Delta Y_{pos}$  is to adopt a unidirectional approach to the hole. As mentioned above, for EDMing of micro holes, multiple electrodes will be needed, therefore the accuracy of positioning of the machine will mainly affect the position of the hole, while the repeatability of positioning will affect the size and shape of the hole.

### **3.3.2. Spark gaps and effective electrode diameter ( $\Delta g_e$ , $\Delta g_d$ and $\Delta D$ )**

#### **3.3.2.1. Gap between electrode and workpiece ( $g_e$ )**

$g_e$  is defined as the spark gap between the electrode and the work-piece. Its nominal value is fixed by the chosen pulse of the generator and the dielectric used. In conventional EDM, the selection of a pulse is directly linked with the removal rate and surface roughness required. In micro EDM, the electrode wear is another important criterion which also needs to be carefully considered. In addition, in order to achieve the micro features, the spark gap should be minimised.

Variation of  $g_e$  ( $\Delta g_e$ ) brings random errors which can appear due to flushing conditions and lack of surface/material integrity (Lim et al, 2003).

#### **3.3.2.2. Gap between electrode and dressing unit ( $g_d$ )**

$g_d$  is defined as the spark gap between the electrode and the dressing unit. As in the case of  $g_e$ , the value of  $g_d$  is fixed by the chosen pulse parameters and dielectric

properties, and variations in  $g_d$  ( $\Delta g_d$ ) can arise due to flushing conditions and lack of surface/material integrity.

The pulse parameters are selected depending on the surface roughness required on the electrode and on the speed of dressing. Because the electrode is rotating, its surface roughness should not significantly affect the roughness of the machined surfaces. However, because of the small dimension involved, a poor roughness will affect the strength of the dressed electrodes, which could break during the process.

Estimation of  $\Delta g_d$  is difficult but it was assumed that it would not exceed  $\Delta g_e$  in the worst case. This is because, during dressing, sparking conditions are better than during drilling itself as dressing involves single point sparking with better flushing conditions.

### 3.3.2.3. Effective Diameter ( $D$ )

The effective diameter of the non-ground electrode  $D$  is determined by the initial diameter  $D_{init}$  of the electrode (WC rod) and the assembly conditions between the electrode and the ceramic guide. The difference between the diameter  $D_{init}$  and the diameter of the ceramic guide  $D_{guide}$  creates a gap that introduces potential errors as shown in Figure 3.12.

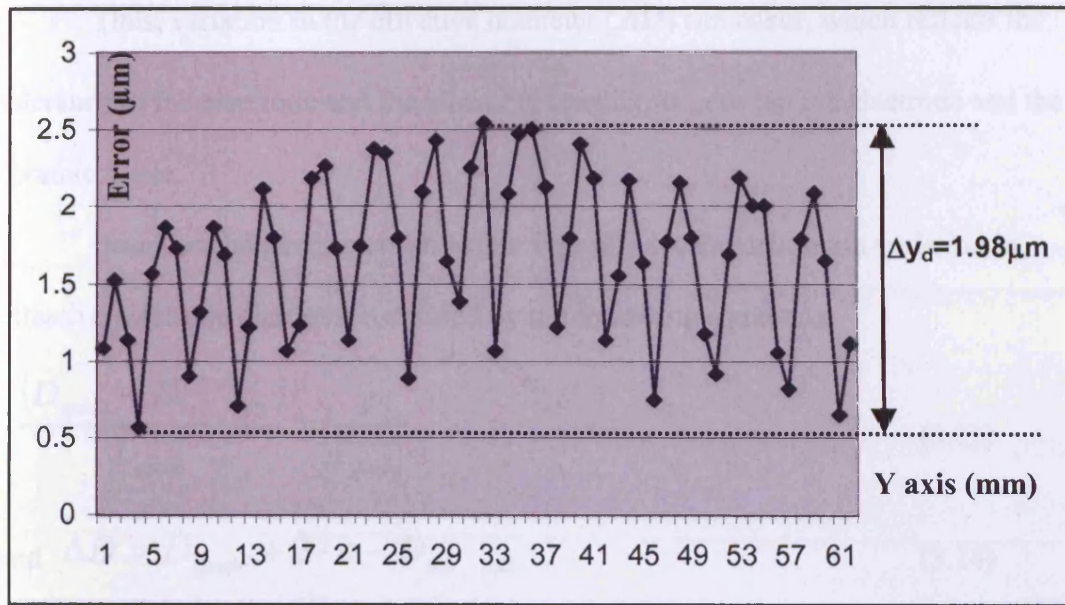


Figure 3.11 Single spot positioning accuracy

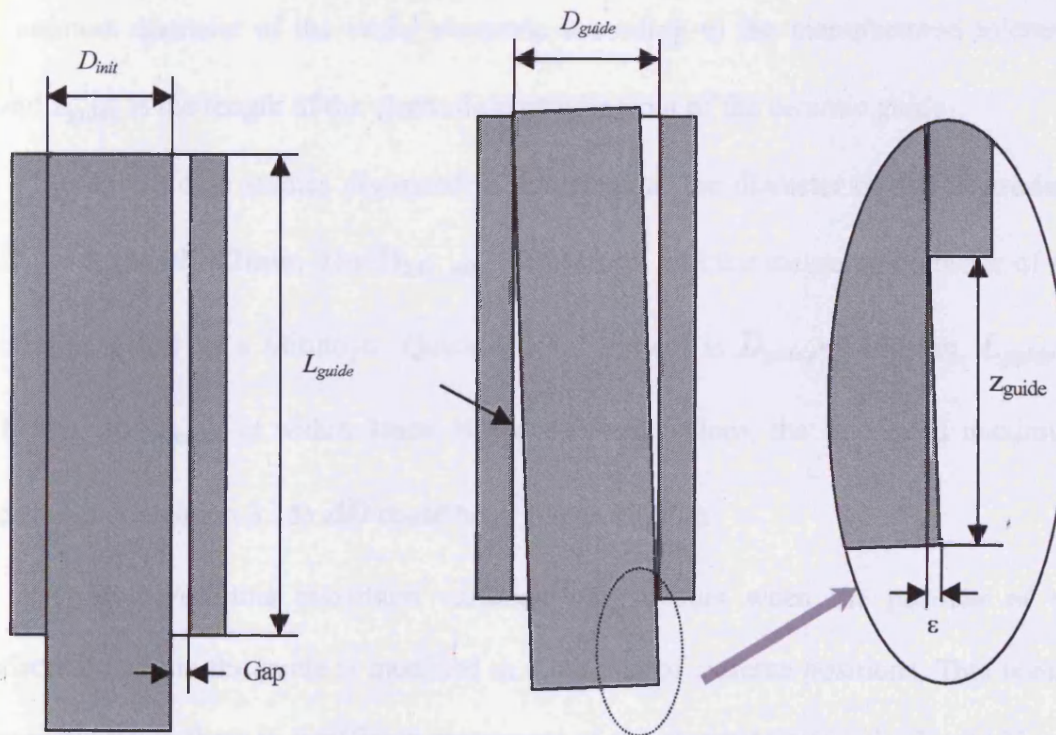


Figure 3.12 Effect of the clearance gap between the ceramic guide and the electrode

Thus, variation in the effective diameter ( $\Delta D$ ) can occur, which reflects the tolerance of the electrode and the assembly conditions between the electrode and the ceramic guide.

Based on the parameters shown in Figure 3.12, the maximum variation in effective electrode diameter is defined by the following equations:

$$\frac{(D_{guide} - D_{init\_min})}{L_{guide}} = \frac{\varepsilon}{z_{guide}} \quad (3.13)$$

$$\text{and } \Delta D = D_{guide} + 2 \cdot \varepsilon - D_{init\_min} \quad (3.14)$$

$$\text{Thus, } \Delta D = D_{guide} + 2 \cdot \frac{(D_{guide} - D_{init\_min}) \cdot z_{guide}}{L_{guide}} - D_{init\_min} \quad (3.15)$$

In the above equations,  $D_{guide}$  is the diameter of the guide,  $D_{init\_min}$  is the minimum diameter of the initial electrode according to the manufactured tolerance and  $z_{guide}$  is the length of the electrode protruding out of the ceramic guide.

In the case studies discussed in this chapter, the diameter of the electrode is  $D_{init} = 0.146 \pm 0.002 \text{ mm}$ , thus  $D_{init\_min} = 0.144 \text{ mm}$ , and the measured diameter of the ceramic guide on a Mitutoyo ‘Quick Vision’ system is  $D_{guide} = 0.154 \text{ mm}$ .  $L_{guide}$  is  $12 \text{ mm}$ , and  $z_{guide}$  is within  $2 \text{ mm}$ . Based on those values, the calculated maximum deviation (equation 3.15)  $\Delta D$  could be as big as  $13.3 \mu\text{m}$ .

However, this maximum variation only occurs when the position of the electrode within the guide is modified to a number of extreme positions. This is only possible when there is significant movement of the electrode along the X and Y axis relative to the guide. This is highly unlikely. To support this point, two cases are considered.

Firstly, when using a non rotating electrode, the position between guide and electrode should not change because the only movement occurring between the guide and electrode is in the Z axis and no force acts along the X or Y axis that would change this position. Significant change should only occur when altering the position of the guide with respect to the head holding the electrode, for instance, when replacing an electrode or after a significant movement in the Z direction because this would affect the angle at which the electrode enters the guide and therefore might create a significant movement along the X and Y axis. Also, changes could arise due to the tolerance of the manufactured electrode, but the variation of diameter along the length of a single manufactured rod is considered negligible. Therefore, it can be assumed that, for a small feed and without change of electrode, the variations in effective diameter when using a non-rotating electrode are negligible,  $\Delta D \approx 0$ .

Second, when the electrode is rotating, X and Y movement can occur due to the rotation and friction between guide and electrode. However, it can be assumed that this movement follows a cycle in phase with the rotation, resulting in a small increase in effective diameter but with negligible variations between two periods of the rotation cycle, therefore  $\Delta D \approx 0$ .

It should be noted that the length of the dressed section on the electrode should be smaller than  $z_{guide}$ . This is to avoid the dressed part of the electrode touching the guide, as this would increase the potential error as shown in Figure 3.13 and the dressed electrode could be damaged. However, this introduces another limitation in the depth achievable using a dressed electrode.



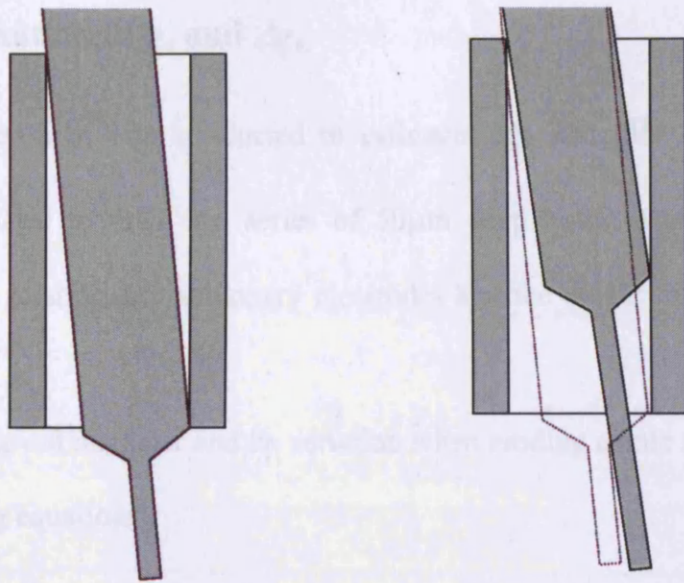


Figure 3.13 Possible error in long dressed electrode

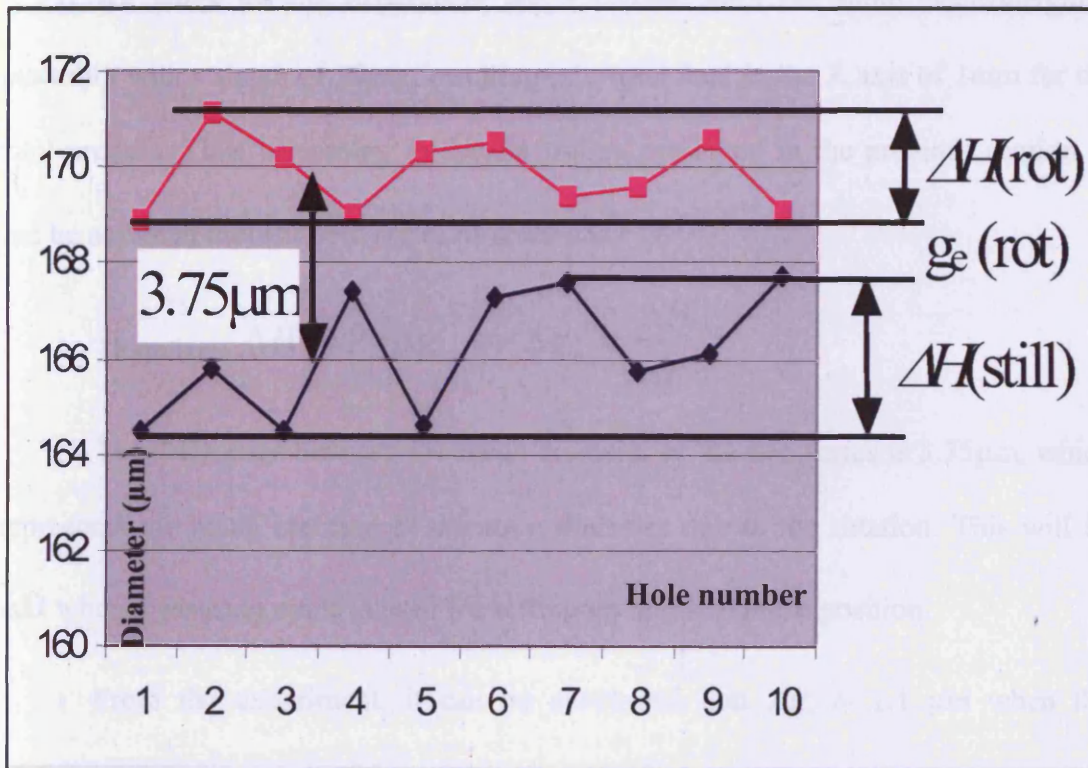


Figure 3.14 Accuracy of a hole produced with rotating and stationary electrodes

### 3.3.2.4. Estimation of $g_e$ and $\Delta g_e$

An experiment was conducted to estimate  $\Delta g_e$  and  $\Delta D$ . A  $\text{Ø}150\mu\text{m}$  WC electrode was used to drill two series of  $50\mu\text{m}$  deep holes. The experiment was conducted with rotating and stationary electrodes and the results are given in Figure 3.14.

The achieved diameter and its variation when eroding a hole are represented by the following equations:

$$H = 2 \cdot g_e + D \quad (3.16)$$

$$\Delta H = 2 \cdot \Delta g_e + \Delta D \quad (3.17)$$

All holes for the experiment are machined with the same electrode/guide assembly with a depth of  $50\mu\text{m}$ , resulting in a total feed in the Z axis of  $1\text{mm}$  for the total process. Thus, according to the discussion presented in the previous section, it can be assumed that for both series of holes  $\Delta D \approx 0$ .

$$\text{Therefore: } \Delta H \approx 2 \cdot \Delta g_e \Leftrightarrow \Delta g_e \approx \frac{\Delta H}{2}.$$

The difference between the mean diameter of the two series is  $3.75\mu\text{m}$ , which represents the mean increase of effective diameter due to the rotation. This will be  $\Delta D$  when measuring cycle is used for setting up the workpiece position.

From the experiment, it can be concluded that  $\Delta g_e = 1.1 \mu\text{m}$  when the electrode is rotating and  $\Delta g_e = 1.6\mu\text{m}$  when the electrode is not rotating.

As seen from Figure 3.14, when the electrode is rotating the  $\Delta g_e$  is smaller which might be due to the better flushing conditions and a better way of removing debris from the sparking zone.



### 3.3.3. Temperature instability error ( $\Delta y_{unit}$ )

$y_{unit}$  is the position of the point of erosion on the dressing unit in the machine co-ordinate system.

Changes in the temperature in the room and in the machine structure create variations in the relative position between the rotating head and the table of the machine and therefore affect the position of the dressing unit with respect to the machine zero point,  $\Delta y_{unit}$  and to the electrode. An example of that error is shown in Figure 3.15. Measurements of displacement along Y axes were done using a laser interferometer during the machine warming up cycle.

The obvious way to minimise the variation is to work in a temperature-controlled room and to ensure thermal stability of the machine structure. Each machine should be tested to find out the time for the temperature of the machine to stabilise for certain ambient conditions and the temperature relative deviation of each axis should be measured in order to plan electrode dressing with minimum error.

Under certain conditions (temperature-controlled room and minimum dielectric temperature variance, short working hours) it can be assumed that:

$$\Delta y_{unit} \approx 0 \mu\text{m}.$$

### 3.3.4. Measurement errors

#### 3.3.4.1. Workpiece surface detection error ( $\Delta X_{meas}$ , $\Delta Y_{meas}$ )

During the setting up of the workpiece, when an electrical contact occurs between the electrode and the workpiece, a contact signal is registered by the machine system processor. The processor has set priorities in checking each machine status signal, which means that the checking of the contact signal is not carried out

continuously. There is a time interval ( $t_{meas}$ ) between each signal check. This causes an error when detecting the position of the measured surface when measuring  $X_{meas}$  and  $Y_{meas}$ . If the speed of approaching the surface is  $V_{meas}$ , the variation will be:

$$\Delta X_{meas}(\Delta Y_{meas})=V_{meas} * t_{meas} \quad (3.18)$$

Usually the measuring signal is checked every 2- 5msec (depending on the controller). Obviously, to minimise the error the approach speed should be as low as possible but fast enough to avoid stick-slip effect on the machine movement. In this case the  $t_{meas}$  is 3msec and the measuring speed is from 20mm/min to 1mm/min. The calculated variation is 0.05 to 1 $\mu$ m.

#### **3.3.4.2. Surface position detection error ( $\Delta g_{meas}$ )**

During the measuring cycle, voltage is applied between the work table and the spindle of the machine. The machine moves until an electrical contact is reached. As the surfaces tend to oxidise, a different gap, or different pressure is needed for the spark to break through. All these factors contribute to an error of surface detection introducing variation in the measuring spark gap  $\Delta g_{meas}$ .

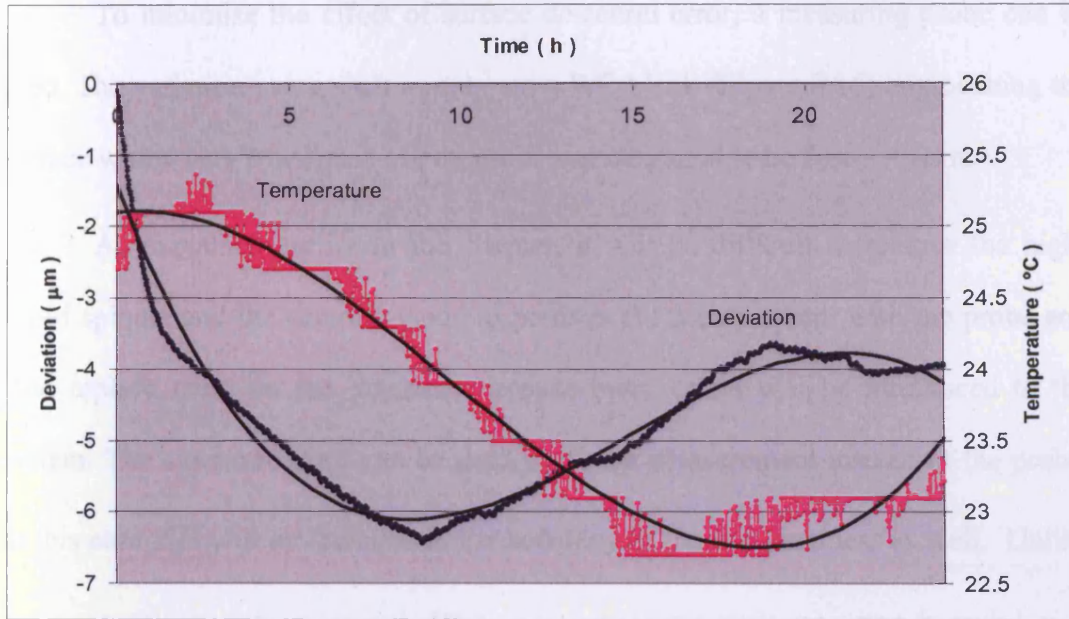


Figure 3.15 Machine body deformation due to temperature variations

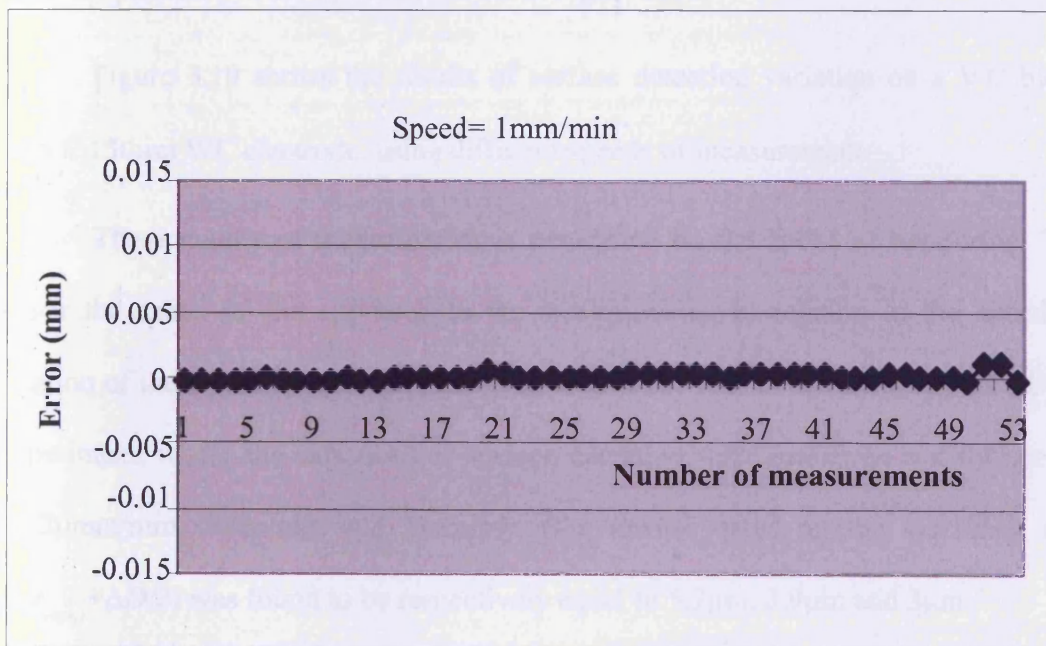


Figure 3.16 Accuracy of surface detection using touch probe on a WC block

To minimise the effect of surface detection error, a measuring probe can be used. The variation using such a probe on a WC block (Figure 3.16) approaching the surface with a very low speed of 1mm/min was measured to be  $\Delta g_{meas} = 1\mu\text{m}$ .

As explained earlier in the chapter, it will be difficult to remove the high-speed spindle and the ceramic guide to perform the measurement with the probe and then replace them on the machine, because more errors will be introduced to the system. The electrode itself can be used to do the measurement instead of the probe. In this case  $\Delta D$  will be included in the accuracy of the measurement as well. Unlike the erosion or dressing process,  $\Delta D$  in this case is not negligible. This is because as mentioned in section 3.3.2.4, the rotation of the electrode creates a cyclic movement in X and Y. Therefore, contact between the electrode and the surface might occur at different positions in the cycle, as shown in Figure 3.17.

Figure 3.19 shows the results of surface detection variation on a WC block with  $\varnothing 150\mu\text{m}$  WC electrode, using different speeds of measurement.

The accuracy of measurement is dependent on the speed of measuring. The lower the speed of the approach to the workpiece is, in relation to the speed of rotation of the electrode, the smaller the error will be. This is confirmed by the above experiment, where the variations of surface detection were measured and for speeds of 20mm/min, 5mm/min and 1mm/min (the lowest speed on the machine), and  $(\Delta g_{meas} + \Delta D/2)$  was found to be respectively equal to  $5.7\mu\text{m}$ ,  $3.9\mu\text{m}$  and  $3\mu\text{m}$ .

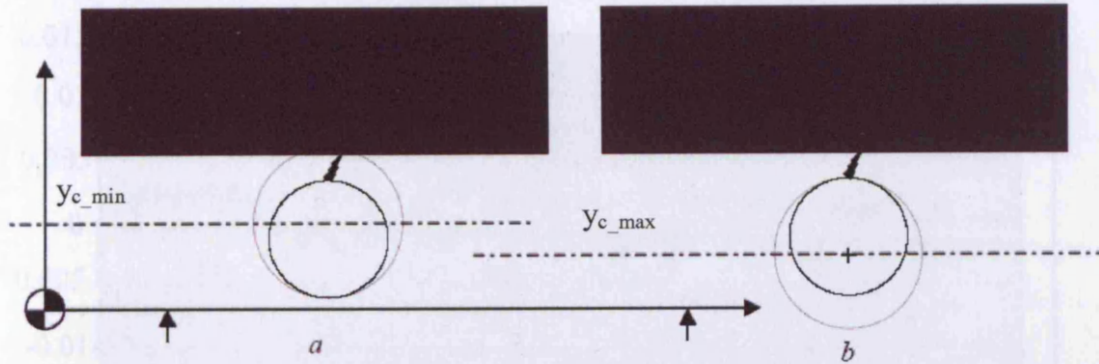


Figure 3.17 Schematic of surface detection with  $\Delta D$  influence

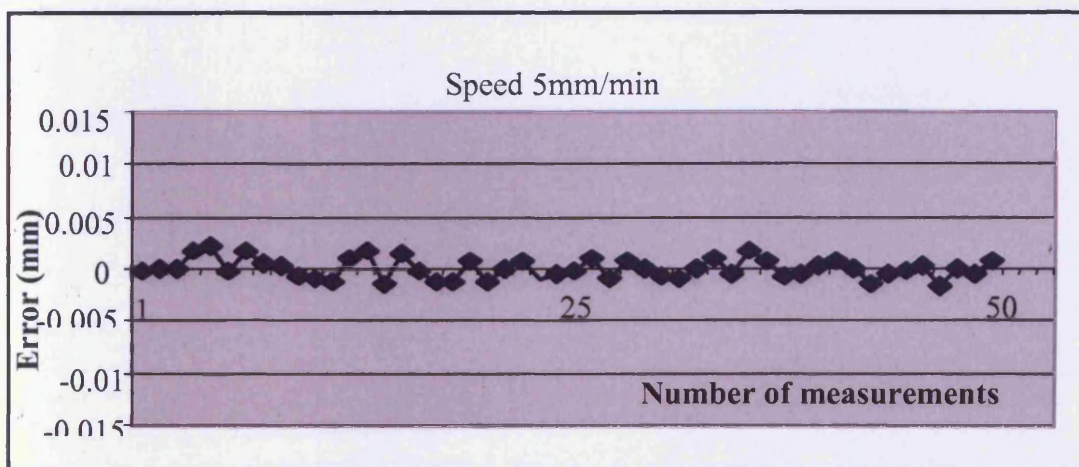
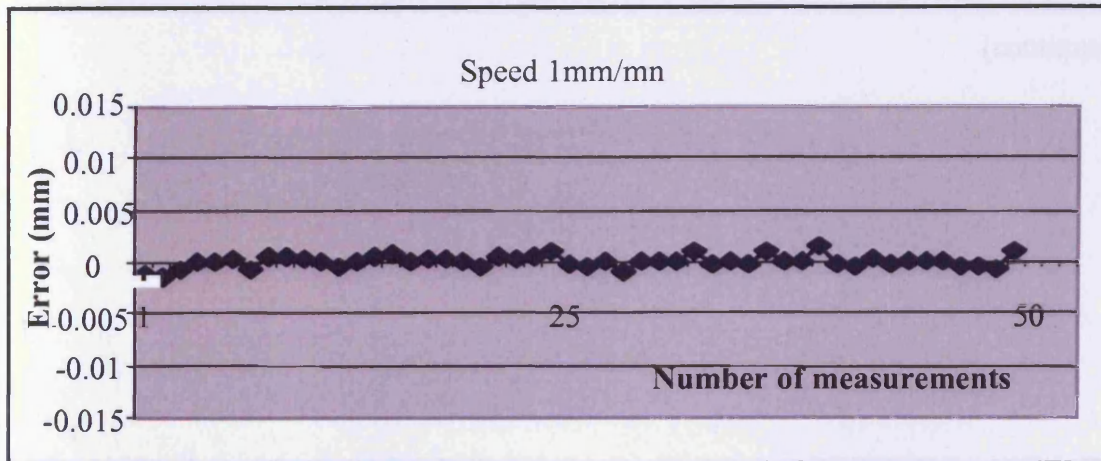


Figure 3.18 Surface detection using electrode on a WC block

(to be continued)



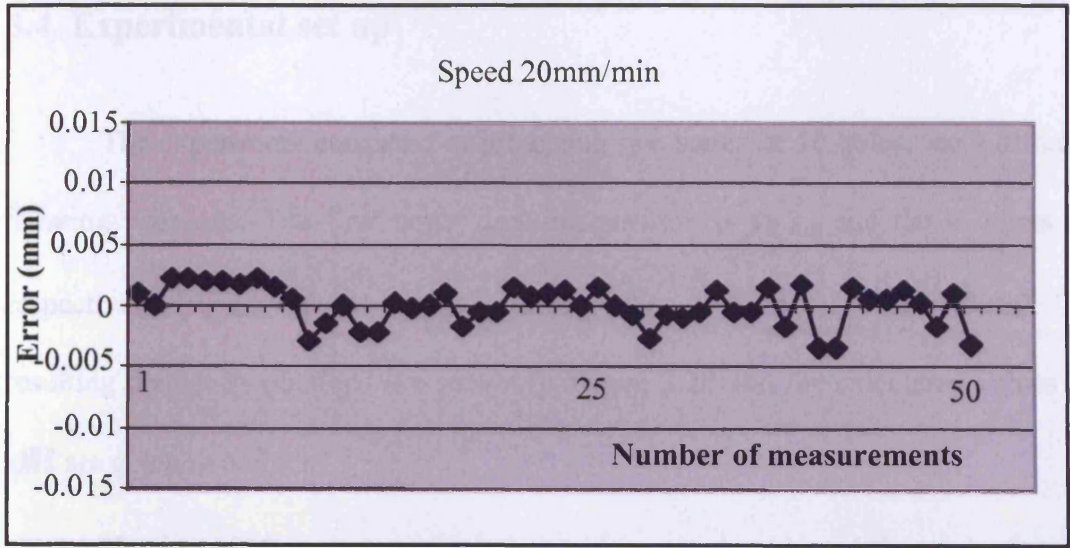


Figure 3.19 Surface detection using electrode on a WC block

(continued)

### 3.4. Experimental set up

The experiment consisted of producing two series of 10 holes, for 5 different dressing positions. The first target dressing position is  $y_{d\_init}$  and the 4 others are respectively  $(y_{d\_init} - 10\mu\text{m})$ ,  $(y_{d\_init} - 20\mu\text{m})$ ,  $(y_{d\_init} - 30\mu\text{m})$ ,  $(y_{d\_init} - 40\mu\text{m})$ . The resulting diameters obtained are shown in Figure 3.20 and the calculated values for  $\Delta H$  are given in table 3.1.

A reduction of  $10\mu\text{m}$  in target dressing position  $y_d$  should result in a reduction of  $20\mu\text{m}$  in diameter for the produced hole. In the experiment, the calculated mean differences between each series of diameters are 20.49, 19.55, 21.31, 19.08, which gives a variation of  $2.23 \mu\text{m}$ . This shows the potential for an accurate dressing process using EDM grinding.

### 5. Summary

This chapter has presented the possible geometry of a microfluidic transducer for

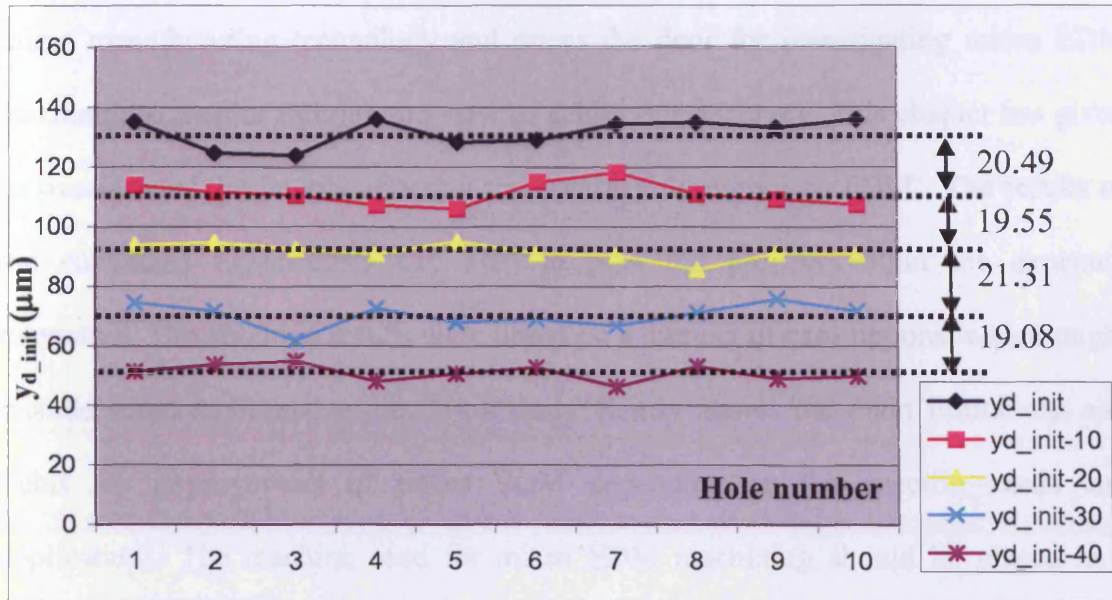


Figure 3.20 Hole diameter variations for 4 dressing positions

	$y_{d\_init}$	$y_{d\_init} - 10\mu\text{m}$	$y_{d\_init} - 20\mu\text{m}$	$y_{d\_init} - 30\mu\text{m}$	$y_{d\_init} - 40\mu\text{m}$
$\Delta H$ exp 1	19.4 $\mu\text{m}$	3.6 $\mu\text{m}$	6.0 $\mu\text{m}$	13.9 $\mu\text{m}$	11.9 $\mu\text{m}$
$\Delta H$ exp 2	12.2 $\mu\text{m}$	12.2 $\mu\text{m}$	9.4 $\mu\text{m}$	13.9 $\mu\text{m}$	8.6 $\mu\text{m}$

Table 3.1 Data for experimentally determined  $\Delta H$



### **3.5. Summary**

This chapter has illustrated the possible accuracy of a micro EDM machine for micro manufacturing technology and opens the door for investigating micro EDM machining strategies through the view of achievable accuracy. This chapter has given an overview of the factors affecting the accuracy during micro EDM. The results of the conducted experiments can help to plan the process within the expected tolerances. The obtained results were based on a number of assumptions, which might include some additional errors. This study clearly shows the main limitations and fields for improvement of micro EDM depending on the specific needs and applications. The machine used for micro EDM machining should be placed in a temperature-controlled environment with a constant ambient and dielectric temperature and should be checked regularly for geometrical accuracy. If a grinding device is used, the type of device should be justified and its position should be selected after careful investigation of the geometrical accuracy of the machine. When assigning process tolerances for micro EDM all activities during the process, such as type of electrode grinding, type of positioning, duration of the operation etc should be considered. All these activities will accumulate errors, which should be taken into account.

A coincidence is when God performs a miracle, and decides to remain anonymous

# Chapter 4

#### 4. Micro EDM electrode wear investigation

In conventional as in micro die-sinking Electro Discharge Machining (EDM), the phenomenon of wear occurring on the tool is well known (Mohri et al, 1995; Ozgedik & Cogun, 2006) and it was described earlier in chapter 2 & 3. This problem is normally overcome by using a number of electrodes to produce a cavity. The errors caused by electrode wear are often negligible when considering the feature sizes and tolerances required in macro EDM.

In micro EDM, it is possible that holes have to be machined with diameters smaller than  $5\mu\text{m}$  and with surface roughness ( $R_{\text{max}}$ ) less than  $0.1\mu\text{m}$  (Masuzawa, 2000). In such cases, in order to produce accurate 3D cavities, it is necessary not only to consider the findings in Chapter 3, but electrode wear becomes an additional very difficult issue and methods to compensate for it are required. The machining conditions in micro EDM differ significantly from those in conventional EDM (Blatnik et al, 2005). The usual die-sinking method based on employing electrodes for roughing followed by electrodes for finishing is not applicable because of the cost of multiple electrodes with micro features. In addition, the micro features will suffer severe wear resulting in the need for even more electrodes.

Thus, in the production of micro 3D cavities, the use of micro EDM milling employing simple-shape electrodes might be the preferred strategy, because the sparking conditions and the wear ratio will not change drastically and the result of the machining will be more predictable, considering all the requirements described in chapter 3. However, because of the physical size of the features and the accuracy required for the methods used in micro EDM milling, wear compensation is much higher than in conventional EDM milling. Many types of electrode wear compensation methods have been studied and applied more or less successfully in research laboratories (Bleys, 2004), but their introduction into an industrial manufacturing environment is not straightforward.

The objectives of this chapter are to study the electrode wear behaviour, pay special attention to the electrode wear variation in different situations and searching for eventual possibilities for applying electrode wear compensation methods.

#### 4.1. Wear estimation

In micro EDM, accurately measuring the amount of wear is a difficult task especially when very small wear volumes are involved (Ferri & Ivanov, 2007).

The first consideration concerns the deformation of the electrode shape due to wear (Rajurkar et al, 2004). This is because wear occurring on the side of the electrode and distorting the shape cannot be ignored. For instance, when eroding with a micro cylindrical (rod or tube) electrode, the shape of the electrode rapidly changes during machining (Pham et al, 2004) (Figure 4.1), which causes geometric errors in the produced micro cavity.

The second consideration is the volumetric wear occurring on both electrode and workpiece and the volumetric wear ratio, which is the ratio of the volume removed due to wear of the electrode  $V_e$  and the volume eroded from the workpiece  $V_p$ . This ratio is the main criterion for electrode wear estimation (Yu et al, 2003).

$$\nu = \frac{V_e}{V_p} \quad (4.1)$$

##### 4.1.1. Electrode shape deformation

A number of experiments were carried out to analyse the shape change of the electrode. These have confirmed that the electrode tends to change during machining towards a constant shape.

Figure 4.2 shows the evolution of the cavity shape when tool steel is EDM drilled and the constant electrode shape obtained after drilling a certain depth.

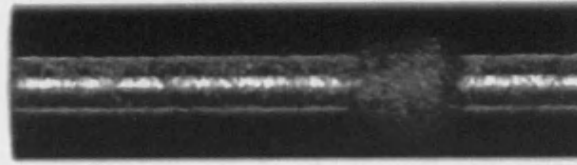
It was noticed that the shape change, under those particular process settings, occurred during the first 180  $\mu\text{m}$  of erosion depth. After this, the electrode continued to wear but its shape remained constant. A logical explanation is that, initially, the intensity of the electrical field is stronger at the edge and it wears first, becoming blunt in the process. Then, the highest intensity of the electric field shifts to the middle of the electrode where there are the most sparks.

It is hypothesised that the shape of the electrode changes in such a way as to achieve uniform electric field intensity eventually (Figure 4.2 b).

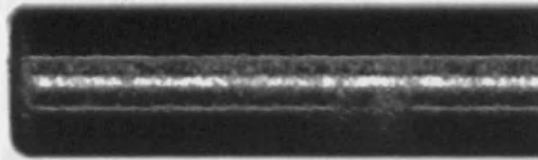
The final shape of the electrode and the cavity were scanned and 3D images of the electrode and the cavity were created together with the initial cylindrical shape and the workpiece and one intermediate shape of the electrode and the related cavity. The three pairs of shapes of the electrode and corresponding cavity were used in electrostatic field modelling software (Vector Fields Ltd, <http://www.vectorfields.com>) to check the above hypothesis. The results are given in Figure 4.3.

Figure 4.3a shows that the intensity of the electric field in the spark gap is highest around the edge when the cylindrical electrode and the workpiece are electrically charged. Figure 4.3b shows the decrease of the intensity of the electric field in the spark gap and shift of the position of highest intensity towards the middle of the electrode as the edge of the electrode wears. Figure 4.3c shows the uniformity of the electric field intensity in the spark gap after the constant electrode shape has been reached.

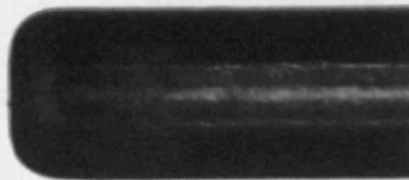
It is not simple to calculate the volume of the electrode material lost in reaching the constant shape (Ferri & Ivanov, 2007). The volumetric wear ratio in this initial period of erosion with non-uniform electric field intensity is difficult to predict as the electric field intensity continuously changes causing sparking to appear at different parts of the electrode.



a) Before Erosion

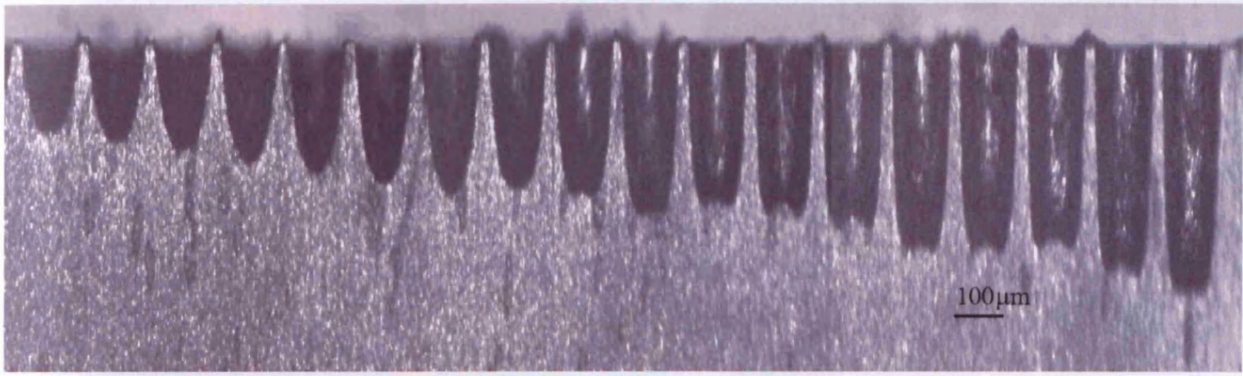


b) After 25  $\mu\text{m}$  erosion depth

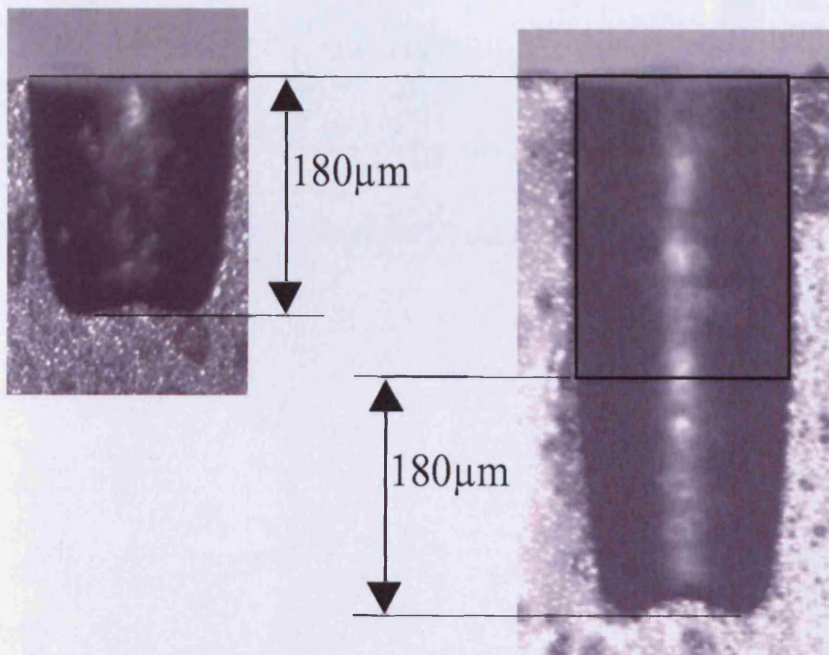


c) After 100  $\mu\text{m}$  depth

Figure 4.1 The shapes of a  $\text{\O}150 \mu\text{m}$  rod electrode (a) before and (b) and (c) after two erosion depths



a) hole/electrode shape evolution during drilling



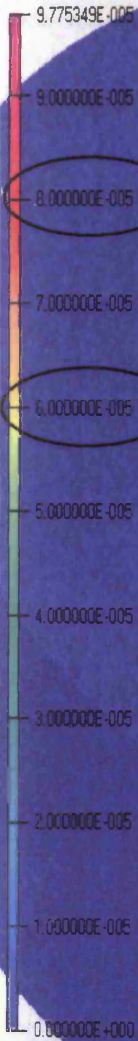
b) constant hole/electrode shape after 180 μm erosion depth

Figure 4.2 Evolution of the cavity/electrode shape during EDM drilling of tool steel with  $\text{Ø}170\text{ }\mu\text{m}$  WC electrode



Electric field intensity (V/m)

Surface contours: DMOD



UNITS	
Length	mm
Magn Flux Density	T
Magn Field	A m <sup>-1</sup>
Magn Scalar Pot	A
Magn Vector Pot	Wb m <sup>-1</sup>
Elec Flux Density	C m <sup>-2</sup>
Elec Field	V m <sup>-1</sup>
Conductivity	S mm <sup>-1</sup>
Current Density	A mm <sup>-2</sup>
Power	W
Force	N
Energy	J

PROBLEM DATA	
cylindrical.op3	
TOSCA Electrostatic	
Linear materials	
Simulation No 1 of 1	
256001 elements	
162166 nodes	
Nodally interpolated fields	
Reflection in XY plane (Z field=0)	

Local Coordinates	
Origin: 0.0, 0.0, 0.0	
Angles: $\phi=90.0$ , $\theta=90.0$ , $\psi=90.0$	

**V VECTOR FIELDS**

a) The highest intensity is on the edge of the cylindrical electrode

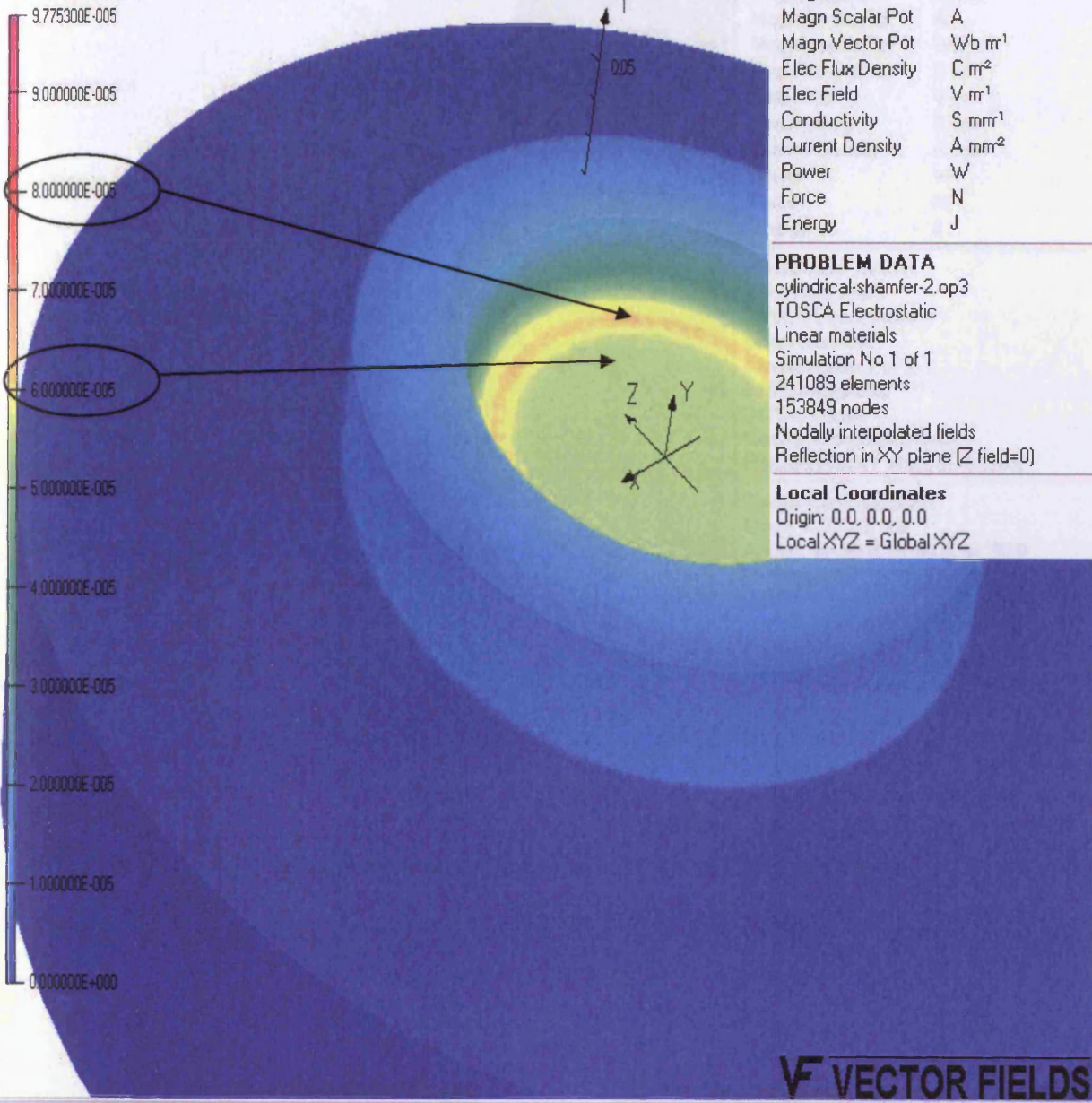
Figure 4.3 Electric field intensity dependency on the electrode shape changes

(to be continued)



Electric field intensity (V/m)

Surface contours: DMOD



**UNITS**

Length	mm
Magn Flux Density	T
Magn Field	A m <sup>-1</sup>
Magn Scalar Pot	A
Magn Vector Pot	Wb m <sup>-1</sup>
Elec Flux Density	C m <sup>-2</sup>
Elec Field	V m <sup>-1</sup>
Conductivity	S mm <sup>-1</sup>
Current Density	A mm <sup>-2</sup>
Power	W
Force	N
Energy	J

**PROBLEM DATA**

cylindrical-shamfer-2.op3  
TOSCA Electrostatic  
Linear materials  
Simulation No 1 of 1  
241089 elements  
153849 nodes  
Nodally interpolated fields  
Reflection in XY plane (Z field=0)

**Local Coordinates**

Origin: 0.0, 0.0, 0.0  
Local XYZ = Global XYZ

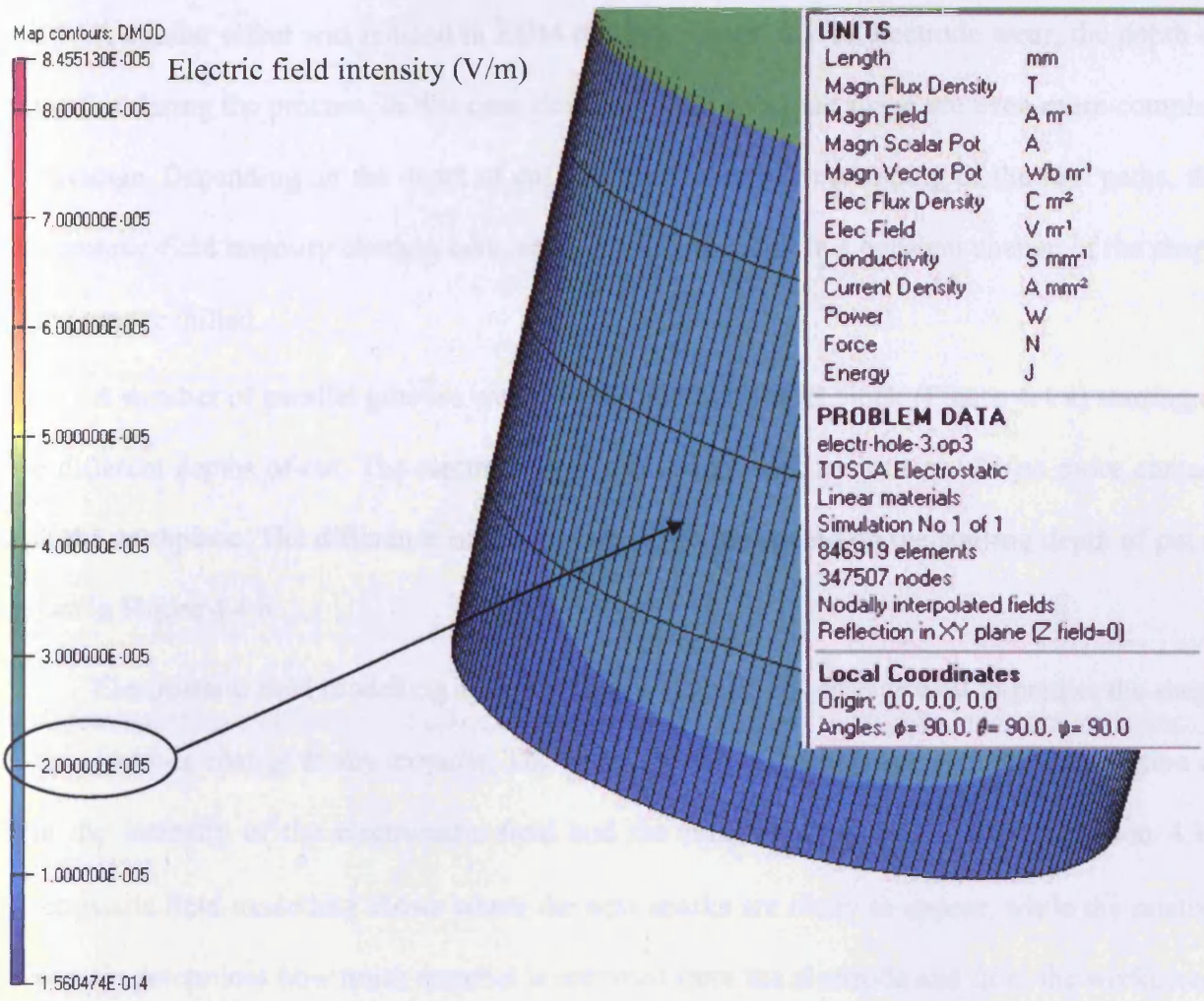
**V VECTOR FIELDS**

b) The position of the highest intensity field shifts towards the centre with the rounding of the edge of the cylindrical electrode

Figure 4.3 Electric field intensity dependency on the electrode shape changes

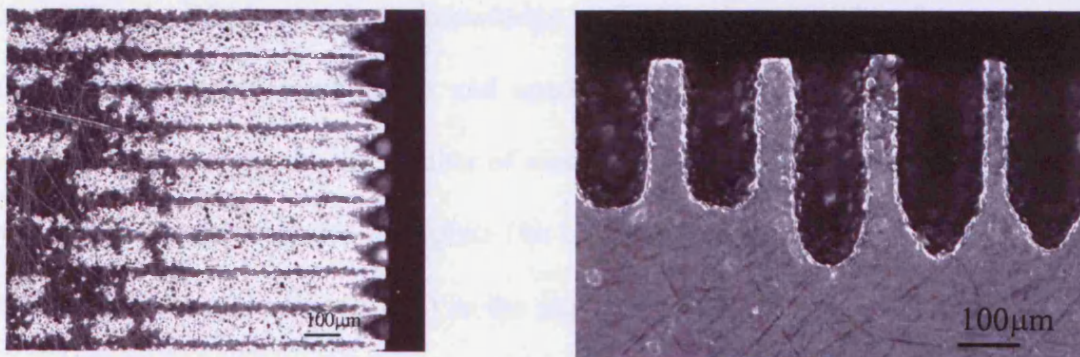
(to be continued)





c) The uniform field intensity with constant electrode shape

Figure 4.3 Electric field intensity dependency on the electrode shape changes (continued)



a) Top view of EDM milling passes

b) End view of the milling passes

Figure 4.4 Groove shapes obtained for two different milling depths

A similar effect was noticed in EDM milling, where, due to electrode wear, the depth of cut varies during the process. In this case changes to the electrode shape are even more complex to envisage. Depending on the depth of cut and the degree of overlapping of the tool paths, the electrostatic field intensity changes constantly which will result in a constant change of the shape of the groove milled.

A number of parallel grooves were EDM milled in a steel block (Figure 4.4 a) starting at two different depths of cut. The electrode was allowed to wear until there was no more contact with the workpiece. The difference of the groove shape depending on the starting depth of cut is shown in Figure 4.4 b.

Electrostatic field modelling software can be used in this case as well to predict the shape of the electrode change at any moment. The electrode shape deformation should be a function of both the intensity of the electrostatic field and the relative wear ratio  $\sigma$  (see Equation 4.1). Electrostatic field modelling shows where the next sparks are likely to appear, while the relative wear ratio determines how much material is removed from the electrode and from the workpiece. By combining different electric field intensities and different wear ratios, various final shapes can be achieved, that give eventually uniform field intensity.

#### **4.1.2. Volumetric wear**

Conventional EDM requires knowledge of the wear ratio for a standard electrode/workpiece material combination and sparking conditions (voltage current, time on, time off, etc.) in order to estimate the number of electrodes needed. The differences of the wear ratio for one material are considered negligible (for instance different quality steels, grain sizes, feature positions, flushing conditions, etc.) as the requirements for the final accuracy are not as high as in micro EDM. In micro EDM, it is not clear how such variations will affect the erosion process and therefore the wear ratio, in spite of the electrode shape being simple. Thus a small change of the sparking conditions (temperature of dielectric, workpiece material structure and

purity, electrode purity, variation of spark energy etc.) might affect the wear ratio in a non negligible way.

The accuracy with which the volumetric wear and the wear ratio can be estimated will determine the accuracy of the compensation method used, the strategy of machining and finally the accuracy of the machined features.

Even in the laboratory, methods such as weighing the electrode and the workpiece before and after erosion, using ultra precision scales, cannot achieve accurate wear measurements and thus cannot yield sufficiently reliable wear ratios. Another approach could be mapping of the electrode and workpiece surfaces before and after EDM machining and using software to calculate the removed volume of material (Ferri & Ivanov, 2007). In this case, the accuracy of the scanning method, software approximation and positioning to scan the same patch before and after machining will determine the accuracy of the approach.

The assessment of the wear ratio should be carried out for each new setting (environment changes, generator parameters etc.) and electrode/workpiece materials combination.

## **4.2. Wear ratio calculation**

As mentioned previously the volumetric wear ratio is the ratio between the volume removed due to wear of the electrode  $V_e$  and the volume eroded from the workpiece  $V_p$ . Measuring each of these volumes would allow calculation of the volumetric wear ratio  $V$  (equation 4.1). A number of electrode wear compensation methods require knowing the value of the volumetric wear ratio (Rajurkar et al, 2004). The usefulness of such compensation methods will depend on how accurately and how repeatable the wear ratio can be determined as it depends on a number of machining conditions, such as the generator parameters (voltage, current, time on, time off, etc.), the flushing conditions and the materials used for both workpiece and electrode. A small modification of any of those conditions might have a non-negligible effect on the value and variation of the volumetric wear ratio. Thus, in order to obtain

an accurate estimation of the wear ratio, rather than relying on existing and approximate data, that ratio should be obtained for each machining problem.

At a macro scale, a constant wear ratio can be assumed, because discrepancies in the machining conditions will on average lead to negligible variations in wear characteristics. However, in micro EDM, it is questionable if the ratio can be assumed constant. This is because uncontrollable factors might affect its value in a non-negligible way due to the small dimensions involved. This casts doubt on the validity of a number of compensation methods which rely on such an assumption.

The method for volumetric wear ratio measurement proposed here could easily be applied even in a production environment. The method is based only on the geometrical information derived from the process.

As mentioned previously, the usual way of assessing the volumes  $V_p$  and  $V_e$  is to measure the weight of the electrode and the workpiece before and after the EDM process. From the weight of each part, based on the material density, the volumes removed in the EDM process are then calculated. This requires removing the electrode and workpiece from the machine and using very accurate scales. In the case of micro EDM, this method is not applicable as it is not sufficiently accurate and will introduce critical errors in the Micro EDM process.

As explained in section 4.1.1, after a certain depth of erosion in EDM drilling, the shape of the electrode remains constant. If drilling proceeds further from that point down to a target depth  $Z$  (Figure 4.5), it can be assumed that the volume of wear  $V_e$  occurring on the electrode is equivalent to a cylinder of diameter  $D_e$ , and length  $W_e$  (Figure 4.5 a).

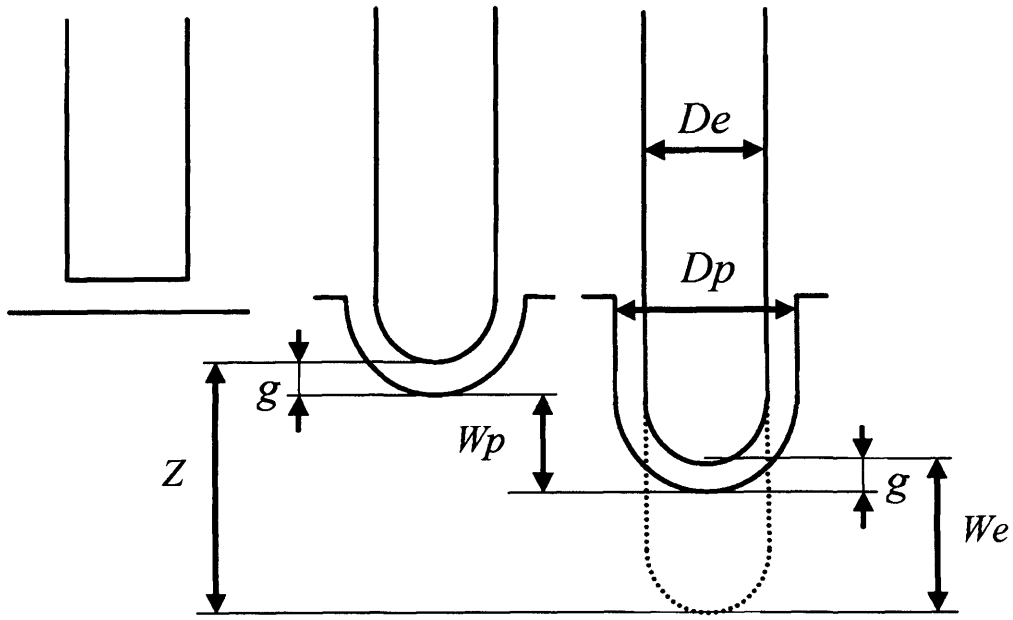
$$V_e = \frac{\pi \cdot D_e^2}{4} \cdot W_e \quad (4.2)$$

A similar assumption can be made when using a tubular electrode (Figure 4.5 b). In this case:

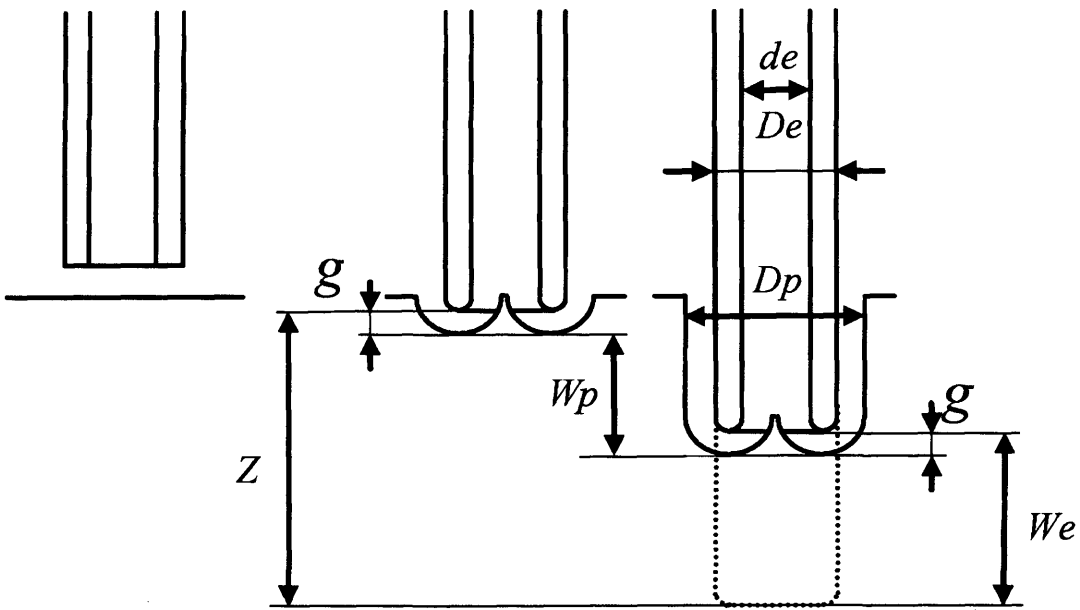
$$V_e = \frac{\pi \cdot (De^2 - de^2)}{4} \cdot We \quad (4.3)$$

The length  $We$  can be measured on the machine by using a datum plane. After each drilling, the electrode tip is brought to the datum plane to establish electrical contact. The position along the  $Z$  axis before and after machining determines the loss of length of the electrode.

The drawback with such a method is that the electrical contact produces a small amount of erosion (Figure 4.6 a) which would cause an error in the measurements of the actual  $We$  value. Figure 4.6 b) shows the deviation in  $Z$  position of 100 attempted measurements on the same spot of the same datum plane.

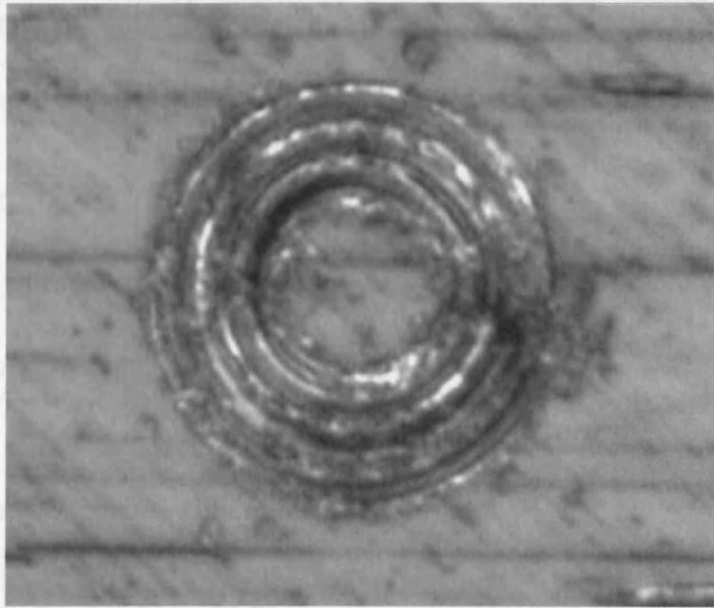


a) Rod electrode

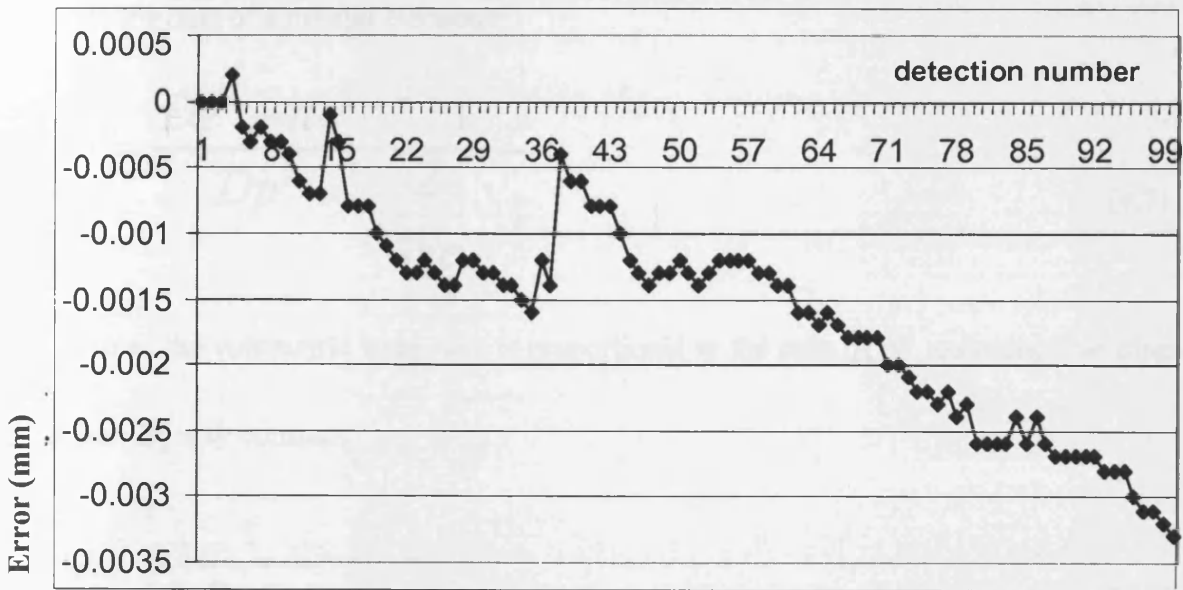


b) Tubular electrode

Figure 4.5 Schematics of erosion to a fixed depth  $Z$  with rod and tubular electrode



a) Datum plane erosion after 100 measurements



b) Error of surface detection

Figure 4.6 Repeatability of electrode measurements



Using a similar assumption for the workpiece regarding the shape deformation and assuming that the spark gap  $g$  is constant, it can be seen from Figure 4.5 that:

$$W_p = Z - W_e \quad (4.4)$$

In the case of a rod electrode:

$$V_p = \frac{\pi \cdot D_p^2}{4} \cdot W_p \quad (4.5)$$

Therefore, the volumetric wear ratio can be defined as:

$$v = \frac{V_e}{V_p} = \frac{D_e^2}{D_p^2} \cdot \frac{W_e}{W_p} = \frac{D_e^2}{D_p^2} \cdot \frac{1}{\frac{Z}{W_e} - 1} \quad (4.6)$$

In the case of a tubular electrode:

$$v = \frac{D_e^2 - d_e^2}{D_p^2} \cdot \frac{1}{\frac{Z}{W_e} - 1} \quad (4.7)$$

Thus, the volumetric wear ratio is proportional to the ratio  $R_w$  assuming that diameters

$D_e$ ,  $d_e$  and  $D_p$  stay constant:

$$R_w = \frac{1}{\frac{Z}{W_e} - 1} \quad (4.8)$$

This method was used to record the evolution of the wear  $W_e$  on the electrode when drilling holes 1 mm in depth with an electrode 170 $\mu$ m in diameter. Drilling was performed in 60 stages and the electrode was measured 60 times to monitor the electrode wear. According to Figure 4.6 b), the error brought due to the electrical contact should not exceed 1.5 $\mu$ m.

### 4.3. Experiments

Three different workpiece materials were investigated: tool steel P20, brass and aluminium. The selection of materials was based on their applicability for conventional tooling and prototype micro tooling.

The electrode material was tungsten carbide (WC) in 170 $\mu$ m diameter tube and rod forms. Before each machining operation, the tip of the electrode was EDM ground flat and taken as a reference in the **Z** direction for further calculations and measurements.

The sparking conditions were as follows:

Voltage ( $U=60$  V);

Current ( $I=0.8$ A);

Time on ( $T_{on}= 1$   $\mu$ sec);

Time off ( $T_{off}= 4.2$   $\mu$ sec);

Electrode Polarity = negative;

Compression =10. The gap compression (a factor between 1 and 50) is the parameter controlling the ignition delay;

Gain=1. The gain (a factor between 1 and 50) is the parameter controlling the sensitivity of the motors to the servo error signals.

The electrode was clamped in a high-speed EDM spindle and was rotated at 2000 rev/min.

Data for electrode wear was collected for the drilling of 6 holes in the three workpiece materials using both rod and tube electrodes. Each hole was drilled in 60 steps. The results obtained for a hole form a data set.

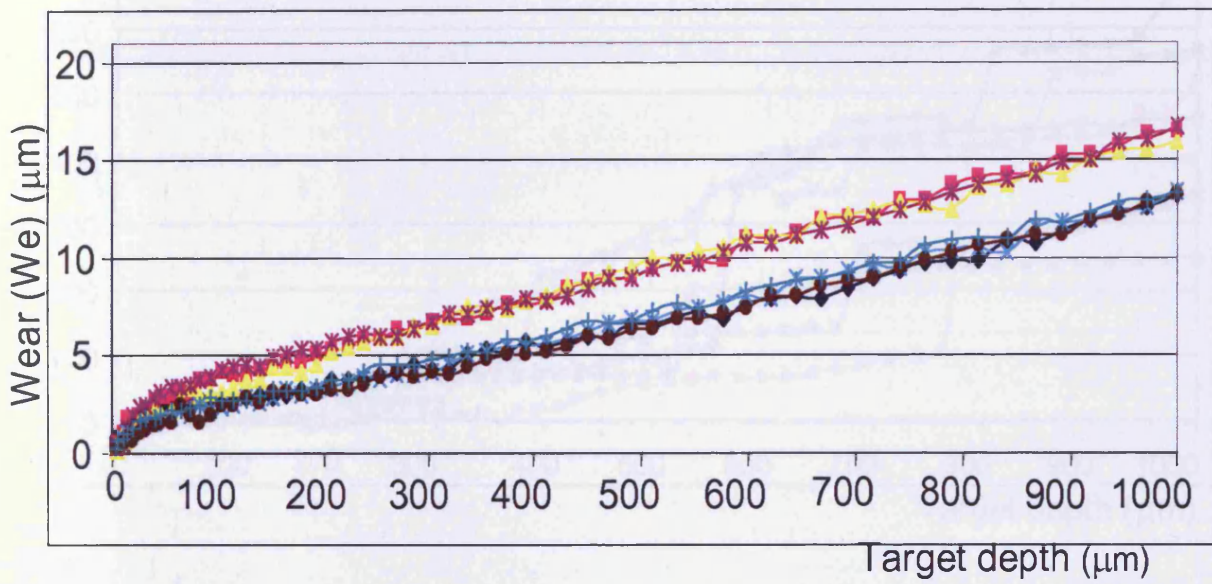
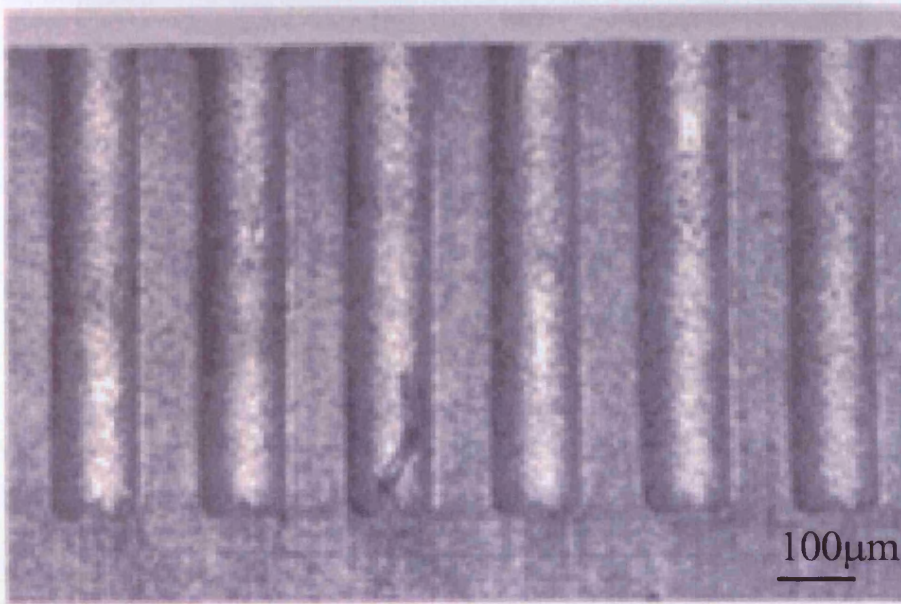
Measurement of electrode wear was performed for each of the 60 steps of the drilling process along the **Z** axis. To avoid long distance positioning errors, the measurement was carried

out by using the top surface of the workpiece as a datum. The accuracy of surface detection for 60 measurements is taken to be  $1.5\mu\text{m}$  (Figure 4.6 b).

#### **4.3.1. Wear measurements for the three different materials**

The evolution of the wear  $We$  was measured for the three workpiece materials and the two types of electrode. Each measurement was repeated 6 times in order to check the repeatability of the process. Figure 4.7 shows the results obtained and a corresponding picture of the cross section of the workpiece. The corresponding data is given in Appendix B.

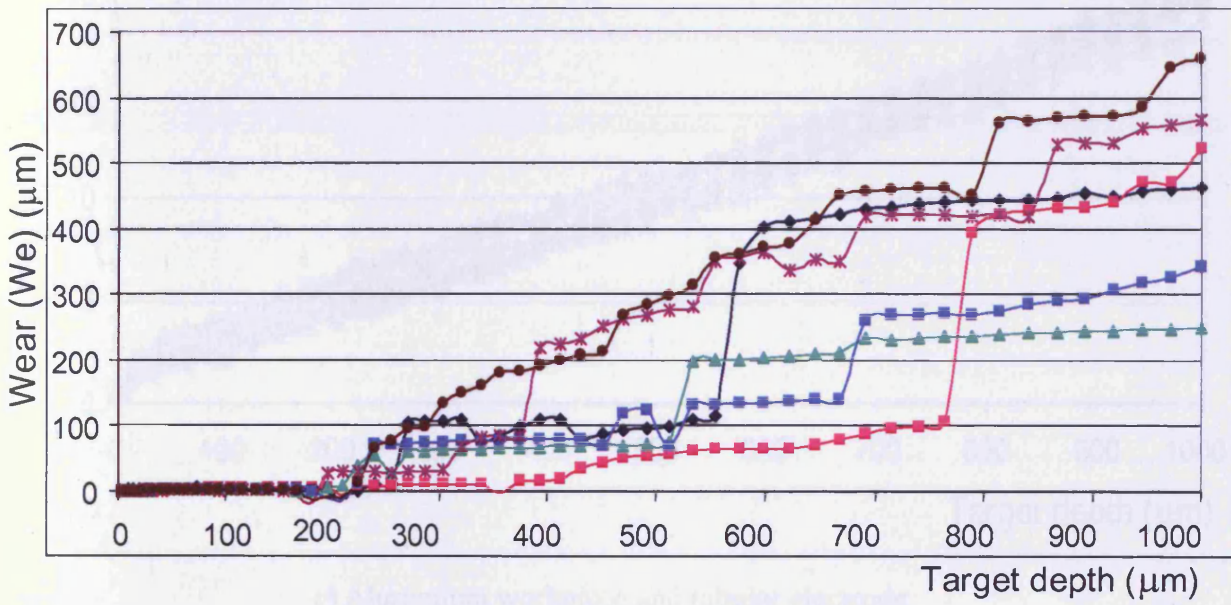
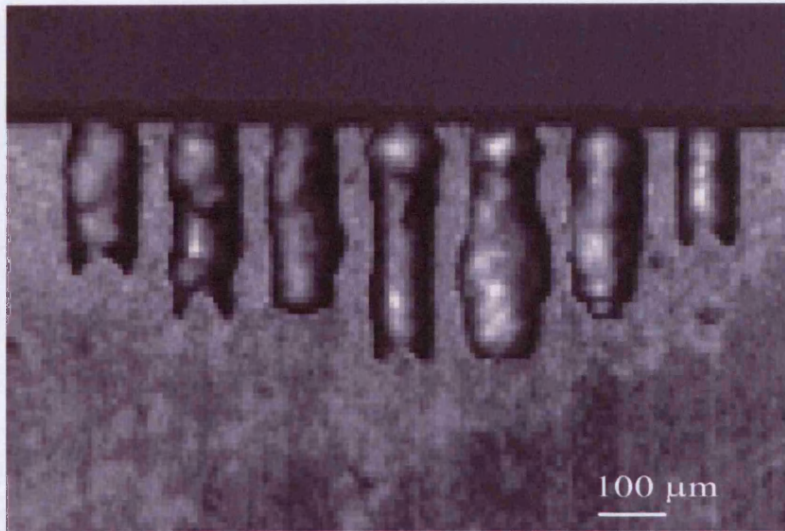
Aluminium and brass have much lower melting points than tool steel and the grain structure consists of much larger grains. With the same spark energy, more material from aluminium and brass will be melted and therefore larger pieces of material will float in the gap as debris than in steel. When using a rod electrode to erode a hole in soft materials like aluminium and brass, after reaching certain depth, the flushing conditions deteriorate rapidly and the larger the debris the more difficult it will be to be flush them out of the sparking area. From that point onwards, debris starts causing sparking on the side of the electrode. This breaks the debris into smaller pieces and finally they are flushed out of the sparking area. This explains the sudden change in electrode wear behaviour, high rate of electrode wear and distortion of the holes as shown in the workpiece cross section pictures when aluminium and brass are drilled using a rod electrode.



a) Brass workpiece and tubular electrode

Figure 4.7 Electrode wear graphs

(to be continued)

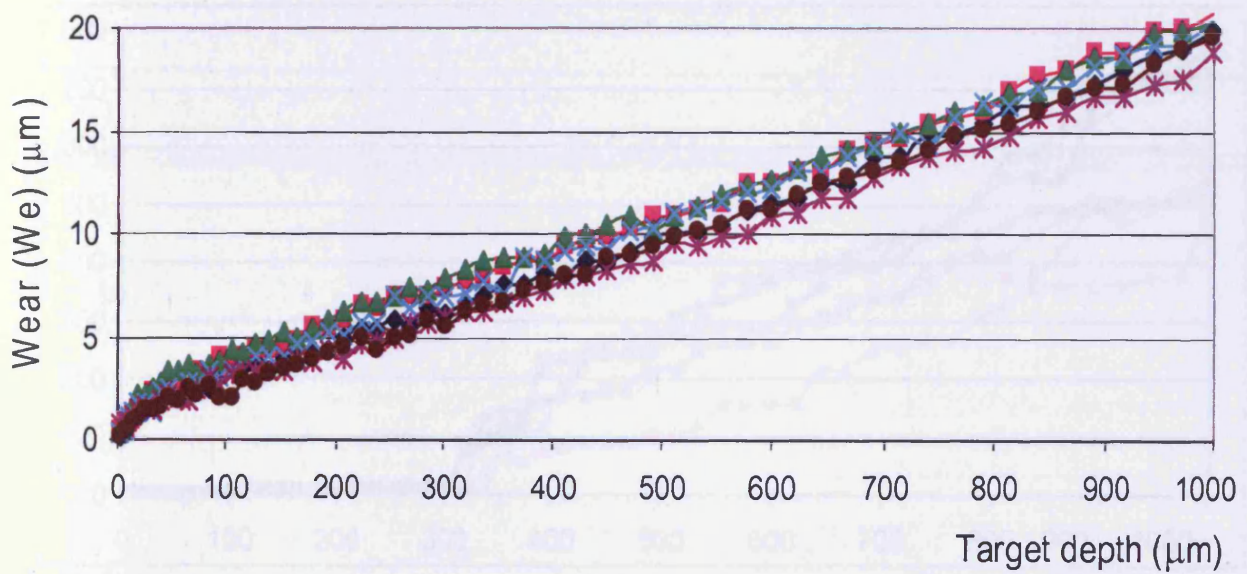
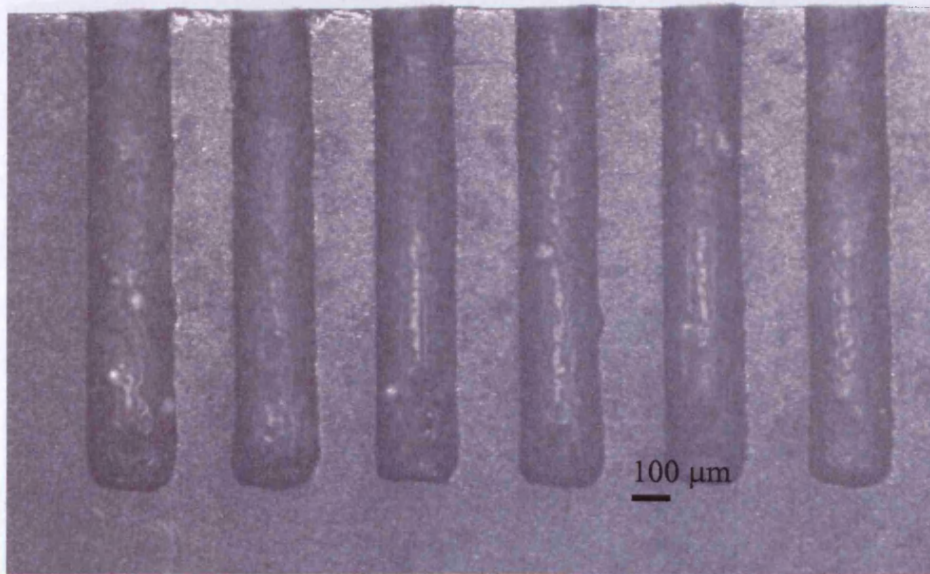


b) Brass workpiece and rod electrode

Figure 4.7 Electrode wear graphs

(to be continued)

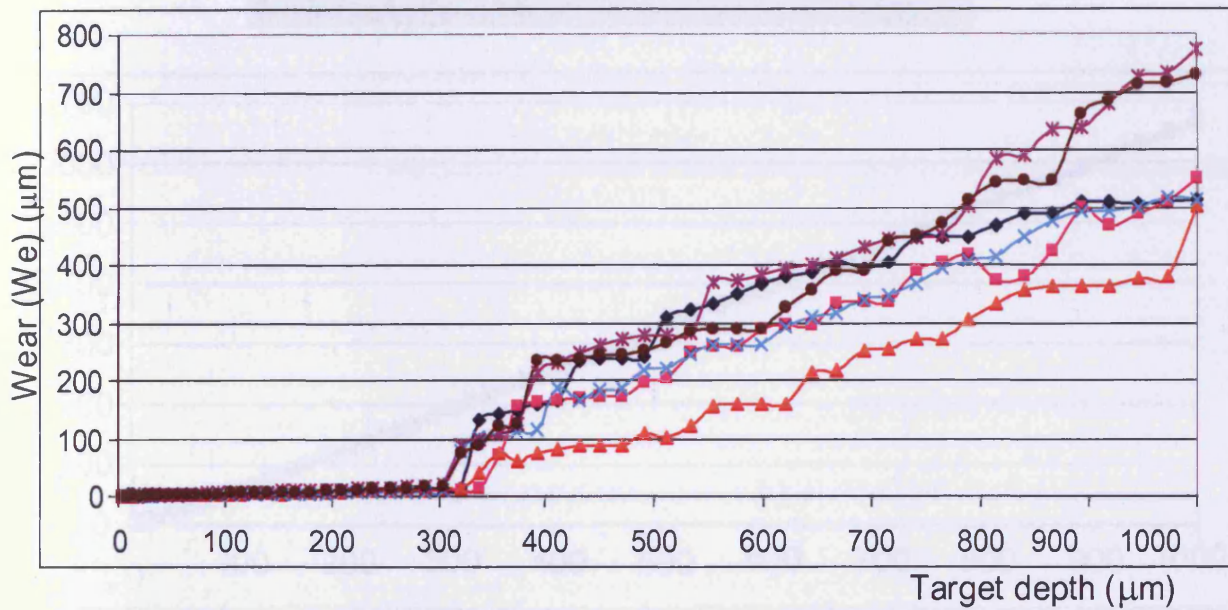
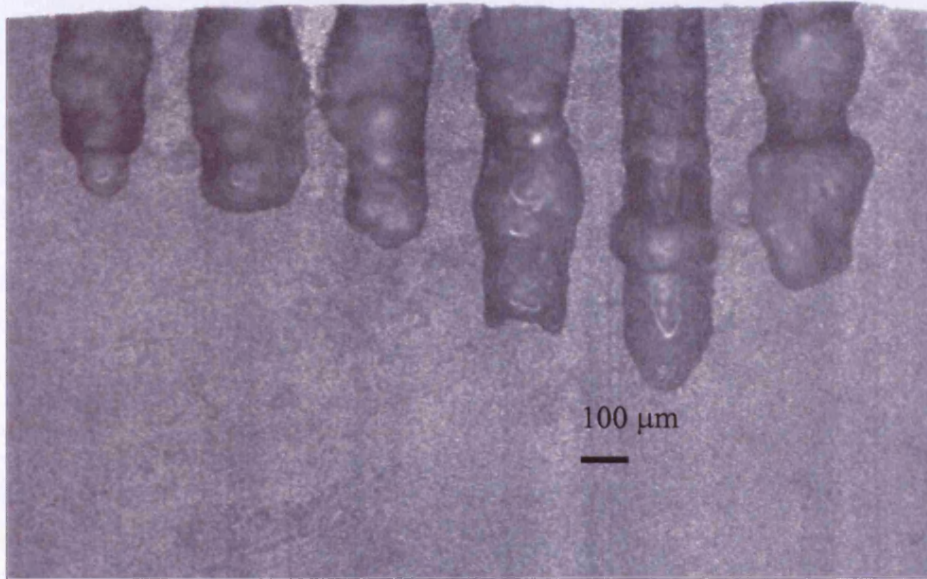




c) Aluminium workpiece and tubular electrode

Figure 4.7 Electrode wear graphs

(to be continued)

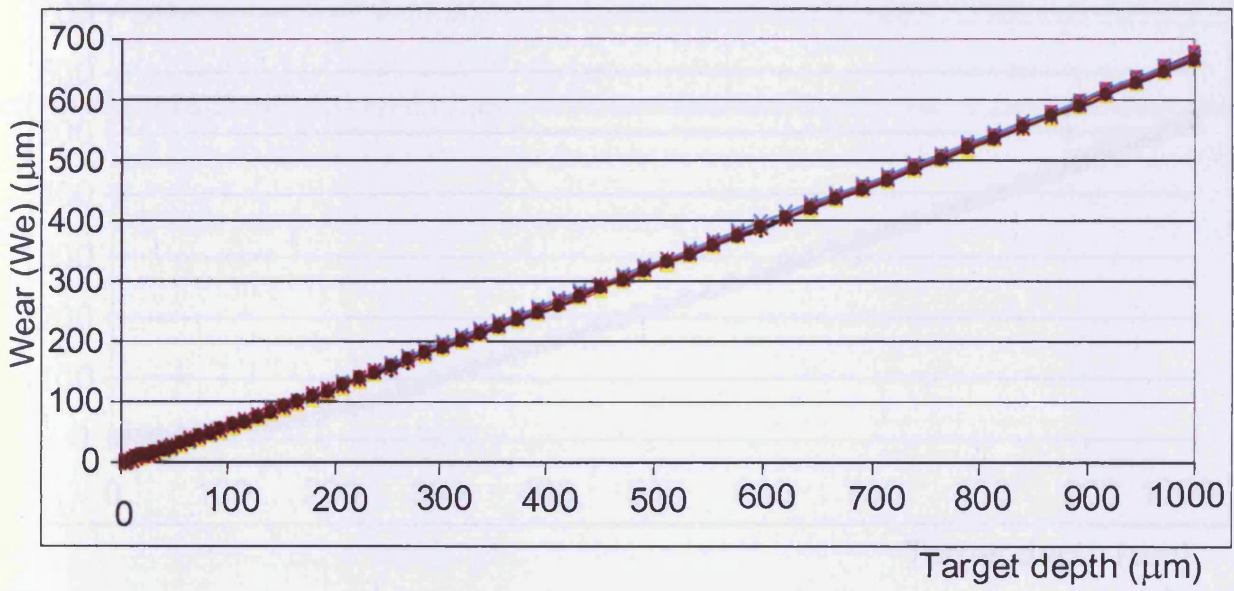
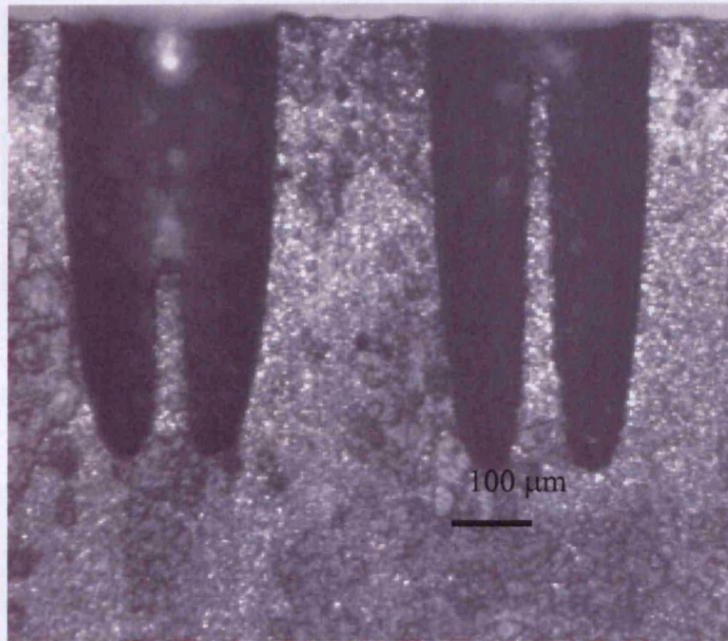


d) Aluminium workpiece and rod electrode

Figure 4.7 Electrode wear graphs

(to be continued)



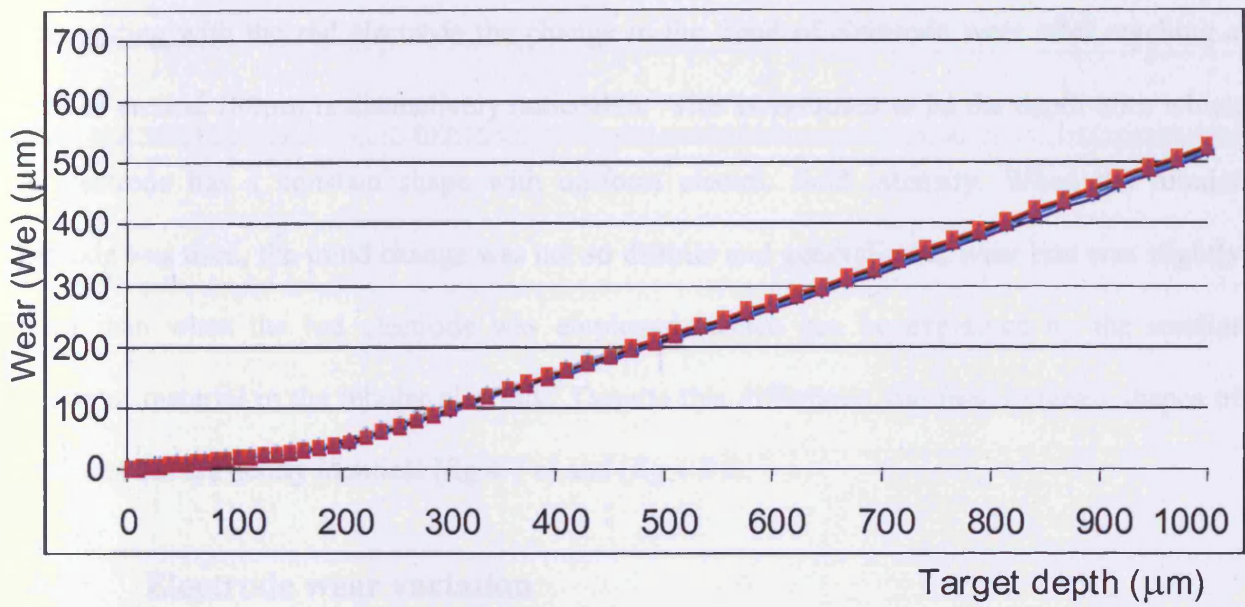
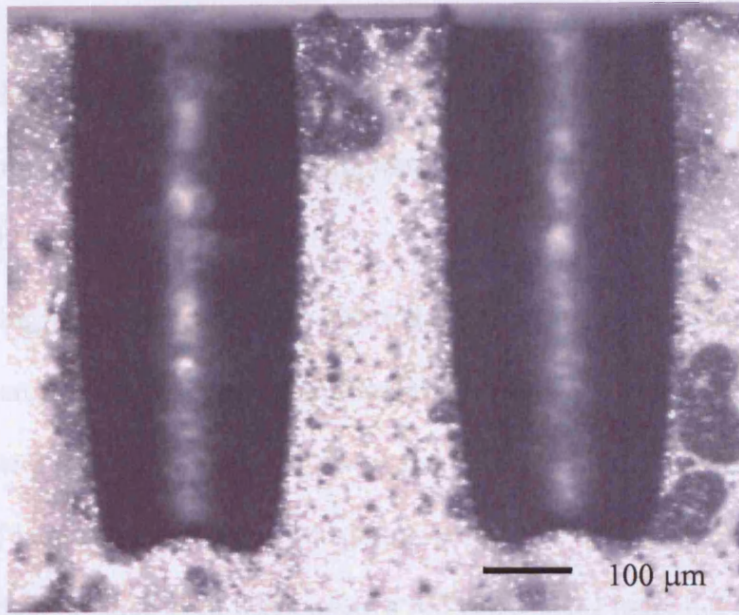


e) Steel workpiece and tubular electrode

Figure 4.7 Electrode wear graphs

(to be continued)





f) Steel workpiece and rod electrode

Figure 4.7 Electrode wear graphs (continued)

If a tubular electrode is used, the flushing conditions do not change much for the whole depth. In spite of the size of the debris, they are forced out of the working area by the constant dielectric flow through the tube and the amounts of electrode wear and variations in wear behaviour are much smaller.

When eroding steel with a tubular electrode, more than 50% of the electrode is worn compared to only around 2% for brass and aluminium. Electrode wear is very similar for rods and tubes in tool steel machining. This can be explained by the much smaller debris size due to the higher melting temperature and smaller grain size of the material. Therefore, the flushing conditions do not change much even when using a rod electrode. Figure 4.7 f) shows that for tool steel eroding with the rod electrode the change in the trend of electrode wear after reaching a depth of around 180µm is distinctively noticeable. This is assumed to be the depth after which the electrode has a constant shape with uniform electric field intensity. When the tubular electrode was used, the trend change was not so distinct and generally the wear rate was slightly higher than when the rod electrode was employed, which can be explained by the smaller volume of material in the tubular electrode. Despite this difference, the final external shapes of the electrodes are nearly identical (fig 4.7 e) and (fig 4.7 f).

### 4.3.2. Electrode wear variation

For the six sets of data, each obtained from drilling in one workpiece material with one electrode shape, the difference  $M_{dif}^z$  between the smallest and largest measured wear for a specific target was calculated. This is used to indicate the variation of the electrode wear for the same sparking conditions.

$$M_{dif}^z = We_{\max}^z - We_{\min}^z \quad (4.9)$$

Figure 4.8 shows the values of  $M_{dif}^z$  for the 6 holes at each targeted depth for each workpiece material and electrode type.

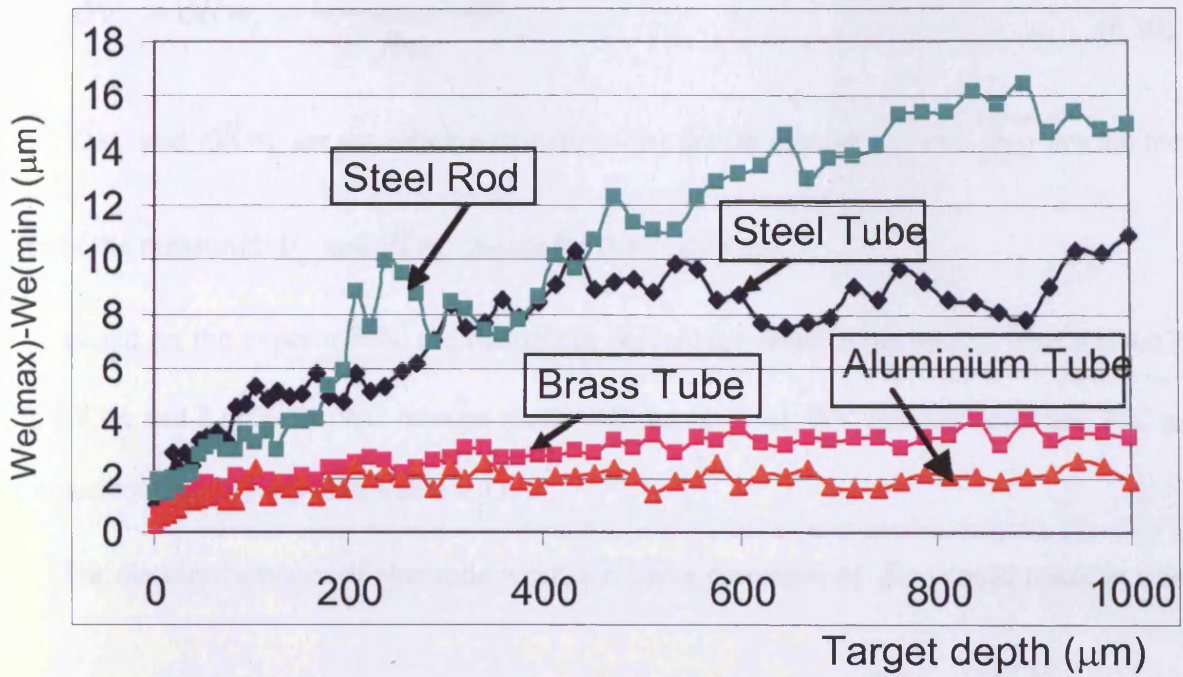
When using a rod electrode on brass and aluminium (Figure 4.8 b), the differences in wear measurement start increasing dramatically from a certain depth. This is mainly because of the deteriorated flushing conditions. Due to the strong stochastic character shown, those measurements could not lead to useful conclusions regarding variations in the amount of wear and the wear ratio.

In the case of the steel workpiece, the flushing conditions do not have such a dramatic effect as explained above, but in comparison to the tubular electrode, the rod electrode shows an increasing variation in the wear ratio with the depth of the hole (Figure 4.8 a).

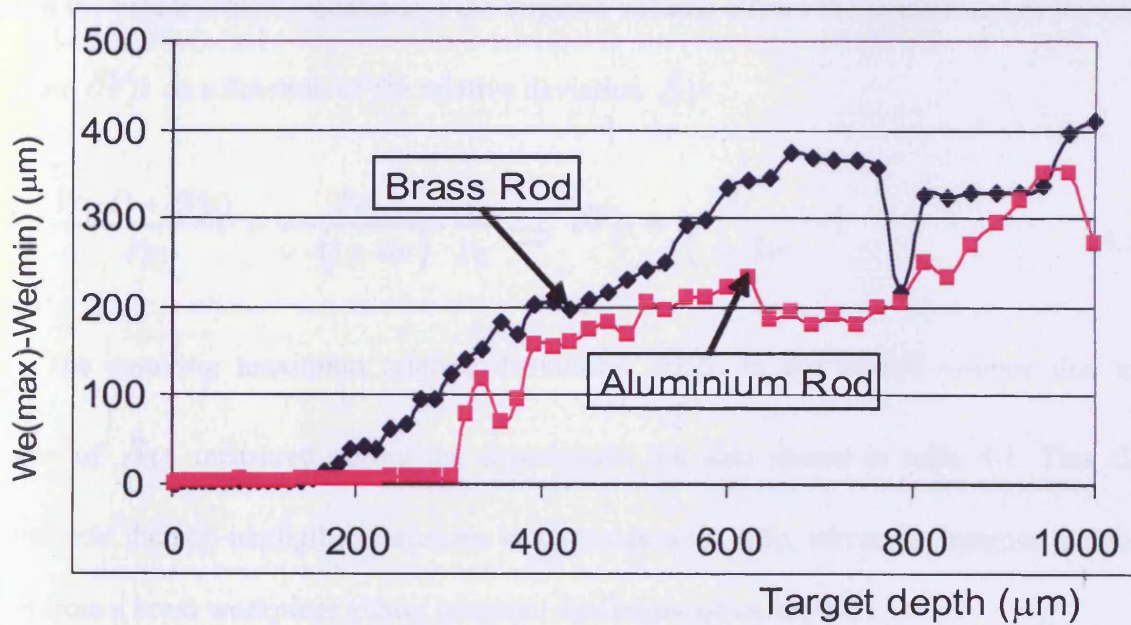
With the tubular electrode used on the three workpiece materials, the variation in the wear ratio after a certain depth shows a tendency to stabilise (Figure 4.8 a). The volumetric wear ratio proportionality factor  $Rw$  (equation 4.8) was evaluated for each of the six data sets. For the purpose of the experiment  $We$  is not the measured value of electrode wear but the amount of wear predicted using the linear regression ( $W_e^{trend}$ ). The regression line was created only for the data obtained after the electrode shape became constant, which eliminates the error from the initial period of erosion with non uniform electric field intensity. Using the predicted wear instead of the measured values not only avoids errors in the measurement of electrode wear but also reveals the stochastic character of the trend lines indicating variations of the systematic factors.

For each of the six data sets, the relative deviation  $\delta v_i = \frac{\Delta v_i}{\bar{v}} = \frac{|v_i - \bar{v}|}{\bar{v}}$  is equal to

the relative deviation,  $\delta Rw_i$  which is defined as follows:



a) wear variation using WC rod and tubular electrode with steel, aluminium and brass workpiece



b) wear variation using WC rod electrode with aluminium and brass workpiece

Figure 4.8 Variation of electrode wear

$$\delta v_i = \delta R w_i = \frac{|R w_i - \overline{R w}|}{\overline{R w}} \quad (4.10)$$

$\delta v_i$  and  $\delta R w_i$  are the relative deviations for the  $i$ th data set,  $\overline{v}$  and  $\overline{R w}$  are the mean values of the measured  $v_i$  and  $R w_i$  values for the  $i^{\text{th}}$  data set.

Based on the experiments, the maximum percentage relative deviations  $\delta v$  are 4.67%, 4.5%, 9.83% and 3.66% for WC tube on steel, WC rod on steel, WC tube on brass and WC tube on aluminium respectively (see Table 4.1).

For the same amount of electrode wear, a relative deviation of  $\delta v$  would result in a non-negligible deviation in the volume eroded from the workpiece  $\delta V p = \frac{\Delta V p}{V p}$ . The ratio between the actual eroded volume and the targeted volume allows the assessment of the relative deviation  $\delta V p$  as a function of the relative deviation  $\delta v$ .

$$\frac{V p \cdot (1 + \delta V p)}{V p} = \frac{V e}{v \cdot (1 + \delta v)} \cdot \frac{v}{V e} \Rightarrow \delta V p = \frac{1}{1 + \delta v} - 1 \quad (4.11)$$

The resulting maximum relative deviations  $\delta V p$  in the eroded volume due to the variation of  $\delta v$  measured during the experiments are also shown in table 4.1. This clearly demonstrates the non-negligible variations in electrode wear ratio, where for instance the volume eroded from a brass workpiece shows potential deviations of up to 9%.

The variations shown in Table 4.1 are not affected by any repeatability and machine positioning errors, because those errors are not cumulative and therefore should not influence the trend line orientation. They are due only to uncontrolled factors which result in an inconstant wear ratio.



### 4.3.3. Spark gap variation

The spark gap is an important criterion for the micro EDM process as it determines the final accuracy of the machined features. According to equations (4.6) and (4.7), the variation in the wear ratio  $v$  depends on the two parameters  $D_p$  and  $W_e$ .  $D_p$  is the diameter of the drilled hole and the main variation in  $D_p$  is due to changes in the spark gap during the EDM process. By assessing both variable parameters ( $D_p$ ,  $W_e$ ), it is possible to draw conclusions regarding the variation of the wear ratio.

For each data set, the diameter of the drilled hole was measured and the results plotted in Figure 4.9. The photographs below each plot show the holes drilled with a WC electrode rod or tube and the marks left from the measurements of  $W_e$ .

Table 4.2 shows the measurements obtained and the calculated 6-sigma ( $6\sigma$ ) variation in hole diameter. Note that this variation includes the error in the positioning repeatability of the machine after each measurement of electrode wear. According to (Pham et al, 2004), for such short movements, this error does not exceed  $\pm 1\mu\text{m}$ .

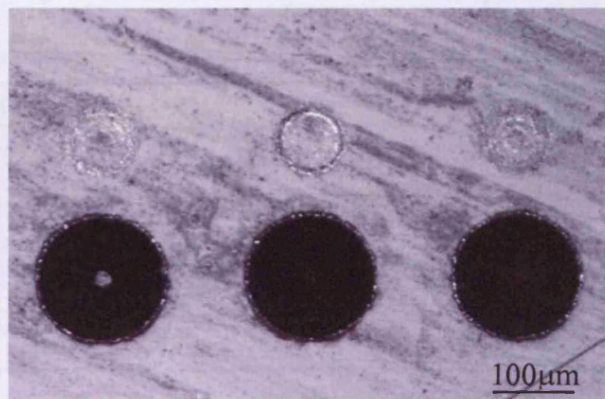
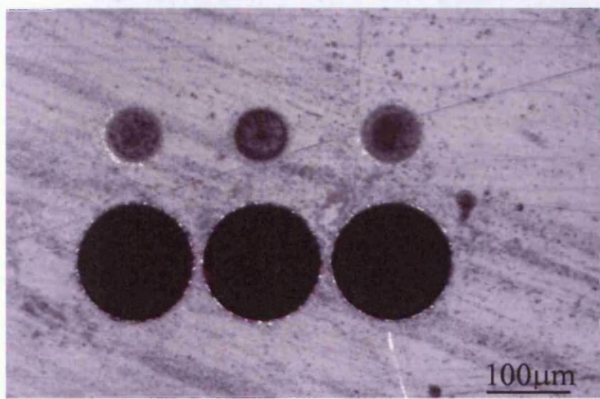
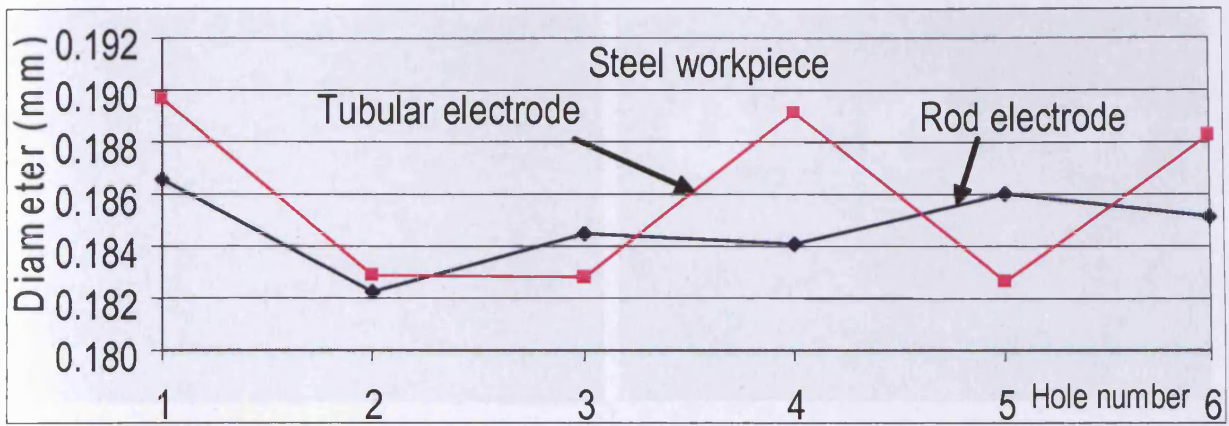
In the cases of holes drilled in aluminium and brass, using rod electrodes, the distortion of the hole is obviously due to the side sparking caused by the debris. Although this makes the hole diameter larger than normal, for aluminium and brass workpieces, the variations in hole diameter were small. In the steel workpiece, there is no noticeable difference in the diameter of the holes, but the variation was larger when the tubular electrode was used. This can be explained by the forced flushing applied in the case of the tubular electrode, where larger debris were forced out of the spark gap possibly causing side sparking. This result also confirms the relative deviations  $\delta v$  shown in Table 4.1, which are similar for the two types of electrodes.

workpiece	electrode	Min Rw	Max Rw	Mean Rw	Max $\delta\sigma$	Max $\delta V_p$
Steel	WC tube	2.123634	2.28415	2.182234	0.046703	-0.0446
Steel	WC rod	1.422847	1.556779	1.489695	0.045032	-0.0431
Brass	WC tube	0.011923	0.014522	0.013223	0.098335	-0.0895
Aluminium	WC tube	0.018228	0.01961	0.01892	0.036581	-0.0353

Table 4.1 Data for electrode wear variation

Workpiece	Steel		Brass		Aluminium	
	Rod	Tube	Rod	Tube	Rod	Tube
1	0.187	0.190	0.195	0.180	0.190	0.182
2	0.182	0.183	0.192	0.179	0.187	0.179
3	0.185	0.183	0.193	0.178	0.189	0.181
4	0.184	0.189	0.190	0.178	0.189	0.179
5	0.186	0.183	0.193	0.178	0.189	0.181
6	0.185	0.188	0.193	0.178	0.188	0.180
<i>Mean</i>	<i>0.185</i>	<i>0.186</i>	<i>0.179</i>	<i>0.193</i>	<i>0.189</i>	<i>0.180</i>
<i>Max. Diff</i>	<i>0.004</i>	<i>0.007</i>	<i>0.003</i>	<i>0.004</i>	<i>0.002</i>	<i>0.003</i>
6 sigma	0.009	0.021	0.008	0.006	0.006	0.0068

Table 4.2 Data for spark gap variation



a) WC rod electrode in steel workpiece

b) WC tube electrode in steel workpiece

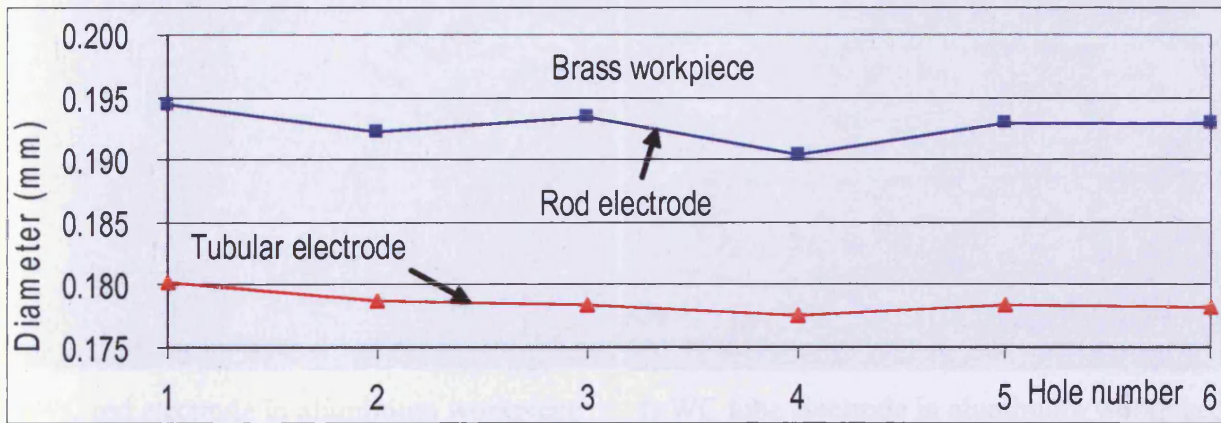
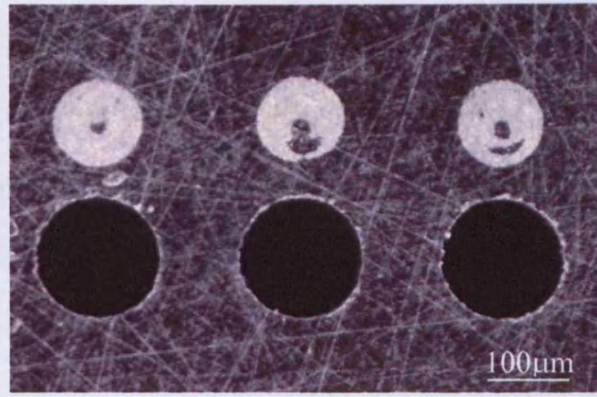
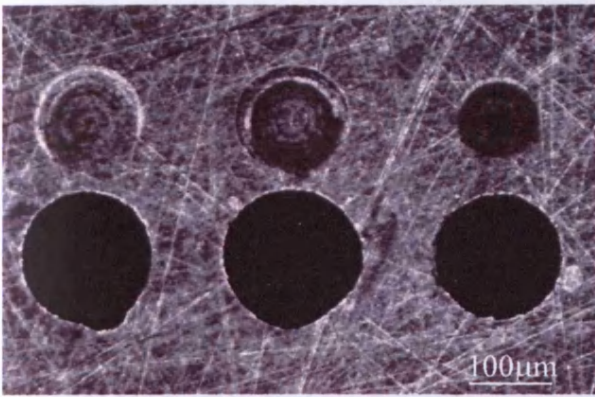


Figure 4.9 Variation of the spark gap

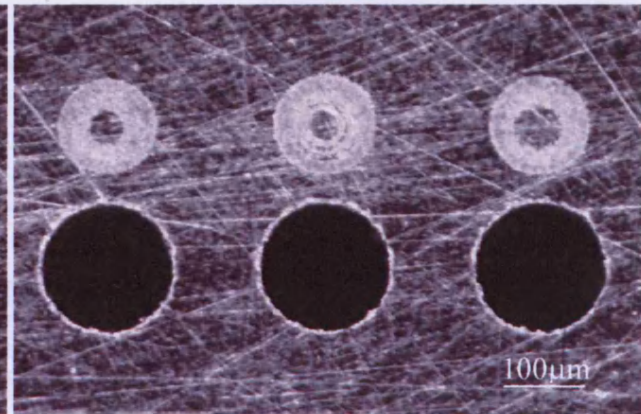
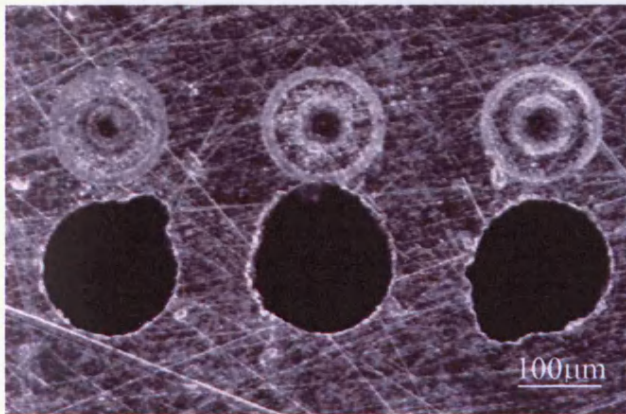
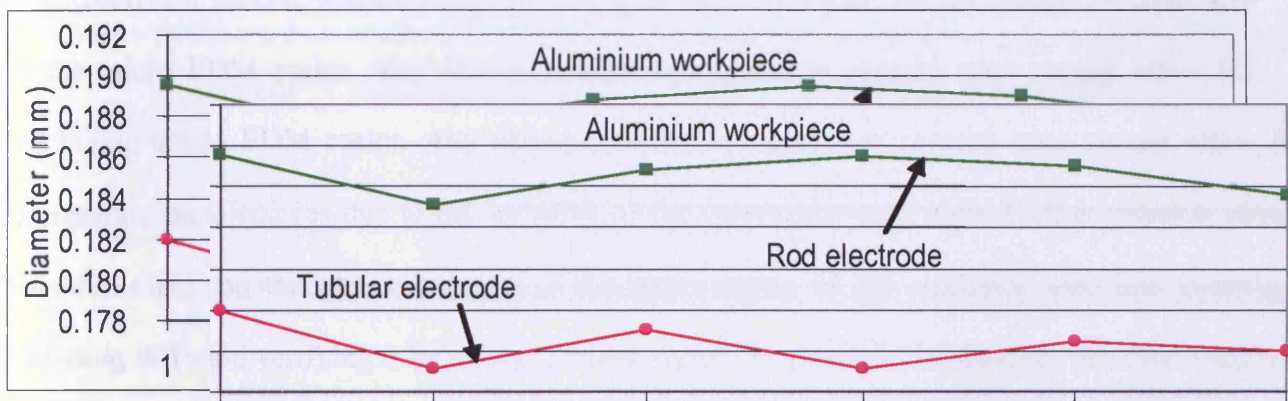
(to be continued)





c) WC rod electrode in brass workpiece

d) WC tube electrode in brass workpiece



e) WC rod electrode in aluminium workpiece

f) WC tube electrode in aluminium workpiece

Figure 4.9 Variation of the spark gap (continued)

#### **4.4. Summary**

In this chapter it was shown that electrode wear is the main phenomenon accompanying the EDM process and contributing to the accuracy and quality achievable. Understanding the electrode wear process and its influencing factors is the key to more accurate and reliable micro EDM. A deeper understanding of electrode wear, particularly for the micro EDM process, is essential for further process improvements and adopting machining strategies or electrode wear compensation methods. The above investigation has shown that variations of the wear ratio due to uncontrolled factors, when machining commonly used materials, are not negligible especially in the micro EDM realm. Any electrode wear compensation method used should allow for machining tolerances due to the variation of the volumetric wear ratio. Further research should concentrate on the physical nature of the phenomenon of the electrode wear and creating a hypothesis and verifying it by testing a wider variety of materials, or specially selected materials, including different grain structures and investigations of inter-grain boundaries and the effect of the material on electrode wear and its variation. When using any new combination of electrode/workpiece materials and for any new diameter of electrode, tests should be conducted on the machine to measure the wear ratio and assess its repeatability. The results should be used to justify a compensation method and strategies for material removal.

"Thou shalt not make unto thee any graven image....." (Exodus 20:4).

# *Chapter 5*

## **5. Natural tolerances of the Micro EDM process**

As mentioned in the previous chapters 2, 3 and 4 electrical discharge machining (EDM) is a process where material is removed from both of the electrodes, the workpiece and the tool.. When the electrical parameters driving the process are set to its minimum, a minimum electric power and respectively minimum energy is released so micro EDM can produce features that are on the micrometric scale. The designation 'micro electric discharge machining' (micro EDM) is therefore used in these cases (Egashira et al, 2006).

The smaller the nominal energy, the smaller the expected value of the unit removal (UR) will be. Unit removal is defined usually only as 'the part of a workpiece removed during one cycle of removal action' (Masuzawa, 2000). In micro EDM, UR is therefore the material removed from the workpiece electrode during one discharge.

When producing features and parts on the micro scale, the phenomenon that takes place between the electrodes in electric discharge machining (EDM) is still not fully understood. A barrier to a complete exploitation of the potential natural tolerance of this process and to the further development of the process towards the production of components on the nano-scale is therefore in place. Improvements in measuring systems contribute to the acquisition of new information that often conflicts with existent theoretical models of the EDM process (Pillans et al, 2002). The objective of this chapter is to advance the theoretical and experimental knowledge of the electrical discharges during micro EDM operations. In particular, the aim of this investigation is to identify the potential boundary phenomenon change for the micro EDM process and what effects the electrode materials have on selected electrical characteristics of the discharge process, if any exists. A possible basis for an analytical micro EDM model of electrode wear is suggested, verification of which requires experimental work with pure metals. This chapter studies the influence of factors contributing to electrode-tool wear during the micro EDM process of pure metals and the effect of the electrode wear on the process accuracy and

process variability (Ivanov et al, 2007, 159-168). An exploratory data analysis (EDA) approach was adopted in order to draw conclusions from the performed experimental activities.

## 5.1 Factors affecting electrode shape change

In Chapter 4 it was explained how with the help of Vector Field software, OPERA-3d, which is a finite element environment for analysis and design of electromagnetic applications in 3 dimensions, it was possible to create a Finite Element Analysis (FEA) model of the electrostatic field, in the medium between the two electrodes in the EDM process. OPERA-3d software contains a suite of analysis modules, capable of solving the complete spectrum of static and low frequency electromagnetic applications. The electrodes used in micro EDM are very simple in shape and during the EDM process are spinning, which therefore creates uniform conditions all round the electrode. These uniform sparking conditions permit the use of electrostatic field modelling of the medium between the electrodes. In this research it is used to predict the shape of the tool-electrode and the workpiece electrode change at any stage of the process.

The electric field between the electrodes is defined as the electric force per unit charge. The direction of the field at a point is defined by the direction of the electric force exerted on a positive test charge placed at that point. The strength of the field is defined by the ratio of the electric force on a charge at a point to the magnitude of the charge placed at that point. It is known that electric fields contain electrical energy with energy density proportional to the square of the field intensity (Hambley, 2002). The electric field is defined as the proportionality constant between charge and force:

$$E = \frac{F}{q} \tag{5.1}$$

**F** is the **electric force** given by Coulomb's law, and **q** is the charge of a "test charge".

The electric field surrounding a point charge is given by Coulomb's law:

$$E = \frac{1}{4\pi\epsilon_0} \frac{Q}{r^2} \hat{r} \quad (5.2)$$

where:

$Q$  is the charge of the particle creating the electric field,

$r$  is the distance from the particle with charge  $Q$  to the E-field evaluation point,

$\hat{r}$  is the Unit vector pointing from the particle with charge  $Q$  to the E-field evaluation point,

$\epsilon_0$  is the permittivity in vacuum (also called **permittivity of free space** or the **electric constant**).

$$\epsilon_0 = \frac{1}{c^2 \mu_0} \approx 8.8541878176 \times 10^{-12} \text{ F/m (or } C^2/(N \text{ m}^2)), \quad (5.3)$$

where:

$c$  is the speed of light

$\mu_0$  is the permeability of vacuum.

The permittivity of a linear isotropic homogeneous material is usually given relative to that of vacuum, as a relative permittivity  $\epsilon_r$  (also called dielectric constant). The actual permittivity is then calculated by multiplying the relative permittivity by  $\epsilon_0$ :

$$\epsilon = \epsilon_r \epsilon_0 = (1 + \chi_e) \epsilon_0 \quad (5.4)$$

where

$\chi_e$  is the electric susceptibility of the material.

According to Equation (5.2) above, the electric field is dependent on position. The electric field due to any single charge falls off as the square of the distance from that charge.

Electric fields also follow the superposition principle. If more than one charge is present, the total electric field at any point is equal to the vector sum of the respective electric fields that each object would create in the absence of the others.

$$E_{total} = \sum_1^n E_i = E_1 + E_2 + \dots E_n \quad (5.5)$$

If this principle is extended to an infinite number of infinitesimally small elements of charge, the following formula results:

$$E = \frac{1}{4\pi\epsilon_0} \int \frac{\rho_{unit}}{r^2} \hat{r} dV \quad (5.6)$$

where:

$\rho_{unit}$  is the charge density, or the amount of charge per unit volume.

For the process of predicting electrode shape change, the process of removing material from both electrodes should be considered as a function on one side of the intensity of the electrostatic field ( $|E|$ ) and, on the other, as a function of the relative wear ratio  $\mathbf{v}$  (equation (4.1)). Finite Element Analysis (FEA) modelling of the intensity of the electrostatic field provides a solution to the prediction of where the next sparks in the EDM process are most likely to be distributed, however the relative wear ratio determines how much material will be removed from both the tool-electrode and the workpiece-electrode. Therefore through the combination of tool and workpiece initial shapes, different tool and workpiece materials and different sparking conditions, various final shapes of electrodes/workpiece can be achieved. Figure 5.1 (Bigot et al 2006) shows an example where the different sparking conditions produce different electrode shapes but at the same time the similarity of the final shapes in the three experiments is striking.

The small differences in the shapes in the three experiments are due to the variability of the process and material parameters.

Figure 5.2 shows a zoom view of the simulated electric field intensity in the sparking gap region. For the simulation the wear ratio is selected to be  $v = \frac{1}{2}$ , which is a common wear ratio for micro EDM process (Kozak, 2001) and all sparking conditions, electrode material and dielectric properties are taken from the real process parameters. The simulation shows higher electric field intensity near the sharp edge, shown in 5a, as the tool-electrode progresses through as in 5 b-d, the electric field intensity region is distributed around the tool-electrode periphery, which is eventually reflected on the wear regions of the tool-electrode. The complete simulation is done for every 10  $\mu\text{m}$  depth and electrode shapes are modified based on the electric field intensity and assumed wear ratio.



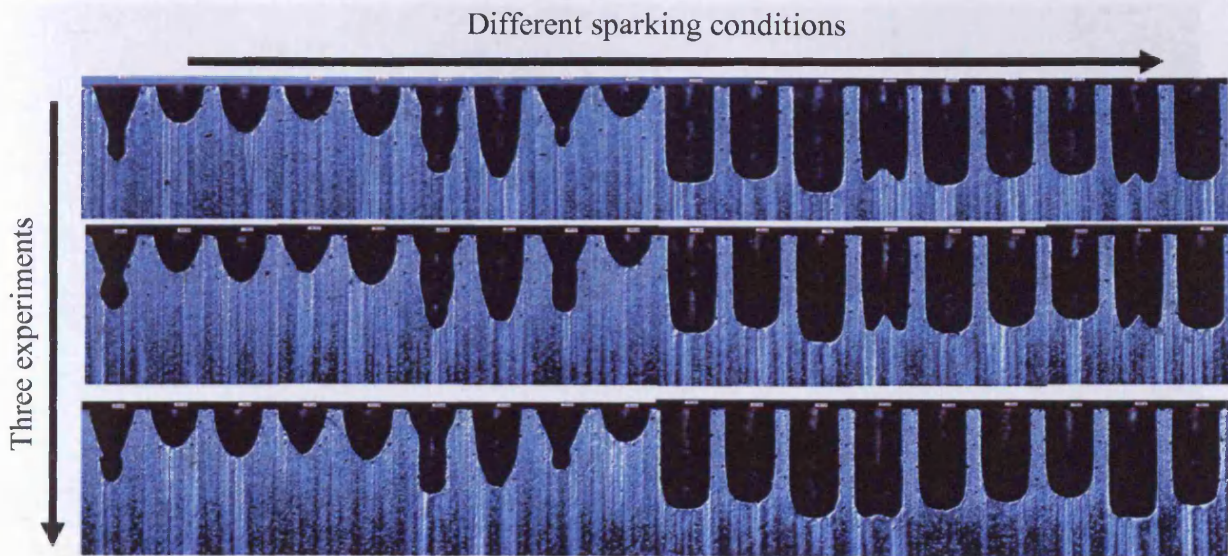
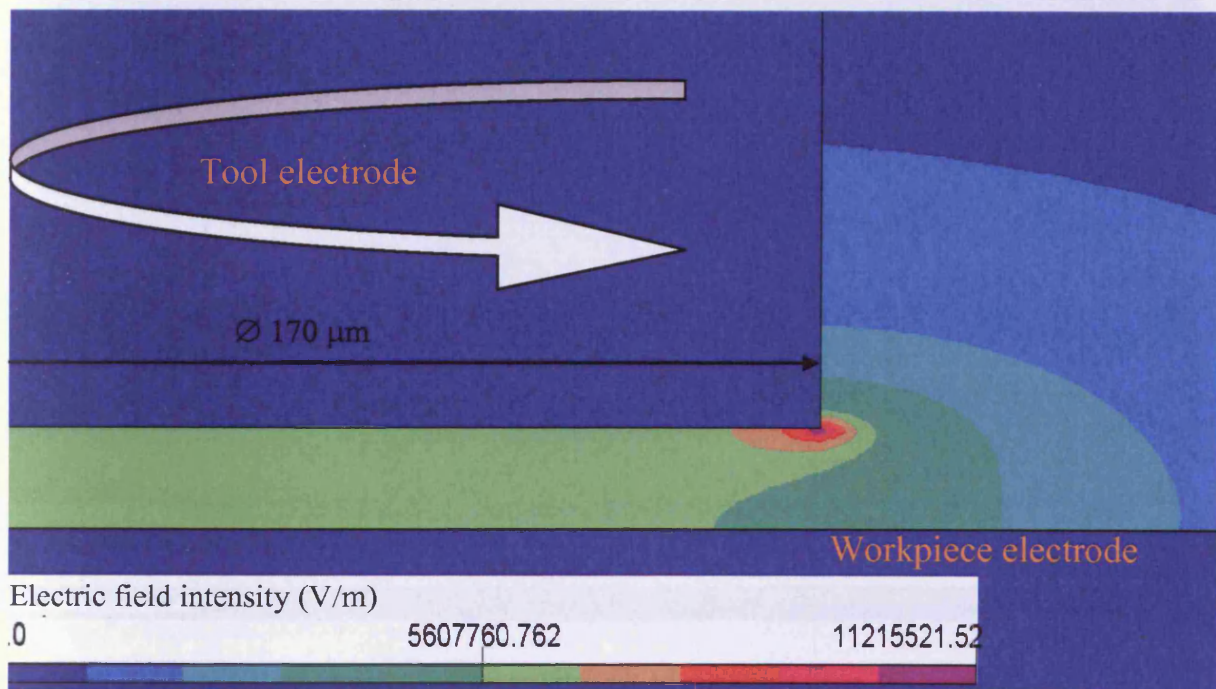


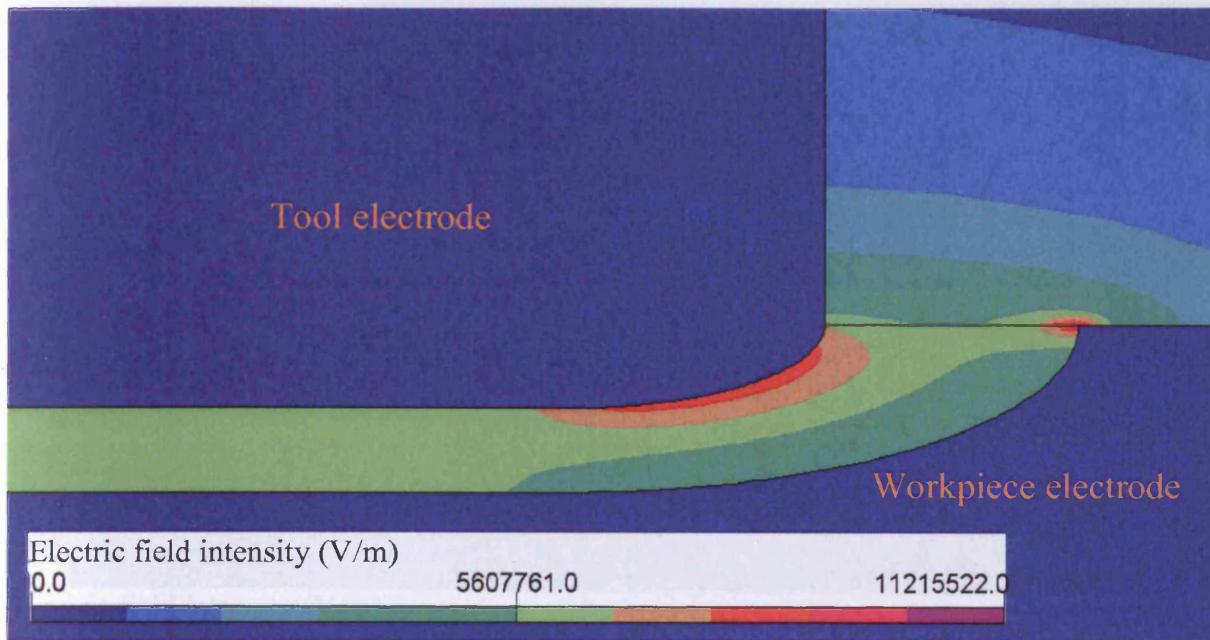
Figure 5.1 Examples of different final shapes achieved by different sparking conditions



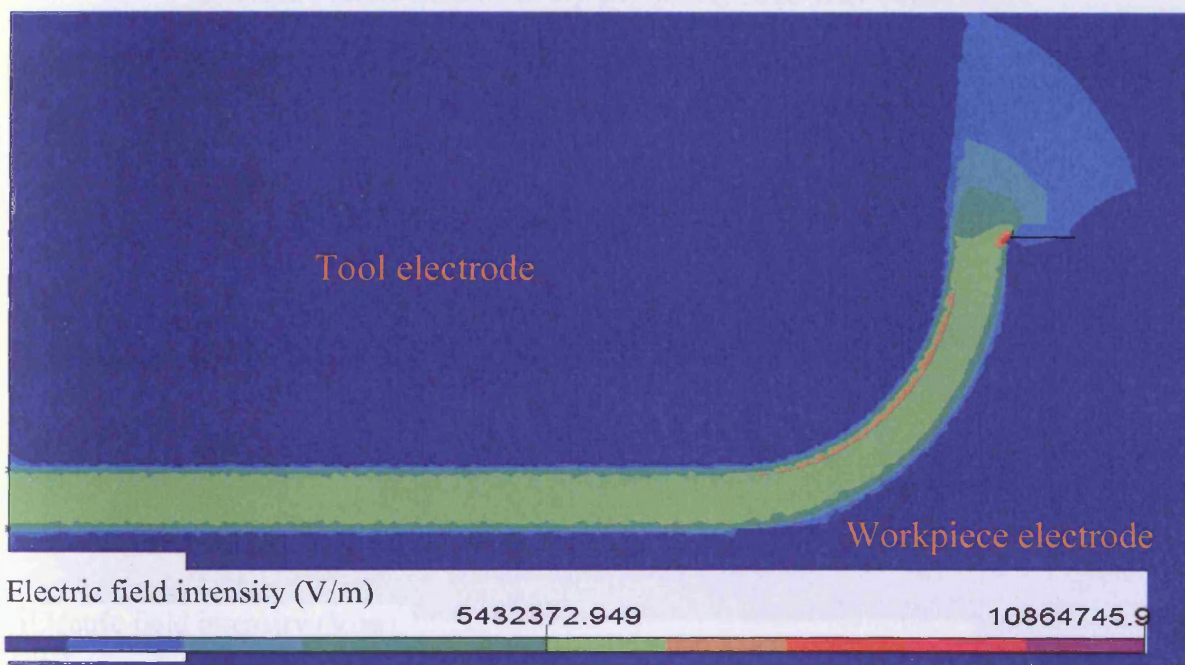
a) Electro static field intensity  $|E|$  of electrode at start

Figure 5.2 Electric field strength  $|E|$  (V/m) in the sparking gap area

(to be continued)



b) Electro static field intensity  $|E|$  of electrode after 10 $\mu$ m depth

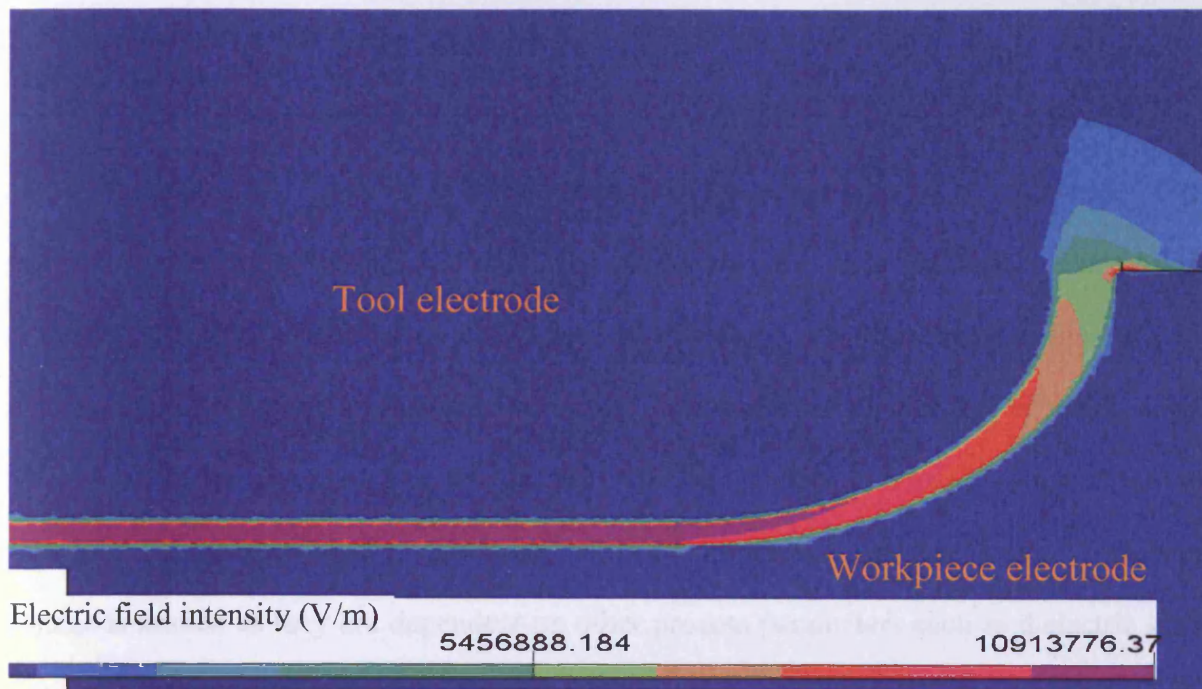


c) Electro static field intensity  $|E|$  of electrode after 40 $\mu$ m depth

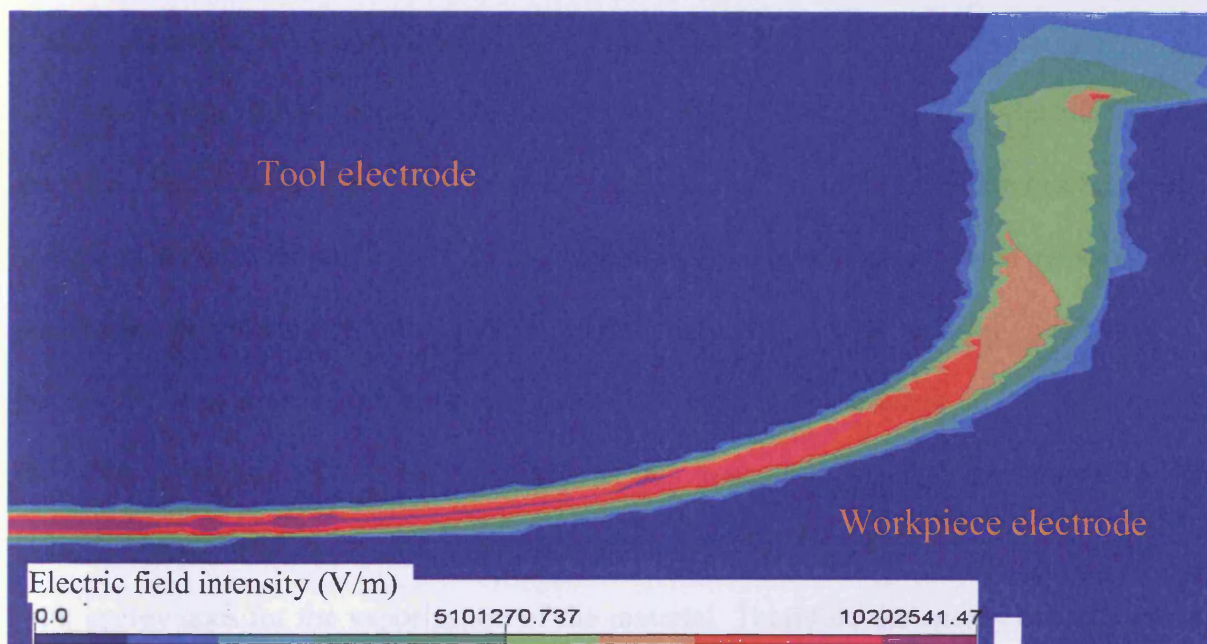
Figure 5.2 Electric field strength  $|E|$  (V/m) in the sparking gap area

(to be continued)





d) Electro static field intensity  $|E|$  of electrode after 60 $\mu$ m depth



e) Electrostatic field intensity  $|E|$  of electrode after 60 $\mu$ m depth and progressing down

Figure 5.2 Electric field strength  $|E|$  (V/m) in the sparking gap area (continued)

## 5.2. Factors affecting electrode wear ratio in micro EDM

In order to feed representative data for the wear ratio from the micro EDM process in to the above simulation, the boundaries of the micro EDM process have to be determined and the mechanism of material removal clarified. For that purpose it is assumed that the spark pulses are as shown in figure 5.3 (Yu et al, 2003; Semon, 1975). To enter the realm of the micro EDM process, the time for the discharge pulse is set to its minimum as it is one of the most crucial parameters in the process. And for the micro EDM process it is used as the main control parameter for the spark energy (Kunieda, et al, 2005). Control over the discharge current and voltage is limited as they are dependent on other process parameters such as dielectric strength, material properties etc. Typically in micro EDM, discharge times of  $1\mu\text{s}$  or less are applied (Kunieda, et al, 2005). Some authors consider that even a discharge time of less than  $5\mu\text{s}$  is enough to consider the process micro EDM (Egashira et al, 2006).

Most of the EDM process models regard the material removal as a combination of melting and vaporization as described in chapter 2, where the volume of material that has been removed through melting is much larger than the volume of material that has been removed through vaporisation. Verification of these models 'suffer' big discrepancies especially in the low energy sparks with very quick discharge times (DiBitonto et al, 1989; Eubank et al, 1993; Patel et al, 1989; Sun & Cheng, 2007). The assumption in this research is that with low energy sparks and quick discharge times there is a negligible amount of molten material and the majority of the spark energy goes for the vaporization of the material. Therefore the energy of the discharge is given by equation 5.7 where:  $t_e$  is the time of the discharge,  $W_t$  is the power of the discharge.

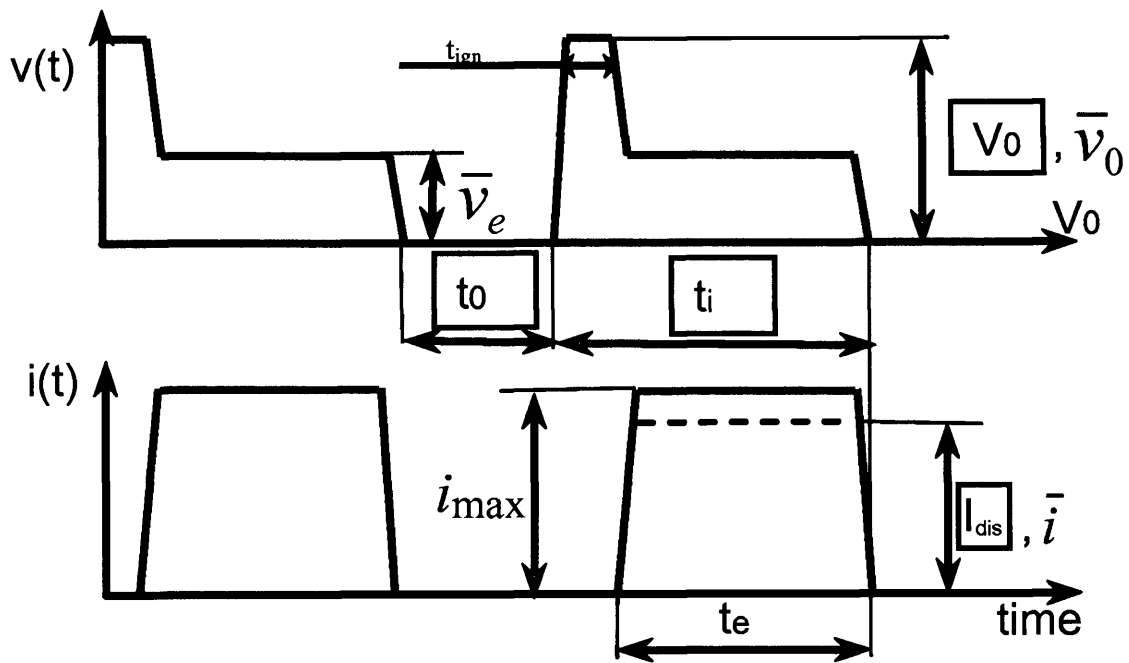


Figure 5.3 Voltage current spark pulses assumption for the wear ratio modelling. Nominal pulse shape: typical set-up parameters of a power generator (in boxes) and measured quantities

$$E_{dis} = \int_0^{t_e} W_t dt \quad (5.7)$$

Power of the discharge can be expressed by equation 5.8

$$W_t = I_{dis}(t)v_e(t) \quad (5.8)$$

where:  $I_{dis}$  is the current of the discharge and  $V_e$  is the discharge voltage, and both could be time dependent.

Finally the discharge energy  $E_{dis}$  can be expressed by equation 5.9

$$E_{dis} = \int_0^{t_e} I_{dis}(t)v_e(t)dt \quad (5.9)$$

The total discharge energy of the spark is divided into 3 sections (Kozak, 2001). Part of it goes to the anode, part of it goes to the cathode and part of it goes into the dielectric.

$$E_{dis} = E_{dis}^{anode} + E_{dis}^{cathode} + E_{dis}^{dial} \quad (5.10)$$

The energies that go to the anode and the cathode melt and vaporise small volumes from the electrodes. The logical assumption at this stage is that the volumes removed from the electrodes are proportional to the share of the energy going to the relevant electrode (5, 6)

$$V_{dis}^{anode} = K_1 E_{dis}^{anode} \quad (5.11)$$

$$V_{dis}^{cathode} = K_2 E_{dis}^{cathode} \quad (5.12)$$

The total volumes removed from the anode and the cathode for some period of time will be:

$$V_{total}^{anode} = \sum_{i=1}^n V_{dis}^{anode} (i) \quad \text{and} \quad V_{total}^{cathode} = \sum_{i=1}^n V_{dis}^{cathode} (i) \quad (5.13)$$

where  $n$  is the number of the effective sparks.

The Volumetric wear ratio ( $v$ ) for a predetermined time period, is the ratio of the volume removed from both electrodes (5.14).

$$v = \frac{V_{total}^{anode}}{V_{total}^{cathode}} = \frac{K_1 E_{total}^{anode}}{K_2 E_{total}^{cathode}} \quad (5.14)$$

The minimum energy required to melt and vaporise one unit of mass is given by the enthalpy of melting and vaporisation (5.15 and 5.16)

Enthalpy of melting:

$$H_m = \int_{T_0}^{T_m} c_p dT + L_m \quad (5.15)$$

Enthalpy of vaporization:

$$H_v = \int_{T_0}^{T_m} c_p dT + L_m + \int_{T_m}^{T_v} c_p dT + L_v \quad (5.16)$$

where:

$c_p$  is the specific heat capacity (J/kg °C)

$L_m$  and  $L_v$  are the latent heats for melting and vaporization (J/kg)

$T_0$  initial (ambient) temperature (°C)

$T_m$  melting temperature (°C)

$T_v$  temperature of vaporization (°C)

The energy required to melt ( $E_m$ ) and to vaporize ( $E_v$ ) a certain amount of material (mass) is given by equation (5.17):

$$E_m = mH_m, \quad E_v = mH_v \quad (5.17)$$

The vaporized mass can be expressed by the total vaporized volume and the density of the

material  $\rho$ ,  $m = V_{total} \rho$ .

The energy required to vaporize material from both the anode and cathode is given by equation (5.18) and (5.19).

$$E_{vap}^{anode} = V_{total}^{anode} \rho^{anode} H_V^{anode} \quad (5.18)$$

$$E_{vap}^{cathode} = V_{total}^{cathode} \rho^{cathode} H_V^{cathode} \quad (5.19)$$

where:

$\rho$  is the density of the material of the anode and the cathode respectively ( $\text{kg/m}^3$ )

$H_m$  is the enthalpy of melting of the anode and the cathode respectively ( $\text{J/kg}$ )

$H_V$  is the enthalpy of vaporization of the anode and the cathode respectively ( $\text{J/kg}$ )

$V_{total}$  is the total vaporized volume ( $\text{m}^3$ )

$m$  is the mass to be melted/vaporized ( $\text{kg}$ )

The relative wear ratio ( $\nu$ ), for this period of time will be given by the ratio of the vaporized volumes. Therefore from equations (5.18) and (5.19) follows:

$$\nu = \frac{V_{total}^{anode}}{V_{total}^{cathode}} = \frac{E_{vap}^{anode}}{E_{vap}^{cathode}} * \frac{\rho^{cathode} H_V^{cathode}}{\rho^{anode} H_V^{anode}} \quad (5.20)$$

Based on equation (5.20) and considering equations (5.11, 5.12), the proportionality coefficients  $K_1$  and  $K_2$  can be determined.

$$\rho^{anode} H_V^{anode} \approx const = K_2 \quad (5.21)$$

$$\rho^{cathode} H_V^{cathode} \approx const = K_1 \quad (5.22)$$

In the case of electrode material and workpiece material being the same ( $K_1=K_2$ ), from equation (5.20) it follows that the wear ratio will be proportional only to the energy distribution between the anode and the cathode. It is not clear from this equation whether the energy



distribution further depends on the material being used as electrodes. This chapter will further investigate the behaviour of pre-selected pure metals in order to study the wear ratios, variations of the wear ratios and make conclusions about the process capabilities.

### **5.2.1. Experimental set up**

This investigation intends to isolate and quantify the contribution to the natural tolerance of the micro EDM process due solely to the wear ratio. Consequently, the experimental activity has been designed so as to block the effect of other potential sources of variability of the micro EDM process. In particular, metals with high purity have been deployed in order to block the effect of other potential sources of variability of the micro EDM process in the removal mechanism due to non-homogeneous chemical-physical properties of the electrodes (thermal and electrical conductivity, density, yield stress, melting point, Energy of ionisation, etc.) and to find an answer to the question which has arisen after equation 5.20, whether the energy distribution between the electrodes further depends on the electrode material properties. In addition, for each individual material, the initial shape of the electrodes is approximately and qualitatively equal in each test carried out. It is anticipated, that the initial shape of the electrodes may constitute a further source of variability of the wear ratio.

A number of electrode materials were selected in order to investigate the energy distribution ratio given in equation (5.20) and the effect of the electrode material on the electrode wear ratio and its variation. In order to cover a broad spectrum of the chemical/physical properties as they appear on the periodic table of the elements, the following materials, with purity equal or higher than 99.95%, were selected: Titanium (Ti), Cobalt (Co), Copper (Cu), Silver (Ag), Gold (Au) and Tungsten (W). Detailed material properties can be seen in Appendix C. All electrode materials were in the shape of  $\varnothing$ 1mm wire apart from Cu which was a pipe of circular cross section with external and internal diameters of  $\varnothing$ 2mm and  $\varnothing$ 1mm, respectively. To block the cross material influence on the process and following the findings in equation (5.20), the experiments were conducted using the same electrode material for the anode and the

cathode. The rods were deployed as electrodes on a commercially available EDM machine equipped with a transistor type generator. The set up of the machine was selected to deliver the minimum discharge energy per pulse to the spark gap. On the basis of Masuzawa (Masuzawa, 2000), this condition is sufficient to place this investigation in the domain of micro-EDM. The detailed generator set up is summarised in Table 5.1.

The dielectric used in this experiment was a commercially available, purpose designed hydrocarbon with the main physical properties shown in Table 5.2.

The experiments were conducted in a submerged bath and the results can be found in Appendix D and Appendix E.

Although the most appealing measurement of wear ratio for manufacturing purposes should be based on volumes, the complexity of the measuring task (Ferri & Ivanov, 2007) has led to an alternative method of assessment being used, which calculated the wear ratio by the measurement of mass (weight). Both the cathode and anode electrodes were weighed before and after electric discharge machining. The ratio of mass removed from the anode and cathode by the machining was measured. The weighing system was an analytical balance with a capacity (maximum measurable mass) of 210 g and readability (resolution) of 0.1 mg. The weighing procedure was carried out in clean room condition of class 6. (BS EN ISO 14644:1 , 1999). A control chart for the standard deviation (Montgomery, 1996, pp 211-221) was designed. On one hand, this resulted in a quantitative assessment of the variability of the measuring system employed in this investigation and on the other hand, the availability of control chart data made provision for an estimation of the capability of the measuring system itself, which is a prerequisite for the subsequent analysis of the variability of the wear ratio. (Montgomery & Runger, 1993-4) The charts for the standard deviation were designed in accordance with the recommendations by Montgomery (Montgomery, 1996), which are:

<b>Parameter, symbol</b>	<b>Unit, symbol</b>	<b>Value</b>
Open circuit voltage, $V_0$	Volt, V	80
Average current from the generator, I	Ampere, A	0.5
Duration of the pulse of voltage at $V_0$ , T-on	microsecond, $\mu s$	1
Programmed time interval between adjacent pulses of voltage, T-off	microsecond, $\mu s$	1
Reference voltage of the servo system <sup>a</sup>	Volts, V	50

Table 5.1 Set up parameters of the EDM generator

<b>Parameter, symbol</b>	<b>Unit, symbol</b>	<b>Value</b>
Density at 15 °C, $\rho$	Grams over cubic centimetres, $g/cm^3$	0.765
Kinematic viscosity at 20 °C,	Centistokes, cSt	1.8
Flash point °C (Pensky-Martens close cup), fp	Degree Celsius, °C	63
Aromatic content, ac	Per cent in weight, %	0.003
Disruptive voltage kV at 2.5 mm	Kilovolts, kV	58

Table 5.2 Main physical properties of the hydrocarbon dielectric

$$UCL_i = \left( 1 + \frac{3}{c_4(n_i)} \cdot \sqrt{1 - c_4(n_i)} \right) \cdot \bar{S} \quad (5.23)$$

$$CL = \bar{S} \quad \text{with} \quad \bar{S} = \left( \frac{(n_i - 1) \cdot S_i^2}{\sum_{i=1}^m (n_i - 1)} \right)^{\frac{1}{2}} \quad (5.24)$$

$$LCL_i = \left( 1 - \frac{3}{c_4(n_i)} \cdot \sqrt{1 - c_4(n_i)} \right) \cdot \bar{S} \quad (5.25)$$

where:  $n_i$  is number of test measurements performed for obtaining the  $i$ -th measurement result, i.e. the sample size associated with the  $i$ -th measurement task. Following Montgomery's recommendations (Montgomery, 1996, page181), 25 measurements results, corresponding to 106 test measurements, were selected for computing  $\bar{S}$ , i.e.  $m = 25$  in equation (5.24). The upper and lower control limits,  $UCL_i$  and  $LCL_i$  were therefore established on the basis of these 25 preliminary samples. The constant  $c_4(n_i)$ , which can be found tabulated or computed directly (Montgomery, 1996, page 212 and Appendix 6), is therefore the sole parameter by which the variable sample sizes exert an influence on the control limits. The experimental results and the chart are presented in the next section.

### 5.2.2. Results

A dedicated 'R' package for statistical process control was employed (Scrucca, 2004). The variability of the weighing system was quantitatively assessed (McGill et al, 1978) and the results are displayed in Figure 5.4. In this figure there are 4 out-of-control points, which can be considered as false alarms. These can be expected every  $1/\alpha$  measurements, where  $\alpha$  is the probability of a false alarm. In fact, a search for assignable causes after each of these alarms did not give any result.

Moreover, an analysis of patterns was conducted on the basis of sections 4-3.5 and 4-3.6 in (Montgomery, 1996). 1 run of length 8 was detected by the chart. The term run refers to a sequence of **S** values with the same characteristics, such as a series of increasing (decreasing) consecutive values and a series of adjacent values above (below) the central line. The violating run was investigated, but no assignable cause was detected.

As a result of the aforementioned observations, experimental evidence supporting the existence of an out of control state of the variability of this process was not found. All the values of standard deviation obtained therefore are considered to have been originated by the same process. Consequently, the unknown variance of the weighing variability,  $\sigma_{balance}^2$ , was estimated by pooling together all the available sample information (148 samples). This resulted in the following estimate (Montgomery, 1996, section 5-31):

$$\hat{\sigma}_{balance}^2 = \bar{S}^2 = \frac{\sum_{i=1}^m (n_i - 1) \cdot S_i^2}{\sum_{i=1}^m (n_i - 1)} = 0.006009 \text{ mg}^2 \quad (5.26)$$

or, equivalently,  $\hat{\sigma}_{balance} = 0.07752 \text{ mg}$ .

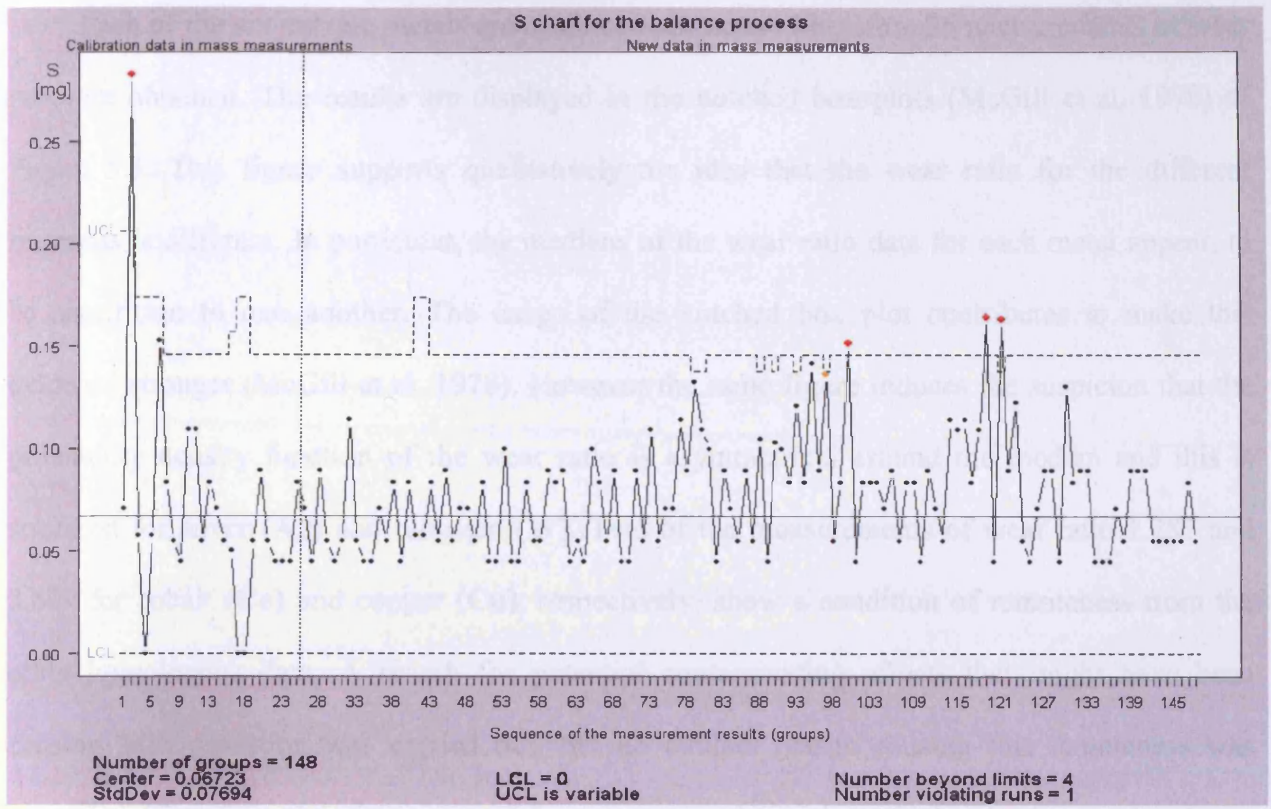


Fig. 5.4 'S' control chart for the mass measuring process

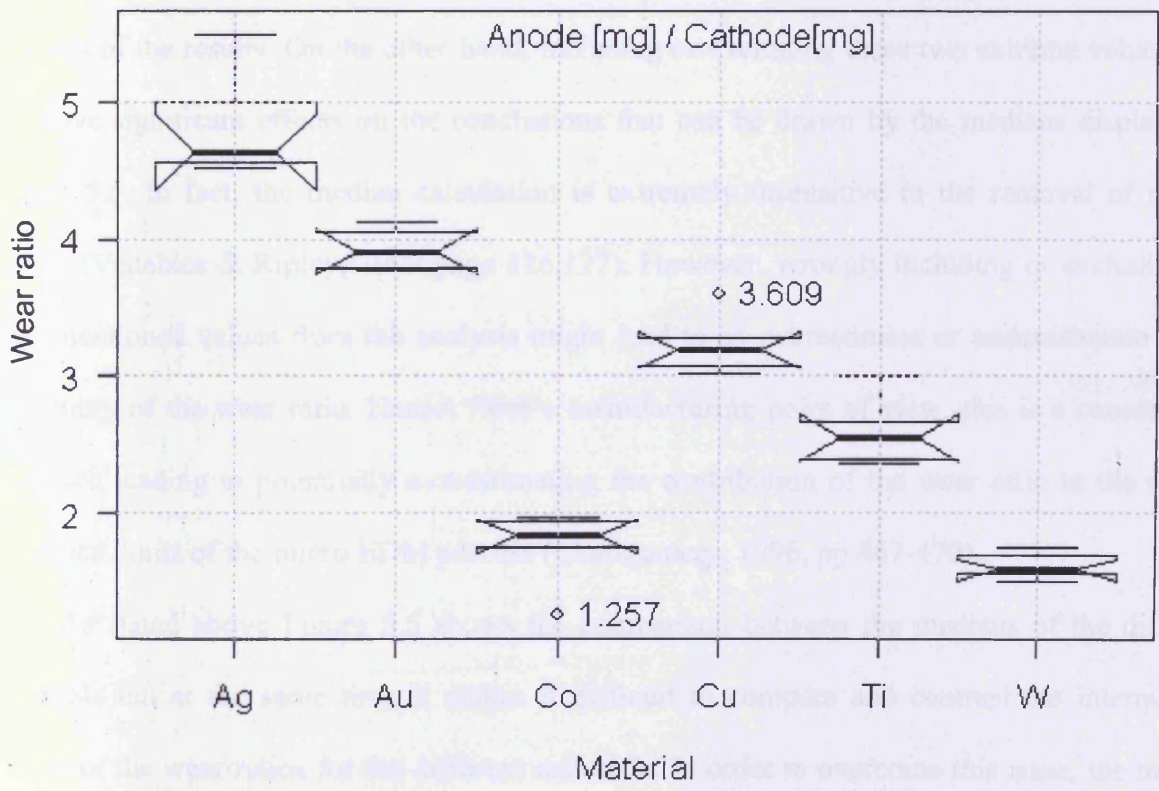


Fig. 5.5 Box plots of the wear ratio in mass (anode over cathode removal)

Each of the six sample metals are machined six times. Therefore 36 measurements of wear ratio are obtained. The results are displayed in the notched box plots (McGill et al, 1978) of Figure 5.5. This figure supports qualitatively the idea that the wear ratio for the different materials is different. In particular, the medians of the wear ratio data for each metal appear, to be significant to one another. The usage of the notched box plot contributes to make this evidence stronger (McGill et al, 1978). However the same figure induces the suspicion that the probability density function of the wear ratio is asymmetrical around the median and this is strongest for silver (**Ag**) and tungsten (**W**). Two of the measurements of wear ratio 1.257 and 3.609 for cobalt (**Co**) and copper (**Cu**), respectively, show a condition of remoteness from the other homologous data. A search for potential contaminating effects that might have been causing such deviation was carried out, but no evident reason causing this remoteness was identified. Therefore, the occurrence of these two experimental results has been considered as a rare but not impossible event originated by the same probability density function that characterises the phenomenon under investigation. They were not, therefore, removed from the analysis of the results. On the other hand, including or excluding these two extreme values does not have significant effects on the conclusions that can be drawn by the medians displayed in Figure 5.5. In fact, the median calculation is extremely insensitive to the removal of remote values (Venables & Ripley, 1999 page 126,127). However, wrongly including or excluding the aforementioned values from the analysis might lead to an overestimate or underestimate of the variability of the wear ratio. Hence, from a manufacturing point of view, this is a conservative approach leading to potentially overestimating the contribution of the wear ratio to the natural tolerance limits of the micro EDM process (Montgomery, 1996, pp 467-470).

As stated above Figure 5.5 shows the comparison between the medians of the different materials but at the same time it makes it difficult to compare and contrast the interquartile ranges of the wear ratios for the different materials. In order to overcome this issue, the median of the wear measurements of each metal was subtracted to each group of measurements. The

resulting box plot with all the medians aligned to 0 (zero) is displayed in Figure 5.6. However, even from this figure, it still appears difficult to ascertain whether a material might have a significant effect on the variability of the wear ratio. A quantitative appraisal of the variability of the wear ratio is presented in the next section.

Images with magnification 480X of the eroded surfaces, of the anode electrode, for each of the investigated six materials were taken on an optical metallographic microscope and are shown in Figure 5.7.

The machined surfaces were first cleaned in an ultrasonic bath to remove the debris from the process. This figure highlights qualitative topographic differences, if any, induced by the different materials. The shape, and also the size of craters is different for the different materials. Craters on the Cobalt and Titanium electrodes are easily visible. However the size of the craters on the Silver, Tungsten and Copper electrodes seems to be smaller. There are also small craters at the surface of the Gold electrode. All this seems a good reason to justify the suspicion that the energy distribution for different materials will be different and that even with the same machining conditions, materials are working differently contingent on their own physical characteristics.



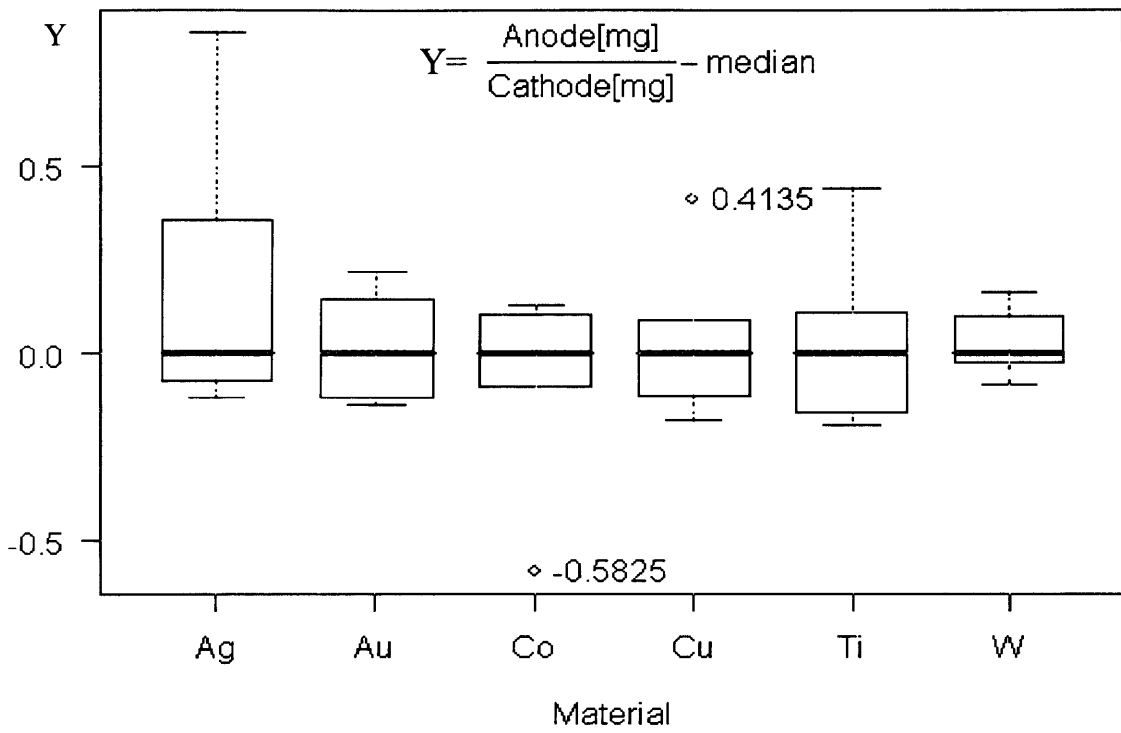
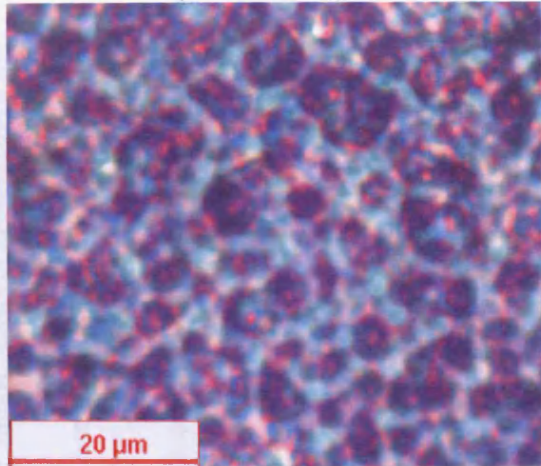
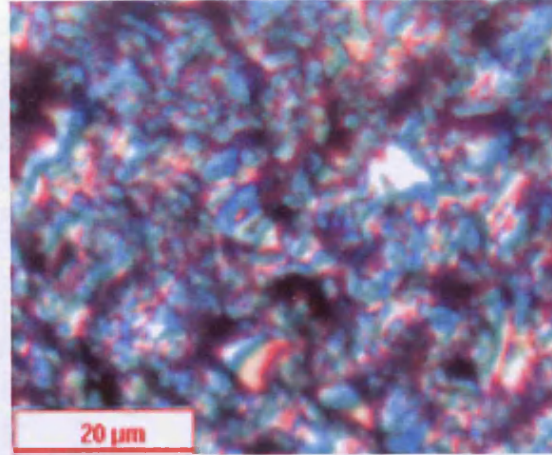


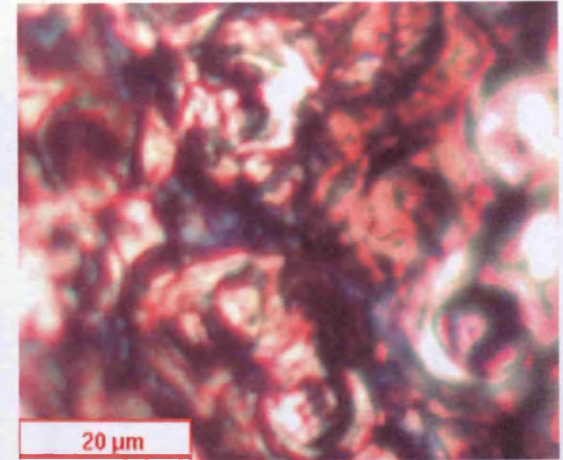
Fig. 5.6 Wear ratio in mass in excess of the median



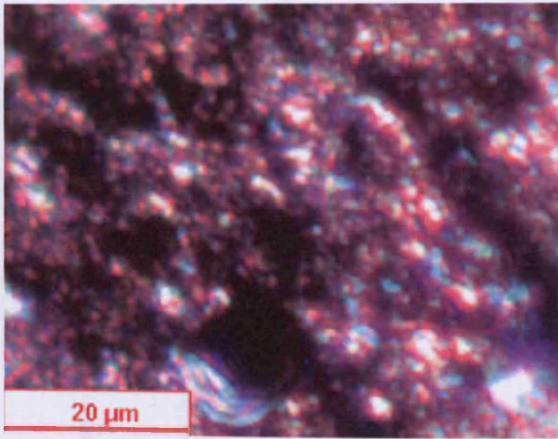
Gold (Au)



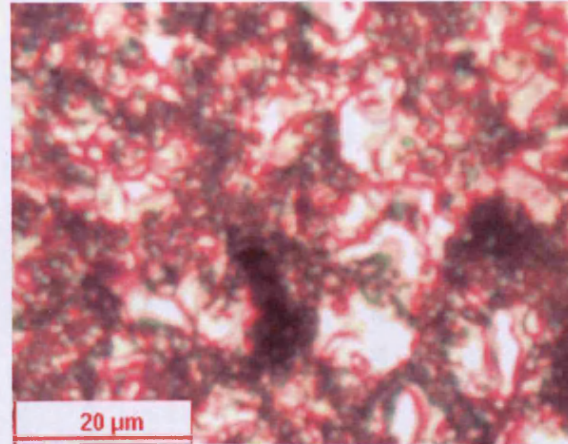
Silver (Ag)



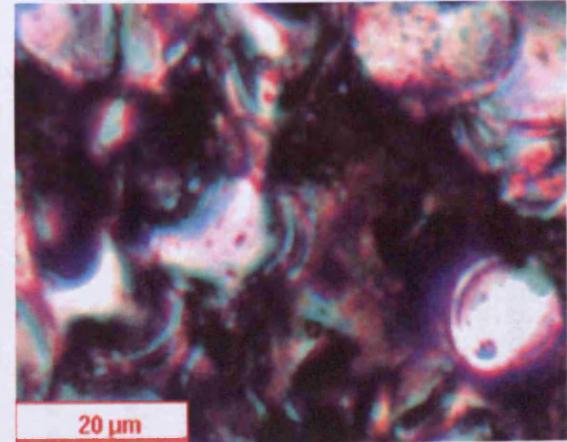
Titanium (Ti)



Copper (Cu)



Tungsten (W)



Cobalt (Co)

Fig. 5.7 Images of the eroded surfaces on the anode

### 5.2.3 Analysis of the results

The potential effect of the materials on the variability of the wear ratios has been tested by using the modification of the Levene's test (Boos & Brownie, 2004) that uses the medians to centre the variables and where the  $p$  value has been computed on the basis of Fisher's distribution. In fact, such a test appears to provide  $I$  type error quite insensitive to the probability density function (pdf) of the parent populations. The simulation studies showed that the significance level of Levene's test is below its nominal value, especially for small sample sizes (Boos & Brownie, 2004). This means that the  $I$  type error is smaller than the nominal. The simulation studies also showed that the Levene's test appears to have greater power than comparable approaches with the same computational simplicity when the number of groups is larger than 4 (Boos & Brownie, 2004). The calculated  $p$  value is equal to 62.63%. **It is therefore not possible to reject the hypothesis of equal dispersions of the wear ratios when considering the erosion of the different metals investigated.** In this case the experimental evidence supports the fact that the variability of the wear ratio does not depend on the metals eroded in this study.

Following the above findings, a more stable (reliable) estimation of the spread of the wear ratio is obtained by aggregating all the experimental results. Therefore the variance of the wear ratio could be estimated by the following equation:

$$\hat{\sigma}_{total}^2 = S_{total}^2 = \frac{\sum_{i=1}^6 \cdot S_i^2}{6} = 0.05634 \quad (5.27)$$

In reality, equation (5.27) represents an estimate of the variance,  $\sigma_{total}^2$ , between the results from the EDM manufacturing process,  $\sigma_{EDM}^2$ , and from the mass measurement process,  $\sigma_{balance}^2$  where the two processes are completely separated. There is no apparent reason for suspecting a correlation between them. Therefore they are assumed independent.

The provided calculated estimation  $\hat{\sigma}_{total}^2$  represents the overall variability of  $\nu$  due to the variability of the volumes (masses) eroded from the electrodes during the micro EDM manufacturing process and due to the variability of the measuring process. On the basis of an approximate expression of the variance of the quotient of two random variables, under the reasonable assumptions of lack of bias in the measurement system and of independence of the micro EDM and the measuring processes, it is derived (Mood & Graybill, 1974):

$$\hat{\sigma}_{total}^2 \cong \left( \frac{\mu_{cathode}}{\mu_{anode}} \right)^2 \cdot \left( \frac{\sigma_{cathode}^2 + \sigma_{balance}^2}{\mu_{cathode}^2} + \frac{\sigma_{anode}^2 + \sigma_{balance}^2}{\mu_{anode}^2} + -2 \cdot \frac{\text{cov}(CAT + BAL, AN + BAL)}{\mu_{cathode} \cdot \mu_{anode}} \right) \quad (5.28)$$

In equation (5.28), CAT and AN are two random variables representing the material removed from the cathode and anode, respectively. Whereas BAL is the random variable associated with the mass measurement process. The expected values (mean) and variances ( $\sigma^2$ ) of CAT, AN and BAL are  $(\mu_{cathode}, \sigma_{cathode}^2)$ ,  $(\mu_{anode}, \sigma_{anode}^2)$  and  $(0, \sigma_{balance}^2)$ , respectively. Although in this investigation an estimate of  $\sigma_{balance}^2$  has been derived in equation (5.26), an estimate of the variability of the wear ratio excluding the balance contribution can be derived from equation (5.28). Nevertheless, it demands further investigation that goes beyond the aims of this research.

From equation (5.26) and (5.27), it is noticed that the variability of the measuring system is about one order of magnitude smaller than the overall variability (wear ratio and balance together). Hence, it is qualitatively argued that the measuring process utilised appears suitable for the performed measuring task.

Due to the further experimental effort required to further elaborate equation (5.28), an approximated method has been followed. It utilises the following equation that hinges on the independence of the measuring and manufacturing processes but neglects deliberately some of the considerations leading to equation (5.28):

$$\sigma_{total}^2 = \sigma_{EDM}^2 + \sigma_{balance}^2 \quad (5.29)$$

Assuming that the estimate  $\hat{\sigma}_{balance}^2$  derived from equation (5.26) is so close to the unknown parameter  $\sigma_{balance}^2$  that they can be considered equal. Then from equation (5.29) it results in:

$$\hat{\sigma}_{EDM}^2 = \hat{\sigma}_{total}^2 - \hat{\sigma}_{balance}^2 = 0.05634 - (0.07752)^2 = 0.050331 \text{ mg}^2 \quad (5.30)$$

$$\hat{\sigma}_{EDM} = \sqrt{\hat{\sigma}_{total}^2 - \hat{\sigma}_{balance}^2} = 0.2243 \text{ mg} \quad (5.31)$$

In order to establish if  $\sigma_{EDM}$  is significantly different from zero, an interval estimate has been proposed using a computationally intensive approach (Johnson, 2001; Boos, 2003). The advantage of such an approach is that it does not require the formulation of any hypothesis on the function of the used estimator. This is also convenient due to the fact that the exact **pdf** of a wear ratio of two random variables appears not straightforward to deal with from a practical perspective, even in the simplest case of the wear ratio of two correlated normal variables (Hinkley, 1969). The computationally intensive approach considered in this study is the bootstrap: a procedure which obtains a reference distribution function by generating a replacement sample from the sample of the experimental results. For each of the newly generated samples, the  $\hat{\sigma}_{EDM}^2$  is computed and a reference empirical distribution for this is created. A number of techniques have been devised to yield a confidence interval from the availability of such a reference distribution (DiCiccio et al, 1996). In this study, a percentile approach was adopted due to its relative simplicity and due to the fact that it does not require any distributional assumption on the data. A value of **M=10000** re-samples were selected for the calculation. The

computations were carried out with **R**, a free language and software environment for statistical computing, and with the “boot” R package in particular. The obtained empirical distribution is shown in Figure 5.8. This figure also shows a quantile-quantile plot comparing the empirical quantiles with the correspondent theoretical quantiles from the normal distribution. Although there is a good agreement between these two **pdf** in the central area, differences have emerged around the ends. These discrepancies indicate that if the normal distribution assumption had been introduced, it would have resulted in deviations of the significance level from its designed value.

The percentile bootstrap confidence interval for  $\hat{\sigma}_{EDM}^2$  at a significance level of  $\alpha=99\%$  resulted in 0.0056, to 0.0759. It is noticeable that this interval does not have zero as an extreme value. The practical implication of such a remark is that all the manufacturing compensation methods of electrode wear that are based on a deterministic knowledge of the wear ratio are by their nature prone to produce an increased number of defective parts due to their inherent underestimate of the natural process variability.

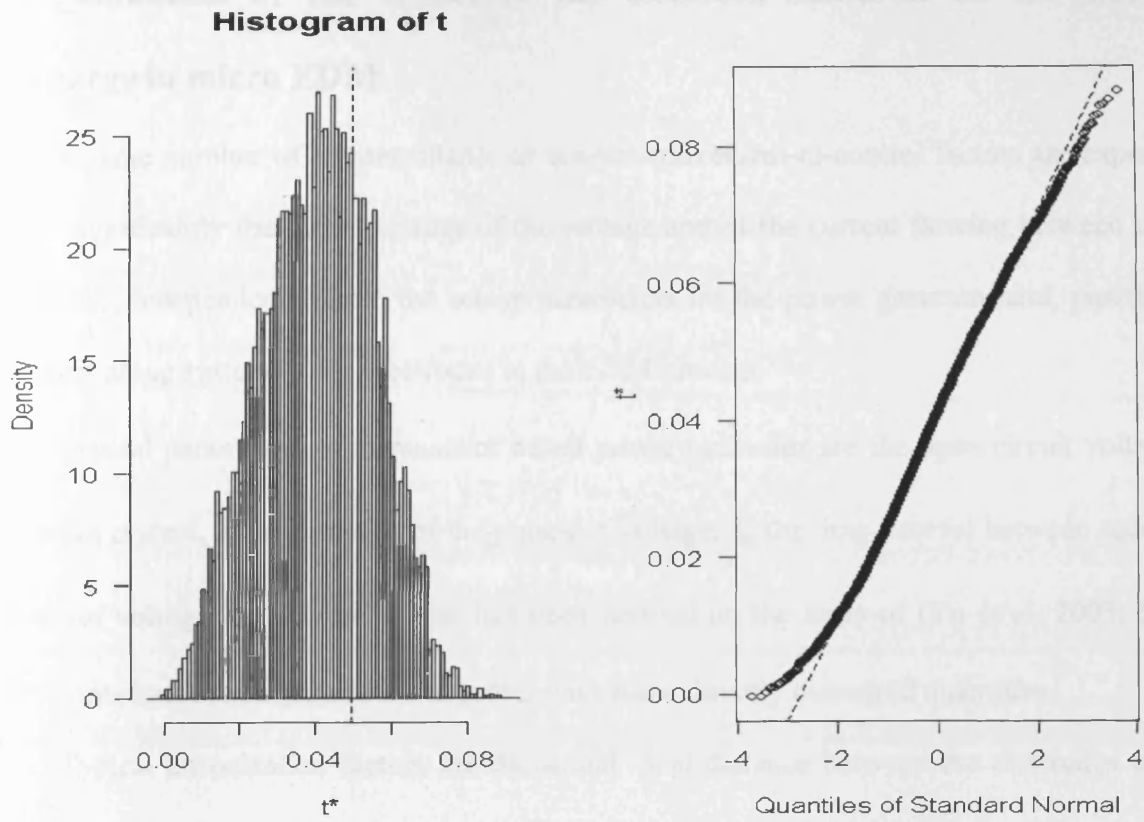


Figure 5.8 The obtained empirical distribution



### 5.3 Estimation of the effects of the electrode material on the electrical discharge in micro EDM

A large number of uncontrollable or not-yet-convenient-to-control factors are expected to affect significantly the instant values of the voltage and of the current flowing between the two electrodes, independently from the set-up parameters for the power generator and, possibly, for the positioning system of the electrodes in the EDM process.

Typical parameters of a transistor based power generator are the open circuit voltage,  $V_0$ , the mean current,  $I$ , the duration of the pulses of voltage,  $t_i$ , the time interval between successive pulses of voltage,  $t_0$ . Figure 1, that has been derived on the basis of (Yu et al, 2003; Semon, 1975), illustrates these parameters together with some directly measured quantities.

Typical uncontrolled factors are the actual local distance between the electrodes where a discharge takes place, the actual strength of the dielectric in the spark gap, the degree of contamination of the spark gap due to the removed material, the degree of potential partial ionisation of the dielectric in the spark gap, the motion characteristics of the liquid dielectric between the electrodes, the local variability of composition, homogeneity and isotropy of the chemical-physical properties of the electrode materials and of the dielectric medium.

The set-up parameters are given in Figure 5.3 and are used for the analytical description of the process. These parameters define ideal functional relationships of the voltage and the current. Hence, the average electrical energy and the instant power as a function of the time can be calculated from them.

However, it is argued that this energy and this power function are just nominal due to the fact that the aforementioned uncontrolled factors make the actual shape of voltage and current to differ significantly and unpredictably from their nominal shape. As a consequence, the Unit Removal (UR) value is expected to be affected by an added source of variability corresponding to the distribution of the electrical discharge characteristics (voltage, current and their



dependence on the time). Ultimately, this variability of the UR is expected to increase the natural tolerance of the process.

It is envisaged that two directions of investigation can significantly contribute to quantify and possibly to reduce the natural tolerance of the EDM process.

The first is an extended effort in limiting the variability of the pulses by analysing the effect that the aforementioned uncontrolled factors exert on the shape of the pulses and, consequently, by extending the control upon them.

The second direction consists of a quantitative identification of the relationship between the UR and the electrical characteristics of the pulse. On one hand, Dauw (Dauw, 2002) undertakes research activities in both of these directions by developing a classification of the pulses and an adaptive control system based upon this classification. Weck (Weck, 1991), on the other hand, focuses his research on the second direction while presenting an adaptive control founded on the identification of the relationship between some pulse characteristics and the removal process. The material removal contribution of pulses previously subdivided into groups is the main purpose of the investigation performed by Cogun (Cogun, 1990).

However, evidence of similar studies in the micro EDM field has not been found. Furthermore, the effect of the material on the electrical characteristics of the discharge pulses has never been explicitly investigated especially in the region of micro EDM. Such an investigation can contribute and cast light upon the nature of the differences between the wear ratios of different electrode materials reported in (Ivanov et al, 2007). It can determine, in fact, whether these differences are solely due to the influence of the material properties on the electrical discharge phenomenon (voltage, current and their time correspondences) or solely due to the material properties affecting directly the removal mechanism (melting and vaporisation temperature, stress resistance, etc.) or are due to both of these reasons and how.

In this section, electrical quantities of interest in both the voltage and the current during a 'generic discharge' are first defined and then measured. The term 'generic discharge' refers to

an actual discharge that can deviate significantly from the ‘nominal discharge’ displayed in Figure 5.3. The potential effects of the electrode material on these electrical parameters are shown using an exploratory data analysis (EDA) approach (NIST: <http://www.itl.nist.gov/div898/handboo>).

### 5.3.1 Investigation set-up

The same commercially available EDM machine was employed in this investigation. The EDM machine was set up to deliver the minimum nominal energy during each discharge. According to Masuzawa (Masuzawa, 2000), this condition is necessary and sufficient to place the manufacturing operation in the micro manufacturing domain. The detailed set up of the particular transistor based generator is the same as described in section 5.2.1 and summarised in Table 5.1.

Current and voltage measurements were taken by means of a current transformer (current probe) and a passive voltage probe (10M $\Omega$ , 14pF, attenuation factor 10X, 200MHz bandwidth at -3dB), respectively.

The overall test rig is illustrated in Figure 5.9. The main characteristics of both the current probe and the oscilloscope are displayed in Table 5.3.

The dielectric used is a commercially available, purpose designed liquid hydrocarbon whose main physical properties were given in section 5.2.1 and are summarised in Table 5.2.

The oscilloscope was set up with a vertical scale of 2V/div for the voltage (corresponding to an actual value of 20 V/div due to the 10X probe), and 500mV/div for the current (corresponding to an actual value of 500mA/div, due to the V/A=1 current probe). The time scale was set at 200 ns/div. A time interval of 2  $\mu$ s was, therefore, globally monitored. A DC coupling option was selected when connecting the two probes to the oscilloscope.

The recording action of the instrument starts when a particular event, called the ‘trigger event’, is detected. In this particular investigation, the trigger event was defined when the current increased more than the pre-specified level of 310mA.

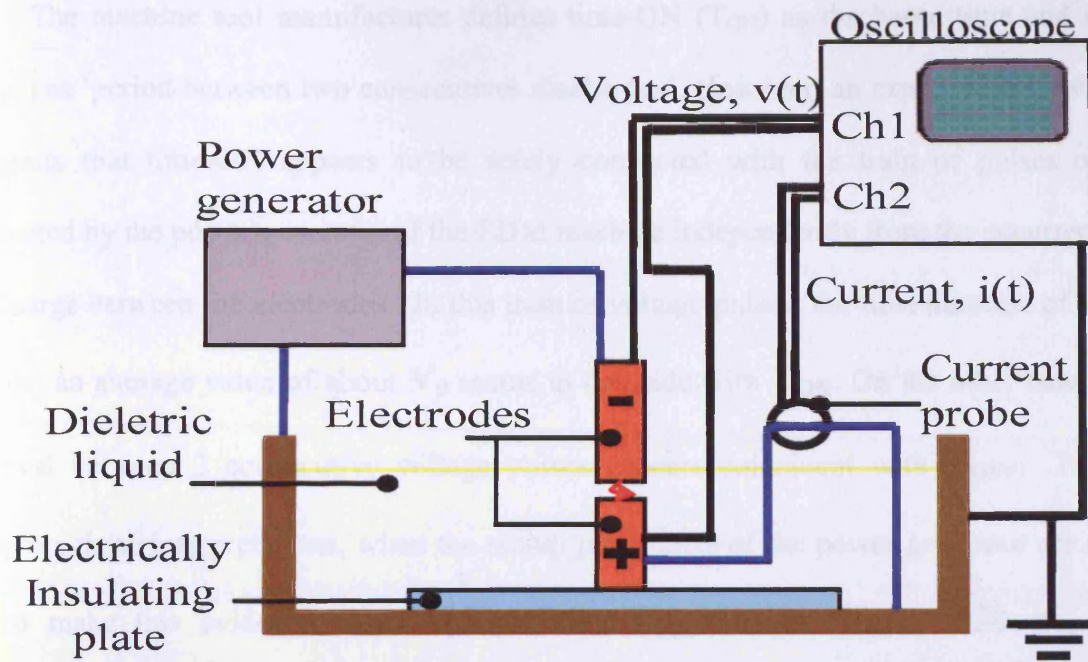


Fig. 5.9 Schema of the test rig.

Oscilloscope		Current probe	
<b>Bandwidth</b>	200MHz	<b>Output (V/A)</b>	1
<b>Sample rate</b>	10S/s to 1GS/s	<b>Rise time</b>	7ns
<b>Vertical Resolution</b>	8bits, 25digitalization levels/div	<b>DC saturation current</b>	3A
<b>Input impedance</b>	$1M\Omega \pm 1\%$ in parallel with $20\text{ pF} \pm 2\text{pF}$	<b>Max. rms current</b>	7A
		<b>3db Bandwidth (Sinewave)</b>	lf : 130Hz (98Hz) hf : 60MHz (100MHz) <sup>a</sup>
		<b>Max Phase shift between signal and current<sup>b</sup></b>	$\leq 6^\circ$

Table 5.3 Oscilloscope and current probe main characteristics

The machine tool manufacturer defines time-ON ( $T_{ON}$ ) as discharge time and time-OFF ( $T_{OFF}$ ) as 'period between two consecutive discharges'. However, an experimental investigation suggests that time-ON appears to be solely connected with the train of pulses of voltage delivered by the power generator of the EDM machine independently from the occurrence of any discharge between the electrodes. In this train of voltage pulses, the time duration of each pulse having an average value of about  $V_0$  seems to coincide with  $T_{ON}$ . On the other hand, the time interval between 2 consecutive voltage pulses appears coincident with  $T_{OFF}$ . Figure 5.10 supports these interpretations, when the set-up parameters of the power generator are chosen so as to make this evidence clearer ( $V_0=80V$   $T_{ON}=40 \mu s$ ,  $T_{OFF}= 130 \mu s$ ,  $I=0.5A$ ,  $V_{servo}=50V$ ). In this figure, only 2 current pulses are visible on channel 2, whereas the train of voltage pulses still continues the  $T_{ON} - T_{OFF}$  pattern. Therefore, the parameters  $T_{ON}$  and  $T_{OFF}$  do not appear directly connected with the occurrence of a discharge between the electrodes. This circumstance, therefore, means that it will be better to measure directly the 'nominal' effects that set-up parameters of a piece of complex equipment such as an EDM power generator actually have on the discharge process.

Each measurement performed by means of the oscilloscope gives a time series of 1000 voltage values where the sampling interval is constant. This time series is acquired on the occurrence of the triggering event. In the 'average acquisition mode', a pre-specified number of time series are detected and their values are averaged into an 'average time series', which is displayed on the oscilloscope screen. In this investigation, the displayed time series (or waveform) is the average of 256 time series. Each of 256 time series represents a 'generic discharge' voltage and current, acquired separately on the two oscilloscope channels. In the following, the waveform resulting from the averaging process is referred to as the 'average discharge pulse'. An average discharge pulse is associated with the measurement of voltage and another with the measurement of current. The average discharge pulses of voltage and current are then used to define the physical quantities of interest, which, in their turn, are measured

directly on the oscilloscope using the built-in functionalities (gated measurements). The product of the average discharge pulses of voltage and current is also obtained directly on the oscilloscope and results in the average discharge pulse of instant power.

**This investigation aims to isolate and quantify the effects of the electrode material on the discharge electrical characteristics in order to answer the question raised in section 5.2 whether the discharge energy further depends on the material properties.** Consequently, the experimental activity has been designed to block the effect of other potential sources of variability in the micro EDM electrical characteristics. This is one reason why metals with high purity have been used in the experiments. In fact, in this manner, potential increments in the variability of the EDM process due to local non-homogeneous chemical-physical properties of the electrodes (thermal and electrical conductivity, energy of ionisation, etc.) are less likely to appear. Therefore, it should be easier to detect differences in the electrical characteristics solely due to the electrode materials. Moreover, the material of the two electrodes was the same in each test in order to prevent potential interaction effects of the pair of materials on the electrical characteristic of the generic discharge. In addition, for each individual material, the initial shape of the electrodes is approximately and qualitatively equal in each test carried out. It is anticipated, in fact, that the initial shape of the electrodes may constitute a further source of variability of the electrical characteristic of the generic discharge.

In this investigation the same materials are used as described in section 5.2.1 in order to cover a broad spectrum of the chemical/physical properties as they appear on the periodic table of the elements and they were selected in order to investigate the effect of the electrode materials on the average discharge pulse. The usage of pure metals is also beneficial due to the fact that the same experimental results might be used in further research to cast light upon the identification of quantitative relationships between chemical/physical material properties and the material removal mechanism in micro EDM (see Appendix F).

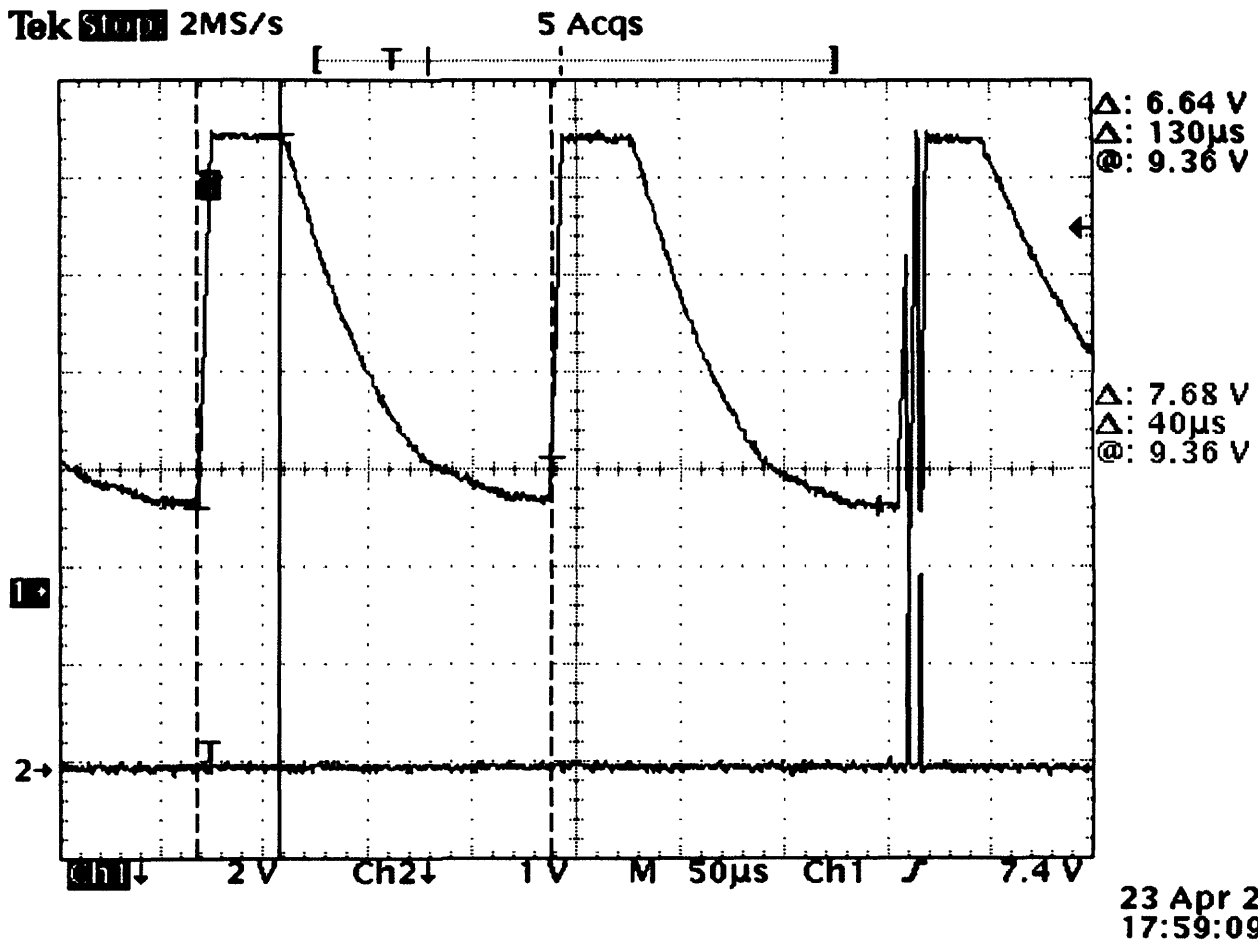


Fig. 5.10 Interpretation of  $T_{ON}$  and  $T_{OFF}$ : on channel 2, just 2 current pulses are visible, whereas the train of voltage still continues the  $T_{ON}$  -  $T_{OFF}$  pattern

### 5.3.2 Results from the investigation

Voltage, current and instant power average discharge pulses for each of the electrode materials investigated is displayed in Figure 5.11. Each component of Figure 5.11 was randomly selected solely for illustrative purposes among all the measurements carried out in this study.

Nine electrical quantities were identified on the average discharge pulse of voltage, current and instant power as they have been defined in the previous section. These quantities are:

- $\bar{V}_0$ , the average open circuit voltage measured from 200 ns before the occurrence of the trigger event to  $A$ , the instant when the beginning of the flow of current is detected (first positive point on the current waveform);
- $\bar{V}_e$ , the average voltage during the discharge measured from  $A$  to  $B$ , the instant after the last positive value on the current waveform.
- $t_e$ , the duration of the discharge, that is the time interval between the instants  $A$  and  $B$ .
- $\bar{i}$ , the average current intensity during the measured time interval  $t_e$ .
- $i_{\max}$ , the maximum value of current intensity during a discharge.
- $t_{\max}$ , the time interval between the initial flow of current, instant  $A$ , and the instant where the current is at its maximum,  $i_{\max}$ .
- $\bar{P}$ , the average discharge electrical power, namely, the average of the instant power waveform during the time interval  $t_e$ .
- $P_{\max}$ , the maximum of the discharge instant power;
- $e$ , the discharge energy of the average discharge pulse, namely, the integral of the instant power during  $t_e$ .

These quantities represent a nine dimensional response variable.

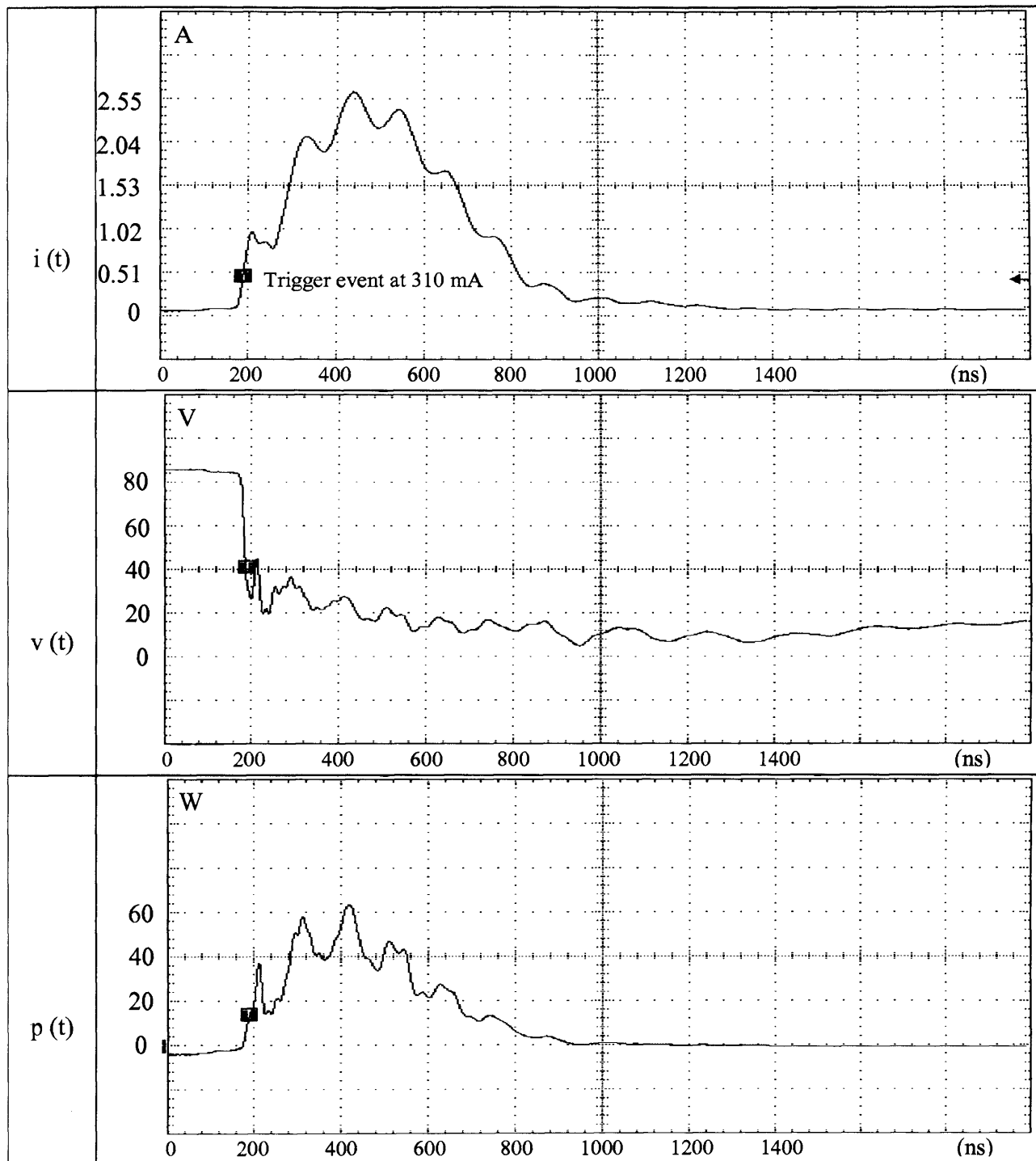
In order to limit the experimental burden, the experiment was carried out in a sequence of 5 experimental units or blocks. In each of these experimental units, 5 measurements of the above 9 electrical characteristics of interest were taken for each pair of electrodes of the same material. This resulted in 25 measurements per each of the 5 materials per each of the 9 response variables. 1125 measurement results were therefore taken in total. Inside each experimental unit, it was not possible to randomise the sequence of tests because it would have increased disproportionately the number of set-ups, and, consequently, the experimental effort. There are two anticipated potential drawbacks of this experimental strategy. On one hand, the effect on the response variables that is attributed to the electrode material can in reality be caused by some unforeseen concomitant nuisance factor. Nevertheless, this circumstance appears only a theoretical possibility, owing to the controlled conditions in which the experiment was performed. On the other hand, an effect on the experimental unit of the response variable can also appear. If this is the case, a contaminant effect on the measurements of the response variables corresponding to different experimental units would appear. This circumstance would, consequently, prevent pooling together response variables belonging to different experimental units, without accepting an increased probability of drawing wrong conclusions from the available data.

For each of the 9 response variables, therefore, the data were grouped by experimental unit and notched box plots (McGill et al, 1978) were produced using R, a free software environment and language for statistical computing and graphics ('R' Development Core Team, 2006). The results are displayed in Figure 5.12 and given in Appendix D. On the basis of this figure it is qualitatively argued that no effect of the blocks is apparent on both the variability and the location of almost all the response variables. In fact, for each response separately, the interquartile range does not appear to change significantly. Similarly, the notches of distinct boxes always display a degree of overlapping. The sole response variables that show some potential problems are  $t_e$ ,  $t_{\max}$  and  $e$ . In the box plot of  $t_e$ , the  $V$  experimental unit presents



a median of the data that appears significantly lower than in the others blocks. It is then argued that the similar deviation present in the box plot for  $e$  is solely due to  $t_e$  because the correspondent plot of  $\bar{P}$  does not present any self-evident anomaly.

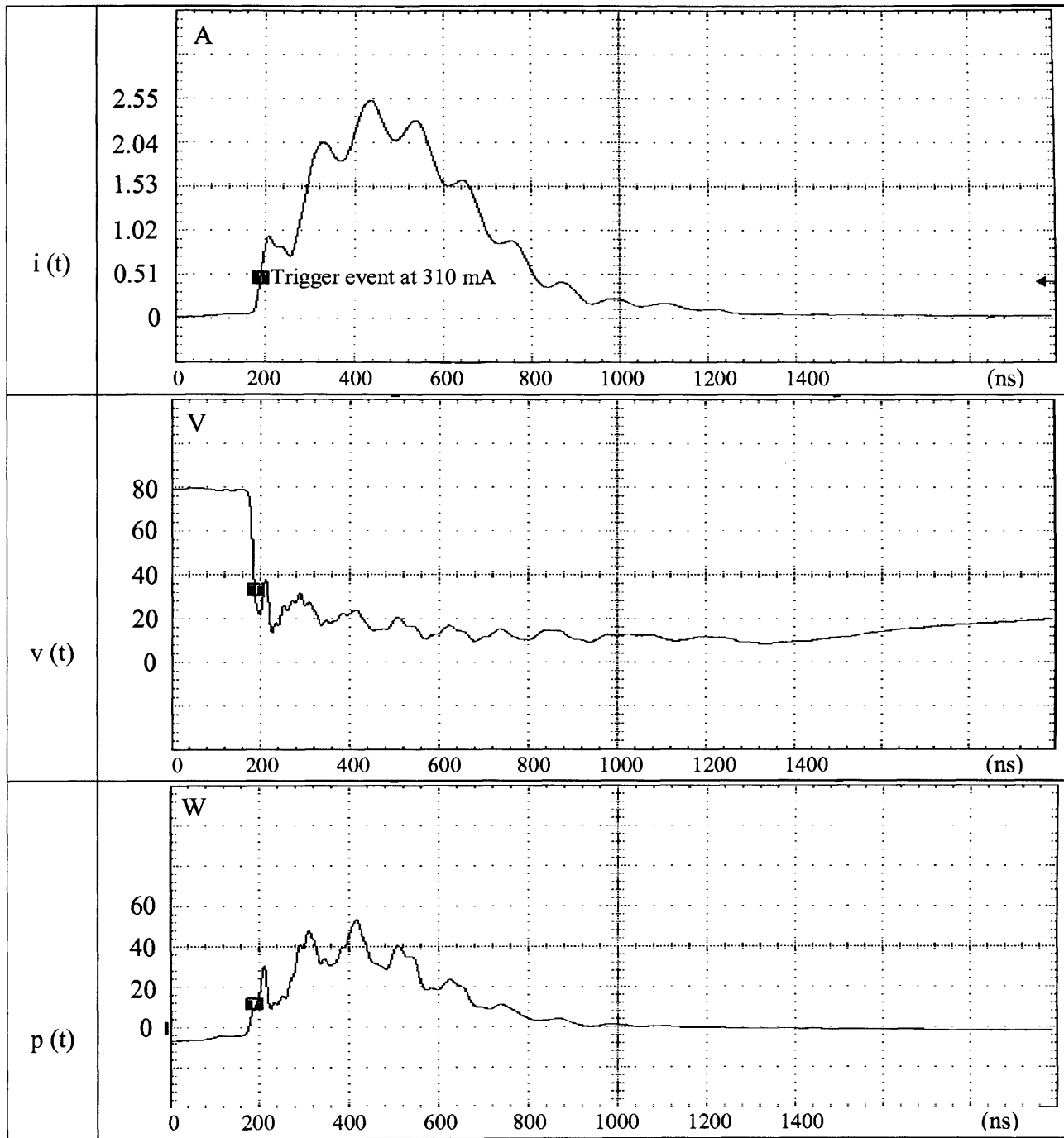
The box plot of  $t_{\max}$  highlights a large number of quite extreme values. However, no significant effect of the blocks on  $t_{\max}$  is qualitatively apparent from the figure in either cases of inclusion or exclusion of these extreme points in the analysis. As a consequence of all these observations, it is concluded that the only  $t_e$  might be sensitive to the different experimental units. However, it appears quite inexplicable that just one of the response variables appears sensitive to the blocks. Therefore, following the Occam's razor principle (*lex parsimoniae – entia non sunt multiplicanda praeter necessitatem*) (entities should not be multiplied beyond necessity); it is argued that such a significance of the blocks is solely due to randomness, or, using a control chart term, it is 'a false alarm'. In the following analysis therefore it is deliberately neglected in the same way as the differences between experimental units are. This course of action is also supported by the fact that an analysis neglecting the  $V$  block that might have been contaminated by some potential nuisance factor, has also been conducted. No changes in the results were observed in such an analysis based on only the first four blocks.



a) Silver (Ag)  $t_e=1080$  ns

Fig. 5.11 Oscilloscope waveforms for each material investigated:  $i(t)$  current average discharge pulses,  $v(t)$  voltage average discharge pulses and  $p(t)$  instant power average discharge pulses

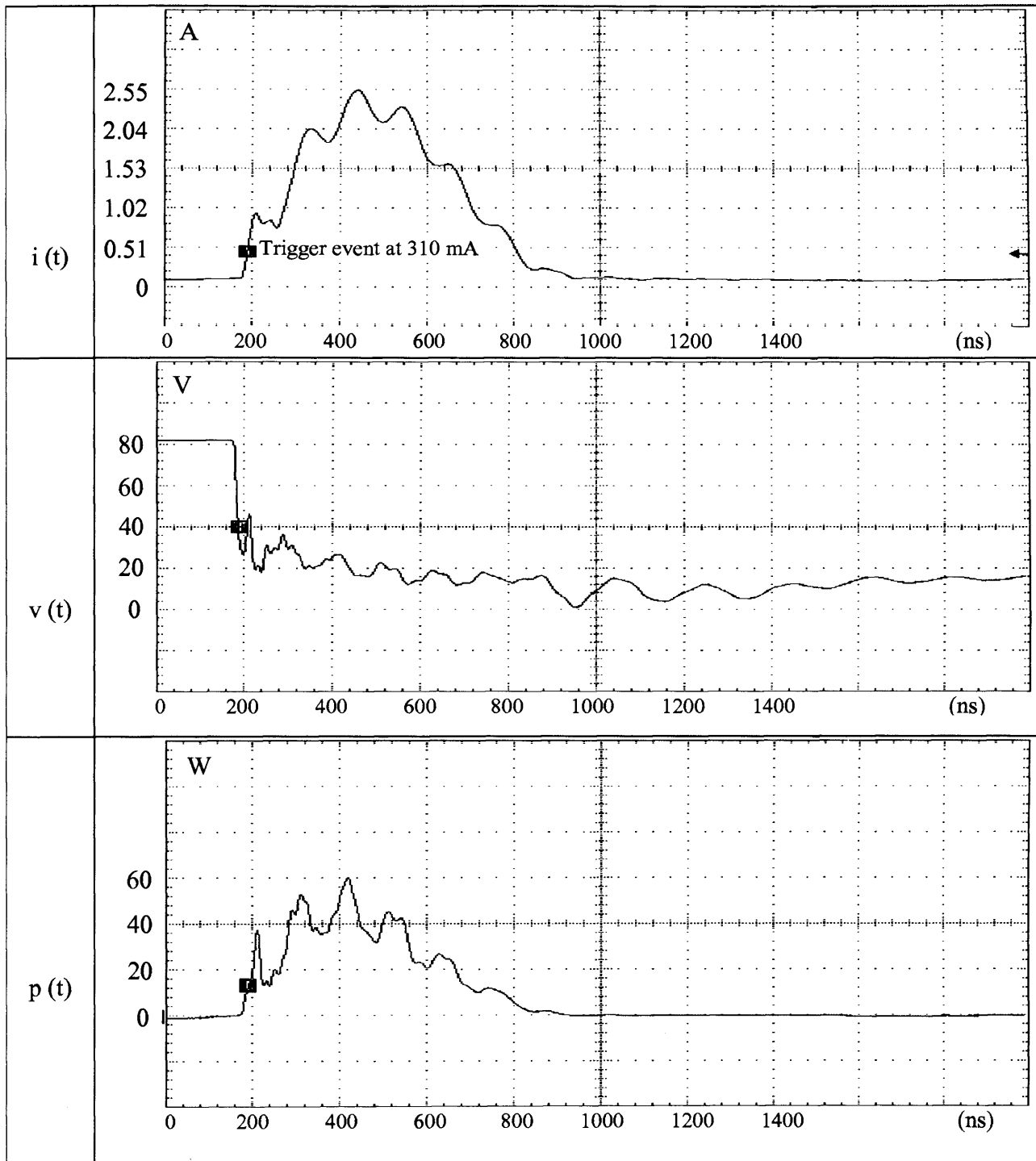
(to be continued)



b) Copper (Cu)  $t_e=976$  ns

Fig. 5.11 Oscilloscope waveforms for each material investigated:  $i(t)$  current average discharge pulses,  $v(t)$  voltage average discharge pulses and  $p(t)$  instant power average discharge pulses

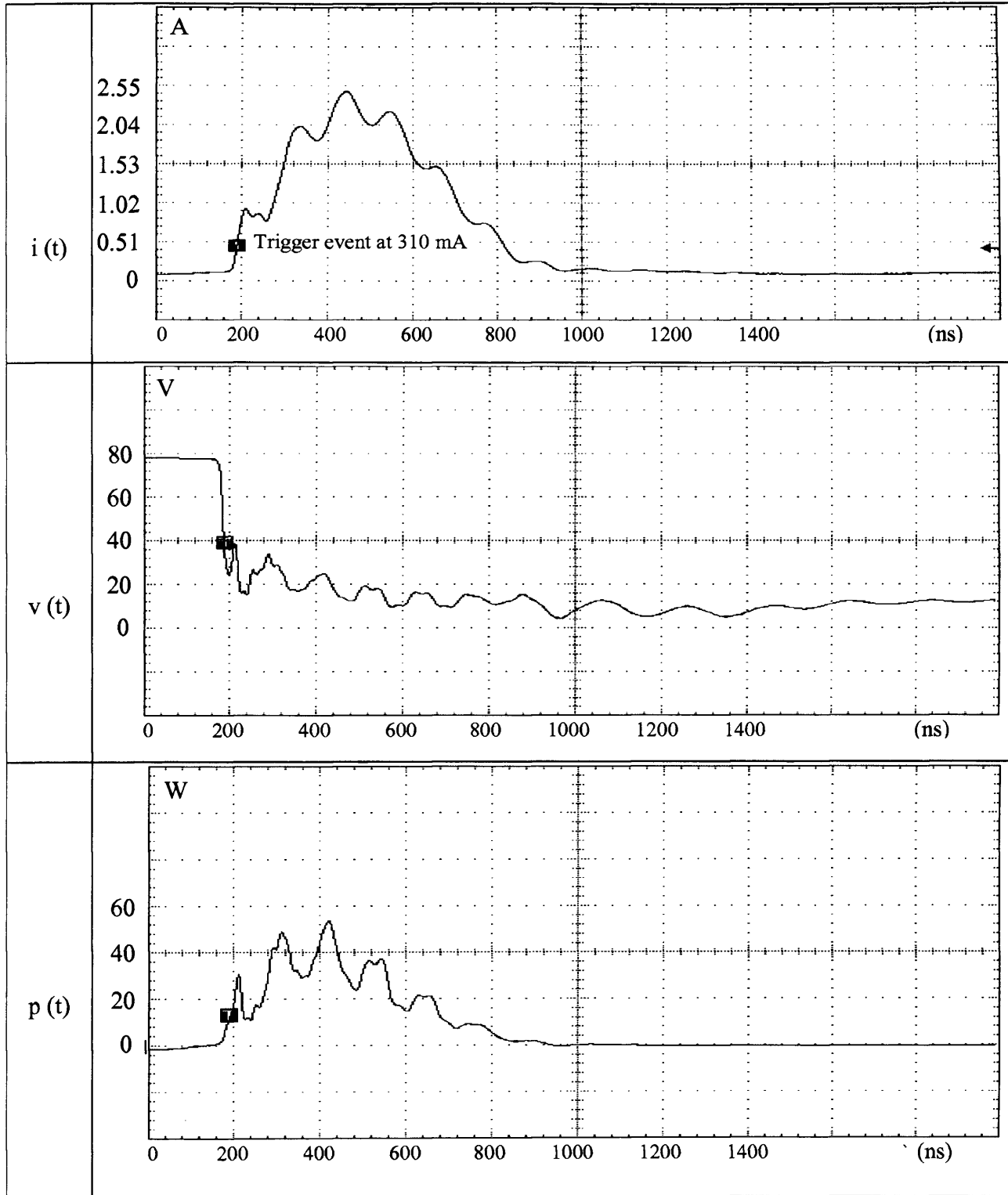
(to be continued)



c) Nickel (Ni)  $t_e=872$  ns

Fig. 5.11 Oscilloscope waveforms for each material investigated:  $i(t)$  current average discharge pulses,  $v(t)$  voltage average discharge pulses and  $p(t)$  instant power average discharge pulses

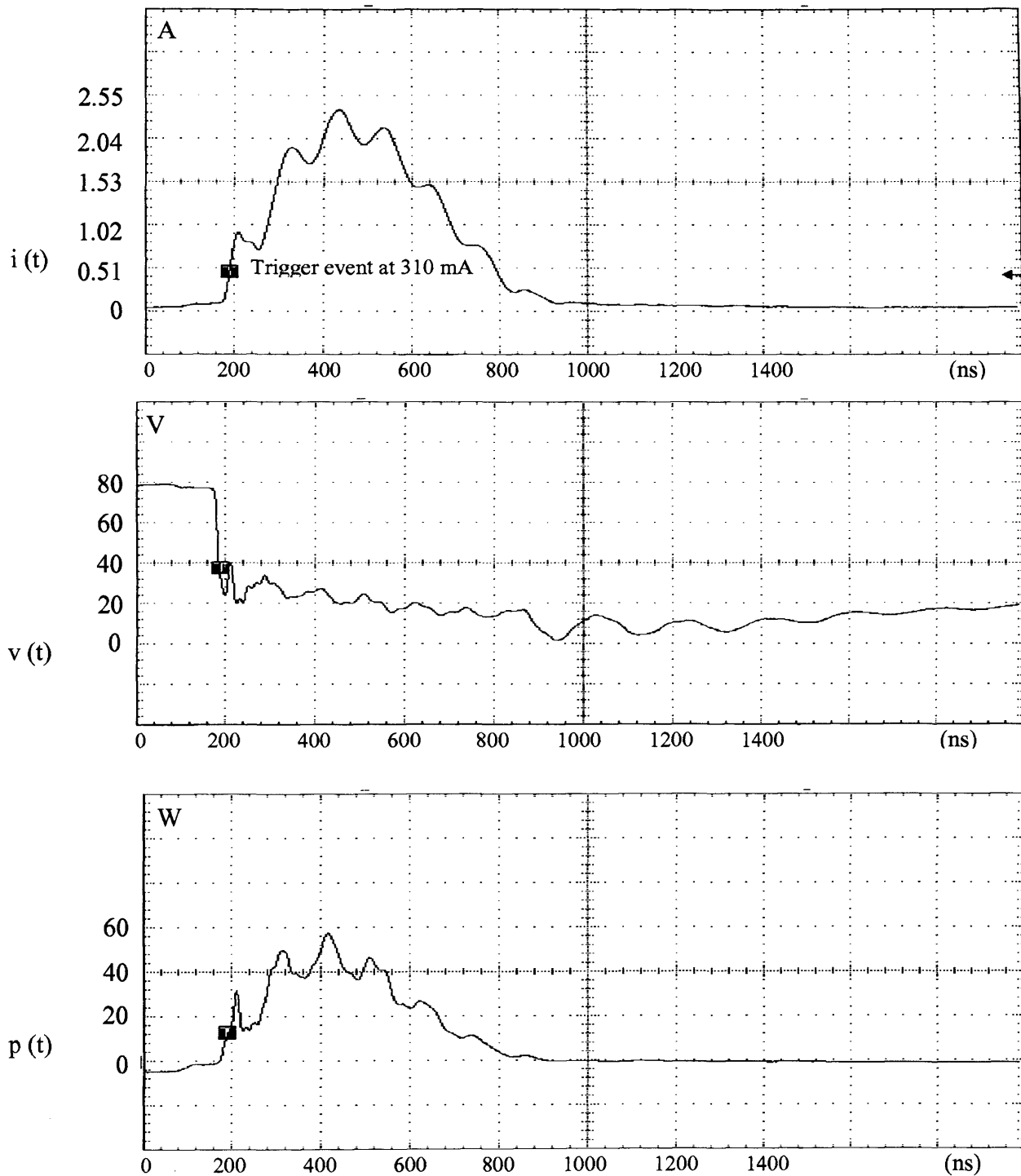
(to be continued)



d) Titanium (Ti)  $t_e=1136$  ns

Fig. 5.11 Oscilloscope waveforms for each material investigated:  $i(t)$  current average discharge pulses,  $v(t)$  voltage average discharge pulses and  $p(t)$  instant power average discharge pulses

(to be continued)



e) Tungsten (W)  $t_e=748$  ns

Fig. 5.11 Oscilloscope waveforms for each material investigated:  $i(t)$  current average discharge pulses,  $v(t)$  voltage average discharge pulses and  $p(t)$  instant power average discharge pulses  
(continued)

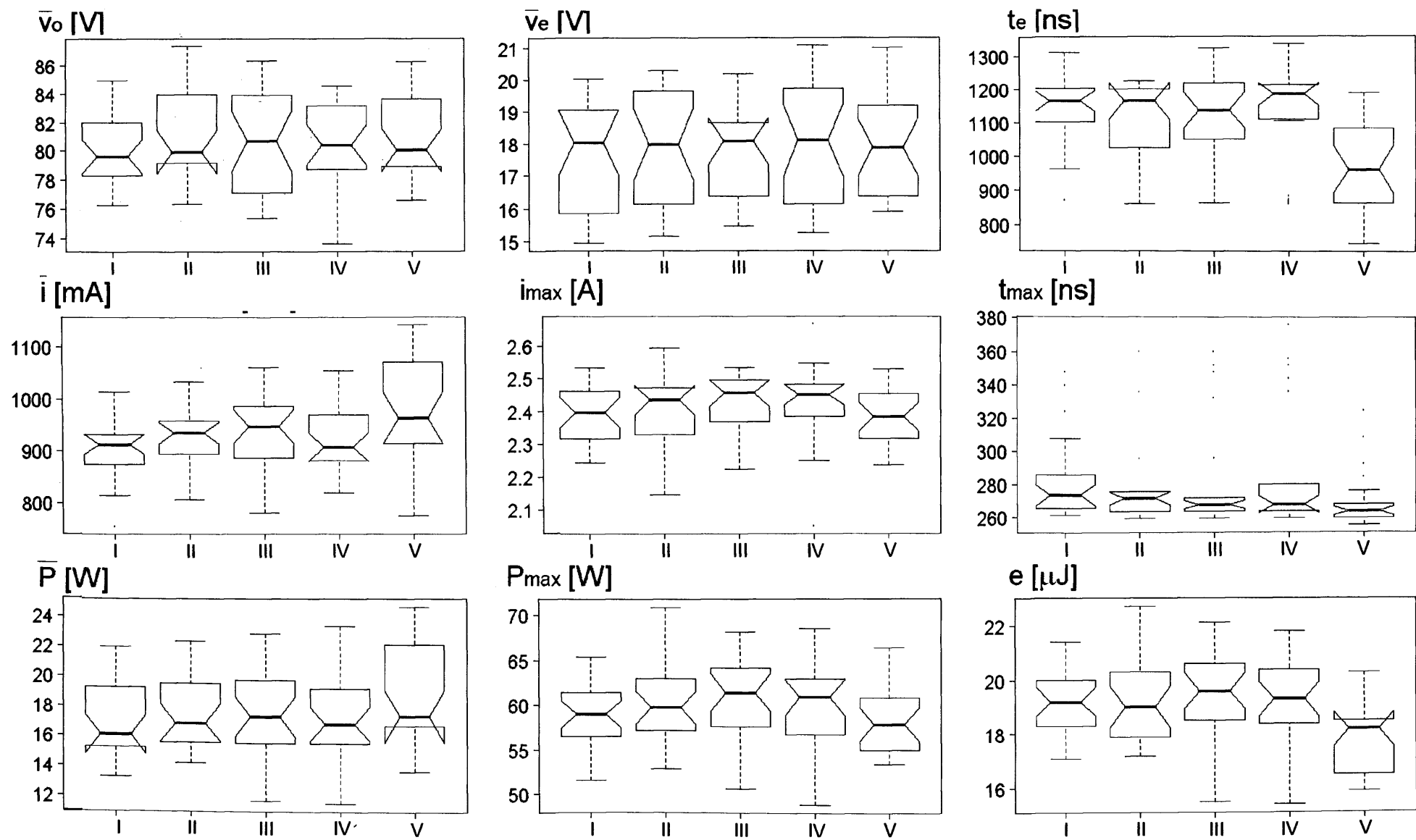


Fig. 5.12 Effect of the five experimental units (I, II, III, IV, V) on the nine response variables

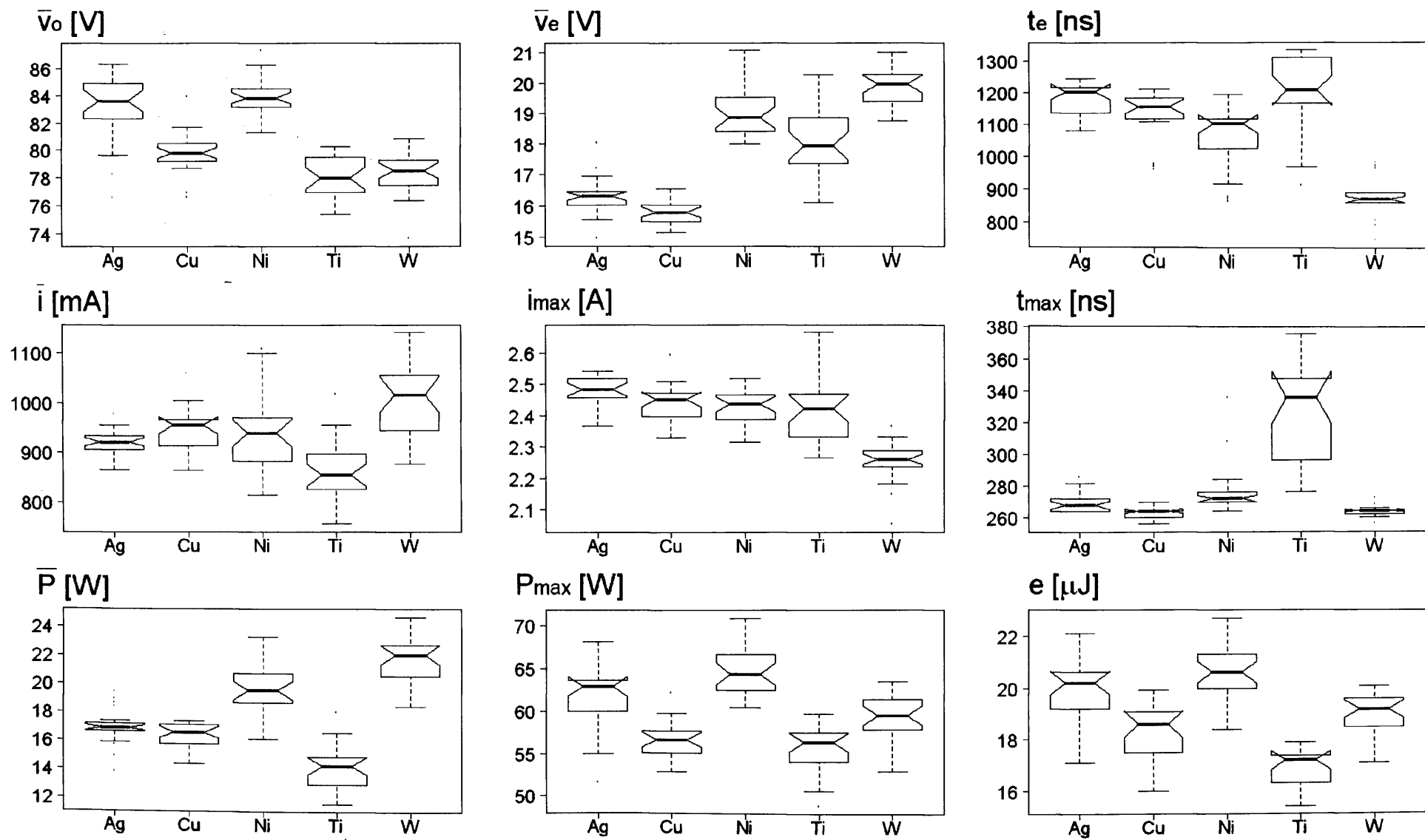


Fig. 5.13 Effect of the five electrode materials considered (Ag, Cu, Ni, Ti, W) on the nine response variables



In analysing qualitatively the effect of the material on the nine dimensional vector of the response variables, therefore, the experimental results related to the same material but originated from all the different experimental units pooled together. In this manner, for each material and for each of the 9 experimental variables, 25 measurement results are available rather than 5. This circumstance is expected to increase the confidence in the conclusions drawn in this study. The set of 9 notched box plots, one for each response variable, having the material as a grouping factor is displayed in Figure 5.13. In this figure it can be observed that, for each of the response variables, there is always at least one material whose effect on the response qualitatively appears significant. This means that micro EDM operations carried out with identical power generator set-up and with identical dielectric, but on different pairs of tool and workpiece electrode materials, show significant differences in the electrical properties of the average discharge. Therefore, there are some as yet unidentified material properties or combination of such that affect the energy conditions in which the dielectric undergoes sequences of breakdowns and recoveries. It is also concluded that a power generator delivering a pre-specified amount of energy per average pulse independently from the electrode material can not be realised.

## 5.4. Summary

In this chapter prediction of the shape change of the electrodes due to the wear phenomenon was demonstrated. Electrostatic field intensity modelling, together with relative wear ratio can give satisfying solution to that problem. A good understanding of the micro EDM process, the phenomenon change in the micro EDM domain, especially electrode wear, is crucial for achieving better results. The above prediction of the shape based on the electric field intensity and relative wear ratio and the following investigations show that some variations of the influencing parameters in micro EDM are not negligible. On one hand the FEA modelling of the electrostatic field caused by the two electrodes can very well represent on a macro level the areas where the sparks will most like take place and on the other the analytical expression of the relative wear ratio gives an answer to the dependency of the wear ratio on the material and energy share on each electrode. Unfortunately the conducted further investigation has confirmed that the energy distribution between the anode and cathode further depends on the electrode material. These results can be trusted because the wear ratio variability for the different materials showed that the material removal phenomenon was the same for all the materials. But still the experimental evidence analysed via an exploratory data analysis approach showed that the material of the electrodes used in micro EDM operations significantly affect the electrical characteristics of the measured average discharge pulses independently from the set-up parameters of the power generator.

Life is a journey not a destination

# *Chapter 6*

## **6. Contributions, conclusions and future work**

This chapter summarises the contributions of this investigation to knowledge in the micro EDM domain and the conclusions reached. Possible directions for further research are also suggested.

### **6.1 Contributions**

The main contribution of this investigation is the physical explanation of the micro EDM phenomenon and development of a procedure for obtaining the electrode shape deformation due to wear, together with the necessary critical analyses of the sources of its variability.

The specific contributions include:

- Identification of the machine tool accuracy requirements for the micro EDM process. The major sources of machining errors affecting the accuracy are identified including the machine positioning, setting up procedure and on-the-machine electrode grinding (dressing).
- Evaluation of the error caused by the on-the-machine measuring cycles which contributes directly to inaccuracy of the positions of the features machined by the micro EDM process.
- Estimate of the accuracy and repeatability of micro EDM machining. This helps the selection of the dressing position and effective electrode diameter calculation.
- Identification and characterisation of the dependence of the electrode shape change on the electrostatic field intensity created by the voltage. A

hypothesis was raised and subsequently verified for the trend of the electrode shape deformation.

- Development of a novel method for wear ratio calculation based on the geometry only which can be used in on-line CAM programming or for adaptive control of the electrode wear.
- Provision of quantitative experimental evidence in order to establish the variation of the electrode wear and possibilities to use compensation methods and machining strategies.
- Verifying the theoretical findings regarding the achievable accuracy.
- Development of a novel procedure for prediction of the electrode shape deformation based on the electrostatic field intensity and the wear ratio.
- Identification of the criterion for phenomenon change for the micro EDM domain based on the vapourisation rather than the melting of the material.
- Use of a novel approach for verifying the importance of material properties in the energy distribution between the electrodes.
- Identification of the limitation (natural tolerances) of the process utilising statistical methods.
- Evaluation of the influence of the material properties on the discharge characteristics of the process.

## **6.2 Discussion and Conclusions**

This research has investigated the micro EDM process using both an experimental and a theoretical approach. The work has been divided into three main different areas:

1. Machine tool requirements and accuracy restrictions, measuring cycles,

electrode preparation and holding;

2. Investigation of the electrode wear phenomenon and its variation in order to estimate the type and accuracy of a possible compensation methods used;
3. Proposal of a method for electrode shape deformation prediction, based on theoretical and experimental analysis. This has involved investigating the phenomenon of electrode wear and defining the boundaries of the natural tolerances of the micro EDM process and the phenomenon change due to the predominantly vaporising than melting material.

The following conclusions may be drawn:

- The machine used for micro EDM machining should be placed in a temperature-controlled environment with a constant ambient and dielectric temperature (Chapter 3).
- The machine should be checked regularly for its geometrical accuracy.
- If a grinding device is used, the type of device should be justified and its position should be selected after careful investigation of the geometrical accuracy of the machine.
- Tests should be made in advance for the preferred sparking conditions and the spark gap deviation should be measured.
- Speed is the main factor contributing to errors when using measuring cycles.
- When assigning process tolerances for micro EDM all activities during the process, such as type of electrode grinding, type of positioning and

duration of the operation should be considered. All these activities will accumulate errors, which should be taken into account.

- The investigation shows that variations of the wear ratio due to uncontrolled factors are not negligible especially in the micro EDM domain. This does not allow the use of compensation methods relying on the ratio staying fixed.
- Any electrode wear compensation method should allow for machining tolerances due to the variation of the volumetric wear ratio.
- When machining soft materials like brass and aluminium, machining strategies that ensure good flushing, should be adopted to avoid side sparking on the electrode.
- In cases where flushing becomes an issue, for instance when drilling small holes, steel is a preferred material because it is less affected by the flushing conditions.
- When using any new combination of electrode/workpiece materials and for any new diameter of the electrode, tests should be conducted on the machine to measure the wear ratio and assess its repeatability. The results should be used to justify the chosen compensation method and strategies for material removal.
- FEA modelling of the electrostatic field caused by the two electrodes can very well represent on a 'macro' level the areas where the sparks most likely will take place.
- The thermodynamic analysis of the relative wear ratio gives an answer to the dependency of the wear ratio on the material and energy share on each electrode.

- The conducted experiments for determining the wear ratio have confirmed that the energy distribution between the anode and cathode also depends on the material.
- The equal wear ratio variability for the different materials shows that the material removal phenomenon was the same for all the materials and is the key to the ultimate process capabilities, but this does not justify the use of compensation methods relying on the wear ratio staying fixed.
- Experimental evidence analysed via an exploratory data analysis approach showed that the material of the electrodes used in micro EDM operations are significantly affecting the electrical characteristics of the measured average discharge pulses independently from the set-up parameters of the power generator. This circumstance may have relevant implications in the current efforts aimed at extending the domain of application of EDM towards the nanoscale. It can also contribute to critical reconsideration of current models describing the erosion mechanism of electric discharge machining.



### 6.3 Future work

In this section a few directions of potential further investigation are suggested. In particular the following broad areas of further investigation have been identified.

1. Due to the large number of variables taking part in the process, extended testing will be required to determine parameters for the variables that will provide stable micro EDM operation when using standard materials. A wider variety of materials or specially selected materials including different grain structures and investigation of inter-grain boundaries and then effects of the material on the electrode wear should be included in further investigations.
2. Material properties and effects on the discharge characteristics are reported in this work, but explanation of this behaviour is beyond the remit of this research. Further investigation devoted only to the material behaviour during the discharge process should be launched, which most likely should consider Cathode Electron Emission Theory and the material ionization process.
3. Existing models of the EDM process claim to cover the whole range of process parameters and do not consider that the sparking phenomenon may change (similar to laser machining). Modelling of the micro EDM process based on the suggested phenomenon change to a vaporisation model is a potential field for further analytical and experimental research activities.

4. Determining the boundaries for a number of pure metals when the vaporisation model is accepted is another area of future research. Similar to high speed cutting where the phenomenon of plastic deformation changes when the speed of cut exceeds certain limits, in micro EDM the vaporisation model will have different limits as regards time of discharge and energy of the discharge for different materials;
5. Adaptive control seems to be a preferred solution for electrode wear compensation. Further investigation into pulse classification and its use for wear compensation could be of interest. In such a situation, introduction of richer and more complex sensory systems will allow the manipulation of the sparks on line compensation using an advanced CAM system will help to utilise a suitable electrode wear compensation method.



## Appendix A

### Measured accuracy of positioning and repeatability of positioning of AGIE Compact 1 micro EDM machine

1. Data for accuracy and repeatability of positioning along Y axes.

Interval number	Travel distance (mm)	$X_{ij}$ (i - measuring interval, j - number of measurement)														
		Two directional measurements ( $\mu\text{m}$ )														
		$\vec{1}$	$\overleftarrow{1}$	$\vec{2}$	$\overleftarrow{2}$	$\vec{3}$	$\overleftarrow{3}$	$\vec{4}$	$\overleftarrow{4}$	$\vec{5}$	$\overleftarrow{5}$	$\overline{X}_i \rightarrow$	$\overline{X}_i \leftarrow$	$\overline{X}_i$	$B_i$	$ B_i $
1	5	-5.22	-2.85	-5.47	-1.22	-3.83	-2.03	-4.81	-0.523	-2.995	-1.483	-4.4654	-1.6206	-3.043	-2.8448	2.8448
2	10	-8.25	-5.47	-8	-4.28	-7.09	-4.37	-7.176	-3.336	-6.234	-3.622	-7.3504	-4.2142	-5.7823	-3.1362	3.1362
3	15	-9.13	-5.89	-8.71	-5.79	-8.4	-5.24	-8.131	-5.294	-7.833	-5.028	-8.4398	-5.448	-6.9439	-2.9918	2.9918
4	20	-6.55	-2.87	-6.07	-2.22	-5.08	-1.63	-4.824	-1.415	-4.206	-0.76	-5.3454	-1.7796	-3.5625	-3.5658	3.5658
5	25	-6.48	-3.8	-6.91	-2.79	-5.31	-2.65	-6.005	-1.526	-4.265	-2.05	-5.7926	-2.5636	-4.1781	-3.229	3.229
6	30	-7.49	-4.97	-7.55	-3.74	-6.4	-3.93	-6.355	-2.551	-5.771	-3.093	-6.7146	-3.6558	-5.1852	-3.0588	3.0588
7	35	-5.93	-2.5	-5.16	-2.28	-5.03	-1.69	-4.743	-1.758	-4.486	-1.598	-5.07	-1.9642	-3.5171	-3.1058	3.1058
8	40	-6.1	-2.92	-6.3	-2.7	-4.86	-1.16	-4.77	-1.084	-3.538	-0.498	-5.1128	-1.6726	-3.3927	-3.4402	3.4402
9	45	-6.11	-3.09	-6.73	-2.86	-5.23	-1.63	-5.977	-1.577	-4.108	-1.122	-5.63	-2.0558	-3.8429	-3.5742	3.5742
10	50	-7.5	-4.97	-7.47	-4.31	-6.74	-3.93	-6.925	-2.913	-6.008	-3.078	-6.928	-3.8394	-5.3837	-3.0886	3.0886
11	55	-5.43	-2.44	-4.84	-1.9	-4.66	-1.67	-4.575	-1.373	-4.079	-1.19	-4.717	-1.7142	-3.2156	-3.0028	3.0028

Interval number	Travel distance (mm)	$X_{ij}$ (l - measuring interval, j - number of measurement)														
		Two directional measurements ( $\mu\text{m}$ )														
		$\rightarrow 1$	$\leftarrow 1$	$\rightarrow 2$	$\leftarrow 2$	$\rightarrow 3$	$\leftarrow 3$	$\rightarrow 4$	$\leftarrow 4$	$\rightarrow 5$	$\leftarrow 5$	$\overline{X}_i \rightarrow$	$\overline{X}_i \leftarrow$	$\overline{X}_i$	$B_i$	$ B_i $
12	60	-6.16	-3.17	-6.64	-3.67	-5.22	-2.12	-5.568	-1.973	-3.914	-0.488	-5.499	-2.2852	-3.8921	-3.2138	3.2138
13	65	-5.92	-3.34	-6.78	-3.36	-5.46	-2.54	-6.285	-2.613	-4.669	-1.433	-5.8212	-2.658	-4.2396	-3.1632	3.1632
14	70	-7.32	-4.68	-7.44	-4.64	-6.95	-4.21	-6.935	-3.621	-6.276	-3.295	-6.986	-4.0872	-5.5366	-2.8988	2.8988
15	75	-5.76	-2.89	-5.64	-2.72	-5.32	-2.5	-5.243	-2.266	-4.844	-2.009	-5.3622	-2.4764	-3.9193	-2.8858	2.8858
16	80	-6.1	-2.96	-6.91	-3.8	-5.7	-2.43	-6.376	-2.916	-4.595	-1.037	-5.935	-2.6278	-4.2814	-3.3072	3.3072
17	85	-5.78	-2.97	-6.84	-3.73	-5.41	-2.53	-6.479	-3.147	-5.214	-2.317	-5.9434	-2.9376	-4.4405	-3.0058	3.0058
18	90	-7.59	-4.33	-7.46	-4.37	-7.42	-4.06	-7.247	-3.921	-6.85	-3.611	-7.314	-4.0576	-5.6858	-3.2564	3.2564
19	95	-5.82	-2.87	-5.59	-2.9	-5.36	-2.33	-5.242	-2.504	-4.904	-2.013	-5.384	-2.5228	-3.9534	-2.8612	2.8612
20	100	-6.6	-3.43	-7.22	-4.15	-6.04	-2.93	-6.932	-4.008	-5.488	-2.433	-6.4564	-3.39	-4.9232	-3.0664	3.0664
21	105	-6.85	-4	-7.72	-4.65	-6.43	-3.44	-7.716	-4.614	-6.293	-3.343	-7.0012	-4.0076	-5.5044	-2.9936	2.9936
22	110	-7.64	-5.15	-7.48	-4.91	-7.36	-4.8	-7.477	-4.886	-7.259	-4.695	-7.4438	-4.887	-6.1654	-2.5568	2.5568
23	115	-7.04	-4.44	-6.85	-4.21	-6.41	-3.84	-6.598	-3.943	-6.188	-3.665	-6.6182	-4.0202	-5.3192	-2.598	2.598
											<b>min</b>	-8.4398	-5.448	-6.9439	<b>B mean</b>	<b>max B</b>
											<b>max</b>	-4.4654	-1.6206	-3.043	-3.08022	3.5742

Interval number	$X_{ij} - \overline{X}_i$										$\overset{\rightarrow}{\sigma}$	$\overset{\leftarrow}{\sigma}$	$R_i \rightarrow$	$R_i \leftarrow$	$2\overset{\rightarrow}{\sigma} + 2\overset{\leftarrow}{\sigma} +  B_i $
	$\overset{\rightarrow}{1}$	$\overset{\leftarrow}{1}$	$\overset{\rightarrow}{2}$	$\overset{\leftarrow}{2}$	$\overset{\rightarrow}{3}$	$\overset{\leftarrow}{3}$	$\overset{\rightarrow}{4}$	$\overset{\leftarrow}{4}$	$\overset{\rightarrow}{5}$	$\overset{\leftarrow}{5}$					
1	-0.75	-1.23	-1	0.401	0.631	-0.4	-0.3446	1.0976	1.4704	0.1376	1.031397	0.875218	4.125588	3.500871	6.658029745
2	-0.9	-1.25	-0.65	-0.06	0.259	-0.15	0.1744	0.8782	1.1164	0.5922	0.802748	0.824829	3.210992	3.299314	6.391353112
3	-0.69	-0.44	-0.27	-0.34	0.041	0.207	0.3088	0.154	0.6068	0.42	0.502479	0.371768	2.009916	1.487072	4.740294254
4	-1.2	-1.09	-0.72	-0.44	0.268	0.146	0.5214	0.3646	1.1394	1.0196	0.951083	0.80307	3.804332	3.21228	7.074105768
5	-0.68	-1.24	-1.12	-0.22	0.487	-0.09	-0.2124	1.0376	1.5276	0.5136	1.04083	0.856106	4.16332	3.424422	7.022871405
6	-0.78	-1.31	-0.84	-0.08	0.313	-0.28	0.3596	1.1048	0.9436	0.5628	0.778569	0.913014	3.114275	3.652054	6.441964555
7	-0.86	-0.53	-0.09	-0.31	0.042	0.271	0.327	0.2062	0.584	0.3662	0.547968	0.397065	2.19187	1.58826	4.995865433
8	-0.99	-1.25	-1.19	-1.02	0.258	0.511	0.3428	0.5886	1.5748	1.1746	1.123517	1.072165	4.494068	4.28866	7.831564235
9	-0.48	-1.03	-1.1	-0.8	0.397	0.423	-0.347	0.4788	1.522	0.9338	1.002629	0.864596	4.010514	3.458383	7.308648462
10	-0.57	-1.13	-0.54	-0.47	0.192	-0.09	0.003	0.9264	0.92	0.7614	0.61348	0.858129	2.453919	3.432516	6.031817563
11	-0.72	-0.72	-0.13	-0.19	0.062	0.045	0.142	0.3412	0.638	0.5242	0.489792	0.487585	1.959167	1.950338	4.957552699
12	-0.66	-0.89	-1.14	-1.38	0.283	0.164	-0.069	0.3122	1.585	1.7972	1.040432	1.231056	4.161728	4.924224	7.756776101
13	-0.1	-0.68	-0.95	-0.71	0.363	0.118	-0.4638	0.045	1.1522	1.225	0.805278	0.787422	3.221111	3.149688	6.348599551
14	-0.34	-0.59	-0.46	-0.55	0.032	-0.12	0.051	0.4662	0.71	0.7922	0.455443	0.614471	1.821773	2.457883	5.038627715
15	-0.4	-0.42	-0.28	-0.24	0.041	-0.02	0.1192	0.2104	0.5182	0.4674	0.361335	0.351514	1.445338	1.406057	4.31149781
16	-0.16	-0.34	-0.97	-1.17	0.235	0.202	-0.441	-0.2882	1.34	1.5908	0.86838	1.016589	3.473519	4.066357	7.077138123
17	0.168	-0.03	-0.9	-0.79	0.536	0.407	-0.5356	-0.2094	0.7294	0.6206	0.69686	0.551878	2.787441	2.20751	5.503275677

Interval number	$X_{ij} - \bar{X}_i$										$\overset{\rightarrow}{\sigma}$	$\overset{\leftarrow}{\sigma}$	$R_i \rightarrow$	$R_i \leftarrow$	$2\overset{\rightarrow}{\sigma} + 2\overset{\leftarrow}{\sigma} +  B_i $
	$\overset{\rightarrow}{1}$	$\overset{\leftarrow}{1}$	$\overset{\rightarrow}{2}$	$\overset{\leftarrow}{2}$	$\overset{\rightarrow}{3}$	$\overset{\leftarrow}{3}$	$\overset{\rightarrow}{4}$	$\overset{\leftarrow}{4}$	$\overset{\rightarrow}{5}$	$\overset{\leftarrow}{5}$					
18	-0.28	-0.27	-0.15	-0.31	-0.11	0.003	0.067	0.1366	0.464	0.4466	0.287191	0.312434	1.148763	1.249735	4.455648752
19	-0.44	-0.34	-0.21	-0.38	0.024	0.191	0.142	0.0188	0.48	0.5098	0.34899	0.372816	1.39596	1.491264	4.304811755
20	-0.14	-0.04	-0.77	-0.76	0.416	0.463	-0.4756	-0.618	0.9684	0.957	0.697611	0.723102	2.790443	2.892408	5.907825556
21	0.148	0.007	-0.71	-0.64	0.573	0.573	-0.7148	-0.6064	0.7082	0.6646	0.684461	0.62121	2.737844	2.48484	5.604941662
22	-0.19	-0.26	-0.04	-0.02	0.082	0.088	-0.0332	0.001	0.1848	0.192	0.142474	0.167462	0.569894	0.669848	3.176670885
23	-0.43	-0.42	-0.23	-0.19	0.208	0.177	0.0202	0.0772	0.4302	0.3552	0.340708	0.305767	1.362834	1.22307	3.89095155

Interval number	$R_i$	$\overline{X}_i + 2\overrightarrow{\sigma}$	$\overline{X}_i + 2\overleftarrow{\sigma}$
1	6.65803	-2.40261	0.129836
2	6.391353	-5.7449	-2.56454
3	4.740294	-7.43484	-4.70446
4	7.074106	-3.44323	-0.17346
5	7.022871	-3.71094	-0.85139
6	6.441965	-5.15746	-1.82977
7	4.995865	-3.97406	-1.17007
8	7.831564	-2.86577	0.47173
9	7.308648	-3.62474	-0.32661
10	6.031818	-5.70104	-2.12314
11	4.957553	-3.73742	-0.73903
12	7.756776	-3.41814	0.176912
13	6.3486	-4.21064	-1.08316
14	5.038628	-6.07511	-2.85826
15	4.311498	-4.63953	-1.77337
16	7.077138	-4.19824	-0.59462
17	5.503276	-4.54968	-1.83384
18	4.455649	-6.73962	-3.43273
19	4.304812	-4.68602	-1.77717
20	5.907826	-5.06118	-1.9438
21	5.604942	-5.63228	-2.76518
22	3.176671	-7.15885	-4.55208
23	3.890952	-5.93678	-3.40867
	min	-7.43484	-4.70446
	max	-2.40261	0.47173

Repeatability of positioning ( $\mu\text{m}$ )		
$\vec{R}$	$\overleftarrow{R}$	R
4.494068	4.924224	7.831564

Systematic positional deviation ( $\mu\text{m}$ )		
$\vec{E}$	$\overrightarrow{E}$	E
3.9744	3.8274	6.8192

M: Mean bidirectional positional deviation ( $\mu\text{m}$ )	3.9009
--	--------

Accuracy of positioning ( $\mu\text{m}$ )		
$\vec{A}$	$\overrightarrow{A}$	A
5.032236	5.176194	7.906572



2. Data for accuracy and repeatability of positioning along X axes.

Interval number	Travel distance (mm)	$X_{ij}$ (l - measuring interval, j - number of measurement)														
		Two directional measurements ( $\mu\text{m}$ )														
		$\vec{1}$	$\overleftarrow{1}$	$\vec{2}$	$\overleftarrow{2}$	$\vec{3}$	$\overleftarrow{3}$	$\vec{4}$	$\overleftarrow{4}$	$\vec{5}$	$\overleftarrow{5}$	$\overline{X}_i \rightarrow$	$\overline{X}_i \leftarrow$	$\overline{X}_i$	$B_i$	$ B_i $
1	5	-1.64	2.725	-1.02	2.679	-0.93	1.454	-0.913	1.377	-0.968	1.258	-1.0934	1.8986	0.4026	-2.992	2.992
2	10	-0.79	3.427	-0.27	3.735	-0.02	2.393	-0.186	2.231	-0.319	2.329	-0.3144	2.823	1.2543	-3.1374	3.1374
3	15	-0.6	3.786	0.009	3.903	0.17	2.995	0.065	2.93	-0.124	2.889	-0.0966	3.3006	1.602	-3.3972	3.3972
4	20	0.009	4.214	0.516	4.201	0.592	3.089	0.417	3.011	0.405	3.215	0.3878	3.546	1.9669	-3.1582	3.1582
5	25	0.58	5.116	1.056	4.666	1.173	3.725	0.968	3.534	0.868	3.756	0.929	4.1594	2.5442	-3.2304	3.2304
6	30	1.378	5.273	1.891	5.479	1.856	4.45	1.77	4.273	1.633	4.6	1.7056	4.815	3.2603	-3.1094	3.1094
7	35	1.847	5.72	2.196	6.204	2.427	5.179	2.208	5.217	2.097	5.374	2.155	5.5388	3.8469	-3.3838	3.3838
8	40	2.184	5.795	2.652	6.216	2.703	5.314	2.602	5.181	2.442	5.538	2.5166	5.6088	4.0627	-3.0922	3.0922
9	45	2.66	5.678	2.761	6.219	2.852	5.323	2.771	5.287	2.713	5.553	2.7514	5.612	4.1817	-2.8606	2.8606
10	50	2.74	5.967	2.873	6.434	2.994	5.594	2.914	5.471	2.837	5.66	2.8716	5.8252	4.3484	-2.9536	2.9536
11	55	2.527	5.982	2.876	6.346	2.923	5.772	2.834	5.491	2.667	5.79	2.7654	5.8762	4.3208	-3.1108	3.1108
12	60	2.397	5.768	2.732	6.068	2.642	5.417	2.592	5.193	2.445	5.502	2.5616	5.5896	4.0756	-3.028	3.028
13	65	2.403	5.751	2.907	5.97	2.863	5.134	2.766	5.069	2.638	5.373	2.7154	5.4594	4.0874	-2.744	2.744

Interval number	Travel distance (mm)	$X_{ij}$ (l - measuring interval, j - number of measurement)														
		Two directional measurements ( $\mu\text{m}$ )														
		$\vec{1}$	$\overleftarrow{1}$	$\vec{2}$	$\overleftarrow{2}$	$\vec{3}$	$\overleftarrow{3}$	$\vec{4}$	$\overleftarrow{4}$	$\vec{5}$	$\overleftarrow{5}$	$\overline{X}_i \rightarrow$	$\overline{X}_i \leftarrow$	$\overline{X}_i$	$B_i$	$ B_i $
14	70	2.433	5.86	2.963	6.201	2.898	5.386	2.768	5.282	2.657	5.776	2.7438	5.701	4.2224	-2.9572	2.9572
15	75	2.826	6.541	3.197	6.712	3.241	6.056	3.177	6.102	3.004	6.416	3.089	6.3654	4.7272	-3.2764	3.2764
16	80	2.912	6.41	3.545	6.76	3.332	6.003	3.328	6.021	3.305	6.394	3.2844	6.3176	4.801	-3.0332	3.0332
17	85	3.213	6.788	3.725	6.963	3.496	6.422	3.607	6.511	3.608	6.727	3.5298	6.6822	5.106	-3.1524	3.1524
18	90	3.684	7.187	4.108	7.29	3.912	6.89	4.029	6.937	3.89	7.171	3.9246	7.095	5.5098	-3.1704	3.1704
19	95	3.761	7.966	4.324	7.736	4.114	7.296	4.257	7.537	4.25	7.749	4.1412	7.6568	5.899	-3.5156	3.5156
20	100	3.808	7.528	4.293	7.496	4.136	7.293	4.178	7.439	4.218	7.468	4.1266	7.4448	5.7857	-3.3182	3.3182
21	105	4.057	7.741	4.597	7.889	4.44	7.514	4.599	7.622	4.681	7.746	4.4748	7.7024	6.0886	-3.2276	3.2276
22	110	4.814	8.453	5.439	8.393	5.063	8.007	5.191	7.938	5.136	7.842	5.1286	8.1266	6.6276	-2.998	2.998
23	115	5.468	9.225	5.931	9.211	5.852	8.859	5.75	8.784	5.862	8.739	5.7726	8.9636	7.3681	-3.191	3.191
24	120	5.376	9.116	5.73	9.029	5.659	8.65	5.561	8.658	5.686	8.556	5.6024	8.8018	7.2021	-3.1994	3.1994
25	125	5.729	9.176	6.002	9.088	6.014	8.785	5.823	8.712	5.843	8.628	5.8822	8.8778	7.38	-2.9956	2.9956
26	130	6.336	9.775	6.854	9.678	6.717	9.338	6.582	9.458	6.632	9.404	6.6242	9.5306	8.0774	-2.9064	2.9064
27	135	6.541	10.25	7.045	10.22	6.922	9.894	6.931	10.049	6.953	9.954	6.8784	10.0734	8.4759	-3.195	3.195
28	140	7.187	10.58	7.696	10.64	7.513	10.28	7.527	10.369	7.596	10.484	7.5038	10.4716	8.9877	-2.9678	2.9678

Interval number	Travel distance (mm)	$X_{ij}$ (I - measuring interval, j - number of measurement)														
		Two directional measurements ( $\mu\text{m}$ )														
		$\vec{1}$	$\overleftarrow{1}$	$\vec{2}$	$\overleftarrow{2}$	$\vec{3}$	$\overleftarrow{3}$	$\vec{4}$	$\overleftarrow{4}$	$\vec{5}$	$\overleftarrow{5}$	$\overline{X}_i \rightarrow$	$\overline{X}_i \leftarrow$	$\overline{X}_i$	$B_i$	$ B_i $
29	145	7.81	11.24	8.259	11.23	8.226	10.9	8.104	10.999	8.222	10.631	8.1242	10.999	9.5616	-2.8748	2.8748
30	150	8.423	11.56	8.59	11.52	8.683	11.33	8.525	11.3	8.593	10.925	8.5628	11.3262	9.9445	-2.7634	2.7634
31	155	8.421	12	8.6	12.06	8.886	11.81	8.793	11.794	8.778	11.492	8.6956	11.832	10.2638	-3.1364	3.1364
32	160	8.719	11.95	8.691	12.01	9.038	11.66	8.833	11.728	8.872	11.591	8.8306	11.7864	10.3085	-2.9558	2.9558
33	165	8.565	12.01	8.922	12.11	9.209	11.85	8.966	11.579	8.92	11.449	8.9164	11.7994	10.3579	-2.883	2.883
34	170	8.343	11.69	8.654	11.72	8.932	11.62	8.732	11.414	8.665	11.163	8.6652	11.5202	10.0927	-2.855	2.855
35	175	7.88	11.53	8.195	11.79	8.566	11.35	8.288	11.392	8.209	11.102	8.2276	11.4312	9.8294	-3.2036	3.2036
36	180	8.181	11.61	8.496	11.75	8.736	11.17	8.475	11.189	8.444	11.064	8.4664	11.3552	9.9108	-2.8888	2.8888
37	185	7.958	11.55	8.588	11.77	9.014	11.41	8.778	11.503	8.87	11.308	8.6416	11.5088	10.0752	-2.8672	2.8672
38	190	8.41	12.21	9.12	12.22	9.367	11.84	9.28	11.853	9.278	11.886	9.091	12.0012	10.5461	-2.9102	2.9102
39	195	8.248	12.36	9.26	12.4	9.553	12.03	9.537	12.396	9.347	12.03	9.189	12.2434	10.7162	-3.0544	3.0544
40	200	8.704	12.67	9.743	12.69	10.08	12.54	10.18	12.733	9.973	12.481	9.7366	12.6218	11.1792	-2.8852	2.8852
41	205	8.569	12.73	9.775	12.74	10.28	12.67	10.275	12.825	10.094	12.556	9.7988	12.702	11.2504	-2.9032	2.9032
42	210	9.163	13.37	10.48	13.33	10.79	13.18	10.722	13.26	10.758	13.178	10.3834	13.2632	11.8233	-2.8798	2.8798
43	215	9.092	14.03	10.85	14	11.28	13.83	11.219	13.926	10.979	13.624	10.6832	13.8826	12.2829	-3.1994	3.1994
44	220	9.666	14.56	11.44	14.31	11.84	14.28	11.87	14.335	11.775	14.052	11.3178	14.3066	12.8122	-2.9888	2.9888

Interval number	Travel distance (mm)	$X_{ij}$ (I - measuring interval, j - number of measurement)															
		Two directional measurements ( $\mu\text{m}$ )															
		$\vec{1}$	$\overleftarrow{1}$	$\vec{2}$	$\overleftarrow{2}$	$\vec{3}$	$\overleftarrow{3}$	$\vec{4}$	$\overleftarrow{4}$	$\vec{5}$	$\overleftarrow{5}$	$\overline{X}_i \rightarrow$	$\overline{X}_i \leftarrow$	$\overline{X}_i$	$B_i$	$ B_i $	
45	225	10.76	15.04	12.16	14.82	12.6	14.76	12.529	14.746	12.235	14.383	12.0582	14.75	13.4041	-2.6918	2.6918	
46	230	10.6	14.71	11.94	14.61	12.21	14.43	12.195	14.374	12.135	14.257	11.8156	14.476	13.1458	-2.6604	2.6604	
47	235	9.3	14.12	11.26	14.1	11.48	13.89	11.505	13.842	11.262	13.603	10.9614	13.9104	12.4359	-2.949	2.949	
												<b>min</b>	-1.0934	1.8986	0.4026	<b>B mean</b>	<b>max B</b>
												<b>max</b>	12.0582	14.75	13.4041	-6.21096	3.5156

Interval number	$X_{ij} - \overline{X}_i$												$R_i \rightarrow$	$R_i \leftarrow$	$2\overrightarrow{\sigma} + 2\overleftarrow{\sigma} +  B_i $
	$\rightarrow 1$	$\leftarrow 1$	$\rightarrow 2$	$\leftarrow 2$	$\rightarrow 3$	$\leftarrow 3$	$\rightarrow 4$	$\leftarrow 4$	$\rightarrow 5$	$\leftarrow 5$	$\rightarrow \sigma$	$\leftarrow \sigma$			
1	-0.54	0.826	0.072	0.78	0.165	-0.44	0.1804	-0.5216	0.1254	-0.6406	0.3067447	0.7368964	1.2269787	2.9475856	5.079282158
2	-0.47	0.604	0.047	0.912	0.299	-0.43	0.1284	-0.592	-0.0046	-0.494	0.2871669	0.7028442	1.1486674	2.8113769	5.117422144
3	-0.51	0.485	0.106	0.602	0.267	-0.31	0.1616	-0.3706	-0.0274	-0.4116	0.3022967	0.4996622	1.2091868	1.9986487	5.001117789
4	-0.38	0.668	0.128	0.655	0.204	-0.46	0.0292	-0.535	0.0172	-0.331	0.2251504	0.6082524	0.9006016	2.4330097	4.825005618
5	-0.35	0.957	0.127	0.507	0.244	-0.43	0.039	-0.6254	-0.061	-0.4034	0.2251155	0.6917888	0.9004621	2.7671554	5.064208733
6	-0.33	0.458	0.185	0.664	0.15	-0.36	0.0644	-0.542	-0.0726	-0.215	0.2084066	0.5300646	0.8336263	2.1202585	4.586342385
7	-0.31	0.181	0.041	0.665	0.272	-0.36	0.053	-0.3218	-0.058	-0.1648	0.2101797	0.428805	0.8407187	1.7152199	4.661769305
8	-0.33	0.186	0.135	0.607	0.186	-0.29	0.0854	-0.4278	-0.0746	-0.0708	0.2100947	0.4117933	0.840379	1.6471731	4.335976028
9	-0.09	0.066	0.01	0.607	0.101	-0.29	0.0196	-0.325	-0.0384	-0.059	0.0714584	0.3759761	0.2858335	1.5039043	3.755468885
10	-0.13	0.142	0.001	0.609	0.122	-0.23	0.0424	-0.3542	-0.0346	-0.1652	0.0939377	0.3863117	0.375751	1.5452466	3.914098814
11	-0.24	0.106	0.111	0.47	0.158	-0.1	0.0686	-0.3852	-0.0984	-0.0862	0.1645397	0.3156631	0.6581586	1.2626524	4.071205545
12	-0.16	0.178	0.17	0.478	0.08	-0.17	0.0304	-0.3966	-0.1166	-0.0876	0.1388463	0.3374349	0.5553853	1.3497395	3.980562401
13	-0.31	0.292	0.192	0.511	0.148	-0.33	0.0506	-0.3904	-0.0774	-0.0864	0.20288	0.390994	0.8115201	1.563976	3.931748007
14	-0.31	0.159	0.219	0.5	0.154	-0.32	0.0242	-0.419	-0.0868	0.075	0.210085	0.3727238	0.8403399	1.490895	4.122817482
15	-0.26	0.176	0.108	0.347	0.152	-0.31	0.088	-0.2634	-0.085	0.0506	0.1724137	0.2822389	0.689655	1.1289556	4.185705305
16	-0.37	0.092	0.261	0.442	0.048	-0.31	0.0436	-0.2966	0.0206	0.0764	0.2297745	0.3150544	0.9190978	1.2602178	4.122857789
17	-0.32	0.106	0.195	0.281	-0.03	-0.26	0.0772	-0.1712	0.0782	0.0448	0.1947324	0.2174068	0.7789295	0.869627	3.976678284

Interval number	$X_{ij} - \overline{X}_i$												$R_i \rightarrow$	$R_i \leftarrow$	$2\overset{\rightarrow}{\sigma} + 2\overset{\leftarrow}{\sigma} +  B_i $
	$\overset{\rightarrow}{1}$	$\overset{\leftarrow}{1}$	$\overset{\rightarrow}{2}$	$\overset{\leftarrow}{2}$	$\overset{\rightarrow}{3}$	$\overset{\leftarrow}{3}$	$\overset{\rightarrow}{4}$	$\overset{\leftarrow}{4}$	$\overset{\rightarrow}{5}$	$\overset{\leftarrow}{5}$	$\overset{\rightarrow}{\sigma}$	$\overset{\leftarrow}{\sigma}$			
18	-0.24	0.092	0.183	0.195	-0.01	-0.21	0.1044	-0.158	-0.0346	0.076	0.1610739	0.1726659	0.6442956	0.6906634	3.837879517
19	-0.38	0.309	0.183	0.079	-0.03	-0.36	0.1158	-0.1198	0.1088	0.0922	0.2258068	0.2524415	0.9032271	1.0097659	4.472096508
20	-0.32	0.083	0.166	0.051	0.009	-0.15	0.0514	-0.0058	0.0914	0.0232	0.1872693	0.0910478	0.7490773	0.3641912	3.874834229
21	-0.42	0.039	0.122	0.187	-0.03	-0.19	0.1242	-0.0804	0.2062	0.0436	0.2493215	0.1415708	0.9972859	0.5662833	4.009384619
22	-0.31	0.326	0.31	0.266	-0.07	-0.12	0.0624	-0.1886	0.0074	-0.2846	0.2255954	0.2776586	0.9023817	1.1106344	4.004508075
23	-0.3	0.261	0.158	0.247	0.079	-0.1	-0.0226	-0.1796	0.0894	-0.2246	0.1821258	0.2362092	0.7285031	0.9448369	4.02767002
24	-0.23	0.314	0.128	0.227	0.057	-0.15	-0.0414	-0.1438	0.0836	-0.2458	0.1409301	0.2522305	0.5637205	1.0089218	3.985721149
25	-0.15	0.298	0.12	0.21	0.132	-0.09	-0.0592	-0.1658	-0.0392	-0.2498	0.1227139	0.2406288	0.4908556	0.962515	3.722285309
26	-0.29	0.244	0.23	0.147	0.093	-0.19	-0.0422	-0.0726	0.0078	-0.1266	0.1912595	0.1869834	0.765038	0.7479337	3.662885863
27	-0.34	0.181	0.167	0.143	0.044	-0.18	0.0526	-0.0244	0.0746	-0.1194	0.194825	0.1581038	0.7793002	0.6324151	3.900857626
28	-0.32	0.108	0.192	0.169	0.009	-0.19	0.0232	-0.1026	0.0922	0.0124	0.1913288	0.1469023	0.7653151	0.5876094	3.644262246
29	-0.31	0.244	0.135	0.228	0.102	-0.1	-0.0202	0	0.0978	-0.368	0.185222	0.2538503	0.7408881	1.0154014	3.752944757
30	-0.14	0.23	0.027	0.192	0.12	0.006	-0.0378	-0.0262	0.0302	-0.4012	0.0962715	0.2506376	0.385086	1.0025503	3.457218156
31	-0.27	0.169	-0.1	0.231	0.19	-0.02	0.0974	-0.038	0.0824	-0.34	0.185117	0.2232991	0.740468	0.8931965	3.953232234
32	-0.11	0.16	-0.14	0.219	0.207	-0.12	0.0024	-0.0584	0.0414	-0.1954	0.1384532	0.1805029	0.553813	0.7220116	3.5937123
33	-0.35	0.208	0.006	0.312	0.293	0.052	0.0496	-0.2204	0.0036	-0.3504	0.2300007	0.2802727	0.9200026	1.1210909	3.903546753
34	-0.32	0.173	-0.01	0.196	0.267	0.095	0.0668	-0.1062	-0.0002	-0.3572	0.2118861	0.2324085	0.8475442	0.9296339	3.743589062
35	-0.35	0.096	-0.03	0.357	0.338	-0.08	0.0604	-0.0392	-0.0186	-0.3292	0.2451516	0.2517354	0.9806063	1.0069415	4.197373925

Interval number	$X_{ij} - \overline{X}_i$														
	$\rightarrow 1$	$\leftarrow 1$	$\rightarrow 2$	$\leftarrow 2$	$\rightarrow 3$	$\leftarrow 3$	$\rightarrow 4$	$\leftarrow 4$	$\rightarrow 5$	$\leftarrow 5$	$\rightarrow \sigma$	$\leftarrow \sigma$	$R_i \rightarrow$	$R_i \leftarrow$	$2\overrightarrow{\sigma} + 2\overleftarrow{\sigma} +  B_i $
36	-0.29	0.25	0.03	0.392	0.27	-0.18	0.0086	-0.1662	-0.0224	-0.2912	0.197224	0.3009389	0.7888959	1.2037555	3.885125697
37	-0.68	0.045	-0.05	0.257	0.372	-0.1	0.1364	-0.0058	0.2284	-0.2008	0.4122	0.1715567	1.6487998	0.6862268	4.034713295
38	-0.68	0.212	0.029	0.214	0.276	-0.16	0.189	-0.1482	0.187	-0.1152	0.3909821	0.1950082	1.5639284	0.7800328	4.082180603
39	-0.94	0.119	0.071	0.156	0.364	-0.21	0.348	0.1526	0.158	-0.2134	0.5406214	0.1953479	2.1624856	0.7813916	4.526338593
40	-1.03	0.043	0.006	0.07	0.346	-0.08	0.4434	0.1112	0.2364	-0.1408	0.5997469	0.107246	2.3989875	0.4289839	4.299185684
41	-1.23	0.024	-0.02	0.036	0.482	-0.04	0.4762	0.123	0.2952	-0.146	0.7175306	0.0996067	2.8701225	0.3984269	4.537474706
42	-1.22	0.102	0.1	0.068	0.408	-0.08	0.3386	-0.0032	0.3746	-0.0852	0.6928941	0.0848864	2.7715766	0.3395456	4.435361085
43	-1.59	0.143	0.162	0.121	0.598	-0.05	0.5358	0.0434	0.2958	-0.2586	0.9069235	0.1631864	3.6276939	0.6527456	5.339619755
44	-1.65	0.248	0.122	0.004	0.52	-0.03	0.5522	0.0284	0.4572	-0.2546	0.9391407	0.1789254	3.7565627	0.7157016	5.224932149
45	-1.3	0.289	0.104	0.071	0.545	0.011	0.4708	-0.004	0.1768	-0.367	0.7484362	0.2363197	2.9937447	0.9452788	4.661311737
46	-1.22	0.233	0.123	0.136	0.393	-0.05	0.3794	-0.102	0.3194	-0.219	0.6880471	0.1826568	2.7521884	0.7306271	4.401807747
47	-1.66	0.21	0.299	0.191	0.519	-0.02	0.5436	-0.0684	0.3006	-0.3074	0.935978	0.2121492	3.743912	0.848597	5.245254462

Interval number	$R_i$	$\overline{X}_i + 2\sigma^{\rightarrow}$	$\overline{X}_i + 2\sigma^{\leftarrow}$
1	5.079282	-0.47991	3.372393
2	5.117422	0.259934	4.228688
3	5.001118	0.507993	4.299924
4	4.825006	0.838101	4.762505
5	5.064209	1.379231	5.542978
6	4.586342	2.122413	5.875129
7	4.661769	2.575359	6.39641
8	4.335976	2.936789	6.432387
9	3.755469	2.894317	6.363952
10	3.914099	3.059475	6.597823
11	4.071206	3.094479	6.507526
12	3.980562	2.839293	6.26447
13	3.931748	3.12116	6.241388
14	4.122817	3.16397	6.446448
15	4.185705	3.433827	6.929878
16	4.122858	3.743949	6.947709
17	3.976678	3.919265	7.117014
18	3.83788	4.246748	7.440332
19	4.472097	4.592814	8.161683
20	3.874834	4.501139	7.626896
21	4.009385	4.973443	7.985542
22	4.004508	5.579791	8.681917
23	4.02767	6.136852	9.436018
24	3.985721	5.88426	9.306261
25	3.722285	6.127628	9.359058
26	3.662886	7.006719	9.904567
27	3.900858	7.26805	10.38961
28	3.644262	7.886458	10.7654
29	3.752945	8.494644	11.5067



Interval number	$R_i$	$\overline{X}_i + 2\vec{\sigma}$	$\overline{X}_i + 2\overleftarrow{\sigma}$
30	3.457218	8.755343	11.82748
31	3.953232	9.065834	12.2786
32	3.593712	9.107506	12.14741
33	3.903547	9.376401	12.35995
34	3.743589	9.088972	11.98502
35	4.197374	8.717903	11.93467
36	3.885126	8.860848	11.95708
37	4.034713	9.466	11.85191
38	4.082181	9.872964	12.39122
39	4.526339	10.27024	12.6341
40	4.299186	10.93609	12.83629
41	4.537475	11.23386	12.90121
42	4.435361	11.76919	13.43297
43	5.33962	12.49705	14.20897
44	5.224932	13.19608	14.66445
45	4.661312	13.55507	15.22264
46	4.401808	13.19169	14.84131
47	5.245254	12.83336	14.3347
	min	-0.47991	3.372393
	max	13.55507	15.22264

repeatability of positioning ( $\mu\text{m}$ )		
$\vec{R}$	$\overleftarrow{R}$	R
3.756563	2.947586	5.33962

Systematic positional deviation ( $\mu\text{m}$ )		
$\vec{E}$	$\overrightarrow{E}$	E
13.1516	12.8514	15.8434

M: Mean bidirectional positional deviation ( $\mu\text{m}$ )	13.0015
--	---------

Accuracy of positioning ( $\mu\text{m}$ )		
$\vec{A}$	$\overrightarrow{A}$	A
14.03498	11.85025	15.70255

3. Data for accuracy and repeatability of positioning along Z axes.

Interval number	Travel distance (mm)	$X_{ij}$ (i - measuring interval, j - number of measurement)														
		Two directional measurements ( $\mu\text{m}$ )														
		$\vec{1}$	$\overleftarrow{1}$	$\vec{2}$	$\overleftarrow{2}$	$\vec{3}$	$\overleftarrow{3}$	$\vec{4}$	$\overleftarrow{4}$	$\vec{5}$	$\overleftarrow{5}$	$\overline{X}_i \rightarrow$	$\overline{X}_i \leftarrow$	$\overline{X}_i$	$B_i$	$ B_i $
1	5	0.288	1.357	0.96	1.105	0.714	1.354	0.887	1.175	0.799	1.322	0.7296	1.2626	0.9961	-0.533	0.533
2	10	0.948	1.295	1.688	1.01	1.517	1.319	1.751	1.186	1.676	1.329	1.516	1.2278	1.3719	0.2882	0.2882
3	15	1.894	1.634	2.446	1.362	2.334	1.62	2.419	1.498	2.422	1.739	2.303	1.5706	1.9368	0.7324	0.7324
4	20	1.086	0.83	1.612	0.587	1.515	0.944	1.739	0.904	1.744	0.991	1.5392	0.8512	1.1952	0.688	0.688
5	25	0.966	0.704	1.479	0.544	1.346	0.871	1.527	0.751	1.335	0.77	1.3306	0.728	1.0293	0.6026	0.6026
6	30	1.492	1.312	2.065	1.056	1.939	1.33	2.101	1.217	1.912	1.194	1.9018	1.2218	1.5618	0.68	0.68
7	35	1.568	1.211	2.031	0.875	1.838	1.223	2.046	1.089	1.873	0.971	1.8712	1.0738	1.4725	0.7974	0.7974
8	40	1.275	1.183	1.69	0.916	1.6	1.236	1.844	1.012	1.655	1.058	1.6128	1.081	1.3469	0.5318	0.5318
9	45	1.482	1.324	1.869	1.131	1.971	1.438	2.087	1.336	1.89	1.379	1.8598	1.3216	1.5907	0.5382	0.5382
10	50	0.846	0.836	1.276	0.549	1.297	0.79	1.354	0.751	1.177	0.616	1.19	0.7084	0.9492	0.4816	0.4816
11	55	0.209	0.12	0.44	-0.31	0.494	-0.12	0.469	-0.294	0.19	-0.386	0.3604	-0.1968	0.0818	0.5572	0.5572
12	60	0.896	0.97	1.322	0.634	1.321	0.786	1.287	0.801	1.15	0.742	1.1952	0.7866	0.9909	0.4086	0.4086
13	65	1.523	1.699	1.964	1.467	2.021	1.691	2.015	1.689	1.889	1.498	1.8824	1.6088	1.7456	0.2736	0.2736
14	70	1.189	1.298	1.483	1.052	1.546	1.08	1.357	0.994	1.257	0.779	1.3664	1.0406	1.2035	0.3258	0.3258

Interval number	Travel distance (mm)	$X_{ij}$ (i - measuring interval, j - number of measurement)														
		Two directional measurements ( $\mu\text{m}$ )										$\bar{X}_i \rightarrow$	$\bar{X}_i \leftarrow$	$\bar{X}_i$	$B_i$	$ B_i $
		$\vec{1}$	$\overleftarrow{1}$	$\vec{2}$	$\overleftarrow{2}$	$\vec{3}$	$\overleftarrow{3}$	$\vec{4}$	$\overleftarrow{4}$	$\vec{5}$	$\overleftarrow{5}$					
15	75	1.332	1.437	1.537	1.25	1.695	1.405	1.636	1.597	1.692	1.281	1.5784	1.394	1.4862	0.1844	0.1844
16	80	0.859	0.934	1.177	0.751	1.334	0.871	1.149	1.026	1.088	0.697	1.1214	0.8558	0.9886	0.2656	0.2656
17	85	0.636	0.679	0.954	0.625	1.111	0.557	0.929	0.712	0.954	0.477	0.9168	0.61	0.7634	0.3068	0.3068
18	90	1.433	1.369	1.684	1.253	1.873	1.094	1.625	1.236	1.495	0.962	1.622	1.1828	1.4024	0.4392	0.4392
19	95	1.024	0.85	1.234	0.729	1.423	0.537	1.193	0.788	1.189	0.551	1.2126	0.691	0.9518	0.5216	0.5216
20	100	1.022	0.722	1.273	0.778	1.669	0.808	1.395	1.034	1.492	0.748	1.3702	0.818	1.0941	0.5522	0.5522
21	105	0.852	0.642	1.244	0.816	1.553	0.67	1.247	0.884	1.311	0.563	1.2414	0.715	0.9782	0.5264	0.5264
22	110	0.581	0.095	0.851	0.165	0.983	0.06	0.722	0.363	0.807	0.051	0.7888	0.1468	0.4678	0.642	0.642
23	115	0.366	-0.18	0.68	0.048	0.828	0.027	0.509	0.18	0.645	-0.153	0.6056	-0.0148	0.2954	0.6204	0.6204
24	120	0.586	0.104	0.989	0.513	1.335	0.388	0.949	0.769	1.319	0.454	1.0356	0.4456	0.7406	0.59	0.59
25	125	1.115	0.516	1.572	0.893	1.761	0.691	1.382	1.065	1.626	0.647	1.4912	0.7624	1.1268	0.7288	0.7288
26	130	1.034	0.518	1.441	0.822	1.532	0.509	1.144	0.919	1.394	0.611	1.309	0.6758	0.9924	0.6332	0.6332
27	135	0.807	0.289	1.273	0.722	1.413	0.529	1.097	0.943	1.512	0.722	1.2204	0.641	0.9307	0.5794	0.5794
28	140	0.758	0.087	1.2	0.533	1.326	0.092	1.026	0.554	1.338	0.335	1.1296	0.3202	0.7249	0.8094	0.8094
29	145	0.684	0.068	1.082	0.483	1.127	-0.03	0.734	0.442	1.044	0.09	0.9342	0.2098	0.572	0.7244	0.7244
30	150	0.692	0.254	1.254	0.868	1.338	0.379	1.054	0.845	1.488	0.696	1.1652	0.6084	0.8868	0.5568	0.5568

Interval number	Travel distance (mm)	$X_{ij}$ (I - measuring interval, j - number of measurement)														
		Two directional measurements ( $\mu\text{m}$ )														
		$\vec{1}$	$\overleftarrow{1}$	$\vec{2}$	$\overleftarrow{2}$	$\vec{3}$	$\overleftarrow{3}$	$\vec{4}$	$\overleftarrow{4}$	$\vec{5}$	$\overleftarrow{5}$	$\overline{X}_i \rightarrow$	$\overline{X}_i \leftarrow$	$\overline{X}_i$	$B_i$	$ B_i $
31	155	0.657	-0.04	1.127	0.463	1.137	-0.06	0.834	0.457	1.326	0.288	1.0162	0.221	0.6186	0.7952	0.7952
32	160	0.665	0	1.125	0.563	1.161	0.109	0.918	0.468	1.232	0.214	1.0202	0.2708	0.6455	0.7494	0.7494
33	165	0.129	-0.33	0.626	0.181	0.568	-0.22	0.445	0.119	0.867	0.095	0.527	-0.0314	0.2478	0.5584	0.5584
34	170	0.22	-0.32	0.763	0.381	0.745	-0.08	0.574	0.151	0.878	0.059	0.636	0.0382	0.3371	0.5978	0.5978
35	175	0.131	-0.62	0.687	0.023	0.501	-0.45	0.217	-0.348	0.585	-0.377	0.4242	-0.3542	0.035	0.7784	0.7784
36	180	-0.46	-0.91	0.272	-0.17	0.231	-0.48	0.118	-0.274	0.527	-0.135	0.1384	-0.3928	-0.1272	0.5312	0.5312
37	185	-0.34	-0.67	0.364	0.007	0.07	-0.43	-0.081	-0.416	0.38	-0.223	0.079	-0.3478	-0.1344	0.4268	0.4268
38	190	-0.74	-0.89	0.055	-0.19	-0.3	-0.63	-0.285	-0.471	-0.003	-0.327	-0.2544	-0.5026	-0.3785	0.2482	0.2482
39	195	-0.61	0.03	0.227	0.718	-0.12	0.211	-0.235	0.276	0.023	0.396	-0.1418	0.3262	0.0922	-0.468	0.468
											<b>min</b>	-0.2544	-0.5026	-0.3785	<b>B mean</b>	<b>max B</b>
											<b>max</b>	2.303	1.6088	1.9368	0.837843	0.8094

Interval number	$X_{ij} - \overline{X}_i$										$\overset{\rightarrow}{\sigma}$	$\overset{\leftarrow}{\sigma}$	$R_i \rightarrow$	$R_i \leftarrow$	$\overset{\rightarrow}{2\sigma} + \overset{\leftarrow}{2\sigma} +  B_i $
	$\overset{\rightarrow}{1}$	$\overset{\leftarrow}{1}$	$\overset{\rightarrow}{2}$	$\overset{\leftarrow}{2}$	$\overset{\rightarrow}{3}$	$\overset{\leftarrow}{3}$	$\overset{\rightarrow}{4}$	$\overset{\leftarrow}{4}$	$\overset{\rightarrow}{5}$	$\overset{\leftarrow}{5}$					
1	-0.44	0.094	0.23	-0.16	-0.02	0.091	0.1574	-0.0876	0.0694	0.0594	0.263595	0.1154396	1.0543798	0.4617584	1.291069098
2	-0.57	0.067	0.172	-0.22	1E-03	0.091	0.235	-0.0418	0.16	0.1012	0.3290266	0.134405	1.3161064	0.5376199	1.215063159
3	-0.41	0.063	0.143	-0.21	0.031	0.049	0.116	-0.0726	0.119	0.1684	0.2325446	0.1445711	0.9301785	0.5782844	1.486631418
4	-0.45	-0.02	0.073	-0.26	-0.02	0.093	0.1998	0.0528	0.2048	0.1398	0.2707115	0.1590557	1.0828459	0.6362226	1.547534241
5	-0.36	-0.02	0.148	-0.18	0.015	0.143	0.1964	0.023	0.0044	0.042	0.2201052	0.1195554	0.8804208	0.4782217	1.281921257
6	-0.41	0.09	0.163	-0.17	0.037	0.108	0.1992	-0.0048	0.0102	-0.0278	0.2427647	0.1096914	0.9710588	0.4387655	1.384912172
7	-0.3	0.137	0.16	-0.2	-0.03	0.149	0.1748	0.0152	0.0018	-0.1028	0.1930847	0.1511661	0.7723388	0.6046645	1.48590166
8	-0.34	0.102	0.077	-0.17	-0.01	0.155	0.2312	-0.069	0.0422	-0.023	0.2094438	0.1293677	0.8377751	0.5174708	1.20942296
9	-0.38	0.002	0.009	-0.19	0.111	0.116	0.2272	0.0144	0.0302	0.0574	0.2278787	0.1155262	0.9115148	0.4621048	1.225009767
10	-0.34	0.128	0.086	-0.16	0.107	0.082	0.164	0.0426	-0.013	-0.0924	0.2026364	0.1211417	0.8105455	0.4845666	1.129156053
11	-0.15	0.317	0.08	-0.11	0.134	0.078	0.1086	-0.0972	-0.1704	-0.1892	0.148271	0.2020933	0.5930841	0.8083732	1.257928662
12	-0.3	0.183	0.127	-0.15	0.126	-0	0.0918	0.0144	-0.0452	-0.0446	0.1815866	0.1215722	0.7263465	0.4862888	1.014917638
13	-0.36	0.09	0.082	-0.14	0.139	0.082	0.1326	0.0802	0.0066	-0.1108	0.2077638	0.1158758	0.8310552	0.4635032	0.920879208
14	-0.18	0.257	0.117	0.011	0.18	0.039	-0.0094	-0.0466	-0.1094	-0.2616	0.1494818	0.186107	0.5979271	0.7444278	0.99697746
15	-0.25	0.043	-0.04	-0.14	0.117	0.011	0.0576	0.203	0.1136	-0.113	0.1518595	0.1384594	0.6074379	0.5538375	0.76503771
16	-0.26	0.078	0.056	-0.1	0.213	0.015	0.0276	0.1702	-0.0334	-0.1588	0.1724972	0.1337113	0.689989	0.534845	0.878017005
17	-0.28	0.069	0.037	0.015	0.194	-0.05	0.0122	0.102	0.0372	-0.133	0.1728285	0.0947206	0.6913141	0.3788826	0.841898339
18	-0.19	0.186	0.062	0.07	0.251	-0.09	0.003	0.0532	-0.127	-0.2208	0.1722672	0.1573744	0.6890689	0.6294976	1.098483257

Interval number	$X_{ij} - \overline{X}_i$										$\overset{\rightarrow}{\sigma}$	$\overset{\leftarrow}{\sigma}$	$R_i \rightarrow$	$R_i \leftarrow$	$2\overset{\rightarrow}{\sigma} + 2\overset{\leftarrow}{\sigma} +  B_i $
	$\overset{\rightarrow}{1}$	$\overset{\leftarrow}{1}$	$\overset{\rightarrow}{2}$	$\overset{\leftarrow}{2}$	$\overset{\rightarrow}{3}$	$\overset{\leftarrow}{3}$	$\overset{\rightarrow}{4}$	$\overset{\leftarrow}{4}$	$\overset{\rightarrow}{5}$	$\overset{\leftarrow}{5}$					
19	-0.19	0.159	0.021	0.038	0.21	-0.15	-0.0196	0.097	-0.0236	-0.14	0.1425107	0.1409344	0.5700428	0.5637375	1.088490166
20	-0.35	-0.1	-0.1	-0.04	0.299	-0.01	0.0248	0.216	0.1218	-0.07	0.2426019	0.124972	0.9704077	0.499888	1.287347868
21	-0.39	-0.07	0.003	0.101	0.312	-0.05	0.0056	0.169	0.0696	-0.152	0.2517981	0.1315485	1.0071925	0.5261939	1.293093207
22	-0.21	-0.05	0.062	0.018	0.194	-0.09	-0.0668	0.2162	0.0182	-0.0958	0.1496302	0.1289077	0.5985208	0.5156309	1.19907586
23	-0.24	-0.16	0.074	0.063	0.222	0.042	-0.0966	0.1948	0.0394	-0.1382	0.1755628	0.1489319	0.7022512	0.5957275	1.269389346
24	-0.45	-0.34	-0.05	0.067	0.299	-0.06	-0.0866	0.3234	0.2834	0.0084	0.3089366	0.239379	1.2357463	0.957516	1.686631103
25	-0.38	-0.25	0.081	0.131	0.27	-0.07	-0.1092	0.3026	0.1348	-0.1154	0.250471	0.2166513	1.0018838	0.8666053	1.663044578
26	-0.28	-0.16	0.132	0.146	0.223	-0.17	-0.165	0.2432	0.085	-0.0648	0.2104923	0.1853664	0.8419691	0.7414656	1.424917348
27	-0.41	-0.35	0.053	0.081	0.193	-0.11	-0.1234	0.302	0.2916	0.081	0.2788455	0.2453436	1.1153819	0.9813745	1.627778227
28	-0.37	-0.23	0.07	0.213	0.196	-0.23	-0.1036	0.2338	0.2084	0.0148	0.2427855	0.2272789	0.971142	0.9091156	1.749528811
29	-0.25	-0.14	0.148	0.273	0.193	-0.24	-0.2002	0.2322	0.1098	-0.1198	0.2084183	0.2358245	0.8336733	0.943298	1.612885681
30	-0.47	-0.35	0.089	0.26	0.173	-0.23	-0.1112	0.2366	0.3228	0.0876	0.3075015	0.2780599	1.2300062	1.1122395	1.727922861
31	-0.36	-0.26	0.111	0.242	0.121	-0.28	-0.1822	0.236	0.3098	0.067	0.2669582	0.2585933	1.0678329	1.0343732	1.846303093
32	-0.36	-0.27	0.105	0.292	0.141	-0.16	-0.1022	0.1972	0.2118	-0.0568	0.2303686	0.2382262	0.9214745	0.9529046	1.686589541
33	-0.4	-0.3	0.099	0.212	0.041	-0.19	-0.082	0.1504	0.34	0.1264	0.2702823	0.2286926	1.081129	0.9147704	1.556349697
34	-0.42	-0.36	0.127	0.343	0.109	-0.12	-0.062	0.1128	0.242	0.0208	0.2566486	0.2609927	1.0265944	1.0439709	1.633082625
35	-0.29	-0.27	0.263	0.377	0.077	-0.09	-0.2072	0.0062	0.1608	-0.0228	0.2396439	0.2358362	0.9585756	0.9433447	1.729360149
36	-0.59	-0.52	0.134	0.223	0.093	-0.08	-0.0204	0.1188	0.3886	0.2578	0.364404	0.3179885	1.4576161	1.2719541	1.895985112

Interval number	$X_{ij} - \bar{X}_i$										$\overset{\rightarrow}{\sigma}$	$\overset{\leftarrow}{\sigma}$	$R_i \rightarrow$	$R_i \leftarrow$	$2\overset{\rightarrow}{\sigma} + 2\overset{\leftarrow}{\sigma} +  B_i $
	$\overset{\rightarrow}{1}$	$\overset{\leftarrow}{1}$	$\overset{\rightarrow}{2}$	$\overset{\leftarrow}{2}$	$\overset{\rightarrow}{3}$	$\overset{\leftarrow}{3}$	$\overset{\rightarrow}{4}$	$\overset{\leftarrow}{4}$	$\overset{\rightarrow}{5}$	$\overset{\leftarrow}{5}$					
37	-0.42	-0.33	0.285	0.355	-0.01	-0.09	-0.16	-0.0682	0.301	0.1248	0.3047113	0.254605	1.2188454	1.01842	1.545432654
38	-0.49	-0.39	0.309	0.309	-0.04	-0.13	-0.0306	0.0316	0.2514	0.1756	0.3167109	0.2716639	1.2668436	1.0866558	1.424949712
39	-0.46	-0.3	0.369	0.392	0.024	-0.12	-0.0932	-0.0502	0.1648	0.0698	0.3114108	0.2558832	1.2456433	1.0235327	1.602587997

Interval number	$R_i$	$\overline{X}_i + 2\sigma^{\rightarrow}$	$\overline{X}_i + 2\sigma^{\leftarrow}$
1	1.291069	1.25679	1.493479
2	1.316106	2.174053	1.49661
3	1.486631	2.768089	1.859742
4	1.547534	2.080623	1.169311
5	1.281921	1.77081	0.967111
6	1.384912	2.387329	1.441183
7	1.485902	2.257369	1.376132
8	1.209423	2.031688	1.339735
9	1.22501	2.315557	1.552652
10	1.129156	1.595273	0.950683
11	1.257929	0.656942	0.207387
12	1.014918	1.558373	1.029744
13	0.920879	2.297928	1.840552
14	0.996977	1.665364	1.412814
15	0.765038	1.882119	1.670919
16	0.878017	1.466394	1.123223
17	0.841898	1.262457	0.799441
18	1.098483	1.966534	1.497549
19	1.08849	1.497621	0.972869
20	1.287348	1.855404	1.067944
21	1.293093	1.744996	0.978097
22	1.199076	1.08806	0.404615
23	1.269389	0.956726	0.283064
24	1.686631	1.653473	0.924358
25	1.663045	1.992142	1.195703
26	1.424917	1.729985	1.046533
27	1.627778	1.778091	1.131687



Interval number	$R_i$	$\overline{X}_i + 2\overrightarrow{\sigma}$	$\overline{X}_i + 2\overleftarrow{\sigma}$
28	1.749529	1.615171	0.774758
29	1.612886	1.351037	0.681449
30	1.727923	1.780203	1.16452
31	1.846303	1.550116	0.738187
32	1.68659	1.480937	0.747252
33	1.55635	1.067565	0.425985
34	1.633083	1.149297	0.560185
35	1.72936	0.903488	0.117472
36	1.895985	0.867208	0.243177
37	1.545433	0.688423	0.16141
38	1.42495	0.379022	0.040728
39	1.602588	0.481022	0.837966
	min	0.379022	0.040728
	max	2.768089	1.859742

repeatability of positioning ( $\mu\text{m}$ )		
$\overrightarrow{R}$	$\overleftarrow{R}$	R
1.457616	1.271954	1.895985

Systematic positional deviation ( $\mu\text{m}$ )		
$\overrightarrow{E}$	$\overleftarrow{E}$	E
2.5574	2.1114	2.8056

M: Mean bidirectional positional deviation ( $\mu\text{m}$ )	2.3153
--	--------

Accuracy of positioning ( $\mu\text{m}$ )		
$\overrightarrow{A}$	$\overleftarrow{A}$	A
2.389067	1.819014	2.727361

## Appendix B

### Data for electrode wear

#### 1. Brass material

Material: Brass (CZ 114)			Electrode diameter: Ø170 µm			Electrode type: Rod		
Programmed depth µm	Wear 1 µm	Wear 2 µm	Wear 3 µm	Wear 4 µm	Wear 6 µm	Wear 7 µm	Wear 8 µm	Wear 9 µm
3	0	0.1	0	-1.3	-0.5	-1.2	-0.5	0
6	0	0.4	0.2	-1.1	-0.7	-0.9	0	0.2
10	1.5	0.9	0.3	0.4	0	0.4	0.6	0.9
14	2	1.3	0.6	1.1	0.6	0.4	1	0.5
20	2	0.6	0.9	1.1	0.5	0.7	1.3	1
26	2.7	1.9	1.3	0.3	0.9	1.3	1.7	1.4
32	2.6	2.5	1.3	1.5	0.9	1.6	2.2	1.5
40	3.4	2.9	1.7	2.4	1.4	1.1	2.5	1.5
47	3.7	3.1	1.8	2.2	1.7	1.6	2.9	1.1
56	3.8	3.2	2.2	2.8	2	1.8	3.1	2.3
65	4	3.6	1.7	3.2	2.1	2	3.3	2.6
74	4.2	4.1	2.6	2.7	2.2	1.4	3	2.3
84	4.7	4.5	2.3	2.6	1.4	2.3	3.1	1.5
94	3.7	4.6	2.1	1.9	2.1	1.3	3	2
105	4	4.9	2.2	2.1	1.6	1.7	2.9	0.9
116	4.1	4.6	2.4	2.7	2.2	2.1	4	1.2
128	2.1	3.9	2.6	3.2	2.5	2.3	3.6	2.7

Material: Brass (CZ 114)			Electrode diameter: Ø170 µm			Electrode type: Rod		
Programmed depth µm	Wear 1 µm	Wear 2 µm	Wear 3 µm	Wear 4 µm	Wear 6 µm	Wear 7 µm	Wear 8 µm	Wear 9 µm
140	4.2	4.9	2.9	3.2	2.6	2	3.8	2.5
153	4.4	5	3.3	3.8	2	-0.2	2.1	-0.8
166	5.5	5.1	1	-2.7	2.3	-7.3	-1.2	-9.6
180	5.1	5.1	-7.7	-9.7	0.6	-16.4	-14.4	6.6
194	-3.2	6.2	6.8	-16.2	-10.1	28.6	-9.5	54
208	-11.6	-6.4	7.7	8.7	-13.1	30	-8.3	28.6
223	0.7	8.4	39.2	106.7	10.6	30.2	13.6	33.7
238	10.1	8.6	55.9	109.1	69.9	30.2	64.7	20.7
254	12.2	9.4	28.7	110.4	70.5	27.8	77.3	22.4
270	104.6	9.6	60.3	111.4	72.3	29.3	96	6.8
286	106.6	10.3	60.7	112.8	73.9	29.8	98.3	19
303	107	10.1	61.8	108.5	72.7	34	133	30
320	108.5	10.3	62.7	105.4	76.3	69.1	150.1	44.1
338	77.4	10.9	63.4	114.3	77	82.6	162.5	54.7
356	83.4	-1.4	64.8	115.8	75.6	85.1	181	54.7
374	98.4	15.2	65.4	112.9	78.1	85.1	184.5	54.7
393	110.7	17.1	66.4	116.4	78.9	219	191	54.7
412	110.4	18.1	67.8	116.8	79.6	224.4	198.5	54.7
431	79.3	34.8	68.8	119.8	79.7	231.6	208.9	54.7
451	87.1	44.6	69.9	120.8	69.6	252.4	213.6	54.7
471	92.7	51.5	69.3	119.9	117.5	263.4	269	54.7
492	95.1	55.5	72.2	110	123.5	267.3	284.7	54.7
512	99.7	57.5	73.4	124.9	67.9	277.3	298.2	54.7
534	109	64.1	196.4	126.3	131.7	282.7	313.3	54.7

Material: Brass (CZ 114)		Electrode diameter: Ø170 µm				Electrode type: Rod			
Programmed depth µm	Wear 1 µm	Wear 2 µm	Wear 3 µm	Wear 4 µm	Wear 6 µm	Wear 7 µm	Wear 8 µm	Wear 9 µm	
555	114.1	64.8	198.8	126.7	132	348.8	356.2	54.7	
577	348.2	65.8	200.9	129.1	133.7	355.7	362.3	54.7	
599	401.5	66.5	202.3	130.7	135.3	363.7	372.9	54.7	
622	409.8	66.6	204.9	130.3	137.1	336.8	376.6	54.7	
645	415.1	69.8	208	305.9	138.5	352.4	413.7	54.7	
668	421.8	78.4	211.6	317.4	139.1	349.1	452.5	54.7	
692	429.7	88.6	231.7	324.2	260.6	419.7	456.1	54.7	
715	433	95	230.7	330.3	267.7	420.6	460.6	54.7	
740	438.4	97.9	232.3	339.7	268.7	421.4	462.3	54.7	
764	439	106.8	234.3	353.9	269.5	422.2	462.6	54.7	
789	442.3	395.1	235.2	368.9	269.2	417.7	451.9	54.7	
814	442.5	421.7	237	370.7	273.3	422.3	561.7	54.7	
840	444	425.6	239.6	375.3	284.2	418.8	563.3	54.7	
866	445.6	431.8	241	378.8	289.1	528.6	568.7	54.7	
892	454.5	432.2	243	383.9	292.7	529.8	571.6	54.7	
918	449	439.1	244.3	441.2	306	531.7	572.2	54.7	
945	456.5	470.5	246	448.2	316.7	552.7	584.1	54.7	
972	459.8	471.5	247.2	458.4	326.2	558.1	644	54.7	
1000	462.6	523.2	248.9	437.4	342.3	565.4	659.6	54.7	
Time	2h18'23"	2h5'56"	2h43'58"	1h42'7"	2h4'8"	2h15'3"	2h24'46"	2h16'35"	

Material: Brass (CZ 114)			Electrode diameter: External Ø170 µm			Electrode type: Tube		
Programmed depth µm	Wear 1 µm	Wear 2 µm	Wear 3 µm	Wear 4 µm	Wear 6 µm	Wear 7 µm	Wear 8 µm	Wear 9 µm
3	0.8	0.5	0.1	0.3	0.2	0.2	0.2	0.3
6	0.8	0.4	-0.1	0.5	-0.1	0.4	0.2	0.6
10	1.2	0.6	0.3	1	0.8	0.5	0.5	0.8
14	1	1	0.6	1.8	1	1.3	0.8	1
20	1.4	1.5	1	1.8	1	1.9	0.6	1.3
26	1.9	1.7	1	1.9	1.4	2.3	1	1.7
32	2.3	2.1	1.5	2.1	1.6	2.5	1.2	1.8
40	2.2	2.5	1.7	2.7	1.6	2.8	1.4	1.8
47	2.4	2.6	1.9	2.8	1.8	3.1	1.5	1.9
56	2.3	2.9	2	2.9	1.8	3.4	1.6	2.2
65	2.6	2.9	2.3	3.3	2.2	3.4	2.5	2.2
74	2.6	3	2.5	2.9	1.9	3.5	2	2.3
84	2.8	3.2	2.3	3.7	2.4	3.7	1.6	2.4
94	2.8	3.4	2.5	3.7	2.2	3.9	1.9	2.8
105	2.9	3.5	2.8	4.1	2.3	4.3	2.4	2.7
116	2.7	3.6	2.8	4	2.5	4.4	2.5	2.7
128	2.8	3.5	3	4	2.8	4.5	2.8	2.7
140	3	4.2	3.2	4.3	2.6	4.4	2.6	3
153	2.9	4.3	3.5	4.4	2.8	4.9	3.1	3.2
166	3	4.5	3.6	4.7	3.2	5	3.1	3.2
180	3.2	4.6	3.7	4.7	3	5.3	3	3.2
194	3.3	4.8	3.6	5	3.2	5.3	3	3.4
208	3.7	5.5	4.1	5.3	3.4	5.7	3.2	3.8
223	3.7	5	4.5	5.4	3.6	5.9	3.2	3.7
238	3.7	5.5	4.1	5.8	3.9	6.1	3.5	4.2

Material: Brass (CZ 114)			Electrode diameter: External Ø170 µm			Electrode type: Tube		
Programmed depth µm	Wear 1 µm	Wear 2 µm	Wear 3 µm	Wear 4 µm	Wear 6 µm	Wear 7 µm	Wear 8 µm	Wear 9 µm
254	4	5.5	4.6	5.8	3.8	5.9	3.9	4.6
270	4.2	6	5	6.3	4	5.9	4.1	4.6
286	4.6	6.2	5	6.4	4	6.4	3.9	4.6
303	4.3	6.6	5.2	6.7	4.2	6.8	4.1	4.8
320	4.3	6.8	5.1	6.9	4.6	7.1	4	4.9
338	5	7	5.9	6.9	5	7.1	4.4	5.2
356	5.3	7	5.7	7.1	5.2	7.4	4.8	5.2
374	5.2	7.7	6.2	7.7	5.4	7.5	5	5.8
393	5.7	8	6.5	7.7	5.4	7.9	5.1	5.7
412	5.4	8.2	6.7	7.8	5.6	7.8	5.2	6
431	5.7	8.5	7.1	8.4	5.8	8.1	5.5	6.3
451	6	8.8	7.2	8.8	6.2	8.4	5.9	6.7
471	6	9.1	6.92	8.9	6.6	8.9	5.8	6.6
492	6.6	9.6	7.6	9.1	6.9	9	6.4	6.8
512	6.6	9.7	8	9.5	6.8	9.5	6.4	7.3
534	7	10	8.3	9.7	7.3	9.7	6.9	7.6
555	7.2	10	8.44	9.9	7.4	9.7	6.9	7.4
577	6.9	10.7	8.6	9.8	7.6	10.3	7.1	7.8
599	7.6	10.7	9	11	8	10.8	7.4	8.3
622	7.9	11.1	9.2	11	7.9	10.7	8	8.6
645	8	11.2	9.7	11.3	8.9	11.1	8.1	8.8
668	7.9	11.7	10.1	11.9	8.9	11.4	8.6	9
692	8.4	11.7	10.5	12.1	9.3	11.7	8.8	9.2
715	9	11.5	10.9	12.1	9.6	12.1	8.9	9.7
740	9.3	12.8	11.2	12.9	9.5	12.5	9.4	9.9

<b>Material:</b> <b>Brass (CZ 114)</b>		<b>Electrode diameter:</b> <b>External Ø170 µm</b>				<b>Electrode type:</b> <b>Tube</b>		
<b>Programmed depth µm</b>	<b>Wear 1 µm</b>	<b>Wear 2 µm</b>	<b>Wear 3 µm</b>	<b>Wear 4 µm</b>	<b>Wear 6 µm</b>	<b>Wear 7 µm</b>	<b>Wear 8 µm</b>	<b>Wear 9 µm</b>
764	9.7	12.7	11.3	12.9	10.3	12.8	9.8	10.6
789	9.8	13.4	11.7	13.7	10.4	13.3	10.2	10.9
814	9.9	13.8	12.2	14.1	10.5	13.7	10.6	11
840	10.9	14.1	12.3	14.3	10.2	14	10.9	11
866	10.8	14.8	12.67	14.4	11.5	14.3	11.2	11.9
892	11.4	15	13.2	15.3	11.8	14.9	11.2	11.8
918	11.9	15.24	13.5	15.3	11.9	15	11.9	12.3
945	12.3	16.1	14	15.7	12.4	15.9	12.2	12.8
972	12.6	16.1	14.3	16.3	12.6	16.1	12.8	13
1000	13.2	16.6	14.3	16.4	13.3	16.7	13.2	13.4
Time	3h37'51"	3h40'24"	3h41'14"	1h41'8"	1h40'56"	1h40'51"	1h41'19'	1h40'35'

## 2. Aluminium material

Material: Aluminium (6082)			Diameter: Ø170 µm			Electrode type: Rod			
Programmed depth µm	Wear 1 µm	Wear 2 µm	Wear 3 µm	Wear 4 µm	Wear 5 µm	Wear 6 µm	Wear 7 µm	Wear 8 µm	Wear 9 µm
3	0.2	0.8	-0.5	0.3	0.3	-0.6	0.3	0.5	0.2
6	2.1	1.1	0.2	0.6	0.4	-0.4	0.7	0.5	0.6
10	5.6	1.7	0	0.2	0.9	-0.8	0.9	0.9	1.1
14	6.1	2.1	0.6	1.8	1.3	0.2	1.1	1.6	1.7
20	10.8	2.6	1	2.8	1.6	0.7	2.1	2.3	1.6
26	13.8	2.8	1.5	3.5	2	0.6	2.7	2.5	2.1
32	23.4	3	1.7	3.9	2.9	1.1	3.4	2.5	2
40	23.8	3.6	1.9	4.4	2.7	1.6	3.3	3	2.7
47	24.1	3.4	2	5	3.1	1.7	4	3.2	3.1
56	24.4	3.8	2.5	5.6	3	1	4.4	3.8	3.1
65	25.1	4.3	3	4.8	3.5	2	5	3.8	3.6
74	25.3	4.6	0.5	5	3.1	2.5	4.9	4	3.6
84	25.8	3.6	1.5	5.9	4	1.7	5.4	4.6	4
94	25	3.8	2	5.6	4.5	2	5.7	4.9	4.7
105	26.1	5.4	3.6	6.8	4.3	2.7	5.8	4.8	5.2
116	26.1	4.6	3.7	7.2	4.7	3	6.5	4.8	5.5
128	26.7	6	3.7	8.1	5.1	3.4	7.3	6	6.2
140	26.4	5.2	3.2	9.2	5.7	2.7	7.8	6.3	6.5
153	26.7	6.6	3.9	10.5	4.9	4.2	8.5	6.9	6.1
166	28.1	6.4	5	11.4	6.7	4	9	7.4	7
180	27.8	7.7	4.7	12	6.6	4.6	9.4	8.3	8
194	28.8	7.3	5.6	86.2	7.7	4.5	10.5	8.8	8.9
208	28.8	8.8	6.5	86.4	8.1	5.5	11.1	9.8	9.3



<b>Material:</b> Aluminium (6082)			<b>Diameter:</b> Ø170 µm			<b>Electrode type:</b> Rod			
<b>Programmed depth µm</b>	<b>Wear 1 µm</b>	<b>Wear 2 µm</b>	<b>Wear 3 µm</b>	<b>Wear 4 µm</b>	<b>Wear 6 µm</b>	<b>Wear 7 µm</b>	<b>Wear 8 µm</b>	<b>Wear 9 µm</b>	<b>Wear 1 µm</b>
223	30.2	9	6.7	87	8.6	5.7	12.3	10.2	10.5
238	29.1	9.3	6.7	87.8	9.5	6.2	13.3	11	11.9
254	30.2	10.3	7.9	89.4	9.4	7	14.1	11.8	13.1
270	31.6	11.1	8.7	91.6	9.9	7.8	15.5	56.3	14.6
286	31.6	12.3	8.7	123.8	11.7	8.4	17	70.6	16.5
303	31.8	13	10.3	164.5	12.4	9.6	18.7	78.5	17.6
320	32.8	14.4	11.5	169	13.5	78.5	89.4	98.6	73.6
338	33.7	131.7	13.6	176.2	39	102.6	97.7	103.4	86.5
356	133.5	141	71.7	187.8	73.6	108.5	109.3	110	122.1
374	186	150.3	156.6	215.8	62.4	113.1	124.9	111.4	126.6
393	192.3	158.6	162.9	209.2	75.3	116.5	214	114.5	234
412	198.1	165.3	165.6	218.2	81.4	185.4	230.9	116.5	235.2
431	200.3	235.3	170.2	219.4	88.4	164.6	247.7	162.6	238.2
451	210.3	236.7	172.7	221	87.5	184.6	262	192.8	243
471	220.4	238.7	173.6	222.9	88.6	185.8	269.8	219.3	244.7
492	265.7	239.8	197.9	223.1	108.7	216.7	277.4	232	251.5
512	266.1	308	204	226.4	101.6	219.6	279.1	352.9	262.9
534	266.7	321	247.9	226.6	123.7	244	279.7	381.3	286.2
555	267.4	333.1	256.6	228.6	157.5	261.7	368.5	390.6	286.7
577	267.2	349.6	258.9	231.1	159.4	261.2	371.3	421.1	286.9
599	270.1	364.7	288.5	231.1	159.9	262.6	382.5	448.2	286.9
622	271.6	379.2	295.7	233.8	161	292.5	393	475.2	323.9
645	274.7	386.4	296.5	236.6	213.9	308.7	399.8	495.1	355.9
668	357.3	404.6	332.2	237.9	216.7	314.6	410.8	511.9	388.7
692	375.8	393	334.3	240.5	250.9	340.6	430.5	546.4	389.7

Material: Aluminium (6082)			Diameter: Ø170 µm			Electrode type: Rod			
Programmed depth µm	Wear 1 µm	Wear 2 µm	Wear 3 µm	Wear 4 µm	Wear 6 µm	Wear 7 µm	Wear 8 µm	Wear 9 µm	Wear 1 µm
715	399.3	404.6	334.6	243.9	253.5	347.1	445.1	556.5	442
740	417.1	446.3	390.6	246.5	270.1	365.5	447.8	561.2	449.2
764	427.2	446.6	402.5	316.9	271.5	392.8	449.4	561.8	472.3
789	478.6	446.6	416.9	324	305.7	407.1	501.9	562.9	510.6
814	464.8	467.4	372.9	354.2	332.9	414.7	581.5	595.9	543.5
840	535	487.6	379.5	361.4	357.3	447.5	590.4	631.4	546.1
866	541.6	487.6	423.9	363.8	364.3	473.1	633.7	652.5	546.7
892	547.4	507.7	498.9	364	364.4	491.4	637	690.9	659.9
918	560.8	508.2	468.6	365.6	364.1	493	677.9	713.5	685.6
945	638.3	506.2	488.9	367.4	375.6	499.5	727.1	742	710.2
972	669.1	508.2	509.6	426.9	381.3	514.6	731.8	769	714.3
1000	687.7	511.6	550.6	432.9	500.9	511.8	773	783.9	729.7
Time	1h59'38"	1h42'23"	1h18'22"	1h30'54"	1h29'32"	1h27'18"	1h52'51"	2h4'7"	1h36'36"

Material: Aluminium (6082)			Diameter: External Ø170 µm			Electrode type: Tube			
Programmed depth µm	Wear 1 µm	Wear 2 µm	Wear 3 µm	Wear 4 µm	Wear 5 µm	Wear 6 µm	Wear 7 µm	Wear 8 µm	Wear 9 µm
3	0.1	-1.1	0.5	0.5	0.3	0.7	0.9	0.1	0.6
6	0.3	-0.1	0.9	0.7	0.4	0.8	1.3	0.4	0.7
10	0.7	0.2	0.5	1.2	1.1	0.9	1.8	0.5	0.6
14	1.3	0.3	0.9	1.6	1.3	1.2	2.3	0.9	1
20	1.1	1	1.5	2.2	1.7	1.4	2.6	1	1.2
26	1.4	0.8	1.7	2.2	1.8	1.6	3.3	1.5	1.2

<b>Material:</b> Aluminium (6082)			<b>Diameter:</b> External Ø170 µm			<b>Electrode type:</b> Tube			
<b>Programmed depth µm</b>	<b>Wear 1 µm</b>	<b>Wear 2 µm</b>	<b>Wear 3 µm</b>	<b>Wear 4 µm</b>	<b>Wear 5 µm</b>	<b>Wear 6 µm</b>	<b>Wear 7 µm</b>	<b>Wear 8 µm</b>	<b>Wear 9 µm</b>
32	1.9	1.4	2.3	2.4	1.3	1.4	3.3	1.4	1.7
40	2.1	0.9	2.3	2.7	2.3	1.9	3.2	1.6	1.8
47	2.3	1.6	2.7	3.3	2.4	2.2	4.1	2.1	1.7
56	2.1	2.3	2.3	3.3	2.2	2	4.4	1.9	2.1
65	2.4	2.6	2.4	3.6	2.8	1.9	5.2	2.4	2.1
74	2.9	2.6	3.3	3.2	2.7	2.4	5.3	2.2	2.4
84	2.5	3.2	2.9	3.6	3.4	3	5.6	2.6	2.5
94	3.1	3.3	4	3.8	3	2.6	5.6	2.1	3.1
105	3.5	3.2	3.4	4.4	3.3	3.2	6.2	2.1	3.1
116	3.5	3.3	4	4.2	3.4	3.4	6.3	2.9	3.1
128	3.7	4.2	4.3	4.6	4.1	3.4	6.6	2.8	4
140	3.4	4.5	4.4	4.8	4.1	3.3	7	3.2	3.2
153	3.9	4.8	4.5	5.2	4.1	3.3	7.1	3.5	4.1
166	4.4	4.6	4.8	4.9	4.7	3.9	7.6	3.6	4.4
180	4.4	5.4	5.5	5.3	4.8	3.7	8	3.9	4.6
194	4.4	5.2	5.4	5.8	5.2	4.4	7.8	4.2	4.8
208	5	6	5.8	6.3	5.1	3.9	8.3	4.5	5.1
223	5.3	6.1	6.5	6.6	5.7	4.6	8.8	4.9	5.2
238	5.3	6.4	6.4	6.6	5.6	4.8	9.1	4.4	5.2
254	5.8	6.8	6.9	6.9	7	5	9.2	5	5.8
270	5.5	7.2	6.9	7.4	6.4	5.6	9.3	5.1	6.4
286	6.4	7.5	6.9	7.3	7	5.7	9.7	5.8	6.8
303	6.1	7.5	7.4	7.8	7	6	10	5.5	7
320	6.7	8	7.7	8.2	7.1	6.2	10.6	6.2	7.1
338	6.9	8.4	7.9	8.7	7.7	6.2	10.6	6.5	6.7

<b>Material:</b> Aluminium (6082)			<b>Diameter:</b> External Ø170 µm			<b>Electrode type:</b> Tube			
<b>Programme d depth µm</b>	<b>Wear 1 µm</b>	<b>Wear 2 µm</b>	<b>Wear 3 µm</b>	<b>Wear 4 µm</b>	<b>Wear 5 µm</b>	<b>Wear 6 µm</b>	<b>Wear 7 µm</b>	<b>Wear 8 µm</b>	<b>Wear 9 µm</b>
356	7.5	8.8	8.4	8.8	7.1	6.7	11.2	6.6	8
374	7.5	9.4	8.7	8.9	8.8	7	11.4	7.2	8.2
393	8.1	9	8.7	9	8.7	7.3	12.1	7.6	8.4
412	8	9.6	9.4	9.9	9.1	7.8	12.3	8	8.8
431	8.7	9.8	9.7	10	9.4	7.9	12.3	8	8.6
451	8.5	10.8	9.8	10.4	9.3	8.2	12.7	8.8	9.1
471	9.1	11	10.3	10.9	10.1	8.6	13.3	9	9.6
492	9.8	10.9	10.8	10.2	10.3	8.7	13.7	9.4	10
512	10	11.4	10.9	10.9	11	9.6	13.8	9.8	10
534	10.1	11.9	11.1	11.3	11.1	9.4	14.8	10.2	10.6
555	10.5	12.6	11.5	11.9	11.6	9.9	15.1	10.5	10.6
577	11.1	13.4	12.5	12.3	12.1	10	15.3	11.1	11.5
599	11.5	13	12.4	12.6	12.2	10.9	15.9	11.1	11.5
622	11.8	14.2	13	13.2	13.1	11	16.4	11.9	11.7
645	12.5	14.6	13.1	13.8	13.1	11.7	17	12.4	12.2
668	12.5	15.1	14	14	13.7	11.7	17.4	12.8	12.8
692	13.7	15.8	14.4	14.3	14.2	12.7	18	13.1	13.2
715	13.7	15.9	14.7	14.9	15	13.4	18.4	13.5	13.1
740	14.8	16.5	15.3	15.3	14.3	13.7	18.3	14.1	13.5
764	14.8	15.8	15.7	15.9	15.7	14	19.5	14.8	12.7
789	15.4	17.3	16	16.2	16.4	14.2	19.6	15.1	14.6
814	16.1	17.8	16.9	16.8	16.3	14.8	20.2	15.4	15.1
840	16.3	18.4	17.7	17	17.1	15.6	21.1	16	15.8
866	16.6	19.2	17.9	17.9	17.1	16	21.3	16.6	15.7
892	17.3	19.8	18.8	18.6	18.1	16.7	22	17.1	16.6

<b>Material:</b>		<b>Diameter:</b>		<b>Electrode type:</b>								
<b>Aluminium (6082)</b>		<b>External Ø170 µm</b>		<b>Tube</b>								
<b>Programmed depth µm</b>	<b>Wear 1 µm</b>	<b>Wear 2 µm</b>	<b>Wear 3 µm</b>	<b>Wear 4 µm</b>	<b>Wear 5 µm</b>	<b>Wear 6 µm</b>	<b>Wear 7 µm</b>	<b>Wear 8 µm</b>	<b>Wear 9 µm</b>			
918	18	19.6	18.9	18.6	18.7	16.7	21.45	17.2	16.8			
945	18.7	21	19.9	19.7	19.1	17.3	23.2	18.2	17.7			
972	19	21.4	20	19.9	19.3	17.6	23.6	19	17.5			
1000	19.9	21.9	20.7	20.3	20.3	18.8	24.3	19.5	18.2			
<b>Time</b>	<b>2h2'</b>	<b>2h0'32"</b>	<b>1h58'57"</b>	<b>1h57'20"</b>	<b>1h56'55"</b>	<b>1h58'15"</b>	<b>1h59'19"</b>	<b>2h0'23"</b>	<b>2h0'35"</b>			

### 3. Steel material

Material: Steel (P 20)			Diameter: Ø170 µm			Electrode type: Rod			
Programmed depth µm	Wear 1 µm	Wear 2 µm	Wear 3 µm	Wear 4 µm	Wear 5 µm	Wear 6 µm	Wear 7 µm	Wear 8 µm	Wear 9 µm
3	1.1	-0.1	0.6	0	0	0.5	0.4	0.9	-0.9
6	1.5	-0.3	1	0.5	-0.7	1	1	1.6	1.1
10	2.1	0.9	1.9	2	2	3	2.1	2.8	0.8
14	3	2.2	2.9	2.9	1.7	3.5	2.4	3.2	2.6
20	5	4	3.9	3.9	3.4	4.1	3.7	4.4	2.9
26	5.6	5.9	4.5	5.8	4.9	5.5	4.7	4.8	4.4
32	6.5	6.7	6	6.9	5.9	6.7	6.1	5.9	5.2
40	8.2	7.7	7.8	7.4	7.2	8.2	7.3	8	6.8
47	10	9.4	8.4	9.4	8.4	9.1	8	9.4	7.6
56	11.7	10.6	8.6	11.6	9.9	10.3	10.3	10.1	9.4
65	13.6	12.4	7.5	12.9	11.8	11.9	11.6	9.9	11.4
74	14.7	13.5	13.4	14.5	12.9	14.4	13.5	13.9	12.6
84	17.1	15.9	14.8	15.5	15.7	16.1	15.7	15.8	13.8
94	18.7	17.4	17.1	18.5	18.2	19.9	20.3	18.5	16.8
105	22.5	20.2	19.9	21.5	22.6	24.3	20.7	22.4	19.4
116	26.2	23.6	25.1	26	26	28.2	27.1	28.9	24.1
128	32.2	29	27.4	31.8	31.9	35	34.7	35.8	30.8
140	38.3	35.3	31.2	38.7	39.4	41.5	37.7	38.2	38.9
153	44.6	41.9	39.4	46.2	46.2	49.2	42.2	42	46.4
166	49	48.6	47.4	52.4	53.3	57.3	50.9	44.9	54.4
180	58.3	56.9	53.5	60.8	62.6	65.2	60.5	55.8	63
194	66.1	65.3	62.6	69.3	71.7	73.9	64.3	59.5	70.7
208	73.9	72.1	71.4	78.6	80.3	82.5	68.1	61.2	80.1

<b>Material:</b> Steel (P 20)			<b>Diameter:</b> Ø170 µm			<b>Electrode type:</b> Rod			
<b>Programmed depth µm</b>	<b>Wear 1 µm</b>	<b>Wear 2 µm</b>	<b>Wear 3 µm</b>	<b>Wear 4 µm</b>	<b>Wear 5 µm</b>	<b>Wear 6 µm</b>	<b>Wear 7 µm</b>	<b>Wear 8 µm</b>	<b>Wear 9 µm</b>
223	80.3	80.9	79.2	86.9	90.3	92.2	72.1	68	88.2
238	89.3	89.7	88.9	96.8	99.2	100.6	84.6	76.9	91.9
254	98.5	99.9	98.8	107.5	110.3	112.1	96.3	89.9	95.2
270	108	108	108.1	117.7	119.8	121.9	99.9	93.4	99.1
286	116	117.5	118.4	127	129.4	131.3	111.9	96.8	102.1
303	125.7	127.7	128	138	139.6	141.9	125	100.5	105.6
320	136.1	139.1	137.9	148.5	150.2	152.1	137.4	104.8	109.6
338	145.8	149.3	148.9	159	161.4	163.5	149.1	112	122
356	156.3	159.7	159.9	170.4	172.2	174.1	161.5	117.2	126.8
374	166.7	170	171.5	181.9	183.9	185.1	174.3	126.8	129.2
393	178	181.6	183.4	193.5	196	196.3	180.1	146.9	141
412	189.2	192.6	194.9	205.3	208.3	208.1	186.7	162.7	151.9
431	201.1	204.7	206.5	217	219.9	219.5	192.5	167.7	159.4
451	213.2	217.1	218.6	229.6	232.7	232.1	199.1	177.4	165.9
471	225.5	229.7	231.8	242	245.3	244.5	205.5	195.2	174.5
492	237	242.1	245.9	255	259.3	257.9	209.5	208.1	188.2
512	250.5	254	258.4	267.9	270.9	270.5	223.1	213.9	201
534	264.5	268	272.1	281	285.2	286	235.3	225.9	217.6
555	277.5	280	286.1	295	298	298.9	242.4	237.8	232.8
577	290.5	294.4	299.5	309.6	311.9	311.7	248.4	249.6	249.9
599	305	306.7	313.2	323	325.7	326.3	261	261.8	265.4
622	318.5	321.1	327.9	338	340	340.3	269.2	273.6	281.8
645	332.3	333.5	342.6	353.2	354	355.9	275.1	282.1	296.1
668	345.5	348.6	356.1	367.5	369	370.7	298.7	296.6	312.6
692	360.1	363.4	371.4	382.2	383.7	385.7	317.5	316.2	328

Material:			Diameter:			Electrode type:			
Steel (P 20)			Ø170 µm			Rod			
Programmed depth µm	Wear 1 µm	Wear 2 µm	Wear 3 µm	Wear 4 µm	Wear 5 µm	Wear 6 µm	Wear 7 µm	Wear 8 µm	Wear 9 µm
715	374.5	377.6	385.1	396.3	398.4	401.2	332	333.6	346.2
740	388.9	394.3	401.2	412.4	413.3	417.1	352.4	349.9	362
764	403.2	409	416.4	427.6	428.6	432.9	366	366.4	378.8
789	419	423.6	432.1	442.9	443.4	448.9	382	383.6	396.4
814	436.1	439.3	448.5	459	459.9	463.9	399.1	398.6	412.6
840	450.9	456.1	465.9	475.8	475.9	480.6	408.1	417.5	431.1
866	466	472.3	483	492.5	491.6	496.6	419.6	436.6	447
892	483.2	489.9	500.1	509.9	509.4	514	429.1	455.6	462.5
918	498.5	505.9	516.6	525.8	526.3	528.7	439.5	473.6	472.4
945	517.6	522.3	533.5	543.3	543.6	544.9	453.5	492.9	488
972	534.7	539.5	551	561	560.9	563.7	469.4	512	499.4
1000	568	556.9	606.5	579.4	578	580.5	487.7	535.6	517.5
Time	1h37'13"	1h33'11"	1h47'45"	1h38'6"	1h34'46"	1h46'5"	4h16'38'	4h4'15"	2h49'34"

Material:			Diameter:			Electrode type:			
Steel (P 20)			External Ø170 µm			Tube			
Programmed depth µm	Wear 1 µm	Wear 2 µm	Wear 3 µm	Wear 4 µm	Wear 5 µm	Wear 6 µm	Wear 7 µm	Wear 8 µm	Wear 9 µm
3	1.1	0.3	0.8	0.4	0.8	0.1	1.8	0.3	0.4
6	1.5	0.9	1.2	1.5	2.3	0.9	2.2	0.9	0.8
10	4.1	3.3	3.8	3.9	4.3	4	4.7	-0.1	1
14	6.1	5.8	7.1	6.2	6.8	6.5	4	1	0.8
20	9.1	7.9	9.3	9.8	9.8	10.8	4.7	1.3	1.4
26	12.7	11.1	11.9	12.9	13.4	13.3	4.2	0.4	1.8



Material: Steel (P 20)			Diameter: External Ø170 µm			Electrode type: Tube			
Programmed depth µm	Wear 1 µm	Wear 2 µm	Wear 3 µm	Wear 4 µm	Wear 5 µm	Wear 6 µm	Wear 7 µm	Wear 8 µm	Wear 9 µm
32	16	14	15.5	16.4	16.9	16.6	3.9	2.6	0.7
40	20.5	19.1	19.7	21	21.5	21	5.3	1.9	0.4
47	25	22.4	23.5	25	25.8	24.8	5.6	-5.7	1.2
56	29.9	27.7	28.3	30.6	31.2	30.8	6.9	-4.6	1.4
65	35.4	33	33.9	36.2	36.7	35.5	5	-2.6	1.3
74	40.5	38.7	39.1	41.5	42.1	41.4	6.2	1.7	1.7
84	46.6	44.8	45.2	47.6	49.4	47.1	5.8	1.4	1.4
94	53.1	50.4	51.1	53.5	55.1	54.4	7.4	1.4	1.2
105	60	56.8	57.9	60.4	62.1	59.7	7.9	1.6	-0.6
116	67.1	64.1	65.3	67.9	69	67	9	1.4	1.1
128	74.5	71.9	72.7	76.2	77.1	74.9	8	1.4	0.7
140	83	80.1	79.5	83	84.5	82	8.8	0.6	0.7
153	91.7	89.7	88	91.8	93.1	91.4	8.2	1.4	0.3
166	99.6	97.9	96	100.5	101.8	99.5	8.8	0.1	0.1
180	108.7	107	105.3	109.6	110.3	108.5	9.2	1.3	-0.9
194	116.9	116.4	114.7	119.5	119.5	117.3	9.3	0.6	-0.2
208	125.7	125.7	123.4	129.2	128.1	126.9	9.3	0.9	-0.4
223	134.5	135.4	134.4	139.6	138.7	137.1	8	-0.5	-0.9
238	145	145.1	144.7	150	149.3	148	9.3	0.1	-0.9
254	155.3	156.3	156.5	161.2	158.7	158.4	8.7	-0.3	-1
270	166.1	166.6	168.8	172.3	169.1	169	8.7	-0.4	-1.4
286	176.3	177.4	178.4	183.3	179.7	179	8.9	0.5	-0.4
303	187.3	188	189.1	195.6	190.4	190.3	9.3	-0.3	-0.3
320	199.5	198.9	200.8	206.4	202	200.9	10.2	0	0.3
338	210.6	210.4	212.3	218.1	214	212.4	11.4	3.9	1.8

Material: Steel (P 20)			Diameter: External Ø170 µm			Electrode type: Tube			
Programmed depth µm	Wear 1 µm	Wear 2 µm	Wear 3 µm	Wear 4 µm	Wear 5 µm	Wear 6 µm	Wear 7 µm	Wear 8 µm	Wear 9 µm
356	222.1	221.9	224	230.4	226.7	223.7	23.7	15.1	13.2
374	234.9	234.9	235.5	242.8	238.4	234.9	36.3	27	24.3
393	248.2	247.4	247.8	255.3	251.4	246.9	50.5	38.6	36.8
412	260.7	259.4	260.4	268.4	264.3	259.3	62	51.9	48.3
431	272.7	271	272.3	281.3	277.1	272.4	74.4	64.4	60.6
451	286.2	285.3	286	294.2	291.8	287.3	89.2	78.6	73.2
471	299.2	299.5	300.1	308.4	304.9	300.1	103.8	92.9	87
492	313.7	314.9	314.9	323	319.4	314.9	117.2	105.7	101.4
512	327.5	327.9	327.9	336.3	332.8	329.1	130.6	119.7	116.4
534	342	343.3	344	351.8	347.2	343.4	145.3	135.9	133.2
555	356.3	358.4	357.4	366	361.4	357.5	162.3	149.1	147.6
577	371.5	372.8	372.3	380	375.2	373.3	176.9	164.6	163.2
599	386.3	388.1	386.7	395	389.1	387.8	192.2	179.5	178.7
622	403.2	403.9	403.7	410.9	405.3	403.5	207.9	196.6	194.1
645	418.6	419.8	418.4	425.9	421.5	419.1	223.9	212.6	209.2
668	434.5	435.7	434.1	441.8	438.9	434.3	241.8	229.7	225
692	450.9	453.5	450.1	458	454.8	450.8	258.3	246.1	241.7
715	468.1	469.3	465.4	474.4	470.3	466.3	274	262.5	258.1
740	485.7	487.4	482.7	491.2	487.9	483.7	292.2	278.3	276.6
764	502.7	505.7	499.7	509.4	503.5	500.3	309.4	295.7	293
789	520.3	521.9	517	526.2	521.5	518	327.4	312.9	310.6
814	538.2	539.8	534.7	543.2	538	535.1	344.6	330.9	328.6
840	556.9	558.1	552.5	560.9	555.4	553.5	364	350	346.8
866	575.2	577.3	570.5	578.6	573.4	571.5	382.8	368.4	364.7
892	594.1	596.9	589.4	597.2	593	589.9	401.3	385.9	383.8

Material:			Diameter:				Electrode type:				
Steel (P 20)			External Ø170 µm				Tube				
Programmed depth µm	Wear 1 µm	Wear 2 µm	Wear 3 µm	Wear 4 µm	Wear 5 µm	Wear 6 µm	Wear 7 µm	Wear 8 µm	Wear 9 µm		
918	612.3	615.4	607.3	616.3	612.1	607.5	420.3	403.7	400.8		
945	632.1	635.4	625.9	636.2	630.8	626	439	422.5	420.2		
972	652.6	655.1	645.1	655.2	649.5	645	459	441.7	439.2		
1000	673.3	676.9	666	674.1	669	666.4	478.4	462.5	459.4		
Time	6h31'55"	6h35'37"	6h17'16"	6h14'6"	6h12'6"	6h11'49"	5h54'8"	5h46'7"	5h46'1"		

## Appendix C

### Pure Materials and their Properties

Average wear ratio and erosion time for 5 samples of each material

Properties	Materials						
	<i>Ti</i>	<i>Co</i>	<i>Ni</i>	<i>Cu</i>	<i>Ag</i>	<i>Au</i>	<i>W</i>
Atomic							
Atomic number	22	27	28	29	47	79	74
Atomic radius (nm)	0.147	0.125	0.125	0.128	0.144	0.144	0.141
Atomic weight (amu)	47.88	58.9332	58.69	63.546	107.8682	196.9665	183.85
Crystal structure	Hexagonal close packed	Hexagonal close packed	Face centred cubic	Face centred cubic	Face centred cubic	Face centred cubic	Body centred cubic
Electronic Structure	Ar 3d <sup>2</sup> 4s <sup>2</sup>	Ar 3d <sup>7</sup> 4s <sup>2</sup>	Ar 3d <sup>8</sup> 4s <sup>2</sup>	Ar 3d <sup>10</sup> 4s <sup>1</sup>	Kr 4d <sup>10</sup> 5s <sup>1</sup>	Xe 4f <sup>14</sup> 5d <sup>10</sup> 6s <sup>1</sup>	Xe 4f <sup>14</sup> 5d <sup>4</sup> 6s <sup>2</sup>
Ionization potential	N eV	N eV	N eV	N eV	N eV	N eV	N eV
	1 6.82	1 7.86	1 7.63	1 7.73	1 7.58	1 9.22	1 7.98
	2 13.6	2 17.06	2 18.2	2 20.29	2 21.5	2 20.5	2 17.7
	3 27.5	3 33.5	3 35.2	3 36.8	3 34.8		
	4 43.3	4 51.3	4 54.9	4 55.2			

Properties	Materials						
	<i>Ti</i>	<i>Co</i>	<i>Ni</i>	<i>Cu</i>	<i>Ag</i>	<i>Au</i>	<i>W</i>
Ionization potential	5 99.2	5 79.5	5 75.5	5 79.9			
	6 119	6 102	6 108	6 103			
Natural isotope distribution	Mass No. %	Mass No. %	Mass No. %	Mass No. %	Mass No. %	Mass No. %	Mass No. %
	46 8	59 100	58 68,27	63 69.2	107 51.83	197 100	180 0.1
	47 7.5		60 26,1	65 30.8	109 48.17		182 26.3
	48 73.7		61 1.13				183 14.3
	49 5.5		62 3.59				184 30.7
	50 5.3		64 0.91				186 28.8
Photo-electric work function (eV)	4.1	5	4.9	4.5	4.7	4.8	4.55
Thermal neutron absorption cross-section (Barns)	6.1	37.5	4.54	3.8	63.8	98.8	18.5
Valences shown	2, 3, 4	2, 3	0, 1, 2, 3	1, 2	1, 2	1, 3	2, 3, 4, 5, 6
<b>Electrical</b>							
Temperature coefficient (K <sup>-1</sup> )	0.0038 @ 0-100C	0.0066 @ 0-100C	0.0068 @ 0-100C	0.0043 @ 0-100C	0.0041 @ 0-100C	0.0040 @ 0-100C	0.0048 @ 0-100C

Properties	Materials						
	<i>Ti</i>	<i>Co</i>	<i>Ni</i>	<i>Cu</i>	<i>Ag</i>	<i>Au</i>	<i>W</i>
Electrical resistivity (uOhmcm)	54 @ 20C	6.34 @ 20C	6.9 @ 20C	1.69 @ 20C	1.63 @ 20C	2.20 @ 20C	5.4 @ 20C
Thermal emf against Pt (cold 0C - hot 100C) ( mV )		-1.33	-1.48	0.76	0.74	0.74	1.12
Superconductivity critical temperature (K)	0.4						0.0154
<b>Physical</b>							
Boiling point ( C )	3287	2870	2732	2567	2212	3080	5660
Density (g/cm3)	4.5 @ 20C	8.9 @ 20C	8.9 @ 20C	8.96 @ 20C	10.5 @ 20C	19.30 @ 20C	19.3 @ 20C
Melting point ( C )	1660	1495	1453	1083	961.9	1064.4	3410
<b>Thermal</b>							
Coefficient of thermal expansion (x 10 <sup>6</sup> K <sup>-1</sup> )	8.9 @ 0-100C	12.5 @ 0-100C	13.3 @ 0-100C	17 @ 0-100C	19.1 @ 0-100C	14.1 @ 0-100C	4.5 @ 0-100C
Latent heat of evaporation (J g <sup>-1</sup> )	8893	6490	6378	4796	2390	1738	4009
Latent heat of fusion (J g <sup>-1</sup> )	365	263	292	205	103	64.9	192

Properties	Materials						
	<i>Ti</i>	<i>Co</i>	<i>Ni</i>	<i>Cu</i>	<i>Ag</i>	<i>Au</i>	<i>W</i>
Specific heat (J K <sup>-1</sup> kg <sup>-1</sup> )	523 @ 25C	456 @ 25C	444 @ 25C	385 @ 25C	237 @ 25C	129 @ 25C	133 @ 25C
Thermal conductivity (W m <sup>-1</sup> K <sup>-1</sup> )	21.9 @ 0-100C	100 @ 0-100C	90.9 @ 0-100C	401 @ 0-100C	429 @ 0-100C	318 @ 0-100C	173 @ 0-100C
<b>Mechanical</b>							
Material condition	Annealed Polycrystall ine	Soft Hard Polycris talline	Soft Hard Polycrystal line	Soft Hard Polycrista lline	Soft Hard Polycristalli ne	Soft Hard Polycristalli ne	Soft Hard Polycrista lline
Bulk modulus ( GPa )	108.4	181.5	177.3	137.8	103.6	171	311
Hardness - Vickers	60	170 320	100 190 Brinell	49 87	25 95	20-30 60	360 500
Izod toughness ( J m-1 )	61		160	58 68	5		
Poisson's ratio	0.361	0.32	0.312	0.343	0.367	0.42	0.28
Tensile modulus ( GPa )	120.2	211	199.5	129.8	82.7	78.5	411
Tensile strength ( MPa )	230- 460	760 1135	400 660	224 314	172 330	130 220	550-620 1920
Yield strength ( MPa )	140- 250	345 -485	150 480	54 270		205	550

Properties	Materials						
	<i>Ti</i>	<i>Co</i>	<i>Ni</i>	<i>Cu</i>	<i>Ag</i>	<i>Au</i>	<i>W</i>
enthalpy	10965.595	8052	7873.24	5980.825	3012.03	2197	4950.854
Enthalpy/ Thermal conductivity	500.71	80.52	86.61	14.91	7.02	6.91	28.62
<b>Electrical results (average of 5 blocks)</b>							
V <sub>o</sub> bar(V)	7.8269826		8.3874	7.98584	8.32176		7.82408
V <sub>e</sub> bar (V)	1.81108		1.90168	1.58016	1.63504		1.98488
V <sub>e</sub> RMS (V)	2.35832		2.19164	1.75084	1.87836		2.16892
t <sub>e</sub> (ns)	1204		1053.12	1123.68	1180.4		876.72
I bar (mV)	860.552		940.612	940.908	920.056		1012.072
I RMS (V)	1.1678		1.26408	1.22468	1.22352		1.25308
I max (V)	2.41384		2.42708	2.44088	2.48008		2.25564
t max (ns)	327.2		276.32	262	269.52		263.92
W bar (VV)	1.4178		1.9666	1.63376	1.6892		2.1732
W RMS(VV)	2.02328		2.71112	2.27848	2.30712		2.77912
W max	5.56132		6.4824	5.66704	6.17172		5.9528
<b>Results</b>							
wear ratio	0.381	0.614	0.622	0.311	0.209	0.248	0.621
erosion time (min)	900	540	900	75	35	13	120



## Appendix D

### DATA FOR DISCHARGE CHARACTERISTICS AND AVERAGE ELECTRODE WEAR RATIO OF PURE METALS

Material	$\bar{V}_o$ (V)	$\bar{V}_e$ (V)	$V_e$ RMS (V)	$t_e$ (ns)	$\bar{i}$ (mA)	$i$ RMS (V)	$i_{max}$ (V)	$t_{max}$ (ns)	$\bar{P}$ (W)	$P$ RMS (W)	$P_{max}$ (W)	Erosion time/ 1.5 mm (min)	AVERAGE wear ratio 1ms
Ti	7.98	2	2.65	1216	875.1	1.194	2.472	348	1.46	2.116	5.938	900	0.381
	8.025	1.776	2.222	1172	903.9	1.209	2.462	308	1.53	2.178	5.981	900	
	7.824	1.865	2.397	1188	852.5	1.15	2.362	324	1.49	2.138	5.761	900	
	7.629	1.695	2.038	1148	854.4	1.134	2.282	292	1.5	2.119	5.548	900	
	7.692	1.803	2.412	1312	755.5	1.07	2.301	340	1.33	2.008	5.675	900	
	7.99	1.707	2.091	1168	955.3	1.259	2.542	296	1.47	2.036	5.641	900	
	7.956	1.907	2.486	1196	895.6	1.206	2.468	336	1.46	2.079	5.753	900	
	7.945	1.728	2.118	1164	896.6	1.198	2.433	296	1.54	2.186	5.928	900	
	7.752	2.027	2.698	1224	812.2	1.12	2.33	360	1.43	2.092	5.786	900	
	7.822	1.918	2.502	1208	807.7	1.111	2.303	336	1.45	2.124	5.775	900	
	7.813	1.736	2.442	1324	825.6	1.127	2.456	360	1.17	1.674	5.061	900	
	7.804	1.787	2.443	1312	831.8	1.145	2.457	352	1.23	1.776	5.202	900	
	7.68	1.886	2.44	1188	835.4	1.133	2.331	332	1.46	2.089	5.642	900	
	7.888	1.626	2.018	1260	836.7	1.151	2.422	296	1.42	2.007	5.759	900	
	7.71	1.816	2.444	1320	781.1	1.101	2.377	348	1.29	1.91	5.422	900	
	8.006	1.786	2.449	1312	908.2	1.238	2.664	344	1.28	1.802	5.531	900	
	7.552	1.81	2.557	1336	868.4	1.173	2.511	376	1.15	1.603	4.883	900	

Material	$\overline{V}_o$ (V)	$\overline{V}_e$ (V)	$V_e$ RMS (V)	$t_e$ (ns)	$\bar{i}$ (mV)	$i$ RMS (V)	$i_{\max}$ (V)	$t_{\max}$ (ns)	$\overline{P}$ (W)	$P$ RMS (W)	$P_{\max}$ (W)	Erosion time/ 1.5 mm (min)	AVER AGE wear ratio 1 $\mu$ s
Ti	7.853	1.892	2.534	1312	883.1	1.2	2.547	356	1.27	1.793	5.283	900	0.381
	7.717	1.793	2.398	1308	827.9	1.141	2.435	344	1.25	1.792	5.22	900	
	7.925	1.988	2.646	1216	894.1	1.206	2.491	352	1.42	1.988	5.503	900	
	8.002	1.788	2.178	912	1018	1.297	2.409	284	1.81	2.41	5.717	900	
	7.889	1.669	1.975	1012	908.8	1.206	2.348	276	1.65	2.306	5.733	900	
	7.656	1.877	2.393	968	908.4	1.186	2.265	308	1.64	2.239	5.381	900	
	7.793	1.787	2.386	1188	776.5	1.113	2.351	324	1.37	2.051	5.498	900	
	7.771	1.61	2.041	1136	801	1.127	2.327	292	1.4	2.066	5.412	900	
Ni	8.276	1.905	2.173	1026	963.9	1.267	2.425	274	1.95	2.653	6.242	900	0.622
	8.316	1.814	2.073	1110	915	1.239	2.466	274	1.82	2.565	6.234	900	
	8.396	1.918	2.169	1102	888	1.212	2.395	270	1.93	2.728	6.537	900	
	8.331	1.882	2.205	1162	834.2	1.518	2.358	278	1.84	2.664	6.503	900	
	8.196	1.995	2.486	1164	815.6	1.139	2.316	308	1.74	2.523	6.341	900	
	8.264	1.798	2.076	1148	876	1.21	2.459	276	1.71	2.445	6.253	900	
	8.343	1.886	2.16	1112	907.6	1.227	2.436	276	1.87	2.622	6.442	900	
	8.41	1.965	2.224	1024	953.1	1.256	2.413	272	2.07	2.828	6.667	900	
	8.733	1.987	2.259	1024	969.9	1.285	2.453	272	2.21	3.034	7.092	900	
	8.627	2.017	2.297	1028	938.5	1.249	2.383	272	2.21	3.039	7.045	900	
	8.386	1.839	2.046	1048	986.4	1.293	2.498	272	1.97	2.668	6.38	900	
	8.361	1.815	2.021	1104	922.2	1.241	2.459	272	1.87	2.605	6.419	900	
	8.357	1.814	2.018	1116	926.6	1.244	2.476	272	1.85	2.583	6.37	900	
8.568	1.864	2.082	1088	953	1.279	2.518	272	1.98	2.748	6.734	900		

Material	$\overline{V}_o$	$\overline{V}_e$	$V_e$ RMS	$t_e$	$\bar{i}$	$i$ RMS	$i_{\max}$	$t_{\max}$	$\overline{P}$	$P$ RMS	$P_{\max}$	Erosion time/ 1.5 mm (min)	AVERAGE wear ratio 1ms
	(V)	(V)	(V)	(ns)	(mV)	(V)	(V)	(ns)	(W)	(W)	(W)		
Ni	8.436	1.845	2.017	1020	1001	1.305	2.494	268	2.01	2.716	6.466	900	0.622
	8.129	2.108	2.707	1196	819.6	1.16	2.409	336	1.61	2.339	6.13	900	
	8.389	1.826	2.047	1104	969.8	1.234	2.452	268	1.89	2.657	6.639	900	
	8.452	1.891	2.185	1108	882.9	1.205	2.387	276	1.97	2.786	6.858	900	
	8.372	1.905	2.258	1120	861.4	1.187	2.385	280	1.88	2.691	6.683	900	
	8.449	1.921	2.256	1132	842.4	1.171	2.354	276	1.92	2.766	6.833	900	
	8.381	1.835	2.081	864	1100	1.374	2.481	264	2.14	2.753	6.089	900	
	8.491	1.844	2.058	864	1109	1.384	2.496	264	2.22	2.855	6.319	900	
	8.198	1.869	2.167	876	1048	1.322	2.395	268	2.11	2.733	6.05	900	
	8.626	1.953	2.25	872	1071	1.354	2.452	264	2.33	3.027	6.639	900	
8.198	2.046	2.476	916	960.2	1.247	2.317	284	2.07	2.75	6.095	900		
Cu	7.926	1.6	1.809	1122	950.2	1.223	2.447	270	1.66	2.266	5.627	25	0.311
	8	1.547	1.78	1198	930.4	1.213	2.484	266	1.6	2.226	5.748	25	
	8.004	1.551	1.727	1202	914.8	1.203	2.477	266	1.59	2.223	5.648	25	
	7.921	1.579	1.784	1180	926.4	1.207	2.462	266	1.61	2.232	5.645	25	
	7.918	1.554	1.742	1202	907.9	1.189	2.449	266	1.57	2.19	5.639	25	
	7.658	1.516	1.73	1196	874.6	1.247	2.361	268	1.44	2.006	5.287	25	
	7.949	1.588	1.775	1120	959.8	1.229	2.457	264	1.63	2.218	5.705	25	
	7.917	1.57	1.75	1180	913	1.191	2.425	264	1.56	2.168	5.662	25	
	8.057	1.642	1.815	1120	966.7	1.239	2.471	264	1.67	2.256	5.717	25	
8.393	1.567	1.73	1196	959.4	1.261	2.594	260	1.66	2.324	6.219	25		

Material	$\overline{V}_o$ (V)	$\overline{V}_e$ (V)	$V_e$ RMS (V)	$t_e$ (ns)	$\bar{i}$ (mV)	$i$ RMS (V)	$i_{max}$ (V)	$t_{max}$ (ns)	$\overline{P}$ (W)	$P$ RMS (W)	$P_{max}$ (W)	Erosion time/ 1.5 mm (min)	AVERAGE wear ratio 1ms
Cu	7.693	1.546	1.72	1168	864.5	1.14	2.328	264	1.5	2.093	5.331	25	0.311
	7.945	1.548	1.694	1184	890.4	1.164	2.385	260	1.56	2.165	5.625	25	
	8.047	1.601	1.749	1116	978.5	1.242	2.454	260	1.71	2.302	5.769	25	
	8.065	1.617	1.768	1116	973.3	1.241	2.466	260	1.74	2.353	5.975	25	
	8.152	1.572	1.724	1156	966.2	1.243	2.501	260	1.69	3.319	5.934	25	
	7.949	1.545	1.74	1212	873.5	1.164	2.41	264	1.53	2.162	5.72	25	
	8.038	1.527	1.685	1180	927.6	1.208	2.47	260	1.6	2.218	5.891	25	
	7.869	1.567	1.747	1184	898	1.174	2.396	264	1.56	2.153	5.673	25	
	8.044	1.616	1.759	1108	970.6	1.235	2.451	264	1.71	2.303	5.872	25	
	8.162	1.6	1.741	1116	1004	1.268	2.51	260	1.73	2.317	5.941	25	
	7.971	1.654	1.809	968	964.1	1.246	2.384	256	1.74	2.339	5.389	25	
	7.977	1.606	1.753	960	955.3	1.289	2.377	256	1.67	2.251	5.341	25	
	7.901	1.594	1.742	976	955.2	1.235	2.378	256	1.67	2.247	5.352	25	
	8.019	1.605	1.751	960	992.3	1.277	2.43	256	1.72	2.31	5.458	25	
8.071	1.592	1.747	972	1006	1.289	2.455	256	1.73	2.321	5.508	25		
Ag	8.491	1.722	1.969	1140	977.7	1.274	2.534	272	1.86	2.575	6.409	35	0.209
	8.214	1.586	1.865	1220	932.5	1.23	2.519	276	1.61	2.269	5.981	35	
	7.661	1.497	1.833	1246	865.5	1.144	2.368	286	1.38	1.939	5.156	35	
	7.961	1.587	1.853	1198	909.1	1.194	2.423	282	1.57	2.195	5.727	35	
	7.83	1.577	1.898	1230	887.9	1.171	2.397	282	1.49	0.089	5.495	35	
	8.309	1.642	1.874	1204	894.9	1.196	2.435	268	1.68	2.408	6.292	35	
	8.5	1.601	1.8	1212	941.3	1.243	2.54	264	1.72	2.441	6.47	35	

Material	$\overline{V}_o$ (V)	$\overline{V}_e$ (V)	$V_e$ RMS (V)	$t_e$ (ns)	$\bar{i}$ (mV)	$i$ RMS (V)	$i_{max}$ (V)	$t_{max}$ (ns)	$\overline{P}$ (W)	$P$ RMS (W)	$P_{max}$ (W)	Erosion time/ 1.5 mm (min)	AVER AGE wear ratio 1ms
Ag	8.402	1.615	1.845	1200	933.2	1.233	2.509	268	1.7	2.393	6.294	35	0.209
	8.442	1.613	1.842	1212	935.7	1.24	2.537	268	1.69	2.396	6.359	35	
	8.226	1.556	1.819	1220	932.2	1.22	2.5	272	1.59	2.23	5.986	35	
	8.629	1.806	2.037	1136	955.9	1.258	2.498	268	1.94	2.719	6.819	35	
	8.266	1.636	1.867	1216	886.8	1.191	2.433	268	1.68	2.4	6.194	35	
	8.486	1.803	2.066	1136	947.7	1.254	2.475	272	1.89	2.631	6.516	35	
	8.528	1.645	1.876	1216	921.8	1.238	2.534	268	1.72	2.448	6.441	35	
	8.531	1.669	1.899	1216	919.4	1.234	2.532	268	1.73	2.463	6.52	35	
	8.232	1.566	1.739	1200	938.5	1.222	2.474	264	1.66	2.325	6.205	35	
	8.313	1.626	1.858	1216	902.4	1.199	2.456	268	1.69	2.396	6.302	35	
	8.391	1.63	1.864	1208	913.6	1.217	2.483	268	1.7	2.415	6.336	35	
	8.32	1.613	1.838	1208	928.5	1.223	2.493	268	1.69	2.368	6.297	35	
	8.176	1.602	1.818	1196	908.6	1.204	2.456	268	1.63	2.291	6.061	35	
	8.493	1.696	1.956	1080	924.2	1.249	2.476	264	1.84	2.615	6.367	35	
	8.484	1.678	1.924	1104	905.6	1.234	2.472	264	1.74	2.481	6.147	35	
	8.51	1.639	1.878	1116	923.8	1.257	2.528	264	1.7	2.427	6.086	35	
8.289	1.635	1.87	1092	899.9	1.222	2.438	264	1.67	2.371	5.839	35		
8.36	1.636	1.871	1088	914.7	1.241	2.492	264	1.68	2.393	5.994	35		
W	7.849	1.885	2.078	982	945.7	1.226	2.317	266	1.99	2.658	5.894	120	0.621
	7.743	1.884	2.085	982	913.8	1.191	2.261	266	1.96	2.634	5.861	120	
	7.79	1.93	2.127	962	920.4	1.191	2.245	262	2	2.677	5.955	120	
	7.99	1.939	2.14	974	941	1.223	2.324	262	2.05	2.757	6.142	120	

Material	$\overline{V}_o$ (V)	$\overline{V}_e$ (V)	$V_e$ RMS (V)	$t_e$ (ns)	$\overline{i}$ (mA)	$i$ RMS (V)	$i_{max}$ (V)	$t_{max}$ (ns)	$\overline{P}$ (W)	$P$ RMS (W)	$P_{max}$ (W)	Erosion time/ 1.5 mm (min)	AVER AGE wear ratio 1ms
W	7.83	2.002	2.177	870	1014	1.253	2.25	262	2.2	2.809	5.956	120	0.621
	7.636	1.873	2.09	984	876.5	1.147	2.181	268	1.84	2.501	5.691	120	
	7.682	2.002	2.237	892	988.1	1.227	2.211	272	2.08	2.679	5.82	120	
	7.939	1.996	2.19	860	977.1	1.205	2.149	272	2.07	2.636	5.619	120	
	7.939	2.029	2.205	864	1033	1.271	2.27	264	2.24	2.856	6.148	120	
	7.811	1.891	2.069	968	937.3	1.208	2.274	264	1.96	2.625	5.969	120	
	7.645	2.017	2.246	892	990.2	1.229	2.224	272	2.12	2.729	5.886	120	
	7.923	2.018	2.196	864	1040	1.28	2.29	264	2.26	2.882	6.144	120	
	7.978	2.016	2.186	868	1061	1.304	2.333	264	2.29	2.913	6.259	120	
	7.683	1.938	2.103	884	1005	1.242	2.234	264	2.1	2.685	5.777	120	
	8.08	1.987	2.168	880	1057	1.309	2.368	264	2.27	2.907	6.35	120	
	7.366	1.975	2.099	868	931.7	1.146	2.053	260	1.97	2.486	5.3	120	
	7.913	2.048	2.224	864	1025	1.265	2.26	264	2.27	2.889	6.138	120	
	7.85	2.046	2.21	872	1022	1.258	2.252	264	2.26	2.879	6.216	120	
	7.991	2.077	2.244	860	1055	1.29	2.291	264	2.34	2.959	6.313	120	
	7.855	1.971	2.141	884	1017	1.264	2.288	264	2.17	2.785	6.092	120	
	7.909	2.09	2.267	748	1142	1.343	2.274	260	2.47	2.986	6.002	120	
	7.802	2.1	2.272	748	1132	1.327	2.237	260	2.47	2.974	5.789	120	
	7.904	1.948	2.127	792	1078	1.302	2.28	256	2.32	2.889	5.986	120	
	7.795	2.042	2.218	748	1139	1.34	2.273	260	2.41	2.908	5.752	120	
7.699	1.918	2.124	808	1060	1.286	2.252	260	2.22	2.775	5.761	120		

## Appendix E

### DATA FOR WEAR RATIO OF PURE METALS

Material	Difference in Weight (mg)		Wear Ratio	Average
	Anode	Cathode		
Au	6.7	1.7	0.254	0.248
	6.9	1.7	0.246	
	6.2	1.5	0.242	
	7.6	2.0	0.263	
	7.0	1.8	0.257	
	6.8	1.8	0.265	
	3.3	0.7	0.212	
Ag	8.0	1.6	0.200	0.209
	8.9	1.9	0.213	
	9.2	2.0	0.217	
	9.6	2.1	0.219	
	8.8	1.6	0.182	
	8.6	1.9	0.221	
Co	4.4	3.5	0.795	0.579
	4.9	2.8	0.571	
	6.3	3.5	0.556	
	6.2	3.3	0.532	
	7	3.6	0.514	

Material	Difference in Weight (mg)		Wear Ratio	Average
	Anode	Cathode		
Co	6.5	3.3	0.508	0.579
Cu	16.6	4.6	0.277	0.311
	15.1	4.9	0.325	
	16.6	5.5	0.331	
	15.0	4.6	0.307	
	16.1	4.9	0.304	
	16.9	5.4	0.320	
Ni	5.3	3.1	0.585	0.601
	5.1	3.3	0.647	
	5.3	3.1	0.585	
	5.5	3.7	0.673	
	6.2	3.5	0.565	
	6	3.3	0.550	
Ti	3.6	1.5	0.417	0.390
	3	1	0.333	
	3.2	1.2	0.375	
	3	1.2	0.400	
	2.6	1.1	0.423	
W	10.7	6.7	0.626	0.621
	9.1	5.2	0.571	



Material	Difference in Weight (mg)		Wear Ratio	Average
	Anode	Cathode		
W	10.8	6.4	0.593	0.621
	12.2	7.8	0.639	
	13.1	8.3	0.634	
	13.4	8.9	0.664	

## Appendix F

### RANKING OF PURE METALS DEPENDING ON THE MATERIAL PROPERTIES AND DISCHARGE CHARACTERISTICS

(1 – Highest numerical value; 7 – Lowest numerical value)

Property	Material						
	Ti	Co	Ni	Cu	Ag	Au	W
Errosion time	1	3	1	6	5	7	4
Wear ratio	4	3	1	5	7	6	2
Enthalpy	1	2	3	4	6	7	5
Enthalpy/Thermal conductivity	1	3	2	5	6	7	4
tensile modulus	3	6	5	4	2	1	7
tensile modulus	5	2	3	4	6	7	1
thermal conductivity	1	3	2	6	7	5	4
specific heat	1	2	3	4	5	7	6
Latent heat of fusion	1	3	2	4	6	7	5
Latent heat of evaporation	1	2	3	4	6	7	5
Coefficient of thermal expansion	2	3	4	6	7	5	1
melting point	2	3	4	5	7	6	1
boiling point	2	4	5	6	7	3	1
Electrical resistivity	7	5	6	2	1	3	4

Property	Material						
	Ti	Co	Ni	Cu	Ag	AU	W
Temperature coefficient	7	2	1	4	5	6	3
Photo-electric work function	1	7	6	2	4	5	3
Atomic weight	1	3	2	4	5	7	6
Atomic radius	7	1	1	3	5	5	4
Atomic number	1	2	3	4	5	7	6
Erosion time	1		1	5	4		3
Wear ratio	3		1	4	5		2
Vobar	1		5	3	4		1
Vebar	3		4	1	2		5
VeRMS	5		4	1	2		3
te	5		2	3	4		1
te	1		4	3	2		5
lbar	1		3	3	2		5
IRMS	1		5	2	2		4
lmax	2		3	4	5		1
tmax	5		4	1	3		2
Wbar	1		4	2	3		5
WRMS	1		4	2	3		5
Wmax	1		5	2	4		3

